National Library of Canada
Acquisitions and Bibliographic Services Branch
395 Wellington Street
Ottawa, Ontario
K1A 0N4

Bibliothèque nationale du Canada
Direction des acquisitions et des services bibliographiques
395, rue Wellington
Ottawa (Ontario)
K1A 0N4

KRAFT CHEMICAL RECOVERY IN A FLUIDIZED BED

by

John A. Fallavollita, B.Eng, M.Eng. (Met.)

A Thesis Submitted to the Faculty of Graduate Studies
and Research in Partial Fulfilment of the
Requirements for the Degree of
Doctor of Philosophy

Department of Chemical Engineering
McGill University
Montréal, Québec
Canada

August 1992

ISBN 0-315-87645-X

Canada

DEDICATION:

To my wife, Lorna Joanne, and my parents, Filomena and Pasquale, for all their love and encouragement throughout the years of my life.

We must not cease from exploration and the end of all our exploration will be to arrive where we began and to know the place for the first time.

T.S. Eliot

ABSTRACT

Pyrolysis and steam gasification of dry kraft black liquor solids were investigated in a fluidized-bed between 500°C and 700°C. Total mass balances were obtained for carbon, sodium, and sulphur in the solid char and gaseous products. Above 600°C the addition of steam resulted in significant increases in CO_2 and H_2, and a decrease in CO; however, the production of CH_4 was unaffected. The global gasification rate of carbon increased fourfold from 0.003 min^{-1} at 600°C to 0.013 min^{-1} at 650°C. It is proposed that the carbon gasification rate for black liquor char is controlled by the kinetics of the C-H_2O reaction.

Catastrophic defluidization was observed at 700°C for steam gasification but not for pyrolysis. SEM micrographs of the char particles revealed that surface melting had occurred. Low-melting-point eutectic mixtures containing chloride and potassium were suggested as the primary cause. It is proposed that the stickiness of the char surface is controlled by the quantity of amorphous carbon under these conditions.

For pyrolysis in N_2, a total mass balance over the temperature range 500-700°C showed that the retention of sulphur in the solid char product increased from 60 ±11 wt% to 91 ±8 wt%. Between 500-550°C, the major sulphur compounds in the char were Na_2SO_4, Na_2SO_3, and Na_2S, in decreasing order. The production of Na_2SO_3 was attributed to the decomposition of sodium thiosulphate, which was present in the kraft black liquor solids. Between 600 and 700°C, the reduction of Na_2SO_4 and Na_2SO_3 by carbon and CO/H_2 led to an increase in the production of sodium sulphide. The reduction efficiency in the fluidized bed was 99.1 ±11.4% at 700°C.

The addition of steam led to a decrease in the concentration of solid Na_2S in the kraft black liquor char throughout the temperature range studied. Between 650-700°C, the emission of H_2S in the particulate phase of the fluidized bed was in equilibrium with the gasification product gases. The results suggest that the sulphur emission could reach unacceptable levels in commercial fluidized-bed gasifiers employing higher steam concentrations.

RÉSUMÉ

On a étudié la pyrolyse et gazéification des solides provenant de la liqueur noire Kraft avec de la vapeur d'eau dans un lit fluidizé à des températures n'excédant pas 700°C. Les balances de masse ont été obtenues pour le carbone, le sodium, et le soufre dans le produit gazeux et la liqueur noire solidifiée. Au-dessus de 600°C, l'addition de la vapeur d'eau est responsable pour l'augmentation de CO_2 et H_2, et une diminution de CO; cependant la production de CH_4 n'a pas été affectée. Les taux globales de gazéification du carbone avec de la vapeur d'eau ont augmentés de 0.003 min^{-1} à 600°C jusqu'à 0.013 min^{-1} à 650°C. On suggère que la gazéification est contrôlée par la cinétique de la réaction C-H_2O pour les conditions employées.

La défluidization catastrophique est observée à 700°C pour la gazéification avec de la vapeur d'eau mais pas pour la pyrolyse. Des photos prises avec un SEM ont révélees que la surface des particules provenant de la liqueur solidifiée était partiellement fondue. Un mélange de composés contenant du chlorure et du potassium est suggéré d'être la cause principale pour la déformation observée. On propose que cette adhésion de la surface est contrôlée par la quantité de carbone organique.

Pour la pyrolyse dans une atmosphère d'azote, la balance de masse indique que la quantité de soufre augmente dans la liqueur noire solidifiée de 60 ±11% à 500°C jusqu'à 91 ±8% à 700°C. Dans l'intervalle 500-550°C, les composés majeurs de soufre dans la liqueur noire solidifiée étaient, en ordre d'importance, Na_2SO_4, Na_2SO_3, et Na_2S. La présence de Na_2SO_3 est le produit de la décomposition du thiosulfate de sodium contenue dans les solides de la liqueur noire. Dans l'intervalle 600-700°C, la réduction de Na_2SO_4 et Na_2SO_3 par le carbone et par le mélange CO/H_2 est résponsable pour la production de Na_2S. L'efficacité de la réduction dans le lit fluidizé était 99.1 ±11.4% à 700°C.

Dans l'intervalle de temperature étudié, l'addition de la vapeur d'eau est responsable pour la diminution de la concentration de Na_2S dans la liqueur noire solidifiée . Dans l'intervalle 650-700°C, l'émission du H_2S est contrôlée par l'équilibre thermodynamique de la réaction entre le solide Na_2S et le mélange de la vapeur d'eau et CO_2. On suggère que l'émission du H_2S peut atteindre un niveau inacceptable dans les systèmes de gazéification commerciaux qui utilisent des concentrations de vapeur d'eau plus élevés.

ACKNOWLEDGMENTS

This project has required copious amounts of both time and money for its completion. I would like to take this opportunity to thank the individuals and organizations mentioned below for their contributions:

- Drs. M.M. Avedesian and A.S. Mujumdar, for their support during the course of this work.
- Dr. A.R.P. van Heiningen, for his thorough criticism of the thesis and immensely helpful suggestions throughout the course of this work - he has been a true inspiration.
- D. Peirce, C. Monasterios, R. Mentore, J. Li, A. Wong and P. Fenchak for assistance in developing the analytical techniques and construction of the pilot plant.
- The members of the CRISP[3] group for their helpful comments: Dr. G. Kubes, P. Stuart and S.K. Sen Gupta.
- Alain, Walter, Herb, Don and Andy (the machine shop crew), for their remarkable workmanship and good cheer.
- J. Dumont, for his excellent organization of the stores, and L. Cusmich for some electrical work on the unit.
- Domtar Inc. and Noranda Inc., for providing some experimental equipment.
- Prof. R.I.L. Guthrie (Dept. of Mining and Met.), for the use of a Leco Carbon Analyzer.
- Prof. M. Wayman and Ms. T. Barker (Dept. of Mining, Met. and Petroleum Eng., Univ. of Alberta, Edmonton), for the cost-effective use of the SEM-EDXA instrument.
- Dr. P. Clark and Mr. K. Lesage (Alberta Sulphur Research Institute, Calgary), for performing the elemental sulphur, organo-sulphur, and some inorganic polysulphide analyses on the char samples.
- The Natural Sciences and Engineering Research Council, for providing a strategic grant throughout this project.
- Les Fonds FCAR and the Pulp and Paper Research Institute of Canada for post-graduate fellowships.
- Last but not least, my wife Lorna, who helped me in many aspects of this work and provided me with the emotional atmosphere necessary to keep the fire burning.

TABLE OF CONTENTS

LIST OF FIGURES

LIST OF TABLES

NOMENCLATURE

a = multiplier indicating the frequency of a reaction step

A = cross-sectional area of a fluidized bed (m^2)

A_o, A_o' = pre-exponential factor for the rate law of Hashimoto et al. (1986) given in Table 9 ($mol \cdot kg^{-1} \cdot s^{-1} \cdot kPa^{-1}$)

A_p = actual external surface area of a particle (m^2)

A', = pre-exponential factor for the rate law, Eq. 26, in Chapter 2 (t^{-1} or $mol \cdot g^{-1} \cdot t^{-1}$)

A_{total} = total external surface area of the particles in the fluidized bed (m^2)

C_{char} = carbon in a char matrix

$C_{H_2O}^{bulk}$ = molar concentration of steam in the bulk gas of the particulate phase ($mol \cdot m^{-3}$)

$C_{H_2O}^{s}$ = molar concentration of steam at the surface of the char-alumina particles ($mol \cdot m^{-3}$)

C_{char}^{c-a} = char content in a char-alumina sample (g char/ 100 g char-alumina)

C_i^{char} = weight percent of component i in the char (g of i/ 100 g char)

C_i^{KBLS} = weight percent of component i in KBLS (g of i/ 100 g KBLS)

C_F, C_F' = free-carbon active sites

C_p = molar heat capacity at constant pressure ($J \cdot K^{-1} \cdot mol^{-1}$)

$[C_{site}]$ = surface concentration of free-carbon active sites ($mol\ sites \cdot m^{-2}$)

$C(O)$ = chemisorbed-oxygen surface complex on carbon

$[C(O)]$ = surface concentration of chemisorbed-oxygen surface complexes ($mol\ sites \cdot m^{-2}$)

$[CO]$ = mole fraction of carbon monoxide

$[CO_2]$ = mole fraction of carbon dioxide

$[C_T]$ = surface concentration of active sites for uncatalyzed gasification ($mol\ sites \cdot m^{-2}$)

$[C_{cT}]$ = surface concentration of active sites for catalysed gasification ($mol\ sites \cdot m^{-2}$)

$CO_2(*)$ = surface complex consisting of a CO_2 molecule adsorbed on an active catalyst site

$CO_3(*)$ = surface complex consisting of a carbonate moiety adsorbed on an active catalyst site

CO_2/M = molar ratio of adsorbed CO_2 to alkali metal

d_p = surface-area-mean diameter of a mixture of particles of different size and same shape; calculated using Eq. 12b in Kunii and Levenspiel (1977, p. 69) (μm)

d_p^* = equivalent diameter of a particle (μm)

$D_{H_2O\text{-}m}$ = overall diffusion coefficient of steam in the bulk fluid ($cm^2 \cdot s^{-1}$)

D_{H_2O-i} = binary diffusion coefficient of steam into i ($cm^2 \cdot s^{-1}$)

$D_{i,char}^{j,KBLS}$ = distribution of i in char (g of i in char/ 100 g of j in KBLS)

$D_{C,i}^{C,KBLS}$ = distribution of carbon in gas i (g carbon in i/ 100 g carbon in KBLS)

$D_{H,i}^{H,input}$ = distribution of hydrogen in the off-gas (g H as H_2/ 100 g H input)

$D_{S,i}^{S,KBLS}$ = distribution of sulphur in gas i (g sulphur in i/ 100 g sulphur in KBLS)

E_{i_1,i_{-1},i_2} = activation energy for the elementary rate constants; i_1, i_{-1}, and i_2 in Eqs. 65, 67 (Table 5) ($kJ \cdot mol^{-1}$)

$E_{m_1,m_{-1}}$ = activation energy for the elementary rate constants; m_1, and m_{-1} in Eq. 69 (Table 5) ($kJ \cdot mol^{-1}$)

E_o, E_o' = apparent activation energy for the rate law of Hashimoto et al. (1986) in Table 9 ($kJ \cdot mol^{-1}$)

E'_r = apparent activation energy for the rate law, Eq. 26, in Chapter 2 ($J \cdot mol^{-1}$)

$f(...)$ = intrinsic reaction rate for carbon gasification ($mol \cdot mol\ sites^{-1} \cdot t^{-1}$)

F_i^{ave} = average molar flow rate of gas i ($mol\ i \cdot min^{-1}$)

F_{KBLS} = feed rate of dry KBLS ($kg \cdot h^{-1}$)

F_{H_2O} = feed rate of H_2O ($mL \cdot min^{-1}$)

$F_{H_2O}^P$ = molar flow rate of steam at the exit of the particulate phase ($mol \cdot min^{-1}$)

$[H_2]$ = mole fraction of H_2

$[H_2O]$ = mole fraction of H_2O

$\Delta H'_{ox}$ = enthalpy change for elementary step, Eq. 84, in Table 6 ($J \cdot mol^{-1}$)

ΔH^o_{298} = standard molar heat of formation at 298 K ($kJ \cdot mol^{-1}$)

ΔH_{tran} = enthalpy change due to a phase transformation ($kJ \cdot mol^{-1}$)

I = term defined by Eq. 22 (Chapter 2)

i_i = rate constants for the elementary steps, i, in uncatalysed CO_2 gasification (units vary)

j_i = rate constants for the elementary steps, i (units vary with reaction order)

k_i = rate constants for the elementary steps, i (units vary with reaction order)

k_c = average mass-transfer coefficient over the char-alumina surface ($m \cdot s^{-1}$)

k_o, k_o' = rate constants for the rate law of Hashimoto et al. (1986) in Table 9 (= $A_o exp(-E_o/RT)$ and $A'_o exp(-E'_o/RT)$, respectively) ($mol/kg \cdot s \cdot kPa$, kPa^{-1})

k''_r = rate constant for the elementary step, Eq. 94, in Table 7 ($mol \cdot mol\ sites^{-1} \cdot t^{-1}$)

k'_r = overall rate constant for the rate law, Eq. 26, in Chapter 2 {= $A'_r\ exp(-E'_r/RT)$} (t^{-1} or $mol \cdot g^{-1} \cdot t^{-1}$)

K^{eq}_{60} = equilibrium constant for the H_2S stripping reaction, Eq. 60, in Chapter 5

K^{p}_{60} = measured value in the particuiate phase of the equilibrium constant for Eq. 60

$K_{CO\text{-}CO_2}$ = equilibrium constant for the elementary oxygen-exchange step, Eq. 65, in Table 5

K_{eq_i} = equilibrium constants for the reversible elementary steps, *i*

K_{gs} = equilibrium constant for the water-gas shift reaction, Eq. 41, in Chapter 4

$K_{H_2\text{-}H_2O}$ = equilibrium constant for the elementary oxygen-exchange step, Eq. 69, in Table 5

K'_{ox} = equilibrium constant for the elementary step, Eq. 84, in Table 6 $[= exp(\Delta S'_{ox}/R) \cdot exp(-\Delta H'_{ox}/RT)]$

K^{H}_{ox} = equilibrium constant for the elementary step, Eq. 93, in Table 7

$K^{C/CO_2}_{overall}$ = equilibrium constant for the reversible, overall C-CO_2 reaction, Eq. 16 (Chapter 2)

$K^{C/H_2O}_{overall}$ = equilibrium constant for the reversible, overall C-H_2O reaction, Eq. 18 (Chapter 2)

K_{surf} = represents a potassium-oxygen surface complex of unknown composition

K_xO_y = non-stoichiometric potassium-oxygen compound, where y < x

K_xO_{y+1} = oxidized non-stoichiometric potassium oxygen compound

k_i = rate constants in the uncatalysed C-H_2O rate law in Table 5 (units vary)

m_i = rate constants for elementary steps *i* of Eq. 69 (Table 5) (units vary)

M_i = molecular weight of species *i* ($g \cdot mol^{-1}$)

M = alkali metal

M/C = molar ratio of alkali metal to carbon

n = amount of carbon present during gasification (mol)

n_{C_0} = initial amount of carbon (mol)

N_{cT}, N_T = total concentration of active sites per amount of carbon for catalysed and uncatalysed gasification, respectively ($mol\ sites \cdot mol^{-1}$)

$O(*)$ = surface complex consisting of an adsorbed oxygen atom on an alkali catalyst site

$[O(*)]$ = surface concentration of oxidized alkali catalyst sites ($mol\ sites \cdot m^{-2}$)

O_{org} = oxygen bound to the organic component of char (mol)

p_i = partial pressure of gas component *i* (kPa)

P_t, P = total pressure (kPa and atm, respectively)

q = exponent for carbon burn-off

Q_b = visible-bubble volumetric flow rate in a fluidized bed ($m^3 \cdot s^{-1}$)

$r^{p}_{H_2S}$ = emission rate of H_2S in the particulate phase ($g\ H_2S \cdot (g\ S^{2-} \cdot min)^{-1}$)

$-r_o$ = initial rate of disappearance of carbon (t^{-1})

$-r_n$ = normalized rate of disappearance of carbon (t^{-1})

$-r_w$ = instantaneous rate of disappearance of carbon (t^{-1})

$-r_w''$ = instantaneous rate of carbon gasification per unit external surface area ($mol \cdot m^{-2} \cdot s^{-1}$)

R = gas constant (8.413 $J \cdot mol^{-1} \cdot K^{-1}$)

Sh = Sherwood number

$\Delta S'_{ox}$ = change in entropy for the elementary step, Eq. 84, in Table 6 ($J \cdot mol^{-1} \cdot K^{-1}$)

S°_{298} = standard molar entropy at 298 K ($J \cdot K^{-1} \cdot mol^{-1}$)

S_a, S_{a0} = specific surface area of carbon for $X>0$ and $X=0$, respectively ($m^2 \cdot mol^{-1}$)

t = time (s or min)

t_{med} = mean residence time of the char, calculated from Eq. 128 in Appendix A (min)

T = temperature (K)

T_{first} = temperature at which liquid first appears for binary and ternary systems (°C)

$Total_{fbc}$ = char content in the dense phase of the fluidized bed (g)

$Total_{char}$ = total char recovered in the pilot plant, including elutriated material (g)

U = superficial gas velocity ($m \cdot s^{-1}$)

U_{mf} = minimum fluidization velocity ($m \cdot s^{-1}$)

W_{H2O} = average molar flux of steam to the char-alumina particles ($mol \cdot m^{-2} \cdot s^{-1}$)

W_j = weight of sample j (g)

X = fractional conversion of carbon

y^p_i = mole fraction of i in the particulate phase

y^{eq}_i = mole fraction of i at equilibrium

Y^{ave}_i = average yield of fixed gas, i (mol $i \cdot kg^{-1}$ KBLS fed)

Y_{char} = total yield of char from the entire pilot plant (g char·100 g^{-1} KBLS fed)

ABBREVIATIONS

BLOX = Black liquor oxidation.

EDXA = Energy Dispersive X-Ray Analysis.

GC-MS = Gas chromatography- mass spectrophotometry.

KBL = Kraft black liquor.

KBLS = Kraft black liquor solids.

MTCI = Manufacturing and Technology Conversion Intl. Inc.

N/A = Not analyzed.

NQ = Not quantifiable.

NSP = New Swedish Process.

OC = Organic carbon.

PI = Proportional-Integral.

SCR = Solid-state control rectifier.

SEM = Scanning Electron Microscope.

STP = Standard temperature (0°C) and pressure (101.33 kPa).

SUM = Comparative bar representing the sum of the measured components: Na, S, or char.

TGA = Thermogravimetric apparatus.

TPP = Triphenylphosphine.

$TPPO_4$ = Triphenylphosphate.

TPPS = Triphenylphosphine Sulphide.

SYMBOLS

(*) = alkali-catalyst site of unknown composition

[(*)] = surface concentration of alkali catalyst sites of unknown composition (mol sites·m^{-2})

Σv = atomic diffusion volume ($cm^3 \cdot g^{-1} \cdot mol^{-1}$)

ϕ = sphericity of a particle as defined in Kunii and Levenspiel (1977)

ξ_{40}, ξ_{41} = reaction rates for Eqs. 40, 41, respectively, in Chapter 4 (mol·min^{-1})

ρ_i = density of species *i* ($kg \cdot m^{-3}$)

INTRODUCTION

Background Information

The liberation of fibres from wood can be accomplished in processes that are dominated by mechanical and chemical steps. The Kraft Pulping Process is the dominant chemical method in present use. In this process the wood chips are dissolved in a digester with white liquor, which is an alkaline solution of the cooking chemicals NaOH and Na_2S. The liberated fibres are then separated from the spent cooking liquor (weak black liquor) and typically bleached to remove any remaining lignin. The spent liquor contains about 15 wt% solids that are composed of about equal parts of dissolved wood and inorganics. The recovery of the cooking chemicals and energy from this black liquor is a key to the commercial success of the Kraft Process. In the recovery section of a kraft mill, the kraft black liquor is concentrated to between 65-80% solids in energy-efficient multiple-effect evaporators. The concentrated black liquor is fired into a high-temperature recovery boiler ($T > 850°C$) with an excess of air. The organics are combusted for energy recovery as high pressure steam, and the molten salts Na_2CO_3 and Na_2S are tapped from the bottom of the boiler into an aqueous solution (green liquor). The Na_2CO_3 in green liquor is then reacted with lime to produce NaOH, thereby regenerating the white liquor.

Some major problems exist in the operation of the recovery boiler mainly because the sodium salts are in a molten state, leading to corrosion and possible smelt-water explosions. Research has been in progress for some time to understand and improve this high-temperature system. The present research focuses on accomplishing the recovery of chemicals/energy using a fluidized bed at low-temperature where the inorganics are in a solid state.

Purpose and Objectives

The purpose of the present study is to determine the conditions for which a low-temperature fluidized-bed process could become a viable alternative to the high-temperature recovery boiler. Several key objectives in this research are:

- To determine the total mass balance for sodium, carbon and sulphur during fast pyrolysis and steam gasification of kraft black liquor solids in a nitrogen atmosphere.
- To determine the global gasification rate of char carbon, and the rate of hydrogen sulphide emission as a function of temperature and steam partial pressure in the fluidized bed.

- To study the composition changes of the inorganic sulphur species in kraft black liquor solids as a function of temperature and steam partial pressure in the fluidized bed.
- To compare the bench-scale fluidized-bed data with equilibrium predictions and kinetic rate laws from thermogravimetric studies available in the literature.

Outline of the Thesis

Chapter 1 provides a general overview of kraft chemical recovery technology. The conventional recovery boiler operation and its attendant problems are reviewed, and the major alternatives are outlined. Some of the relevant experimental data on low-temperature pyrolysis of kraft black liquor are presented. Equilibrium calculations are performed to show the effect of moisture content, temperature, and thermochemical data for Na_2S on the sulphur recovery.

The CO_2 and steam gasification of uncatalysed and alkali-catalysed carbon are discussed in Chapter 2. The reaction mechanisms that have been proposed in the literature for these systems are discussed, and the important variables that affect the overall gasification are explained. The reactivity of kraft black liquor char is compared with that of alkali-catalysed coal and activated carbon. Langmuir-Hinshelwood rate laws that successfully correlate the gasification data of black liquor char are reviewed. A new mechanism for the alkali-catalysed steam gasification is proposed that leads to the correct form of the rate law for the primary CO_2 formation.

A description of the fluidized-bed pilot plant system and operating procedures is given in Chapter 3. A major effort in this work involved the development of analytical methods to characterize the char-alumina product and the major fixed and sulphur-containing gases. A brief description of these methods is included along with some mass balance results that validate the experimental techniques. The reproducibility of the experimental data for the char and gases is also discussed.

Chapter 4 details the results for the fluidized-bed pyrolysis and steam gasification of kraft black liquor solids in a N_2 environment. Total mass balances for carbon and sodium are also measured. The effect of temperature and the steam:solids weight ratio on the distribution of organic carbon and fixed gases are quantified. The global gasification rate of carbon is estimated from the fluidized-bed operating data, and compared with a known kinetic rate law prediction. Bed agglomeration at 700°C during steam gasification is explained by the factors that determine the stickiness of char particles.

In Chapter 5 the sulphur distribution in the fluidized-bed pilot plant is reported. The major reactions involving the inorganic sulphur species - Na_2S, Na_2SO_4, Na_2SO_3 and $Na_2S_2O_3$ - are established. The emission of sulphur as H_2S, CH_3SH and $(CH_3)_2S$ is related to the interaction of both inorganic and organic sulphur in kraft black liquor solids.

Chapter 6 extends the findings of the experimental program to the industrial situation by allowing for the addition of O_2 to the reactor. The equilibrium sulphur distribution is calculated as a function of O_2 and temperature. A novel process for the treatment of kraft black liquor at low-temperature using fluidized-beds is proposed that may fulfil the dual objectives of chemical and energy recovery.

The raw experimental data and details of the mass balance calculations for both char and gases are provided in Appendix A. A comprehensive list of all the equipment, including specifications and suppliers, is tabulated in Appendix B. The derivation of the Langmuir-Hinshelwood rate laws for the proposed mechanism of alkali-catalysed steam gasification is outlined in Appendix C. In Appendix D an estimate of the mass transfer rate of steam to the char-alumina particles is outlined.

CHAPTER 1

KRAFT BLACK LIQUOR RECOVERY TECHNOLOGY - A REVIEW

ABSTRACT

The Tomlinson recovery boiler has been the mainstay of the kraft pulping industry for over fifty years. It is clear, however, that the main drawbacks to this process are the large capital costs of new plant and the smelt-water explosion hazard. This chapter reviews the main alternatives to the conventional kraft recovery system. The alternatives are generally based on the gasification of kraft black liquor, using air or steam, at temperatures where the inorganic salts are either molten or in the solid state. The former are referred to as high-temperature processes and include cyclone or plasma reactors, while the latter are low-temperature processes that employ fluidized beds.

Some of the relevant literature on the pyrolysis of kraft black liquor at low-temperature is reviewed. It is seen that the reactions during pyrolysis lead to the production of a solid char (mostly carbon, Na_2CO_3, and Na-S salts), fixed and sulphurous gases, and condensable hydrocarbons. The relative proportion of these products is a complex function of the black liquor composition and process conditions.

Thermodynamic calculations were performed to determine the effect of temperature and moisture content on the recovery of sulphur as Na_2S. It was found that the equilibrium predictions varied significantly, depending on the literature source for the thermochemical data of Na_2S. Between 500-700°C, the equilibrium yield of solid Na_2S increases with increasing temperature and decreasing moisture content in the kraft black liquor. These results suggest the use of dry kraft black liquor solids as the feed to a low-temperature fluidized-bed process.

CONVENTIONAL KRAFT RECOVERY

The process of recovering energy and valuable cooking chemicals from kraft black liquor (KBL) has been practised for nearly one hundred years. Equipment upgrading has improved the operability and throughput of the process. Reviews are available in the literature that discuss the basic unit operations (Hough, 1985), the chemistry of alkaline pulping (Bryce, 1980), and the recovery boiler complex (Blackwell and King, 1985). Research has been under way in the areas of fume formation (Cameron et al., 1985: Li and van Heiningen, 1990a), smelt reduction (Grace et al., 1985), char combustion and gasification (Milanova and Kubes, 1985: Li and van Heiningen, 1990a; 1990b; 1991b), and sulphonation reactions (Backman et al., 1985). This work has provided a better understanding of the chemistry in the kraft recovery boiler.

The main advantages that have traditionally maintained the kraft process as the dominant chemical pulping method are: the improved strength of the pulp fibres, the ability to handle a variety of wood species, and the ease of recovering both the energy in KBL and the valuable cooking chemicals, Na_2S and NaOH. The Tomlinson recovery boiler is the key unit operation in which the energy of the organics in kraft black liquor is converted to high pressure steam, and Na_2SO_4 in the inorganic smelt is reduced to Na_2S in a char layer at the bottom of the furnace. For a kraft mill producing 1000 tonne/day of pulp, the boiler would process about 70 m^3/h of black liquor at 65% solids. Steam production would be in the order of $3.0 \cdot 10^5$ kg/h (6500 kPa and 500°C), and the smelt flow from the furnace would be about $2.7 \cdot 10^4$ kg/h. The conversion of sulphur in the black liquor to Na_2S in the smelt is typically about 90%. The overall energy efficiency (useful steam out compared with the total enthalpy input) for a 65% solids feed liquor would be around 64%. The cost of such a unit could be between 100-150 million U.S. dollars.

Due to the high cost of installing new recovery boilers, the time is approaching where the kraft process may start to price itself out of the pulp market (Gundersby, 1985). In particular, it is desirable to develop technology that could allow for incremental capacity for new plant installation at reduced capital cost (Grace, 1981). The conventional recovery boiler has also had a notorious safety record, with explosions that seem to defy preventive measures. It is generally believed that water contact with the smelt bed is a major contributor to this recurring problem.

PROPOSED ALTERNATIVE RECOVERY SCHEMES

Development work on alternative recovery processes has intensified over the last fifteen years in industrial, government and academic institutions in various parts of the world. The International Forum on Recovery Alternatives held at the Institute of Paper Chemistry in 1976 was the first attempt to examine some of the more advanced processes on a comparative basis (IPC, 1976). From a group of six alternatives at that conference, only the NSP gasification process progressed beyond the pilot plant stage. It should be noted that the Domtar-Copeland Process was used commercially at Cornwall (Tomlinson et al., 1976) but did not represent an alternative to the Tomlinson boiler.

Recently, several interesting proposals have entered the scene that are based on molten salt, plasma or fluidized-bed technology. The following process descriptions are based on the published reviews of Fallavollita et al. (1987) and Empie (1991).

NSP Process

The main idea in the NSP process was to perform the various physical and chemical steps of moisture removal, KBL pyrolysis, char gasification and sulphate reduction, in a cyclone reactor that was external to the recovery boiler. The products were a molten smelt, combustible gases and fume. The smelt was tapped outside the power boiler, eliminating the possibility of smelt-water explosions. Bjorklund et al. (1985) presented results for a pilot-scale cyclone furnace (2 tonnes dry solids/h) that was mounted on a conventional recovery boiler. As expected, smelt reduction in the cyclone varied with the air/black liquor solids ratio, but was generally above 85%. Further commercial development of this process does not appear likely and development efforts have been halted (Warnqvist, 1986).

Molten Salt Gasification

The molten salt gasification process outlined by Kelleher (1984) was essentially the design developed by Rockwell International for coal gasification. The KBL and oxidant (air or oxygen) were fed to a molten salt bath at 1000°C. The products were a gas of low- to medium-calorific value and a smelt consisting of Na_2CO_3 and Na_2S. Early results on a bench-scale unit suggested a potential to achieve 95% reduction of sulphate to sulphide in the smelt, and a higher heating value for the gas of 4700 kJ/m^3 (STP). Further experimental work on a pilot scale unit (4 m high by 0.8 m I.D.) showed a poor reduction efficiency and product gas composition (Kelleher, 1985a).

Kohl (1986) has presented details of the plant economics and flowsheet for this process. Champion International was seeking to form a consortium to build a demonstration plant (Kelleher, 1985b), but presently these plans have been shelved.

Kignell (1989) recently proposed a process that was very similar to that of Champion International. The main difference was that it operated at higher pressure (10^3-10^4 kPa) for the purpose of reducing the smelt-water explosion hazard. These conditions also lead to higher sulphur volatilization. For example, Warnqvist (1987) performed thermodynamic calculations at 827°C, $5 \cdot 10^3$ kPa total pressure, and 0-50% stoichiometric air. He found that all the sulphur in KBL would report to the gas phase. In this process, the sulphur recovery would take place via gas absorption in a solution containing green liquor (Na_2CO_3 + Na_2S) and NaOH.

Plasma Gasification

A plasma gasification process was initially conceived as a joint development between SKF Steel and Stora Kopparberg of Sweden. The idea involves feeding oxygen and black liquor into a plasma reactor operating at a temperature around 1250°C. In this temperature region the main products of gasification are liquid Na_2S, sodium vapour, and NaOH vapour (Bernhard and Martenson, 1985). By quenching this mixture quickly, the developers claim that it is possible to recover the inorganics as NaOH and Na_2S in an aqueous scrubbing solution. Therefore, this process would eliminate the need for the causticizing section in the mill.

The idea seems very appealing from an economic standpoint and would simplify the process flowsheet considerably. The claimed advantages of the plasma process are incremental capacity, lower capital cost, and no smelt-water explosion hazard. A major technical problem that needs further study is the possible recombination reactions leading to Na_2CO_3 formation during rapid cooling, such as:

$$2NaOH_{(v)} + CO_2 \Leftrightarrow Na_2CO_{3\,(l)} + H_2O_{(v)} \quad (1)$$

$$2Na_{(v)} + CO_2 + H_2O_{(v)} \Leftrightarrow Na_2CO_{3\,(l)} + H_2 \quad (2)$$

Empie (1991) has confirmed that the cooling and separation of the sodium compounds has been difficult, and this technology is still in the development stage.

Recent work has shifted to a temperature of between 900-950°C. The inorganics are recovered as molten droplets of Na_2CO_3-Na_2S in an aqueous scrubbing solution, and a fuel gas

is produced consisting of H_2, CO, CO_2, H_2O, and traces of H_2S (Stigsson, 1989; 1991). Kamyr AB. (1990) is commercializing this technology via a license agreement with Chemrec AB. of Sweden. A demonstration unit has been installed at the Frövifors Kraft Mill in Sweden with a capacity of 4 tonne/h of kraft black liquor.

Fluidized-Bed Gasification

Fluidized-bed gasification centres around the idea of low-temperature processing (i.e., below the inorganic-salts eutectic melting point). The products of gasification are a solid char and a combustible gas. The gas phase consists mostly of CO, H_2, CO_2, CH_4, H_2O, N_2 and volatile sulphur compounds such as CH_3SH and H_2S. Fluidized-bed gasification would eliminate the possibility of smelt-water explosions and associated corrosion problems inherent in the conventional high-temperature recovery boiler.

The fluidized bed approach to the processing of KBL has appeared in various patents over the past 20 years (Nguyen, 1985: Cook, 1981: DiNovo and Ballantyne, 1981: Tomlinson, 1977: DeHaas et al., 1976: Shah, 1971: Osterman and Klei, 1970: Flood, 1967). To the author's knowledge, none of these systems has reached the commercial stage. However, the earlier work of DiNovo and Ballantyne (1981) was developed further and is embodied in the International Paper Co. (IP) Fluidized Bed. Also, the process patented by Nguyen (1985), which uses a TiO_2 autocausticizing agent, has been extended by the work of Zou et al. (1990). Recently, two new entrants have focused serious attention on fluidized-bed technology. These are the Manufacturing and Technology Conversion Intl. (MTCI) Indirect Black Liquor Gasifier, and the Technical Research Centre of Finland (VTT) Pressurized Gasifier.

International Paper Co. Fluidized-Bed Process

Two key steps underpin the IP Fluidized Bed Process. First, KBL is combusted with excess air in a circulating fluidized bed. This produces a solid Na_2CO_3-Na_2SO_4 mixture and a gas consisting of mostly CO_2 and steam. Second, sodium sulphate is reduced to Na_2S in a molten salt reactor at 900°C with petroleum coke and/or natural gas. Since the reduction is endothermic, energy needs to be added to this reactor. This technology eliminates the need for a water-wall construction that is used in the conventional recovery boiler, and also the smelt-water explosion hazard. Unfortunately, the progress toward commercialization is presently not known (Empie, 1991).

Autocausticizing Process

Based on chemical equilibrium calculations, Zou et al. (1990) propose a fluidized-bed process whereby KBL is gasified with 70% stoichiometric air at 900°C and a molar ratio of TiO_2/Na_2 greater than 1. The addition of TiO_2 results in the formation of solid sodium titanates, $Na_2O{:}xTiO_2$, at temperatures where the inorganics, Na_2CO_3 and Na_2S, would otherwise be molten. In a subsequent step, the sodium titanates dissolve in water to produce NaOH and regenerate TiO_2. Under these conditions, the products consist of solid TiO_2 and $Na_2O{:}xTiO_2$. All the sulphur reports to the gas phase with 90 wt% as H_2S and 9 wt% as COS; the remainder is S_2 and SO_2. Negligible amounts of sodium vapour are predicted. One benefit of this process would be the elimination of the conventional causticizing step with CaO. However, the details of recovering sulphur as Na_2S from H_2S and COS were not given. This process is at the research stage with bench-scale fluidized bed work to commence shortly (van Heiningen, 1991).

MTCI Indirect Gasifier

MTCI has developed an atmospheric, indirectly-heated fluidized-bed gasifier that uses steam and recycled process gas as fluidizing medium and oxidant (Durai-Swamy et al., 1989). Kraft black liquor at 65% solids is sprayed onto a bed of Na_2CO_3 particles between 590-650°C. Heat is provided by immersed resonance tubes of a pulse combustor. Product gas from the fluidized bed is cooled in a heat recovery system, and then scrubbed with a sodium carbonate solution to produce green liquor. The scrubbed gas is split into two streams: some gas is diverted to the pulse combustor and the remainder flows to a gas boiler.

A key feature of the process is the pulse combustor. The design of this unit allows self-induced pressure fluctuations with frequencies between 30-300 Hz. As a result, high velocity pulses (180 $m{\cdot}s^{-1}$) in the resonance tube of the combustor result in heat transfer coefficients that are 3-5 times greater than steady-flow combustion systems. This leads to the design of compact systems that can be installed in the side-walls of fluidized-bed reactors.

The authors claim that the process is compatible with combined-cycle cogeneration, in which the gasification and gas scrubbing would be performed at a pressure of ~2000 kPa. However, it is still economical when operated at atmospheric pressure. Scale-up to a 22 tonne/day demonstration plant for the Weyerhaeuser Co. is in progress.

VTT Pressurized Gasifier

Because this work is at an early stage of development only some general information is available in the literature (McKeough and Saviharju, 1991). The process envisaged would employ a circulating fluidized bed operating at low-temperature and with pressures between 3-5 MPa (Empie, 1991). Both steam and air are being considered as oxidants. The product gases would be cleaned in a pressurized gas-liquid scrubber.

A combined-cycle power generation system is employed downstream for electricity and steam generation for the mill. Therefore, the clean fuel gas is combusted and expanded in a gas turbine thereby producing electricity, followed by heat recovery in a boiler. In the boiler, steam is heated to high temperatures and then expanded in a steam turbine for electricity production. The gas turbine allows a higher conversion efficiency of heat to electricity. This is because a gas turbine presently operates at inlet temperatures that are 300°C - 400°C higher than a steam turbine (van den Berg et al., 1977). Hence, the plant operates with a ratio of electricity to steam that is several times higher than a conventional recovery boiler (i.e., ~0.7 versus ~0.25).

The availability of published operating data from these fluidized-bed processes are limited. Therefore, to better understand the technology of some of these systems, it is useful to examine some available basic knowledge concerning the physical and chemical processes occurring in the low-temperature regime.

LOW-TEMPERATURE CHEMICAL RECOVERY

Pyrolysis may be defined as the irreversible thermal decomposition of organic matter in the absence of air. It is generally understood that pyrolysis is an endothermic process and is usually the first stage of gasification or combustion (Probstein and Hicks, 1982). The pyrolysis products of KBL (kraft black liquor) are typically a solid residue and volatile fraction. The solid residue contains mostly Na-S compounds, Na_2CO_3, and amorphous carbon. The volatiles consist mostly of the fixed gases CO, CO_2, H_2, CH_4, and sulphur gases such as CH_3SH and H_2S (Bjorkman and Warnqvist, 1985: Prahacs, 1976: Bjorkman, 1968: Feuerstein et al., 1967: Feuerstein, 1966). The condensable fraction of the volatiles consists mainly of water vapour and long-chain hydrocarbons (tar). The relative distribution of solid char and volatiles is a complex function of the following variables:

- composition and swelling behaviour of the KBL;
- composition of the ambient gas;
- final temperature of KBL droplets;
- time and rate of heating; and,
- droplet size.

For the subsequent gasification of solid char by CO_2 and steam, it is also of interest to understand the catalytic effect of Na_2CO_3. This subject is discussed in detail in Chapter 2. Because of the multivariable nature of this system it is difficult to compare and interpret data of different workers in this field. However, some general observations can be noted.

Hupa et al. (1985) showed results for a 1.5 mm droplet suspended in stagnant air at 600°C. They observed with a ciné film that it took about 3 seconds for drying, 1 second for volatilization, and about 1.5 seconds for char combustion. The droplet showed signs of boiling and the interior temperature rose to about 150°C, remaining at this temperature until all the water evaporated. The temperature then continued to rise and pyrolysis began. At a particle temperature above 600°C, combustion of the volatiles with air was evident by a burning yellow flame envelope. During this period the particle swelled to several times its original diameter. After pyrolysis, the yellow flame extinguished and char combustion began because of high temperatures and an excess of oxygen in the furnace environment. The diameter of the porous particle was reduced considerably during heterogeneous burning. Noopila et al. (1989) extended this work to include the effect of KBL composition (i.e., lignin, aliphatic acids, extractives, and inorganics) on char burning kinetics.

Milanova and Kubes (1985) have shown by differential thermal analysis that the low-temperature reactions were endothermic during the heat-up period to the ignition temperature in a gasification environment.

Miller et al. (1986) investigated the effect of heating rate, moisture content, particle size, and composition on the swelling behaviour of dry kraft black liquor solids (KBLS). The heating rate changed only the rate of swelling, not the final swollen volume. Completely dry solids swelled about 50 percent less than 65-80% solids. For particles sizes between 1-4 mm, no effect on the maximum particle volume was observed. The composition variables studied were kraft lignin, sugar acids, inorganic salts, and extractives. Kraft lignin did not swell during pyrolysis, whereas

sugar acids swelled extensively, even more than KBL. The combination of KBL and sugar acids in a 1:1 weight ratio produced the highest swollen volumes. Sodium sulphate and sodium carbonate acted as diluents in the swelling of KBL and were not directly involved in the swelling mechanism. The extractives significantly reduced the swelling behaviour of KBL by reducing the viscosity of black liquor and did not influence the extent of volatilization reactions during pyrolysis.

Harper (1989) studied the pyrolysis behaviour of the individual inorganic sulphur compounds Na_2S, $Na_2S_2O_3$, Na_2SO_4, and Na_2SO_3 mixed with a soda black liquor (T= 350-700°C, N_2 atmosphere). One conclusion of this work was that swelling had no significant effect on the emission of sulphur from these compounds.

Prahacs (1976) noted that black liquor gasification with air at 800°C resulted in a large emission of H_2S gas and no observable reduction of the Na_2SO_4 to Na_2S. In the absence of air he noted that some reduction of sulphate to sulphide was observed. These tests were done in an atomized-suspension reactor with residence times for the droplets in the order of 10-25 s.

Bjorkman (1968) and Feuerstein (1966) observed that a maximum production of H_2S for pyrolysis of KBL occurred at a reactor temperature of about 700°C. In an attempt to isolate the origin of the sulphur emission during pyrolysis, Strohbeen (1981) studied model organic compounds with different inorganics such as Na_2S, $Na_2S_2O_3$, Na_2SO_3, and Na_2SO_4. He found that Na_2SO_4 did not release a significant amount of its sulphur into the gas phase, while Na_2S released nearly 100% of its sulphur as hydrogen sulphide.

Li (1986) reported the results of a study on the pyrolysis and gasification of KBLS in a thermogravimetric apparatus. As part of his work, dry KBLS from laboratory cooks were heated at a rate of 20°C/min in a helium gas stream to a final temperature between 600 and 750°C. In the temperature range 250-500°C, the sulphur emissions were mainly $(CH_3)_2S$, CH_3SH, and H_2S in decreasing order. Above 610°C it was observed that solid sodium sulphide was produced. Table 1 shows that it is possible to obtain a reduction efficiency of 90% without the addition of a reducing gas such as CO. From thermodynamic considerations it should be possible to achieve nearly 100 percent reduction at 750°C. However, a higher reduction efficiency was not achieved in this study mainly due to oxidation problems encountered when handling the char residue (van Heiningen and Li, 1986). These results imply that, in an inert environment, the

carbon in the char reduces the solid Na_2SO_4 to solid Na_2S; thereby confirming the earlier work of Kubelka and Hojnos (1956).

The key points resulting from experimental investigations for low-temperature processing can be summarized as follows:

- Pyrolysis of dry black liquor solids will precede gasification and lead to organic-bound sulphur emission;
- If the inorganic sulphur present in black liquor solids is Na_2SO_4 then a minimum of H_2S evolution is expected; and,
- In the pyrolysis char, carbon begins to reduce solid Na_2SO_4 to solid Na_2S at temperatures above 610°C in an inert atmosphere.

THERMODYNAMICS

Sulphur in KBL

KBL (kraft black liquor) is a complex colloidal solution that is very difficult to characterize analytically. It contains both organics from the wood and inorganics from the cooking liquor. Typical ultimate and proximate analyses for the dry solids comprising KBL are shown in Table 2. The distribution of sulphur between the organic and inorganic fraction has been inferred by Strohbeen (1981) to be 10 and 90 wt%, respectively; whereas Blackwell and King (1985) have attributed up to 33% as organic sulphur.

For a particular KBL, the organic sulphur pyrolyses to form mostly CH_3SH, $(CH_3)_2S$, and H_2S. The quantity of these species will depend on the KBL source, temperature, heating rate, and droplet size. Sulphur gas emission also may originate from the inorganic fraction of KBL as shown in Eq. 5 below. This implies that during gasification in a fluidized bed these species will be present. Strohbeen's work with model compounds for KBL showed that if the inorganic sulphur is present as Na_2SO_4 then, during the initial pyrolysis, almost no inorganic sulphur is emitted as H_2S.

Key Chemical Reactions

For a 1 mm diameter droplet of KBL, pyrolysis occurs within 1-2 seconds. If air gasification is performed then the resulting porous char and gaseous products will react with an oxygen-rich environment in a complex way. Some of the major reactions that can occur are shown below:

Heterogeneous reactions

$$2C_{char} + O_2 \rightarrow 2CO \quad (3)$$

$$C_{char} + 2H_2 \rightarrow CH_4 \quad (4)$$

$$Na_2CO_{3\,(s)} + H_2S \Leftrightarrow Na_2S_{(s)} + CO_2 + H_2O_{(v)} \quad (5)$$

$$Na_2S_{(s)} + 2O_2 \rightarrow Na_2SO_{4\,(s)} \quad (6)$$

$$C_{char} + CO_2 \rightarrow 2CO \quad (7)$$

$$C_{char} + H_2O_{(v)} \rightarrow CO + H_2 \quad (8)$$

$$Na_2SO_{4\,(s)} + 2C_{char} \rightarrow Na_2S_{(s)} + 2CO_2 \quad (9)$$

Gas-phase reactions

$$2CO + O_2 \rightarrow 2CO_2 \quad (10)$$

$$CO + H_2O_{(v)} \Leftrightarrow CO_2 + H_2 \quad (11)$$

$$H_2 + \frac{1}{2}O_2 \rightarrow H_2O_{(v)} \quad (12)$$

Rosén (1961) has shown by equilibrium calculations that the presence of large quantities of water in the KBL feed will impact negatively on the objective of sulphur recovery as Na_2S at low-temperatures. This is understood by considering Eq. 5 since an increase in the partial pressure of water shifts the equilibrium to the left. Therefore, it would be advantageous from this perspective to use dry KBLS (kraft black liquor solids) as feed to a fluidized-bed gasifier.

Equilibrium Calculations

Since this thesis deals with fluidized-bed pyrolysis and steam gasification without the presence of oxygen, it is useful to examine thermodynamic predictions for these conditions. The equilibrium calculations were performed with a computer code named "EQUILIB" from the F*A*C*T program (Thompson et al., 1988). The ensuing discussion gives a brief account of the calculation method employed, underlying assumptions made, and the results obtained.

"EQUILIB" calculates the equilibrium composition of systems containing one gaseous phase, condensed mixtures, and condensed phases of invariant or variable stoichiometry. This program is an updated version of the algorithm, SOLGASMIX, originally developed by Eriksson (1975). The numerical technique is based on the minimization of the total free-energy of the system, with mass balance relationships among the various species as constraints. Eriksson and Rosén (1973) provide more details of the calculations.

Chemical Species Considered

Pejryd and Hupa (1984) have performed detailed equilibrium calculations for the lower part of a conventional recovery boiler including the smelt bed. As part of their work, they presented a listing of compounds that were present in significant quantity (i.e., > 1 ppm_v in the gas; > 0.01 mol% in the smelt). This tabulation is used as a guide in selecting the chemical species. Their results show that the elements K and Cl do not affect the observed distribution of sulphur in the equilibrium calculations. Therefore, compounds of these elements were not used in the calculations.

Table 4 shows the chemical species considered and the relevant thermodynamic properties obtained from the F*A*C*T database. This tabulation gives the standard molar heat of formation, ΔH°_{298}, and entropy, S°_{298}, at 298 K; the enthalpy change due to phase transformation, ΔH_{tran}; and, the constant-pressure molar heat capacity, C_p. The original sources of this data are the compilation made by Wagman et al. (1971; 1982), Barin et al. (1977), and Mills (1974). Warnqvist (1980) comments that the data for the melting point of Na_2S are in error in these references as well as those given by Kubaschewski et al. (1977) and Stull and Prophet (1970). He reports that the correct value is 1170 ±10°C, whereas the above references quote 914-980°C. He also notes that the most reliable compilation of thermochemical data for the common Na-S compounds is that of Rosén (1960). A comparison between Warnqvist's accepted data and that found in the F*A*C*T database is shown in Table 3.

Assumptions

The gaseous phase is treated as an ideal mixture with a total pressure of 101.3 kPa absolute. The solid phases are taken as pure phases with unit activity. The properties of graphite are used for the carbon phase since Kapteijn and Moulijn (1986) showed that this does not introduce significant error when dealing with alkali-catalysed gasification of various amorphous carbons. The inorganic salts Na_2CO_3 and Na_2S are the only stable salts at equilibrium. These salts display mutual solid-solubility (Magnusson and Warnqvist, 1975: Ovechkin et al., 1971). However, it is unlikely that any significant alloying is achieved within the time frame of the experiment. This is due to the random dispersion of these salts throughout the char matrix, and the extremely slow process of solid-state diffusion.

Results

To perform the equilibrium calculations, "EQUILIB" requires the user to specify the system temperature, total pressure, molar feed rate of dry KBLS and H_2O, besides the selected chemical species mentioned previously. Two specific sets of calculations were performed. In the first set, the equilibrium calculations were performed using the data of Warnqvist (1980) and Rosén (1960) for the specific conditions of each experiment shown in Table 22 - Table 35. These results are discussed in Chapters 4-5 and compared with actual fluidized-bed operating data.

The second set of calculations was obtained by using the composition of KBLS in this work (Table 10), and varying the moisture content over a wide range. Figure 1 shows the equilibrium composition of sulphur as Na_2S in the char as a function of reactor temperature and wt% solids. The sensitivity of these results to the thermodynamic values chosen for solid Na_2S is evident. It can be seen that the data supported by Warnqvist and Rosén give higher sulphur retention in the char for any specified operating temperature.

Thermodynamic calculations using these data for Na_2S have been reported by Fallavollita (1984) for the case of air gasification. The calculated Na_2S content in the char followed a similar trend as shown in Figure 1. Some key results for O_2 gasification will be presented in Chapter 6, together with a discussion of the industrial applications of the thesis results.

Regardless of which thermodynamic data are used for Na_2S, the sulphur retention in the char is favoured by higher temperatures and lower H_2O levels. The bulk of the experimental work in this thesis has been performed to find out the extent to which these trends are observed in a pilot scale fluidized-bed reactor system.

CONCLUSION

High-temperature gasification of kraft black liquor (i.e., NSP, Champion Intl., and Chemrec) favours the direct formation of liquid Na_2S over a broad range of operating conditions as predicted by equilibrium calculations. The main technical challenge for the Chemrec process may be the adequate recovery of sodium fume prior to combustion of the fuel gas. Also, if an acid gas scrubber installation is required, due to the presence of H_2S and organo-sulphur gases, then only limited advantage is offered over the fluidized-bed approach.

The low-temperature fluidized-bed processes, using steam or air, appear more sensitive to variations in temperature and gasifying agent - leading to a broader range of combustible fuel composition and sulphur species. Therefore, it is important to examine the rates of both the char gasification reactions with steam/CO_2 (Chapters 2 and 4), and the emission of sulphur as H_2S and other sulphur gases (Chapter 5). The fluidized-bed data obtained on a bench-scale are important for making a proper assessment of this technology for kraft chemical recovery.

CHAPTER 2

CARBON GASIFICATION BY CO_2 AND H_2O - A REVIEW

ABSTRACT

The gasification of carbon by CO_2 and H_2O is discussed for both uncatalyzed and alkali-carbonate catalysed systems. Single-site mechanisms for the uncatalysed gasification consist of two steps. Initially, a rapid oxygen exchange occurs between the oxidizing gas (CO_2 or H_2O) and an active carbon site that produces a chemisorbed oxygen on the carbon, C(O), and CO or H_2, respectively. This is followed by a slow desorption of the chemisorbed surface species, C(O), leading to gasification of the carbon. The addition of alkali carbonate complicates the interpretation of the gasification process. Many studies are reviewed describing the mechanisms and the identity of the active surface complex. The recent literature shows that (a) the slow step is the same as the uncatalyzed case, (b) the catalyst increases the surface concentration of C(O) sites, and (c) the oxygen exchange reactions occur at the catalyst complex and are in quasi-equilibrium.

The available literature on the gasification of kraft black liquor char with CO_2 and H_2O at atmospheric pressure is reviewed. A major difference between black liquor char and other alkali-catalysed carbons is its higher reactivity. For CO_2 gasification, the instantaneous rate for black liquor char is one order of magnitude higher than activated carbon with an optimum catalyst loading. The higher reactivity of kraft black liquor is explained by a fine, bulk dispersion of the alkali catalyst. The gasification rate of black liquor char with steam is several times higher than with CO_2. This is probably due to a lower apparent activation energy and higher concentration of oxidized catalyst sites.

The mechanism for the CO_2 gasification of black liquor char is taken to be the same as for other carbons, and a Langmuir-Hinshelwood rate law adequately correlates the rate data. However, for steam gasification, the mechanism presented in the literature does not properly account for the primary production of CO_2. Therefore, a new mechanism is proposed in this work that results in the correct form of the rate law for both CO and CO_2 production during steam gasification.

UNCATALYSED GASIFICATION OF CARBON

Introduction

The char obtained from the pyrolysis of kraft black liquor solids (KBLS) consists mainly of a mixture of carbon, sodium carbonate, and Na-S salts (Table 11). Therefore, alkali-catalysed carbon gasification studies can serve as a useful reference. The gasification of carbonaceous materials by CO_2 and steam has been the subject of many investigations over the past forty years. Important reviews on the subject of uncatalysed gasification have been written by Walker et al. (1959), von Fredersdorff and Elliott (1963), and Laurendeau (1978). The kinetic investigations have used either impure or relatively pure carbons: coal and coke chars (amorphous carbons) are examples of the former, while polycrystalline graphite and diamond (crystalline carbons) are in the latter category. Since almost any trace impurity can affect gasification rates (Walker et al., 1968), it should be realized that most of the published kinetic studies are only approximations to the ideal "uncatalysed" case.

Carbon Reactivity

The carbon reactivity has been reported as either the normalized reaction rate, $-r_n$, or some variation thereof, where:

$$-r_n = -\frac{1}{n_{C_o}} \cdot \frac{dn}{dt} \tag{13}$$

For instance, the instantaneous rate, $-r_w$, would be obtained as the ratio $(-r_n/1\text{-}X)$ and the initial reaction rate, $-r_o$, is simply $-r_n$ evaluated at t=0.

Gasification occurs preferentially at active sites on the surface of carbon. Active sites can be generated by dislocations and edge planes in carbon (Walker et al., 1959); inorganic mineral matter (McKee, 1981); and, the O and H content of the carbon (van Krevelen, 1961).

For chemically-controlled gasification, the reactivity is a function of the total surface concentration of active sites ($[C_T]$), specific surface area (S_g), temperature, partial pressures of gaseous reactants and products, and the rate- and equilibrium constants for the various elementary reaction steps that describe the overall reaction (Kapteijn and Moulijn, 1986):

$$-r_n = N_T \cdot f(T, p_i, k_i, K_{eq_i}) \tag{14}$$

$$\textit{where} \quad N_T = [C_T] \cdot S_g \tag{15}$$

For a specific pure carbon, $[C_T]$ is equal to the sum of the concentration of occupied sites, $[C(O)]$, and free-carbon sites, $[C_{site}]$. The total number of active sites varies with carbon type, pretreatment temperature and carbon burn-off (100·X). For coal chars, S_a is either constant or exhibits a maximum during burn-off. The variation of surface area with burn-off may be described by substituting S_a in Eq. 15 with $S_{ao}(1-X)^q$; where S_{ao} is the initial specific surface area and X is the fractional conversion of carbon. Also, the exponent, q, usually varies between 2/3 and 1 during uncatalysed gasification. The specific surface area can be readily obtained by CO_2 or N_2 equilibrium adsorption measurements. However, a direct measurement of $[C_T]$ can only be obtained using transient kinetic techniques (Kapteijn and Moulijn, 1986).

Although the intrinsic reaction rate given by the function, f, in Eq. 14 can be expressed by an empirical power law, the semi-empirical approach based on Langmuir-Hinshelwood kinetics has been preferred. This incorporates an analysis of the reaction mechanism and gives a rate expression that applies over a wider range of temperature and pressure (Laurendeau, 1978). This approach involves developing a set of elementary reaction steps, deriving a rate equation based on these steps and then obtaining the kinetic parameters by experiment. Most of the postulated elementary reaction steps given in the literature involve one free-carbon active site and are known as single-site mechanisms.

C-CO_2 Reaction

The so-called Boudouard reaction (Eq. 16) accounts for the stoichiometry of the CO_2 gasification of pure carbon but does not describe the elementary reaction steps involved.

$$C + CO_2 \Leftrightarrow 2CO \qquad (16)$$

A single-site mechanism of gasification that accounts for this reaction is given by Eqs. 65, 67 in Table 5. In the first elementary step, a reversible oxygen-exchange occurs in which an oxygen atom or radical from gaseous CO_2 chemisorbs on a free-carbon active site, C_f, thereby producing a surface complex $C(O)$ and a CO gas molecule. The second elementary step (i.e., gasification) involves desorption of $C(O)$, resulting in carbon loss via a CO gas molecule (Ergun and Mentser, 1965). This step is considered irreversible for total pressures of 101.3 kPa or less, implying that the overall gasification reaction is also irreversible.

Oxygen exchange rates between CO/CO_2 and carbon, in the temperature range 750-850°C, are several orders of magnitude greater than the gasification step (Mentser and Ergun, 1967).

Therefore, oxygen exchange is considered to be in quasi-equilibrium, while the desorption step controls the reaction rate (Ergun, 1956). The presence of CO in the gas will inhibit gasification by shifting Eq. 65 to the left, and reduce the steady state concentration of *C(O)* (Reif, 1952).

Ergun and Mentser (1965) have studied the effect of varying p_{N_2} on the reaction rate. They found that the rate was independent of N_2 partial pressure but increased with the CO_2/CO ratio, confirming that N_2 does not chemisorb onto carbon active-sites at gasification temperatures (Ergun, 1956). Therefore, nitrogen can be neglected in the formulation of rate expressions.

Walker et al. (1959), Reif (1952), and Laurendeau (1978) state that the rate law for this mechanism is given by Eq. 66 in Table 5. Derivation of this rate law requires that the desorption step, Eq. 67, is rate limiting and [*C(O)*] is at steady state. For gasification at atmospheric pressure, Ergun (1956) suggested that i_2 may be dropped from this expression, since $i_2 << i_1 p_{CO_2}$ and $i_2 << i_{-1} p_{CO}$. This implies that the oxygen exchange step is in quasi-equilibrium. Based on these assumptions, the rate law can be written as Eq. 68, where $K_{CO\text{-}CO_2}$ is the equilibrium constant for the oxygen exchange step. Ergun and Mentser (1965) also stated that the inequalities mentioned above do not hold for gasification under vacuum (i.e., below 0.001 kPa) due to the low partial pressures of CO and CO_2; therefore, Eq. 66 would be more appropriate.

Kapteijn and Moulijn (1986) presented the more general case where the elementary gasification step, Eq. 67 (Table 5), was considered reversible with a rate constant, i_{-2}. This implies that the carbon dioxide gasification reaction, Eq. 16, is reversible and an equilibrium constant may be defined as, $K_{overall}^{C/CO_2}$. Assuming that *C(O)* desorption, Eq. 67, determines the gasification rate, then the following rate law can be derived:

$$-r_n = \frac{i_1 i_2 N_T \left(p_{CO_2} - \dfrac{p_{CO}^2}{K_{overall}^{C/CO_2}} \right)}{i_2 + (i_{-2} + i_{-1})\, p_{CO} + i_1 p_{CO_2}} \qquad (17)$$

Note that for high pressure gasification with p_{CO} >>101 kPa, the inhibiting effect of CO would be predicted to increase roughly in proportion to p_{CO}^2, at constant p_{CO_2}. Such a large inhibiting effect would not be predicted by Eq. 68 (Table 5).

Data is available on the parameters in the rate expressions, Eqs. 66, 68. For coal char data, Laurendeau (1978) suggested that the activation energy (kJ/mol) for the elementary rate

constants i_1, i_{-1} and i_2 are E_{i1}~230, E_{i-1}~147, and E_{i2}~250, respectively. Kapteijn and Moulijn (1986) gave apparent activation energies that varied between 220-260 kJ·mol^{-1} for the C-CO_2 reaction, Eq. 16, at 101 kPa p_{CO_2} for various coal chars. Also, the equilibrium constant for the elementary oxygen exchange Eq. 65, $K_{CO\text{-}CO_2}$, was shown to vary only with temperature and was independent of the carbon type (Ergun, 1956). An expression for $K_{CO\text{-}CO_2}$ that fit the data of Ergun (1956) for 800-1400°C was given by Kapteijn and Moulijn (1986) as, $4.15 \cdot 10^3 \exp(-96300/RT)$. In the temperature range of interest in this work (i.e., 500-700°C), $K_{CO\text{-}CO_2}$ is small and varies between 0.002-0.03.

C-H_2O Reaction

The stoichiometry of the steam gasification reaction for a pure carbon can be written as,

$$C + H_2O_{(v)} \Leftrightarrow CO_{(g)} + H_{2\,(g)} \tag{18}$$

Laurendeau (1978) espoused the single-site oxygen exchange mechanism (Eqs. 67, 69, Table 5) based on evidence from the experimental data of Ergun (1961). Analogous to the C-CO_2 case, the slow step is given by an irreversible desorption of chemisorbed *C(O)* (Eq. 67) which implies that Eq. 18 can be considered irreversible. Hydrogen inhibits the reaction rate by a fast, reversible oxygen exchange step, Eq. 69.

Walker et al. (1959) and von Fredersdorff and Elliott (1963) have stated that the rate law for this mechanism is given by Eq. 70 (Table 5). The derivation of this expression requires that the desorption step, Eq. 67, is rate limiting and [*C(O)*] is at steady state. For p_{H_2} and p_{H_2O} much larger than 0.001 kPa, the rate constant i_2 may be dropped, since $i_2 << m_1 p_{H_2O}$ and $i_2 << m_{-1} p_{H_2}$. This implies that the oxygen exchange step is in quasi-equilibrium. Based on these assumptions, the rate law can be written as Eq. 71, where $K_{H_2\text{-}H_2O}$ is the equilibrium constant for the oxygen exchange step, Eq. 69.

For the more general case where the gasification step is considered reversible with a rate constant, i_{-2}, then the steam gasification reaction Eq. 18 would be considered reversible and an equilibrium constant, $K_{overall}^{C/H_2O}$, may be defined. With the assumption that Eq. 67 determines the overall gasification rate and [*C(O)*] is at steady state, Kapteijn and Moulijn (1986) derive the following rate law:

$$-r_n = \frac{m_1 i_2 N_T \left(p_{H_2O} - \frac{p_{CO}\, p_{H_2}}{K_{overall}^{C/H_2O}} \right)}{i_2 + i_{-2}\, p_{CO} + m_{-1}\, p_{H_2} + m_1\, p_{H_2O}} \qquad (19)$$

Based on a critical evaluation of coal char data, Laurendeau (1978) suggested that the activation energies (kJ/mol) for the elementary rate constants, m_1 and m_{-1}, are E_{m1}~189 and E_{m-1}~105. It was also noted that further research would be useful to improve the reliability of this data. Also, for gasification of various carbons in pure steam, Kapteijn and Moulijn (1986) pointed out that the apparent activation energy for the C-H_2O reaction, Eq. 18, was between 140 and 200 kJ·mol^{-1}. This was lower than the apparent activation energy for C-CO_2.

C-H_2O-CO_2 Reaction

In addition to the H_2 and CO primary products from steam gasification shown in Eq. 18, CO_2 is also found as a secondary product in systems where extensive steam conversion has occurred or the water-gas shift reaction (Chapter 1, Eq. 11) is favourable. Ergun (1961) proposed that the CO produced from the gasification step also could reduce a chemisorbed-oxygen surface complex *C(O)* by the reverse of Eq. 65, thereby accounting for CO_2 formation. Then the mechanism is given by Eqs. 67, 69, reverse 65 (Table 5), where this sequence of steps accounts for both steam gasification (Eqs. 67, 69), and the water-gas shift reaction (Eqs. 69, reverse 65). The mechanism assumes that identical sites are used for oxygen exchange by H_2-H_2O and CO-CO_2 (Kapteijn and Moulijn, 1986). The rate determining step would be that of Eq. 67, and both CO and H_2 inhibit the gasification.

Laurendeau (1978) has presented a rate law of the form given by Eq. 72 in Table 5. This expression may be simplified by using Ergun's quasi-equilibrium assumption for the oxygen exchange reactions, implying that the water-gas shift reaction is also in quasi-equilibrium. The resulting rate law, Eq. 73, shows that the gasification rate can be described by either the C-CO_2 rate law (Eq. 68) or the C-H_2O expression (Eq. 71). However, Ergun (1961) also showed that the water-gas shift equilibrium was achieved only for steam conversions above 60% at 1000°C, thereby constraining the general applicability of this approach.

Kapteijn and Moulijn (1986) have noted that if the gasification step (Eq. 67) is considered reversible then a more general rate law can be derived:

$$-r_n = \frac{m_1 i_2 N_T \left(p_{H_2O} - \frac{p_{CO}\, p_{H_2}}{K^{C/H_2O}_{overall}} \right) + i_1 i_2 N_T \left(p_{CO_2} - \frac{p^2_{CO}}{K^{C/CO_2}_{overall}} \right)}{i_2 + m_{-1} p_{H_2} + m_1 p_{H_2O} + (i_{-1} + i_{-2}) p_{CO} + i_1 p_{CO_2}} \qquad (20)$$

The previous rate laws were based on the assumption that the same sites were used in both oxygen exchange reactions, Eqs. 65, 69. Kapteijn and Moulijn (1986) have noted some experimental evidence which contradicts this assumption. For different sites, Bliek (1984) has used the sum of the separate general rate laws for C-CO_2 and C-H_2O (Eqs. 17, 19) to correlate his data on coal gasification.

ALKALI-METAL-SALT CATALYSIS OF CARBON GASIFICATION

Introduction

Alkali metal salts will increase carbon reactivity only if pore diffusion or chemical kinetics control the reaction rate (Juntgen, 1983). The catalysis is explained by oxygen exchange mechanisms, accelerated exposure of reactive carbon edges by catalyst pitting, and other complex chemical phenomena (Walker et al., 1968). More recently, oxygen exchange mechanisms have gained wide acceptance in explaining catalytic behaviour, therefore these will be discussed exclusively. Interestingly, a recent paper by Moulijn et al. (1984) suggested that catalysis in the C-CO_2 system could be explained by its impact on the uncatalysed Eqs. 65, 67 in Table 5. They argued that the gasification rate could be increased by either shifting the equilibrium of Eq. 65 to the right and/or accelerating the desorption step, Eq. 67. Redox mechanisms have been proposed for the former. In the latter case, increasing the oxygen chemisorption coverage *C(O)* and decreasing the activation energy for *C(O)* desorption may be possible.

Much of the literature has dealt with K_2CO_3-catalysed CO_2 gasification and only a few studies are available for Na_2CO_3-catalysed steam gasification. The reasons for this are twofold: the potential application of K_2CO_3 in commercial coal gasification processes (Nahas, 1983); and, the ease of working with the C-CO_2 system since there is only one reaction product (Moulijn and Kapteijn, 1986). However, the usefulness of this section is not undermined since many results also apply to Na_2CO_3-catalysed steam gasification.

Mechanisms for C-CO_2

Catalytic Cycles of Alkali Carbonate

Fox and White (1931) described a mechanism which assumed that the homogeneous reactions in the gas phase resulted in enhanced mass transfer at the carbon surface, thereby increasing the reaction rate (Eqs. 74-77, Table 6). McKee and Chatterji (1975; 1978) adapted these reaction steps to a heterogenous mechanism occurring on the carbon surface (Eqs. 78-80, Table 6) and showed via thermodynamics that the postulated reactions were feasible. Their experimental observations supported the idea that carbothermic reduction with carbon (Eq. 78) was rate-determining and responsible for CO inhibition of the gasification. Wen (1980) argued that the alkali metal produced in the elementary step, Eq. 78, could react with carbon to form intercalates (C_nM) that act as intermediates (Eqs. 78, 81-83, Table 6).

Recent work by some investigators has argued against the participation of sodium metal, intercalates, and bulk alkali-carbonate crystals in the catalytic cycle. Sodium metal probably does not exist on the carbon surface without being associated with oxygen, otherwise it would easily vaporize. Also, it is generally acknowledged that alkali intercalates do not exist during gasification except perhaps at temperatures above 1400 K (Rao et al., 1982: Ferguson et al., 1984: Moulijn et al., 1984; Moulijn and Kapteijn, 1986). Experimental evidence suggests that bulk Na_2CO_3 crystals do not participate in the catalytic cycle, instead these decompose irreversibly at lower temperatures (i.e., 873 K) in contact with carbon to produce CO_2 and an active alkali oxide (Saber et al., 1984;1988: Mims and Pabst, 1980a;1983;1987: Wood et al., 1985: Freriks et al., 1981: Huhn et al., 1983).

Catalytic Cycles of Alkali Oxide

Experimental data suggest that the alkali oxide formed by carbonate decomposition will be the active species participating in the gasification. The active species was thought to be an oxide of the alkali metal and several compositions were suggested: a phenoxide surface group K^+-O^--C (Mims and Pabst, 1983: Sams and Shadman, 1986); a non-stoichiometric compound, M_xO_y (Moulijn et al., 1984); and, M_2O (Saber et al., 1988).

Cerfontain et al. (1987a; 1988) have presented a more complex picture of the actual carbon surface during gasification. Their work suggests that several types of surface oxides exist and that the predominant active species changes with alkali loading. At low alkali loading the

predominant form is alkali phenolate (i.e., C-O-K) while for higher loadings the active form is an alkali oxide cluster consisting of 5-6 K atoms and chemisorbed CO_2. Some bulk alkali carbonate crystals are also present during gasification but these are essentially inactive.

A key difference between alkali-catalysed and uncatalysed gasification is that, in the former, the oxygen exchange between CO/CO_2 occurs at an active catalyst site, while in the latter, the exchange occurs at an active carbon site (Moulijn and Kapteijn, 1986). Mechanisms which account for oxygen exchange at the catalyst site have been proposed by Kapteijn and Moulijn (1983) and Sams and Shadman (1986) and are shown in Table 6. The only difference between the two mechanisms is the composition of the active catalytic species. The first step in both mechanisms is a rapid oxygen exchange followed by a rate limiting step in which an oxidized catalyst site is reduced by carbon. In a later paper by Kapteijn et al. (1986) it was proposed that the rate determining step was the same as uncatalysed gasification, Eq. 67. Moulijn and Kapteijn (1987) further explained that the catalyst increased the gasification rate by increasing the number of *C(O)* sites on the carbon surface due to the mobility of the catalyst cluster. They postulated that the cluster was anchored by a phenolate surface group (*C-O-K*) in association with (*CO_2 K-O-K*) groups.

Cerfontain et al. (1987b) were the only workers that also accounted for the inhibiting effect of CO on gasification by extending the single-site mechanism for uncatalysed gasification (Eqs. 65, 67, Table 5) to explain oxygen exchange and carbon gasification in CO/CO_2 atmospheres over alkali-carbonate/carbon systems (Table 6, Eqs. 65, 67, 88-89). First, CO_2 can react directly with a carbon "vacant site" to produce *C(O)* and gaseous CO (Eq. 65). Also, it has been shown that the presence of an alkali carbonate will produce an unknown active species that can be designated as *(*)*. Because the concentration of *(*)* is much larger than that of the active carbon sites, the forward step of Eq. 65 is ignored. There is strong evidence that the active surface species is tightly bound to an adsorbed CO_2 molecule during gasification and represented by *CO_2(*)*. However, there was no evidence that CO_2 could adsorb directly onto C_f. In Eq. 88 this adsorbed species interacts further with CO_2 to produce a carbonate moiety, *CO_3(*)*. The equilibrium constant for this elementary step is large, therefore most of the catalyst surface species are in the *CO_3(*)* form. Oxygen exchange between CO_2 and CO occurs primarily at this site. This mechanism reveals the fact that the catalyst sites act to increase the *C(O)* surface

concentration by the irreversible, CO_2-assisted Eq. 89. As in the uncatalysed case, the CO inhibition of gasification is explained by the reverse of Eq. 65, and the rate determining step is Eq. 67. The rate law for this mechanism is similar in form to the uncatalysed gasification (Eq. 68, Table 5) and given by:

$$-r_n = \frac{i_2 N_T}{1 + \left(\frac{p_{CO} \cdot i_{-1} \cdot I}{p_{CO_2} \cdot k_{10} \cdot N_{cT}} \right)} \tag{21}$$

$$\text{where} \quad I = 1 + \frac{k_{-8} p_{CO}}{k_8 p_{CO_2}} + \frac{k_{10} [C_{site}]}{k_8} \tag{22}$$

Noting that the oxygen exchange, Eq. 88, occurs at a higher rate than the carbon oxidation, Eq. 89, this means that $k_8 >> k_{10}$. Also, since the equilibrium constant for Eq. 88 is large then $k_{-8}/k_8 << 1$. Therefore, it is seen that I approaches 1, and Eq. 21 takes the form of the rate law for the uncatalyzed gasification, Eq. 68 (Table 5). The denominator contains the term, N_{cT}, which is the surface concentration of catalyst sites on carbon. If it is assumed that all of the alkali carbonate added is in the active form during gasification then the catalyst loading may replace this term in the rate law. As will be seen in a later section, this assumption is more suitable for K_2CO_3 catalysis of carbon.

Mechanisms for C-H_2O

As previously shown for the uncatalysed steam gasification of carbon, the primary products are CO and H_2 according to Eq. 18, and the water-gas shift reaction is responsible for the production of CO_2, as follows:

$$CO_{(g)} + H_2O_{(v)} \Leftrightarrow CO_{2\,(g)} + H_{2\,(g)} \tag{11}$$

This section will review the key mechanisms that have been proposed in the literature to explain the catalytic effect of alkali carbonate on the production of CO, H_2, and CO_2 during steam gasification.

McKee and Chatterji (1978) and McKee (1982) suggested a mechanism for the catalysis of the steam gasification reaction, Eq. 18, which assumed that the active species was alkali carbonate. The elementary steps shown in Table 7 include: the irreversible carbothermic reduction reaction (Eq. 90); hydrolysis of alkali metal (Eq. 91); and, reforming of the carbonate

(Eq. 92). Experimental identification of the carbonate, alkali metal, and alkali hydroxide on the surface of carbon were not made. Instead, thermodynamic calculations showed these reactions to be favourable at T > 973 K for Na and K. Wood et al. (1985) also supported the occurrence of both Eqs. 90, 91 by the indirect method of observing the gas phase composition during gasification. Without any further proof, Veraa and Bell (1978) adopted this mechanism and specifically introduced the water-gas shift reaction, Eq. 11, to explain the formation of CO_2.

Mims and Pabst (1983) showed experimentally that the active species in steam gasification was an ionic potassium phenoxide (K^+-O^--C) that is represented in Table 7 by K_{surf}. The mechanism proposed to explain CO and H_2 formation consisted of a rapid, reversible oxidation of the catalyst active sites followed by a slower decomposition step. Carbon dioxide formation was assumed to be due to the homogeneous water-gas shift reaction, Eq. 11.

Kapteijn and Moulijn (1986) gave a mechanism to explain the CO and H_2 formation (Eqs. 93, 94 in Table 7). In this case, the catalyst was an active alkali-metal cluster denoted by (*). The oxygen exchange between CO/CO_2 occurred at the catalyst site and was very rapid (Eq. 93). The slow step was the reduction of an oxidized catalyst site, O(*), by carbon (Eq. 94).

The mechanisms described by Wigmans et al. (1983b) and Huttinger and Minges (1985a, b) also accounted for the primary production of CO_2, albeit via different active species (Table 7). Water vapour reacts with an active surface group (i.e., K_{surf}, K_xO_y) by exchanging oxygen and forming H_2; the oxidized catalyst site reacts with a neighbouring carbon active site to reform the active surface site and produce chemisorbed C(O). The C(O) could either reduce an oxidized catalyst site and produce CO_2 directly (Eqs. 97, 100) or desorb to form CO (Eq. 67). The rate limiting step in both mechanisms is the desorption of C(O). Wigmans et al. (1983b) also noted that the formation of CO_2 was favoured at higher alkali/carbon ratios.

Saber et al. (1988) presented a mechanism for the Na_2CO_3- catalysed steam gasification in which the rate determining step was the reduction of an oxidized catalyst site (Eq. 102). The production of CO_2 was due to the CO reduction of the oxidized site (Eq. 103), and the water-gas shift reaction was the result of heterogeneous reactions, Eqs. 101, 103.

It has been shown that alkali carbonates catalyse the water-gas shift reaction. Huttinger et al. (1986) proposed the two step sequence given by Eqs. 98, 104 to explain their results for potassium carbonate catalysis in the temperature range 400-500°C. Meijer et al. (1989b)

highlighted the important role of CO_2 chemisorption on the active alkali-metal cluster (*). First, water vapour reacts with the cluster to exchange oxygen and produce H_2 (Eq. 105, Table 7). Second, carbon monoxide reacts with the oxidized site to form a strongly adsorbed CO_2(*) species (Eq. 106) that subsequently desorbs to form CO_2 and the active alkali-metal cluster via Eq. 107. By performing oxygen exchange experiments with mixtures of CO-H_2O and H_2-CO_2, they determined that the forward rate of the water-gas shift reaction (CO + $H_2O \rightarrow$) was about ten times faster than the reverse step (CO_2 + $H_2 \rightarrow$). For example, at 850 K and a K/C molar ratio of 0.018, the conversion of CO in a CO-H_2O mixture over alkali/carbon was 0.3, whereas, conversion of CO_2 in a H_2-CO_2 mixture was 0.03.

Overall Gasification Rates

The initial gasification rate, $-r_o$, for catalyzed gasification with steam or CO_2 is a function of: the amount, type, and state of the catalyst; temperature; and, concentration of reactant gases. During gasification, the normalized rate, $-r_n$, or the instantaneous rate, $-r_w$, also may change with carbon burn-off and deactivation of the catalyst.

Effect of Catalyst Loading

Sams and Shadman (1983) found that a plot of $-r_o$ versus the initial potassium-carbon molar ratio (K/C) showed three distinct regions. Between 0 and 0.04 K/C (region I) the rate increased linearly from 1 to 25 $mg \cdot g^{-1} \cdot min^{-1}$ at 800°C. This type of linear behaviour has also been observed by Spiro et al. (1983), Moulijn et al. (1984), Yuh (1984), Sams et al. (1985), and Mims and Pabst (1980a) for chars impregnated with either K- or Na- carbonate. In region II, $-r_o$ increased only about 5% as the K/C ratio was more than doubled from 0.04 to 0.1. At higher K/C levels the initial rate declined nearly 50% (region III). It was argued that in region I the catalytic sites increased with K addition until saturation of the surface was reached as exemplified by region II. The decrease in $-r_o$ for region III was thought to be the result of pore blockage of the carbon matrix by K salts. Therefore, $-r_o$ was not only a function of initial K/C but also the carbon pore size distribution.

Cerfontain et al. (1985a) found for the C-CO_2 gasification at 1000 K that a plot of $-r_n$ versus M/C atomic ratio showed a maximum rate of $0.1 \cdot 10^{-3}$ s^{-1} at 0.05 M/C for Na_2CO_3, and $0.4 \cdot 10^{-3}$ s^{-1} at 0.1 M/C for K_2CO_3. Therefore, the saturation level was lower for Na than K-

carbonate. This behaviour was attributed to the difference in extent of decomposition of these two alkali salts to form the active species during gasification.

Cerfontain et al. (1987b) also found that the amount of chemisorbed CO_2 per alkali metal (CO_2/M) increased with M/C loading. However, as M/C increased the alkali atoms first formed clusters and then at higher metal loading carbonate crystals were observed. These crystals did not exchange oxygen with either gaseous CO_2 or CO. Sodium carbonate behaved in this manner and a maximum CO_2/M occurred at M/C = 0.04. Potassium carbonate did not exhibit a maximum and it was likely that inactive carbonate crystals did not form.

Effect of Catalyst Composition

Type of Cation

Potassium carbonate is a more effective catalyst than Na_2CO_3; based on studies involving a variety of carbons, gasifying agents, catalyst loadings and catalyst/carbon mixing methods (Miura et al., 1986: Adjorlolo and Rao, 1984: Kapteijn et al., 1986: McKee and Chatterji, 1978: Spiro et al., 1983: Lang, 1986). An explanation for this behaviour has recently been advanced by Moulijn and Kapteijn (1986). They argue that the carbon surface contains more inactive bulk carbonate crystals during gasification with Na_2CO_3. Therefore, the total number of active catalytic sites per mol of initial catalyst added is greater for K_2CO_3. Formation of carbonate crystals is favoured at lower temperature (T ~700 K) and high CO_2 pressure. Mims and Pabst (1981) also explain the higher gasification rate of K_2CO_3 as the result of a larger concentration of phenoxide surface groups during gasification.

Type of Anion

Steam and CO_2 gasification studies have shown that the type of anion affects catalytic activity: with $NO_3^- > SO_4^{2-} > HCO_3^- >> CO_3^{2-} > OH^-$ (Yuh and Wolf, 1984: McKee, 1982: Veraa and Bell, 1978). Although adequate explanations for this ordering are lacking, some information is available. The carbonate, sulphate and hydroxide compounds of potassium are activated in an inert atmosphere during carbonization up to 1000 K. Nitrates and sulphates decompose to form alkali monoxides on heating and are therefore capable of participating in catalytic cycles. Huttinger and Minges (1985c) noted that, for the steam gasification of graphite at 1173 K, both K_2SO_4 and K_2S were remarkable gasification catalysts. To account for this behaviour, they

proposed a reaction sequence in which these sulphur compounds readily hydrolysed to the active form K-O-H.

Effect of the Catalyst State

In obtaining reaction rate data from laboratory experiments, the time-temperature history prior to introducing the reactant gas may affect the observed gasification rate. For instance, Wigmans et al. (1983a) found that Na_2CO_3- or K_2CO_3- impregnated samples which were pretreated in He for 30 minutes from 1025 to 1100 K, showed a reduced gasification rate in steam at 1025 K. Also, studies by Sams and Shadman (1986) and Shadman et al. (1987) provided experimental evidence that the alkali carbonate was transformed to the active state during sample heat-up; with the total time required for transformation being proportional to the initial Na/C atomic ratio. Therefore, the degree to which the alkali carbonate is reduced to the active state during heat-up determines the subsequent reaction rate.

Effect of Catalyst Dispersion

The initial surface dispersion of catalyst over carbon is unimportant since physical mixtures and impregnated carbons show comparable activity. However, dispersion enhancement during thermal treatment is an important factor (Moulijn et al. 1984). The work of Spiro et al. (1984) using hot-stage microscopy revealed that the catalyst particles are mobile during gasification, well below the melting point of the pure carbonate. Wood et al. (1985) found from potassium x-ray emission maps that thermal treatment at 800 K caused spreading from discrete regions to a broad, nearly-uniform distribution over the char. McKee et al. (1985) rationalized that a three-phase interface must be maintained between the carbonaceous substrate, the catalyst phase, and the gaseous oxidant. Thus, melting of the catalyst phase and subsequent dispersion over the carbon surface would promote reactivity through the generation of additional active sites.

Effect of Catalyst Deactivation

Although very little data are available on this topic, Meijer et al. (1989a) state that alkali metal can be lost by: evaporation; formation of inactive species by reaction with other inorganics (ash); formation of bulk alkali carbonate; and, diffusion of metal from the reactive surface into the carbon matrix.

In mixtures of catalyst and relatively pure carbon, deactivation has been mostly attributed to catalyst loss by vaporization (Sams et al., 1985). The vaporization rate correlates poorly with

the melting point of the catalyst and strongly with the oxygen content of the carbon matrix. Data presented by Sams et al. (1985) show that, in an inert atmosphere at 973 K, a similar weight loss of 5 wt% was obtained for both K_2CO_3 (m.p. 891°C) and KOH (m.p. 380°C). In the work of Saber et al. (1986) it was shown that with an oxygen content in the carbon of 880 μmol/g (K:O ~1 mol/mol), a 7 wt% K loss was observed at 1350 K. For a carbon containing 30 μmol O·g C^{-1} with a K:O molar ratio of 40, the loss increased to 40 wt% K. Meijer et al. (1989a) confirm that the amount of potassium remaining on the surface is primarily dependent on the oxygen content bound with the carbon. Also, they claim that the intrinsic reactivity (rate per K atom) is not affected by catalyst loss.

Effect of Carbon Burn-Off

The relationship between carbon reactivity and burn-off varies considerably depending on experimental conditions (Table 8). Unfortunately, an important parameter that is not given in this table is the specific surface area of carbon, S_a, due to a lack of available data. Since the catalyst is mobile during gasification then the larger the surface area available, the greater the dispersion and corresponding concentration of active sites. Also, the concentration of active sites for catalysed gasification, N_{cT}, is the sum of catalyst sites, [(*)], and oxidized catalyst sites, [O(*)]. Kapteijn and Moulijn (1986) noted that two limiting cases exist for the normalized gasification rate, $-r_n$:

$$-r_n = N_{cT} \cdot (1-X)^q \cdot f(T, p_i, k_i, K_{eq_i}) \tag{24}$$

$$where \quad N_{cT} = [C_{cT}] \cdot S_{ao} \tag{25}$$

First, the reaction rate will be zero order with respect to burn-off (i.e., q=0) if the surface area of the carbon is large enough so that the catalyst concentration determines the concentration of total active sites, N_{cT}. This behaviour has been observed for C-CO_2 and C-H_2O (Table 8) by Kapteijn and Moulijn (1983), Mims and Pabst (1980a), and Huhn et al. (1983).

Second, at high carbon burn-off (greater than 60%) or with char of initially low surface area, the carbon surface will be saturated with catalyst. Therefore, the reaction rate is limited by the carbon surface area and a positive reaction order in carbon is observed (q>0). The results of Sams et al. (1985) and Veraa and Bell (1978) in Table 8 may have been influenced in this way.

The work of Miura et al. (1986) is noteworthy since they employed a mixing technique whereby the catalyst was dispersed uniformly within the bulk char volume, and not simply on the surface. This volumetric dispersion resulted in a constant reactivity up to 90% burn-off for both CO_2 and H_2O gasification.

Rate Law for C-CO_2

McKee (1981) and Walker et al. (1959) have suggested that the rate law for uncatalysed C-CO_2 gasification, Eq. 66, also applies to the alkali carbonate- catalysed gasification. However, more recent studies by Mims and Pabst (1983) and Kapteijn and Moulijn (1986) have shown that another form is more applicable:

$$-r_n = \frac{k'_r N_{cT}}{1 + \left(\frac{p_{CO}}{p_{CO_2} \cdot K'_{ox}} \right)} \qquad (26)$$

The mechanism that is used to derive this equation can be of the form given in Table 6 by Moulijn et al. (Eqs. 84, 85) or Sams and Shadman (Eqs. 86, 87). As an example, consider the gasification mechanism of Moulijn et al., with rate constants for the forward and reverse elementary chemisorption step, Eq. 84, as k_f and k_b, respectively; and, the rate constant for the irreversible elementary step, Eq. 85, as k_d. The following assumptions are used to derive the rate law: the catalyst reduction step given by Eq. 85 is rate limiting; Eq. 84 is much faster than Eq. 85; and, the oxygen exchange step Eq. 84 is in quasi-equilibrium (i.e., $k_b\, p_{CO} >> k_d$ and $k_f\, p_{CO_2} >> k_d$). Then the parameters in Eq. 26 are: $k'_r = k_d$, $K'_{ox} = k_f/k_b$, and N_{cT} is the total concentration of active catalyst sites. Kapteijn and Moulijn (1986) note that this equation is useful in correlating gasification data for T= 873-1273 K and P_t= 10-101 kPa. They also compared a wide range of coal char data from Johnson (1979) and found that the K'_{ox} values were close to Ergun's data for $K_{CO\text{-}CO_2}$ (Eq. 68, Table 5). Therefore, they suggested that the equilibrium oxygen exchange step was independent of carbon type. The wide variation in char reactivity for different coals was therefore attributed to differing N_{cT} values.

Kapteijn and Moulijn (1983) performed a series of experiments with high-surface-area peat char at a constant temperature of 1050 K, and total pressure varying between 50-2000 kPa. The results are summarized in Table 9. The normalized gasification rate, $-r_n$, was independent of

the total system pressure and constant between 20% and 60% burn-off: q=0 in Eq. 24. The equilibrium constant (i.e., $K'_{\alpha r}$) for the elementary step Eq. 84 was constant with burn-off while $k'_r N_{cT}$ decreased above 60% burn-off. It was concluded that this decrease was due to a lowering of N_{cT}, since k'_r is constant due to isothermal conditions.

Kapteijn et al. (1986) extended this work by determining k'_r and $K'_{\alpha r}$ for uncatalysed, Na_2CO_3-, and K_2CO_3- catalysed carbon gasification in the burn-off range where $-r_n$ is constant (i.e., 20-60% burn-off). Table 9 shows data for the rate law parameters. Several observations can be made. First, $K'_{\alpha r}$ for both Na- and K-catalysed gasification are similar and within the experimental error range of the equilibrium constant, $K_{CO\text{-}CO_2}$, for the reversible oxygen chemisorption on a carbon active site during uncatalysed gasification (Ergun, 1956). Cerfontain et al. (1987b) state that $K'_{\alpha r}$ and $K_{CO\text{-}CO_2}$ vary between 0.05 and 0.2. This suggests that the chemisorption of oxygen onto a carbon site occurs near an alkali surface complex. Second, the decrease in the activation energy, E'_r, due to potassium addition is responsible for the large increase in $-r_n$. It was suggested for K_2CO_3 catalysis that the active catalyst concentration may lower the activation energy for the C(O) desorption step by providing more oxygen coverage on the carbon surface. Third, for Na-catalysis, the increase in activation energy for the elementary step given by Eq. 85 (Table 6) implies that the Na active site interacts less with carbon and therefore produces less C(O). This is supported by the previous observation that Na_2CO_3 does not dissociate and disperse over the carbon as easily as K_2CO_3.

Freund (1985) adopted the single-site oxygen exchange mechanism for uncatalysed gasification (Eqs. 65, 67, Table 5), and the rate law shown in Table 9 to compare uncatalysed and K_2CO_3-catalysed gasification for P_t=10 kPa. A plot of $i_2 N_{cT}$ versus $1/T$ gave a value of 240 kJ/mol for the activation energy of the desorption step, E_{i_2}, which was very close to that given by Ergun (1956). Also, $K_{CO\text{-}CO_2}$ was not significantly different with the addition of catalyst. This leads to the conclusion that the catalyst affects neither the equilibrium of Eq. 65, nor the activation energy of the desorption step Eq. 67. Instead, it is the concentration of surface complex C(O) that increases. Freund (1986) showed that this was true for the case of $Ca(NO_3)_2$-catalysed gasification by using transient kinetic methods to uncouple the i_2 and N_{cf} terms. He found that for both uncatalysed and Ca-catalysed case, i_2 was statistically the same. However, experiments with another carbon system and K_2CO_3 did not confirm these results.

Cerfontain et al. (1985b) performed transient kinetic experiments in which they studied Eq. 67. They found that the rate constant i_2 was similar for both Na- and K-carbonate, but the concentration of $C(O)$ was twice as large for K than Na (i.e., M/C = 0.018 for both catalysts). Therefore, the difference in reactivity between Na and K can be ascribed to the number of active species present during gasification. The alkali metals can form either active surface species or react with CO_2 to form inactive bulk carbonate crystals, and they suggested that Na promotes the latter behaviour.

Rate Law for C-H_2O

Kapteijn and Moulijn (1986) derived a rate law for steam gasification that was similar in form to that for C-CO_2, as follows:

$$-r_n = \frac{k_r^H N_{cT}}{1 + \left(\frac{p_{H_2}}{p_{H_2O} \cdot K_{ox}^H} \right)} \tag{27}$$

The postulated mechanism from which this equation is derived is given by Eqs. 93, 94 (Table 7). The parameter, K^H_{ox}, is the equilibrium constant for Eq. 93, and k^H_r is the rate constant for the irreversible step Eq. 94. Using data from Mims and Pabst (1983), Kapteijn and Moulijn found that K^H_{ox} = 0.1 at 977 K. When this value was corrected for the water-gas shift equilibrium constant, a value of 0.06 was obtained for $K^{'}_{ox}$ which is similar to direct kinetic measurements for the C-CO_2 gasification.

Mims and Pabst (1980b) state that the concentration of active sites, N_{cT}, remains constant up to high carbon conversion. Since the gasification rate is proportional to the concentration of catalytic sites, $-r_n$ is constant up to high carbon conversion. Also, the gasification rate is proportional to the oxygen activity of the reactant gas, which could be quantified by the equilibrium constant, K^H_{ox}, for the elementary step given by Eq. 93 (Table 7). Wood and Sancier (1984) and Matsumoto and Walker (1986) note that hydrogen inhibits steam gasification of carbon with alkali carbonates of K, Na, and Ca, while Mims and Pabst (1983) confirm that the rate depends on the ratio p_{H_2}/p_{H_2O}.

Hashimoto et al. (1986) developed a rate law for the initial reaction rate, $-r_o$, using the mechanism of Wigmans et al. (1983b) given in Table 7. Since they measured the initial reaction

rate, the effect of H_2 production was ignored and the reverse of Eqs. 95, 97 could be neglected. Experimentally, it was found that the forward Eq. 95 was the fastest and the formation of CO was much slower than CO_2, therefore Eq. 67 was also neglected. The gasification was proportional to the amount of oxygen trapped by the alkali metal on the carbon surface and the rate parameters are shown in Table 9. They found that the initial rate of CO_2 formation was 70-80% of the initial carbon gasification rate, $-r_o$. However, the initial CO formation rate was only about 30% of $-r_o$, and almost constant for any alkali salt used. These findings suggest that the CO_2 formation is significant during the alkali-catalysed steam gasification of carbon.

GASIFICATION OF KBLS CHAR

Gasification with CO_2

Reactivity of Carbon

A major difference between KBLS char and alkali-catalysed carbons is the higher reactivity of the former in CO_2 atmospheres. Li and van Heiningen (1990b) determined the instantaneous gasification rate, $-r_w$, for an activated carbon with 13 wt% Na_2CO_3 loading, and a fast-pyrolysis KBLS char. The surface areas were 1000 and 160 m^2/g, respectively. For T = 750°C, p_{CO_2} = 20 kPa, and P_{CO} = 5 kPa, the gasification rate was one order of magnitude higher for KBLS char (i.e., 0.4 min^{-1} versus 0.04 min^{-1}). By comparison, for the CO_2 gasification of a coal char with 20 wt% Na_2CO_3 loading, p_{CO_2} = 101 kPa, and T = 700°C; the instantaneous rate was two orders of magnitude lower at 0.002 min^{-1}.

The kraft black liquor solids (KBLS) char has a higher reactivity for a catalyst loading that is an order of magnitude higher than the optimum for other carbons. As noted previously, the optimum Na/C atomic ratio is 0.05 for an activated carbon, and above this loading the rate usually decreases. However, the Na/C atomic ratio was 0.61 in the KBLS char gasification work discussed above.

The higher gasification rates of KBLS char can be explained by the unique dispersion characteristics of the alkali-metal. Kraft black liquor contains sodium that is mixed with water-soluble lignin and carbohydrate degradation products on a molecular scale. Therefore, the dried solids obtained from black liquor exhibit a 3-dimensional dispersion of sodium. After pyrolysis, the resultant char has been shown to have a very high dispersion of sodium (Li, 1989) compared

to activated chars doped with alkali-metal salts. Therefore, it is the higher value of the total mass concentration of active sites, N_{cT}, and the 3-dimensional dispersion of the catalyst that give KBLS char its superior gasification properties, even at very high Na_2CO_3 loading.

The gasification rate, $-r_w$, for KBLS char increases by a factor of 3-4 with carbon burn-off for fast-pyrolysis char. However, with slow-pyrolysis char, $-r_w$ remains constant up to X = 0.9 (Li and van Heiningen, 1990b). Recalling that $-r_w$ is equal to $-r_n/(1 - X)$, then it is seen that the normalized rate is first order in carbon (i.e., $q = 1$) for the slow pyrolysis char, and $q > 1$ for fast pyrolysis char. In both cases, these results imply that the surface of char is saturated with catalyst and the amount of carbon remaining determines the gasification rate.

The rate at high conversions is several times higher for fast-pyrolysis char than slow-pyrolysis char (i.e., 0.5 min^{-1} versus 0.09 min^{-1}). This difference is attributed to the higher initial specific surface area of the fast-pyrolysis char of 160 m^2/g, compared to only 30 m^2/g for slow pyrolysis char.

Mechanisms and Rate Laws

Li and van Heiningen (1989) correlated the initial gasification rate, $-r_o$, with the rate law given by Eq. 66 based on the mechanism for the uncatalysed gasification, Eqs. 65, 67. Using char from the slow pyrolysis of KBLS and the experimental conditions T = 700-775°C, p_{CO_2} = 101 kPa, they found an apparent activation energy of 187 kJ/mol.

In a later paper, Li and van Heiningen (1990b) used the mechanism of Sams and Shadman (1986) to derive rate laws that have the form of Eq. 66 (Table 5) and Eq. 26. The instantaneous gasification rate, $-r_w$, could not be correlated with Eq. 66 (Table 5) since the rate coefficients k_1, k_2, and k_3 were negative. This is contrary to their findings for $-r_o$ shown above, and no explanation was given for this behaviour. However, $-r_w$ did correlate with Eq. 26 and the coefficients, $k'_r \cdot N_{cT}$ and K'_{ox} were found to be 0.24 min^{-1} and 0.25, respectively. This fit was obtained for the following experimental conditions; X = 0.25, T = 998K, p_{CO_2} = 20 kPa, and p_{CO} = 5 kPa. Interestingly, the K'_{ox} value is in the range of 0.05-0.2 obtained for catalysed and uncatalysed gasification of coal and activated carbon. This confirms the hypothesis that the equilibrium oxygen-exchange step is independent of the carbon type. Also, the apparent activation energy was 250 kJ/mol for T = 675-725°C. This is similar to the value of 240 kJ/mol given for catalysed and uncatalysed gasification (Kapteijn and Moulijn, 1986). Therefore, from

Eq. 26 it is seen that the differences in reactivity for different carbons is due to the differing total concentration of catalyst active sites, N_{cT}.

Gasification with Steam

Reactivity of Carbon

As in the C-CO_2 gasification, the KBLS char reactivity in steam gasification is much higher than for other carbonaceous materials catalysed by alkali salts. Li and van Heiningen (1991b) compared the instantaneous rate, $-r_w$, at 723°C and 2.67 vol% H_2O for KBLS char, coal char (10 wt% K_2CO_3), and activated carbon (10 wt% K_2CO_3). The rates were 1.6 min^{-1}, $3.9 \cdot 10^{-3}$ min^{-1}, and $2.4 \cdot 10^{-2}$ min^{-1}, respectively.

The reactivity of KBLS char is several times higher for steam gasification than CO_2 gasification at the same temperature and comparable oxidizing power of the gas mixtures. For example, the rate for C-CO_2 gasification was previously shown as 0.4 min^{-1} at 750°C and $p_{CO_2}/p_{CO} = 4$. For these experimental conditions, and the thermochemical data given in Gaskell (1981), an effective partial pressure of oxygen of $1.6 \cdot 10^{-3}$ kPa can be calculated, based on the equilibrium reaction: $CO + \frac{1}{2}O_2 \Leftrightarrow CO_2$. Similarly, an equivalent p_{H_2O}/p_{H_2} ratio of ~3 can be calculated from the reaction, $H_2 + \frac{1}{2}O_2 \Leftrightarrow H_2O$, which results in the same partial pressure of oxygen. Therefore, using the rate law given below (Eq. 28) with $p_{H_2O}/p_{H_2} \sim 3$, then $-r_w$ is calculated as 2.45 min^{-1}, or about 6 times greater than that for C-CO_2. A higher carbon reactivity for steam gasification has been noted since the early work of Walker et al. (1959). They estimated that the relative rates of the uncatalysed C-H_2O reaction were 3 times that of the C-CO_2 for T = 800°C and P_t = 10 kPa. A proposed explanation for this behaviour is deferred to the next section.

The instantaneous rate, $-r_w$, is constant up to about 90% carbon burn-off for a fast-pyrolysis KBLS char (Li and van Heiningen, 1991b). This differs with results for C-CO_2, using a similar KBLS source and the same Na/C ratio. In this case it was shown that $-r_w$ increased with carbon burn-off. No explanation was given by these authors. Assuming that both chars have similar surface areas then the different reactivity could only be explained by changes in $[C_{cT}]$ with burn-off. The gaseous atmosphere is another variable that could account for a change in the total surface concentration of catalyst sites. It may be possible that the composition of the active surface species is different in H_2/H_2O, and that this complex may tend to form clusters of

inactive crystals as the carbon is depleted. Further work is required to completely explain the observed rate behaviour with carbon burn-off.

Mechanisms and Rate Laws

Li (1989) used the mechanism of Kapteijn and Moulijn (1986) given by Eqs. 93, 94 (Table 7) to derive the following rate law, accounting for CO and H_2 production,

$$-r_w\,(\text{min}^{-1}) = \frac{1.9\cdot10^{11}\exp(-210000/RT)}{1+\left(\dfrac{p_{H_2}}{p_{H_2O}\cdot 0.704}\right)} \tag{28}$$

Note that this equation has the same form as Eq. 27 with the coefficients $k_r^H N_{cT}$ equal to the numerator, and $K^H_{ox} = 0.704$. The apparent activation energy is 210 kJ/mol. Compared to C-CO_2, the activation energy is smaller and the equilibrium constant for the oxygen-exchange is 3 times larger. These differences contribute to the higher carbon gasification rates with steam.

Li (1989) also presented a two-step mechanism to explain the primary production of CO_2 during steam gasification, as follows,

$$(*) + H_2O \underset{k_{-L}}{\overset{k_L}{\Leftrightarrow}} O(*) + H_2 \tag{29}$$

$$O(*) + H_2O + C \xrightarrow{k_{3b}} (*) + CO_2 + H_2 \tag{30}$$

The catalyst sites were assumed to be phenolic and carboxylic surface complexes. Equation 29 is that of Kapteijn and Moulijn (1986) given in Table 7. Li gave a rate law for this mechanism with the same form as Eq. 28. However, the author does not agree with this finding. Assuming that Eq. 30 is the rate determining step, and that Eq. 29 is in quasi-equilibrium (i.e., $k_{3b} << k_L\, p_{H_2O}$ and $k_{3b} << k_{-L}\, p_{H_2}$), then the rate law is given by,

$$-r_w = \frac{k_{3b}\, N_{cT}}{\left(1+\dfrac{k_{-L}\, p_{H_2}}{k_L\, p_{H_2O}}\right)\dfrac{1}{p_{H_2O}}} \tag{31}$$

Since the measured gasification rate is proportional to p_{H_2O}/p_{H_2}, and Eq. 31 is quadratic in p_{H_2O}, it is concluded that the elementary step of Eq. 30 is not correct. A mechanism is proposed below that accounts for both CO and CO_2 production.

From the review on alkali-catalysed gasification, it is seen that the recent mechanisms proposed for C-H_2O gasification are based partly on analogies with the C-CO_2 system. Therefore, the proposed mechanism combines ideas from the most recent work in both gasification systems.

Cerfontain et al. (1987b) presented a unified view of the carbon surface for C-CO_2 gasification where the active catalyst sites (i.e., (*) and O(*)) and active carbon sites (i.e., C_f and C(O)) participate in the overall reaction mechanism for alkali-catalysed C-CO_2 gasification. They noted the following: oxygen-exchange occurs at the catalyst sites; CO inhibition occurs by lowering [C(O)] via the reverse of Eq. 65 (Table 6); the catalyst acts to increase the concentration of gasification sites [C(O)] by a CO_2-assisted reduction of oxidized catalyst, Eq. 89 (Table 6); and, the rate determining step is given by the desorption of C(O) in Eq. 67 (Table 6).

By analogy with the C-CO_2 gasification it is proposed that the overall C-H_2O gasification reaction for the production of CO and H_2 can be accomplished with the following steps,

$$C_f + H_2O \underset{m_{-1}}{\overset{m_1}{\Leftrightarrow}} C(O) + H_2 \tag{69}$$

$$C_f + CO_2 \underset{i_{-1}}{\overset{i_1}{\Leftrightarrow}} C(O) + CO \tag{65}$$

$$(*) + H_2O \underset{j_{-1}}{\overset{j_1}{\Leftrightarrow}} O(*) + H_2 \tag{84}$$

$$O(*) + C_f \overset{H_2O}{\underset{j_2}{\rightarrow}} (*) + C(O) \tag{32}$$

$$C(O) \overset{i_2}{\rightarrow} CO + C_f' \tag{67}$$

The inhibition of steam gasification by CO is given by the reverse of Eq. 65. By analogy, it is suggested that H_2 inhibits the gasification by the reverse of Eq. 69, and not by shifting the quasi-equilibrium of Eq. 84. The forward rates of Eqs. 65, 69 can be neglected in catalysed gasification.

The oxygen-exchange reaction on the catalyst sites, Eq. 84, has also been proposed by various workers as shown in Table 7. Cerfontain et al. (1987b) noted that the oxygen exchange rates between H_2/H_2O are even higher than those of CO/CO_2, possibly due to the lower bond strength of the oxygen in steam (i.e., 498 kJ/mol) compared to CO_2 (i.e., 531 kJ/mol). Lastly, it is proposed that the reduction of oxidized catalyst sites by carbon is assisted by H_2O, analogous to the C-CO_2 reaction.

From the elementary steps given above a rate law is derived in Appendix C and is given by,

$$-r_n = \frac{i_2 N_T}{1 + \left(\frac{m_{-1} p_{H_2}}{j_2 \cdot N_{cT} \cdot p_{H_2O}} \right)} \tag{141}$$

A modification of the elementary step, Eq. 97 (Table 7), originally proposed by Wigmans et al. (1983b) is added to the above mechanism to account for the direct production of CO_2. The reduction of an oxidized catalyst site by $C(O)$ is assisted by H_2O according to,

$$O(*) + C(O) \xrightarrow[j_3]{H_2O} (*) + CO_2 \tag{33}$$

This is based on the assumption that H_2O assists the reduction of oxidized catalyst sites, (O^*), by both $C(O)$ and C_f. It also allows for the effect of p_{H_2O} on the CO_2 production that was suggested by Li and embodied in Eq. 30.

The details of the rate law derivation for CO_2 production are given in Appendix C, and the simplified rate law is given by,

$$-r_n = \frac{i_2 N_T}{1 + \left(\frac{m_{-1} p_{H_2}}{j_2 N_{cT} p_{H_2O}} + \frac{j_3}{j_2} \right)} \tag{146}$$

Equation 146 is of the form given by Eq. 141 except that the rate constant ratio j_3/j_2 is also present. These constants are functions of temperature only and do not change the fact that $1/-r_n$ varies with p_{H_2}/p_{H_2O}. The production of gasification sites via Eq. 32 is very fast and mainly responsible for the increased $[C(O)]$, implying that j_2 is larger than j_3. This rate law also shows that the rate of carbon gasification resulting in CO_2 production should be less than that for CO

production. This is reasonable since CO and H_2 are the principal products of the heterogenous C-H_2O gasification given by Eq. 18 . Therefore, the production of CO_2 arises mainly from the secondary water-gas shift reaction, and to a lesser degree via the primary route shown above.

CONCLUSION

The addition of alkali carbonates to activated carbon and coal leads to higher rates than the uncatalysed gasification. Studies show that the catalyst interacts with the carbon surface by increasing the total concentration of carbon active sites. The effect of gas composition on the rate can be adequately described by Langmuir-Hinshelwood type rate laws for both gasification media. Assuming that the overall rate of gasification for either CO_2 or H_2O is controlled by the irreversible desorption of oxidized carbon complexes, C(O), then the derived rate laws show that the reciprocal of the carbon gasification rate is proportional to p_{CO_2}/p_{CO} or p_{H_2O}/p_{H_2}, respectively.

The CO_2 gasification rate of KBLS char is at least one order of magnitude greater than for activated carbon and coal char catalysed by an optimum loading of alkali carbonate. The higher rates are sustained to burn-off levels of up to 90%. The fine, bulk dispersion of sodium in KBLS char is given as the main reason for the unique gasification properties of KBLS char. Steam gasification rates for KBLS char are several times larger than for CO_2 gasification at the same temperature and effective oxygen partial pressure in the gas. This is because of the lower apparent activation energy and higher concentration of oxidized catalyst sites.

The rate law for CO_2 gasification of KBLS char is based on the same mechanisms as for other alkali-catalysed carbons. For steam gasification the only published rate mechanism that also accounts for the primary production of CO_2 does not give the proper rate law. Therefore, a new mechanism is proposed that accounts for CO_2 production, as well as the inhibiting effects of CO and H_2 on the gasification. The rate law derived from this mechanism also shows that the carbon gasification leading to CO_2 formation is less than that for CO and H_2 production.

CHAPTER 3

EXPERIMENTAL APPARATUS AND ANALYTICAL METHODS

ABSTRACT

A description is given of a 0.1 m diameter fluidized-bed pilot plant that was used for pyrolysis and steam gasification of dry kraft black liquor solids between 500-700°C. Details are given concerning operating procedures, kraft black liquor solids composition, and the fluidized-bed reactor.

Analytical methods are presented for the characterization of char and gas products. The char was characterized completely for the major sulphur species (Total Sulphur, S^{2-}, SO_3^{2-}, SO_4^{2-}, S_x^{2-}, S^0), other major components (Total C, CO_3^{2-}, Na^+), and minor elements (K^+, Cl^-). Scanning electron micrographs of char and kraft black liquor solids were taken to study the particle shapes and surface morphology changes during processing. Energy-dispersive x-ray maps of the char surfaces also showed the relative distribution of major and minor elements. Gas samples of the pilot plant off-gases were taken at discrete times to analyze for the fixed gases CO, CO_2, CH_4, and H_2 as well as the sulphur-bearing gases H_2S, CH_3SH, $(CH_3)_2S$, SO_2, and COS.

Independent estimates of total sulphur, char, and sodium content were used to validate the analytical techniques developed for char. Duplicate and triplicate runs at temperatures ranging from 500-600°C showed that the char and gas data were generally reproducible.

INTRODUCTION

This experimental study was initiated to examine the distribution of products from the pyrolysis and steam gasification of dry kraft black liquor solids (KBLS) in a semi-batch fluidized-bed system. The experimental facility was designed, constructed, and commissioned over a three year period. It was located in the Chemical Engineering wing of the Pulp and Paper Research Institute Building on the McGill University campus. The present location is in the laboratories of the Industrial Research Chair in Pulping Technology at the University of New Brunswick in Fredericton, N.B.

The experiments consisted of continuously feeding dry KBLS into a fluidized bed of Al_2O_3 particles at temperatures between 500-700°C in nitrogen and steam/nitrogen atmospheres. After a run, the char-coated alumina particles were analyzed to determine the degree of sodium sulphate reduction and the extent of carbon gasification. The gas phase was analyzed at discrete times for the permanent gases CO, H_2, CO_2, CH_4, and sulphur-bearing gases H_2S, CH_3SH, $(CH_3)_2S$, and COS. Operating conditions for each experiment can be found in Table 22 - Table 35, and an explanation of the entries is given in Appendix A. Specifications and suppliers of major equipment are listed in Appendix B.

FLUIDIZED-BED PILOT PLANT

Process Flowsheet

Figure 2 shows a flowsheet of the bench-scale facility. Nitrogen or laboratory air was metered into four packed-bed gas preheaters in series. For steam gasification runs, distilled water was fed and superheated in a Lindberg tube furnace and then injected at the inlet to the preheaters. The gas was preheated to 500°C and then fed into the windbox of the fluidized bed.

Dry KBLS were fed continuously into a fluidized bed of alumina particles using a combination of metering screw and nitrogen carrier gas. Reactor products consisted of char-coated alumina particles which remained in the bed, and a continuous stream of gases containing elutriated fines and condensables. After a run, bed samples were withdrawn and rapidly quenched to room temperature in a nitrogen atmosphere.

The gas cleaning train consisted of two heated cyclones in series, a vertical shell-and-tube condenser, a primary water scrubber, and a packed-tower caustic scrubber (4 wt% NaOH

aqueous solution). Entrained particles that were trapped by the cyclones and condenser were dried and weighed and included in the mass balance. It was not possible to separate the condensable hydrocarbons and water for mass balance purposes since, besides the condenser, these collected in the primary water and caustic scrubbers. Therefore, the mass balance closure included the uncollected dust, tars and pyrolysis water.

A gas-tight syringe was inserted into an in-line septum port between the primary water scrubber and caustic scrubber to sample the gas at regular intervals during a run. The caustic scrubber removed H_2S from the gas stream and kept total sulphur emissions at ~5 ppm. The product gas volumetric flow rate was recorded by an optical sensor attached to the analog display of a dry test meter. The gas was then sent to either a natural gas burner or fume hood for final discharge.

Fluidizing Gas and Steam Feeding Systems

The fluidizing gases used in this work were industrial grade N_2 (less than 20 ppm O_2) and a steam/N_2 mixture. A glass-tube rotameter and needle valve were used to measure and control the inlet flow at 50 ±3 L/min (STP). Laboratory compressed air, cleaned of oil and moisture, was used as the fluidizing gas only during the start-up period to minimize operating costs.

In the steam feeding system, distilled water was contained in a cylindrical plexiglass reservoir that was deaerated periodically with nitrogen. A peristaltic metering pump controlled the flow of water between 4-10 mL/min. A toggle switch started the metering pump and opened a solenoid valve to the main gas stream. The distilled water entered a Lindberg tubular furnace and was superheated to a temperature of about 400°C before being fed to the entrance of the gas preheaters.

KBLS Feeding System

Figure 3 shows a schematic diagram of the feeding system. The major components of the feeder were: horizontal and vertical motors, metering auger, mixing chamber, and injector lance. A 250 watt DC horizontal motor was connected to a high-torque gear box and controlled by a potentiometer to maintain a rotational speed of 10 rpm. The vertical motor turned a mixing blade that kept the solids in the hopper from bridging and ensured a uniform feed rate to the metering auger. About 5 kg of solids could be placed in the hopper. The solids were metered into the mixing chamber via a 380 mm long x 9.5 mm OD auger with a 100 mm long x

120 mm OD overwrap. The feed rate of solids was in the range 0.26-0.36 kg/h. For safety reasons, an electronic control system was installed to cease solids feeding in the event of a high or low pressure signal in the feeder hopper.

The cylindrical mixing chamber was 25.4 mm OD x 76 mm long. The N_2 carrier was injected into the chamber at a rate of 3-7 L/min (STP) through a 0.5 mm ID nozzle attached to the top plate. On the bottom plate a 25.4 mm Swagelok fitting allowed removal and cleaning of the chamber after an experiment. A vibration mechanism was started every five minutes to prevent the accumulation of solids on the chamber wall.

The solids were transported pneumatically around a bend in a 4.8 mm OD tube and through an isolating ball valve on the injector lance. An auxiliary N_2 gas purge was established through the injector lance during the reactor heat-up period. The injector lance was 610 mm long and fitted with an external water-cooled heat exchanger along the entire length. To avoid agglomeration of bed material onto its cooled exterior surface, the lance protruded only 6 mm into the fluidized bed.

Fluidized-Bed Reactor

The fluidized-bed reactor system shown in Figure 4 provided a uniform bed temperature, good mixing, and rapid sample quenching of the bed material. The cylindrical, bolted-flange reactor shell was constructed with Schedule 40, 316 SS to withstand a corrosive environment containing H_2S. It had an internal diameter of 0.1 m and a length of 1.22 m. An external resistance heater with a maximum temperature rating of 1200°C was used to heat a section of ~500 mm in height. Temperature control was provided by a Barber-Coleman PI controller and SCR power unit. A 75 mm layer of Kaowool insulation was contained in a steel enclosure that surrounded the entire reactor shell. Three Type K chromel-alumel thermocouples were placed along the length of the bed to measure temperature.

Dry KBLS were fed pneumatically with nitrogen gas via an injector lance into a bed of angular alumina particles (Figure 5a; d_p = 180μm; Geldart Group B; 99.43% Al_2O_3 min.) at a height of 200 mm above the distributor. The carrier N_2 gas was six to twelve percent of the main fluidizing flow rate. The KBL particles pyrolysed in the bed and coated the alumina with char. Henceforth, these particles are referred to as char-alumina. Figure 5b shows a scanning electron micrograph of char-alumina particles for steam gasification at 700°C. Note that the

original shape of the pure alumina was maintained and that a thin coating of char can be observed. Figure 5c gives a higher resolution of the surface. The small clumps (~ 3μm) on the surface are fragments of KBLS that may have shattered due to pyrolysis processes occurring in-flight prior to striking the alumina surface. Alumina was chosen as the preferred bed material instead of sand for two reasons. First, alumina has been used successfully by Thorman and Macur (1985) as containment material for molten sodium salts at a much higher temperature (1050°C) than was used in this work. Secondly, sodium salts react with SiO_2.

The carrier N_2 gas could not be preheated due to the swelling nature of the solids. However, this did not alter the bed temperature profile. Temperature measurements showed that the gas near the injector nozzle reached the bed temperature within 20 mm of the lance tip. Also, axial and radial bed temperature measurements showed a variation of only ±2°C, indicating uniform fluidization and good particle mixing.

The gas distributor was a layered structure consisting of a multi-orifice plate (1 mm openings) and wire-mesh stainless steel screen (100 μm aperture). The design of the multi-orifice plate followed the criteria set out by Kunii and Levenspiel (1977). The average pressure drop across the distributor for all experimental runs was 3.5 kPa compared to ~ 7 kPa for the fluidized bed. Sealing of the distributor plate with grafoil gaskets was critical to avoid gas leakage.

The bed was sampled after each experiment by dropping one-third of the bed material into a quench vessel. The char-alumina was quenched to room temperature within five minutes in a nitrogen gas atmosphere. This procedure minimized the oxidation of Na_2S to $Na_2S_2O_3$ with ambient air. The composition of the char-alumina samples for each run is tabulated in Table 22 - Table 35.

CHARACTERIZATION OF KBLS

Oxidized weak kraft black liquor from hardwood pulping was obtained from the Domtar Fine Paper mill in Cornwall, Ontario. It was spray dried using N_2 at the Domtar Research Centre, Senneville, Québec, and subsequently stored in air-tight, sealed containers. The mean moisture content of the solids for the entire experimental program was 4.50 ±0.21 wt% (95% confidence interval). The particle size distribution was determined by sieving with Tyler screens

in an inert N_2 environment: the surface-area mean particle size, d_p, was 46μm (Geldart Group A powder). An Hitachi S-2700 scanning electron microscope was used to obtain micrographs of two representative KBLS samples shown in Figure 6 (a, b). The KBLS particles appear spheroidal with diameters ranging from ~10 μm to over 100 μm.

Dry solids were used for two reasons. First, thermodynamic calculations (Fallavollita et al., 1987) suggest that chemical recovery of Na_2S is favoured as the water partial pressure in the reactor is reduced. Second, the trend in industrial practice is to increase the solids content of the kraft black liquor feed to the recovery boiler to decrease energy costs (Harrison et al., 1988).

Table 10 shows the elemental and inorganic ion analyses for KBLS. The inorganic sulphur species analyses were repeated during the experiments, and it was shown that storage time did not affect the results. The total sulphur content of the black liquor was 1.67 ±0.05 wt%. This was low in comparison with typical values of 3-4 wt% usually encountered in kraft mills. This may be due to volatile sulphur release during drying and to the low sulphidity in this mill. Analogous to coal chemistry, the organic sulphur was determined as the difference between total sulphur and inorganic sulphur (Attar and Corcoran, 1977). It was found that the sulphur bound to the hydrocarbon matrix of KBLS accounted for 19 ±4 wt% of the total sulphur. The presence of sulphite was detected but could not be quantified. Polysulphide sulphur, S_x^{2-}, could not be detected by potentiometric titration.

The majority of carbon is associated with alkali lignin and hydroxy acids, with the remainder bound as inorganic carbonate. Sodium is present as the cation in inorganic salts or as sodium phenolate (R-ONa) and the sodium salt of carboxylic acids (R-COONa). Based on Table 10, about 60% is associated with the organic fraction in the KBLS. This agrees with the findings of Blackwell and King (1985). Based on mill data they found that 55-80 wt% of the sodium is bound to the organics in KBLS. Potassium, chloride and calcium are present in small quantities compared to sodium. However, their presence is noteworthy because potassium and chloride affect the agglomeration behaviour of the char-alumina particles (Chapter 4), and both K- and Ca- salts are known catalysts for the CO_2 gasification of carbon (Spiro et al., 1983).

EXPERIMENTAL PROCEDURE

Start-up

Before each experiment the following operations were performed: the gas chromatographs were calibrated; the quench vessel and reactor were pressure tested for leaks; the cooling water lines and scrubber pumps were checked; the toxic gas monitors were calibrated; and, the operation of the induction fan was tested. The top of the fluidized-bed reactor was removed and between 4.4 and 6.3 kg of alumina were added. The KBLS feeder-lance was installed and after pressure testing of the reactor, a stream of N_2 was passed through the lance at 0.5 L/min. Fluidizing air was then introduced into the reactor at 50 L/min. All heaters were turned on and the system was allowed to heat up over a period of 3-4 hours.

During the heating period the KBLS feeder was weighed and then continuously purged with N_2. One hour prior to the start of solids feeding, the air flow was turned off and the reactor system was purged with 50 L/min of N_2. A gas sample was taken before the start of solids feeding to ensure that the oxygen was completely purged from the reactor. After the fluidized bed reached the desired temperature, the product gas flow rate recording was started, the auxiliary N_2 to the injector lance was closed, the main carrier N_2 flow was directed to the reactor, and both scrubber pumps and feeder were started.

Data Acquisition

During an experiment the pressure and temperature were measured at various locations, the average volumetric flow rate of product gas was recorded, and syringe samples of product gas were taken every five to ten minutes. The feeder was weighed after an experiment and the average dry KBLS feed rate calculated by dividing the feeder weight change by the elapsed feeding time. The data acquisition locations are shown in Figure 2 - Figure 4.

Bed Sampling

After a run was completed, the quench vessel was evacuated and purged several times with N_2 gas. Liquid nitrogen was then poured into the holding vessel and the temperature of the quench vessel reached about -50°C. A ball valve on the fluidized bed underflow pipe was opened that allowed the bed material to empty into the quench vessel. During this time, the temperature inside the quench vessel was monitored with several thermocouples. Bed sampling stopped when an increase in temperature was observed. About five minutes were required to

bring the bed sample temperature to 0°C. The quench vessel was then sealed under a blanket of nitrogen and placed in a nitrogen-filled glove box. Over forty individual samples were placed into glass vials and stored in a desiccator overnight. The analyses for sulphur species were performed the next day and all other analyses were usually completed within two weeks, except for the analyses of K^+, Cl^-, elemental sulphur, and polysulphide.

ANALYTICAL METHODS

Introduction

Products from the fluidized-bed reactor consist of solid char, gases, and condensable vapours. Studies on the distribution of condensable vapours from pyrolysis of kraft black liquor can be found in Feuerstein (1966) and Jones (1968). This work will consider only the analysis and characterization of important gases and solids. A brief summary of the in-house chemical analyses is discussed in subsequent sections.

Several analyses were performed by outside laboratories owing primarily to a lack of adequate in-house facilities. The KBLS analysis of Cl^-, K^+, Ca^{2+}, OH^-, elemental O, and elemental H were performed by the Pulp and Paper Research Institute at their laboratory in Pointe Claire, Québec. As a check, they also provided OH^- analyses for several char-alumina samples and some comparative analyses for the inorganic sulphur ions in KBLS. All the analyses for K^+ and Cl^- in char-alumina samples were done by Norwest Labs, Edmonton. They also provided some Na^+ analyses that acted as a check for in-house results. Analyses for elemental sulphur, S°, were performed by Alberta Sulphur Research Ltd. (Calgary, AB) on both char and KBLS samples. They also analyzed for polysulphide, S_x^{2-}, in char samples and provided comparative data for the in-house results on KBLS.

Gas Analyses

Gas-tight syringe samples containing the sulphur gases H_2S, CH_3SH, $(CH_3)_2S$, SO_2, $(CH_3)_2S_2$ and COS were analyzed using a Hewlett-Packard 5790A dual-column gas chromatograph. This instrument was equipped with a single-flame photometric detector (FPD) using a sulphur interference filter. DeSouza et al. (1975) discuss the column preparation, conditioning, and details of the operating conditions required for effective separation of ppm levels of these gases. Calibration standards were prepared with the aid of permeation tubes (VICI Metronics, Santa

Clara, CA) containing the above sulphur compounds. The tubes were kept at 30°C in a water bath. A variable flow of diluent nitrogen allowed different concentrations of gases to be prepared.

A Fisher Model 1200 Gas Partitioner with thermal conductivity detector was used to analyze syringe samples of the permanent gases: CO, CO_2, CH_4, and H_2. Isothermal separations at 50°C were made using a helium carrier gas flow rate of 30 mL/min and two columns: Porapak Q and Molecular Sieve 13X.

KBLS and Char Analyses

Total Sulphur

A method was developed that incorporated an oxygen bomb combustion technique (ASTM, 1984) with a Dionex Model 2000i Ion Chromatograph (Dionex Corp., Sunnyvale, CA) to measure total sulphur in char-alumina and KBLS samples. This new technique has some advantages over the wet digestion method (CPPA, 1981) that is used for KBL analysis: a shorter analysis time by about 50%, and the elimination of a fume hood that is resistant to perchloric acid fumes.

Oxygen-bomb combustion has been used extensively for determining total sulphur in coal and coke. Most of the sulphur in these materials is in the organic form, with smaller amounts of inorganic-bound sulphur. In KBLS and char, it is inorganic sulphur that is the dominant form. Therefore, various analyses were performed to find out if the method could be adequate for inorganic sulphur and samples containing alumina. Using high purity (99.9 wt%) sodium thiosulphate as a standard inorganic sulphur compound, it was determined that the total sulphur analysis was accurate to within 3 wt%. Also, blank analyses using only pure alumina showed that its contribution to the total sulphur content was not measurable.

The method begins by drying about 0.5 g of KBLS or char-alumina for 1 h at 105°C. The material is then pelletized into a disc shape and placed in the stainless steel crucible of an oxygen-bomb apparatus (Parr Instrument Co., Moline, Illinois). For char-alumina, a combustion aid such as paraffin oil is added in a 1:1 weight ratio. Ten millilitres of distilled water are pipetted into the bottom of the bomb cylinder to absorb any SO_2 that may be released during combustion. The bomb is then filled with 3 MPa of pure O_2 and ignited. The bomb is left standing for about 10 minutes and then the pressure is released slowly. All inside surfaces of the cylinder are washed with distilled water and all the liquid is poured into a 250 mL beaker.

Any char-alumina particles remaining in the stainless-steel crucible are also mixed with this liquid. After filtration, the total sulphur content is calculated from the SO_4^{2-} concentration in the solution, as determined by ion chromatography.

Inorganic Sulphur Species

Kraft black liquor solids were analyzed in-house for the sulphur species; sulphide (S^{2-}), polysulphide (S_x^{2-}), thiosulphate ($S_2O_3^{2-}$), sulphite (SO_3^{2-}), and sulphate (SO_4^{2-}). Potentiometric titration (CPPA standard method J.15P) was used to analyze for polysulphide and sulphide. The other sulphur anions were determined by ion chromatography (Krishnagopalan et al., 1985) with eluent (1 mM Na_2CO_3, 5 mM NaOH, and 0.8 mM p-cyanophenol) and separator column (HPIC-AG4 or HPIC-AS5) as stipulated in technical note 30R (Dionex, 1984).

The char-alumina samples from the fluidized bed contained much smaller concentrations of these sulphur species due to the much larger fraction of alumina (92-97 wt%). Development work revealed that the ion chromatograph was best suited to analyze for the sulphoxy anions. However, for runs performed between 650-700°C, the S^{2-} analysis was problematic owing to oxidative losses during dilution (Easty and Johnson, 1987). For these cases the potentiometric method provided more reliable results. Several runs between 500-650°C showed that the $S_2O_3^{2-}$ concentration was small. Therefore, due to the long analysis time (i.e., 25 minutes) and low availability of the ion chromatograph, $S_2O_3^{2-}$ was checked only for a few experiments.

Inorganic polysulphide determinations for char samples were also made by Alberta Sulphur Research, Calgary, using a technique described in Borchardt and Easty (1984). The method involves mixing the following chemicals for 48 h in sealed septum vials: 1 mL of buffer (pH 4.0; 50 mL 0.1 M potassium acid phthalate with 36.6 mL 0.1 M NaOH); 1 mL of a stock solution of 3 g/L triphenylphosphine (TPP) and 0.25 g/L triphenylphosphate ($TPPO_4$) in toluene; and, 1 g of char-alumina. At this low pH, polysulphide is converted quantitatively to elemental sulphur that is then derivatized with TPP to form triphenylphosphine sulphide (TPPS). Details for quantifying TPPS are given in the next section.

Elemental Sulphur

Analyses of elemental sulphur, S^o, in the char and KBLS were performed by Alberta Sulphur Research Ltd., Calgary. The method employed is described in Clark and Lesage (1989) and is summarized below. This technique is quantitative and selective for elemental sulphur in a

hydrocarbon matrix. Inorganic polysulphides do not interfere with this analysis since an organic solvent (toluene) was used (Lesage, 1991). The analytical method is based on the rapid, quantitative reaction between elemental sulphur in the char sample and TPP to form TPPS. The TPPS is stable at room temperature and can be volatilized upon heating thereby making it suitable for analysis by gas chromatography.

A stock solution is prepared by adding 3 g TPP and 0.25 g $TPPO_4$ to 1 L of toluene. Approximately 1 g of char-alumina is added to a 15 mL aliquot of the TPP/$TPPO_4$ solution. The mixture is shaken for 3 h in a stoppered container to prevent oxidation of TPP. After filtering, a 1 µL sample of filtrate is analyzed by a Varian Vista 6000 gas chromatograph coupled with an FPD detector using a phosphorous interference filter. The separation is achieved in a DB-5 megabore column (0.53 mm x 30 m, J&W Scientific, Inc.) maintained at 260°C and a He carrier flow rate of 5 mL/min. The chromatogram peaks for TPP, $TPPO_4$, and TPPS are obtained at retention times of about 3.5, 5.2 and 8.8 minutes, respectively. The elemental sulphur content is obtained by calculating the proportion of sulphur as TPPS.

Total Carbon

About 30 g of KBLS were first oven dried for 2 h at 105°C under an inert atmosphere and then placed in a desiccator. A smaller sample weighing approximately 0.1 g was prepared and transferred to the combustion crucible of a LECO Carbon Determinator, Model WR-12 (LECO Corp., St. Joseph, MI). For the char-alumina material, sample sizes between 0.3-0.5 g were used without the need for drying since the moisture content was low (less than 0.1 wt%).

This instrument used an induction heater and copper flux to combust completely the carbon in the sample to CO_2, which was measured by a thermal conductivity cell. The signal was integrated and the total carbon content was calculated for each sample. Development work was done to ascertain if the instrument could analyze for inorganic carbon in the char and KBLS. Combustion of pure sodium carbonate samples showed that the accuracy of the total carbon determination was about ±2 wt%. Also, it was found that alumina did not contain significant amounts of carbon.

Carbonate and Organic Carbon

Carbonate analyses were performed on a Dionex Ion Chromatograph Model 2000i equipped with a conductivity detector. The eluent was deionized water pumped at a rate of 1.0 mL/min.

Samples of KBLS or char-alumina were diluted with deionized-deaerated water and injected into an ion-exclusion separator column (HPICE-AS1). The carbonate content was determined from the peak area of the resulting chromatogram by reference to a calibration standard.

The amount of organic carbon in char was obtained as the difference between the Total Carbon measurement and the carbon present as carbonate.

Sodium

The in-house determination of sodium in KBLS and char-alumina samples was made with a Perkin-Elmer Atomic Absorption Spectrophotometer Model 403. Solutions of KBLS and char-alumina were prepared with distilled-deionized water with sodium content between 0.1-1.0 mg/L. The pH of these samples was first adjusted to between 8.2-8.5 with 1:6 (v/v) HCl or NH_4OH and then the samples were aspirated into the flame. For the KBLS, a correction was made for the distilled-deionized water blank absorbance, whereas for the char-alumina samples an estimate of the contribution of the sodium in the alumina fraction was also obtained. This estimate was based on multiplying the amount of alumina in a sample by the weight percent of sodium in alumina (i.e, ~0.05 wt%). Typically, the Na content attributable to alumina was less than 3.8% of the total Na measured.

For runs P1 and SG4, the sodium analysis for char was performed by Norwest Labs (Edmonton, AB). The method is identical with that used for potassium and is detailed in a subsequent section. Only two samples were analyzed for each run compared to five for the in-house method. Therefore, the 95% confidence intervals reported are much larger for these runs.

Char Content

During an experiment the alumina particles became coated with char. For mass balance purposes it was important to know the amount of char present in the bed. A gravimetric procedure was developed that involved three steps. First, a 1 g sample of char-alumina was placed in a muffle furnace at 900°C to burn off the organic carbon. Second, the remaining inorganic fraction (Na_2SO_4 and Na_2CO_3) covering the alumina was dissolved in boiling distilled water. Third, the remaining material was weighed and the percentage of char calculated. An alumina blank was analyzed in the manner mentioned above to correct for any weight loss (i.e., ~0.06 wt%) resulting from soluble fractions in the original alumina matrix. Therefore, less than 2% of the reported char content was attributed to alumina dissolution.

Surface Morphology/Composition

A study of the surface appearance and composition of alumina powder and char-alumina was also initiated. A SEM (Model ISI-60, International Scientific Instruments) and EDXA (System 4, Princeton Gamma-Tech Co.) probe were used for this purpose. A random sample of the powder was pasted with a graphite binder onto a holder before introduction to the instrument. Surface appearance was investigated for magnifications of 72X, 400X, and 1100X. Semi-quantitative composition variation over the entire sample surface was accomplished by energy-dispersive x-ray (EDXA) maps for the elements Al, Si, Na, Fe, K, S, Cl, and Ca. The depth of penetration for the analysis is typically 1 μm. It should be noted that Na usually volatilizes during this type of analysis and therefore the actual content may be up to 30% more than what is observed.

A SEM micrograph of a random sample of char-covered alumina particles for a pyrolysis run at 700°C is shown in Figure 7a. Because the powder samples were not provided with a flat surface with respect to the x-ray beam, some signal noise is introduced due to particle edges. Therefore the reported surface compositions are semi-quantitative. The corresponding EDXA maps for the major char elements sodium and sulphur are displayed in Figure 7b and Figure 7c, respectively. EDXA surface scans of char-alumina particles from a steam gasification run also revealed the presence of aluminum (Figure 8b) and iron (Figure 8d), as well as sulphur (Figure 8c).

The relative proportion of surface elements observed for a pyrolysis run at 600°C is shown in Figure 9a. The surface composition scale is based on the total amount of elements scanned, not the total weight of char. Clearly, the most abundant surface element is aluminum. It constitutes about 75 wt% of the total elements detected. The implication is that the surface of the alumina may not be completely covered by char. The elements Cl, K, Ca, and Fe were also detected. Calcium originates from the causticizing step in the kraft process and the wood itself, and is present as $CaCO_3$. The effect of potassium and chlorine compounds on char agglomeration will be discussed in Chapter 4. Huttinger and Minges (1985a) have shown that some compounds of K, Cl and Ca are able to catalyse the steam gasification of carbon. However, since their concentration is very small compared to sodium, their effect is generally

ignored. Iron has been shown to catalyse the reduction of sodium sulphate (Birk et al., 1971). An estimate of iron concentration in the char for the pyrolysis runs is 0.2-0.35 wt%.

The variation in sulphur surface concentration for pyrolysis runs between 500-700°C is shown in Figure 9b. The EDXA surface scans reveal that sulphur increases from about 6 to 10 wt% of the total elements detected. Though these are semi-quantitative data, the trend of increasing sulphur with temperature supports the results of more precise data given in Chapter 5.

Moisture Content

A porcelain crucible was placed in an oven at 105°C for one hour, allowed to cool in a desiccator, and then weighed. These steps were repeated until the weight reading (W_1) varied by less than 0.0005 g. Between 1-3 g of KBLS or char-alumina were then placed in the crucible and weighed (W_2). The crucible and sample were then placed in an oven for 1 h at 105°C, followed by a cooling period in a desiccator and final weighing (W_3). The moisture content was calculated as: $\{(W_2-W_3)/(W_2-W_1)\}\cdot 100$.

Chloride and Potassium

Both chloride and potassium analyses were performed by Norwest Labs, Edmonton. The chloride content was obtained as follows. A 1 g sample was placed in a 250 mL erlenmeyer flask, 5 mL of deionized water was added and then the flask was shaken for 1 hour. The solution was filtered and the extract was analyzed colorimetrically at 480 nm. The amount of chloride in Al_2O_3 was less than 0.0025 wt%. This value was subtracted from the char-alumina chloride concentration and was usually less than 5 wt% of the total Cl^- measured.

For potassium analysis, a 0.2 g sample of material was weighed into a Teflon bomb and then 1 mL of aqua regia and 6 mL of HF were added. The bombs were sealed and placed in a pressure cooker for 2 h. After cooling, the bomb contents were placed into a 125 mL polyethylene wide-mouth bottle containing 5.6 g of boric acid crystals and 20 mL of distilled water. The bottle was shaken for several hours, stored in a refrigerator, and later analyzed for potassium by atomic emission spectroscopy. The potassium content of an Al_2O_3 blank was 0.016 wt%. Knowing the char/Al_2O_3 weight ratio for each run, it was possible to subtract this contribution. Typically, this was about 15 wt% of the K^+ content in char-alumina.

VALIDATION OF ANALYTICAL METHODS FOR CHAR-ALUMINA COMPOSITE

The char-alumina composite particles are complex and difficult to analyze. For these reasons the methods developed in this work for the total sulphur, sodium, and char content needed to be validated in some way. It was thought that two independent estimates of these quantities may provide further support.

Sodium Content in the Char

Figure 10 shows independent estimates of the sodium content for some pyrolysis and gasification runs. The sodium content of the char-alumina mixture for these runs was measured directly by atomic absorption spectroscopy. An independent estimate of the sodium content can be also obtained by assuming that it is bound mostly with the anions CO_3^{2-}, S^{2-}, SO_3^{2-} and SO_4^{2-}. The amount of sodium associated with these anions is calculated by noting that two moles of sodium are associated with one mol of carbonate, and one mol of each sulphur anion. The comparative bar, SUM, represents the sodium combined with these anions and independently measured. For each run, the 95% confidence interval for this independent estimate compares well with the direct measurement of sodium by atomic absorption spectroscopy.

Sulphur Content in the Char

Figure 11 shows a comparison between two independent measurements, with their 95% confidence intervals, of the sulphur content in char-alumina for some pyrolysis and gasification runs. The measurement labelled Total S was obtained by direct oxygen-bomb combustion/ion chromatography of a bed sample. The comparative bar, SUM, is the addition of the independent measurements of the individual sulphur species from a separate bed sample. For most experiments, the Total S determination was consistently higher than the SUM. An explanation for this discrepancy is proposed.

It is well known that KBL char consists mostly of a 3-dimensional dispersion of inorganic sodium salts in an amorphous carbon matrix. The oxygen bomb technique completely consumes the carbon in char and the sulphur reports quantitatively as solid Na_2SO_4. These inorganic salts are completely soluble and stable in the aqueous solution used for ion chromatography. However, in the analysis of char for individual sulphur species by ion chromatography, the carbon matrix acts as a diffusion barrier for rapid dissolution of the sulphur species. This is

supported by the fact that the differences between the two estimates decrease as the operating temperature increases (e.g., compare P4 with P8). The higher temperature samples contain less organic carbon in the char matrix that may impede dissolution. Also, the analysis time for the individual anions is very short (i.e., less than 10 minutes) to prevent rapid oxidation of S^{2-} and SO_3^{2-} with dissolved oxygen in solution. The combination of short dissolution times and the carbon barrier likely result in the incomplete dissolution of the inorganic sulphur ions.

It is concluded that a more accurate estimate of the total sulphur content is achieved by the direct oxygen bomb/ion chromatography method. However, the analyses for the individual sulphur species are expected to give reasonable estimates of the overall trends.

Char Content

The total mass balance results presented in Chapters 4, 5 rely on an acceptable estimate of the char content in the fluidized bed. Figure 12 shows a subset of the complete series of results shown in Table 22 - Table 35 for pyrolysis and gasification runs. The char content as measured directly by the gravimetric method was compared with the weight percent of the sum of individual char components (SUM). This was done to determine the accuracy of the method and to account for all the material in the bed. The agreement between these independent estimates is excellent and typical for all the experiments. Indeed, the 95% confidence intervals either overlap or differ by no more than about 8%.

REPRODUCIBILITY OF EXPERIMENTAL DATA

Char Analyses

To obtain information on the reproducibility of the char and gas data as a function of reactor temperature, several repeat runs were performed. In Chapters 4, 5 the total mass balances for sodium and sulphur in the pilot plant are presented to further support the experimental methods. The compositions of the individual char species are stated in terms of the 95% confidence interval for the population mean and given in Table 22 - Table 35. Between 5-10 samples of the char component were analyzed for each run. All mathematical manipulation of the data were done to minimize error propagation. A detailed discussion of the statistical approach used is given in Skoog (1985).

For pyrolysis in nitrogen, Table 11 gives data for the major species in the char for triplicate runs at 550°C and duplicate runs at 600°C. It can be seen that the 95% confidence intervals overlap for all the analyses, except runs P2, P4 for SO_3^{2-}, and the runs P5, P6 for S^{2-}. These sulphur species tend to be oxidized by dissolved oxygen in solution during the analytical procedures.

Gas Analyses

Table 12 gives data for both fixed and sulphur gases for duplicate pyrolysis runs at 550°C and 600°C, and steam gasification runs at 500°C. The raw data for the time-sampled gas flow rates are given in Figure 40 - Figure 51. The average flow rate was taken as the mean of several time-samples during a run. The 95% confidence interval was calculated based on the number of time-samples and the statistical formula given in Skoog (1985).

Table 12 shows that the 95% confidence intervals overlap for CH_4, H_2S, CH_3SH and $(CH_3)_2S$. For CO and CO_2, differences of 5-13% are seen for duplicate runs at 500-550°C. The data for H_2 differ by as much as 30-60% for runs performed at 500 and 550°C. The reason for this behaviour may be due to the low concentration of H_2 in the gas stream combined with its tendency to leak from the syringe sampler. The run at 600°C supports this explanation. In this case the H_2 concentrations are about an order of magnitude higher than at 500°C, and the H_2 confidence intervals do overlap.

CONCLUSION

Dry KBLS are easily pyrolysed between 500-700°C and the resultant char is retained as a coating on the fluidized bed alumina particles. This property allows steam gasification and sulphate reduction reactions to be monitored at the bench-scale.

Analyses of random samples of bed material showed that the sodium, total sulphur, and char content data were reliable. Duplicate runs showed that the key inorganic species data were reproducible. The gas analyses data were reproducible for all the sulphur-bearing species analyzed. The fixed gases data showed more variability for duplicate experiments, especially for H_2. Considering the complexity of the pilot plant, the data appear sufficiently reliable to allow an adequate mass balance of Na, S and C.

CHAPTER 4

PYROLYSIS OF KRAFT BLACK LIQUOR SOLIDS AND STEAM GASIFICATION OF CHAR CARBON

ABSTRACT

Pyrolysis and steam gasification of dry kraft black liquor solids were carried out using a 0.1 m diameter fluidized-bed reactor. The dry solids having a surface-area mean particle size of 48 μm were injected continuously into a fluidized bed of alumina particles of 180 μm. For the entire experimental program the feed rate of solids ranged from 0.26 to 0.36 kg/h while the bed temperature was varied between 500°C to 700°C. The alumina particles became coated with a char containing amorphous carbon and the inorganics. This char was analyzed for sodium, total carbon, and carbonate. The off-gas from the fluidized bed was analyzed for the permanent gases, H_2, CO, CO_2, and CH_4.

Total mass balance results for char and gases are given for fluidized-bed pyrolysis in N_2 and steam/N_2 atmospheres in the temperature range 500-700°C. During pyrolysis, the carbon content of char decreased from 71 ±8 wt% to 41 ±4 wt% between 500 to 700°C, while carbon in the gas increased from 14 ±2 wt% to 40 ±3 wt%, respectively. Sodium volatilization in the range 8-15 wt% was observed above 600°C. The loss occurs as a result of rapid pyrolysis during KBLS particle heat-up. Prolonged exposure at these temperatures does not lead to further volatilization because of the presence of CO/CO_2 gases and the high organic oxygen content of the char.

Above 600°C, the addition of steam resulted in significant increases in CO_2 and H_2, a decrease in CO, and the production of CH_4 was unaffected. It was found that the CO_2 concentration increased with temperature, contrary to equilibrium predictions. This is explained by the fact that CO_2 is a primary product of the C-H_2O reaction, and that the reaction rate of the water-gas shift reaction is comparable to carbon gasification. It was also found that the water-gas shift reaction approached equilibrium with increasing temperature. The volatilization of sodium was not observed between 600-650°C. This could be due to surface reactions involving steam that lead to Na_2CO_3 production, and to the larger H_2O/H_2 ratio that increases the adsorbed oxygen on char. The global gasification rate of carbon with steam was found to be kinetic-controlled in the temperature range 600-650°C.

The fluidized bed agglomerated for steam gasification runs at 700°C. Scanning electron micrographs of char particles revealed partial surface melting. Low-melting-point eutectic mixtures containing chloride and potassium were suggested as the primary cause. It is proposed that the stickiness of the char surface is controlled by the quantity of amorphous carbon under these conditions.

INTRODUCTION

Part of the critical requirements for development of an alternative low-temperature process for kraft chemical recovery is obtaining kraft black liquor solids (KBLS) pyrolysis and char gasification data under actual fluidized-bed operating conditions (Fallavollita et al., 1987). While references to such systems have been made in the literature, there has been no detailed study reported on the actual behaviour of dry KBLS in a fluidized-bed reactor.

DeHaas et al. (1976) sketched a process flowsheet for processing dry KBLS in a fluidized bed operating at 500°C with a recycled combustion gas atmosphere; however, no details were given regarding KBLS particle size and gases/char composition. Recently, Durai-Swamy et al. (1989) presented a low-temperature technique in which kraft black liquor (KBL) at 65% solids was fired into a fluidized-bed reactor operated at 550-625°C. Heat was supplied to the reactor via immersed resonance tubes of a gas-fired Helmholtz pulse combustor. The bed consisted of 600 μm Na_2CO_3 particles fluidized by steam. Clay et al. (1987) studied the pyrolysis of large KBL droplets (i.e., d_p > 1 mm) in a counter-current dilute phase reactor. However, differences in heat transfer rates, droplet residence time, and gas/droplet interactions lead to inadequacies in extrapolating their results to a fluidized bed.

A key objective of this investigation was to develop process data for the fluidized-bed pyrolysis (H_2O:solids = 0.05 $g \cdot g^{-1}$) and steam gasification (H_2O:solids = 0.87, 1.75 $g \cdot g^{-1}$) of dry KBLS. The dry solids, having a surface-area mean particle size of 48 μm, were injected continuously into a bed of alumina particles of 180 μm size fluidized by nitrogen gas at 50 L/min (STP). The alumina particles became coated with char and remained in the bed while the gases were withdrawn continuously. The feed rate of KBLS and reactor temperature were constant during a run. After a run, the char was analyzed for sodium, total carbon, and carbonate. Time-samples of the off-gas were analyzed for H_2, CO, CO_2, and CH_4. For the entire experimental program the KBLS feed rate was varied between 0.26-0.3 kg/h while the temperature ranged from 500 to 700°C.

The global rate of carbon gasification was estimated from the change in composition of the off-gases and char carbon between pyrolysis and steam gasification runs. Also, the water-gas shift reaction constant was estimated based on the off-gas composition.

PYROLYSIS OF DRY KRAFT BLACK LIQUOR SOLIDS

Total Mass Balance

Pyrolysis consists of competing fragmentation and polymerization reactions; forming volatiles (gases and condensables) and char, respectively. Pyrolysis affects the subsequent gasification reactions by controlling the formation of surface area, volatiles, char production and spatial distribution of alkali salts in the amorphous carbon matrix. Important factors that may affect pyrolysis are: KBLS particle size and composition, heating rate, ambient temperature and atmosphere, mixing and contact time between char and gases. Some of these factors are interrelated. For instance, the ambient temperature will influence the heating rate if the particle size changes.

Char Yield

A reliable estimate of the total char yield in the fluidized-bed pilot plant is necessary to obtain mass balances for the elements Na, C, and S. Figure 13 shows a graph of the total char yield as a function of the fluidized-bed temperature and feed weight ratio of steam to KBLS (i.e., H_2O:solids). For comparison, some relevant data from other studies are also included.

The fluidized-bed char yield is highest for 500-550°C and decreases markedly above 600°C for both pyrolysis and steam gasification runs. It is also evident that the fluidized-bed results straddle those of Jones (1968) and Feuerstein (1966) at lower temperatures, but approach the data from Bhattacharya et al. (1986) at 700°C. Note that the temperature dependency (i.e., slope) of the char yield curve for the other studies is very similar and much smaller than in the present work.

The relative distribution of char and volatiles is a complex function of: the composition of KBLS and ambient gas; final particle temperature; residence time; rate of heating; and, particle size. For the various studies in Figure 13, the final temperatures are identical and the residence times are in the range of this study. Also, the work of Bhattacharya et al., Feuerstein, and Jones can be compared to fluidized-bed pyrolysis data (i.e., H_2O:solids = 0.05) since N_2 was the main ambient gas. The larger H_2O:solids ratios reported for Jones and Feuerstein are due to the use of black liquor of varying solids content. The contribution of the remaining factors to the differences in char yield is outlined briefly below.

The composition of KBLS can have a strong impact on the char yield during pyrolysis. Frederick (1991) showed that the residual carbon content, a major component of char, varied by ±25% of the average for several softwood and hardwood kraft liquors. Therefore, for the same operating temperature, composition differences could explain the variation in char yield between the studies of Bhattacharya, Jones and Feuerstein. But, the char yield temperature dependency for fluidized-bed pyrolysis cannot be explained by this factor alone.

During pyrolysis of KBLS, the net endothermic heat requirement has a significant effect on the temperature-time history of a particle. As a result, pyrolysis can be controlled by heat transfer, chemical kinetics or a combination of these. In some cases, the heating rate and particle size may determine which of these is dominant.

From empirical data on the related topic of coal pyrolysis, it has been shown that the amount of char or volatiles was not size dependent for particles up to 400 μm in diameter; for larger particles, more char was produced (Anthony and Howard, 1976). Also, theoretical calculations showed that chemical kinetics control the pyrolysis for 275 μm particles exposed to 972 K (Mills et al., 1976).

In Feuerstein's work, KBL was heated very slowly (5°C/min) in an evacuated batch reactor. Jones injected between 1-3 g of KBL (40% solids) from a syringe into a heated cylinder. Bhattacharya's experiments involved placing 2 g of dry KBLS of 150 μm size in a ceramic holder and quickly introducing these into a preheated tube furnace. A heating rate of 20°C/s was reported. In this case, the apparent activation energy for pyrolysis was particle size dependent.

In the present study, a continuous stream of dry KBLS particles of ~50 μm was injected into a fluidizing bed of alumina particles. The heat transfer rates in the particulate phase of the fluidized bed are high due to the frequent collisions of particles. The present study used the smallest particles and the highest heating rates. Therefore, the temperature dependency of the char yield may be due to a different controlling mechanism for pyrolysis compared to the other investigations.

Yield of Gases and Condensables

KBLS fragmentation reactions lead to the production of gases and condensable volatiles. The gases consist of fixed, sulphur-bearing, and hydrocarbon species. The major fixed and sulphur gases were measured in this study. The volatile hydrocarbons, except CH_4, were not analyzed

because of a lack of adequate analytical facilities. This does not impact the carbon balance since their concentration is less than 1 wt% of the total fixed gases (Jones, 1968).

The condensables consist primarily of pyrolysis water and heavy hydrocarbon fractions such as tar and oils. Feuerstein (1966), Jones (1968), and Bhattacharya et al. (1986) found that pyrolysis water and organic liquid products were constant at 30 wt% (on a dry solids basis) between 500-700°C. In addition, Feuerstein's data also revealed that only 10 wt% consisted of organic liquid, the other 20 wt% was pyrolysis water.

Because of the small scale of the pilot plant, the collection and separation of condensables proved to be difficult. In the present work, a maximum value for the condensables was obtained by closing the mass balance and assigning the difference to the condensables stream. This difference is reported in the rest of the text as: mass balance closure. Also, when needed for calculation purposes, the amount of pyrolysis water produced by KBLS during pyrolysis will be taken as 20 wt%.

Elemental Balance

Table 13 summarizes the total mass balance of sodium and carbon for the pyrolysis experiments: data reduction procedures are detailed in Appendix A. Briefly, the char data was obtained by multiplying the analytical measurements for total carbon and sodium content by the char yield previously presented in Figure 13. For the gas phase, the carbon content was determined by summation of the carbon content associated with the fixed gases CO, CO_2, and CH_4. Sodium was not analyzed in the gas phase and was therefore not included in this stream. Closure of the mass balance for both elements was made by difference and listed as: mass balance closure. A larger 95% confidence interval for the sodium balance in runs P1 and SG4 is noted. This was because only two samples were analyzed compared to five samples for the remaining experiments.

Carbon Balance

In the char, carbon is present as either amorphous organic carbon or inorganic CO_3^{2-}. The amount of Total Carbon (i.e., organic and inorganic) in KBLS that reported to the char was constant at 70 ±8 wt% between 500-600°C. Above 650°C, a significant carbon transfer to the gas phase began, and only 41 ±4 wt% remained in the char at 700°C. In comparison, for pyrolysis

of a 67% solids black liquor in flowing N_2 for a stationary single-particle reactor, the carbon steadily decreased from 70% at 500°C down to 60 wt% at 700°C (Grace, 1987).

Figure 14 shows a plot of the organic carbon yield in char as a function of temperature for pyrolysis. Equilibrium values obtained using the F*A*C*T program (Thompson et al., 1988) are also included. The agreement between these data appears adequate between 500-600°C. However, at 700°C the experimental data show that about 10% less carbon is found in char than is predicted.

Figure 15 shows that the experimental CO_3^{2-} content in the char agrees with the equilibrium calculations between 500-600°C. The graph also shows that carbonate increases over 150 wt% compared to the amount of carbonate in KBLS. This is comparable to the increase of 120 wt% found by Li and van Heiningen (1990a) for the slow pyrolysis of dry KBLS to a final temperature of 675°C.

Figure 15 also shows that the measured CO_3^{2-} is about 10% lower than the equilibrium predictions at 700°C. The apparent loss of CO_3^{2-} at this temperature is likely due to the decomposition reactions of Na_2CO_3 with amorphous carbon in an inert gas atmosphere above 675°C (Li and van Heiningen, 1990a). In their experiments, the loss of CO_3^{2-} was 11 wt% during the heat-up period in which pyrolysis reactions were also occurring. These reactions also account for up to 1/3 of the decrease in organic carbon at 700°C previously shown in Figure 14. Li and van Heiningen concluded that all the organic sodium compounds in KBLS are converted to Na_2CO_3 during pyrolysis be ,w 675°C.

Douglass and Price (1968) and Blackwell and King (1985) speculated that Na_2CO_3 forms by reaction of NaOH and CO_2 that are released during pyrolysis. Some evidence which supports the possibility of this reaction was obtained in this work. For example, analysis of the KBLS and char for runs at 500 and 700°C showed that the OH^- decreased by 50 wt% during pyrolysis.

Carbon in the fixed gases also remained somewhat constant between 500-650°C, climbing sharply after that until about 40% of the carbon was gasified at 700°C (Table 13). Interestingly, the amount of carbon in the mass balance closure stayed somewhat constant as a function of temperature. This supports the general conclusion presented above for the gross yield of condensables given as mass balance closure (i.e., total mass yield with no reference to composition).

Sodium Balance

Table 13 gives a summary of the sodium balance for pyrolysis experiments. For the runs at 500-550°C, the solid char accounts for all the input sodium in KBLS. The mean sodium content of char varies between 95-96 wt% and the 95% confidence levels overlap completely with that of the input sodium in KBLS.

Between 600-700°C, the data become more difficult to interpret. For instance, the mean sodium content in char varies between 82-87 wt%, indicating a sodium loss between 13-18 wt%. Only the run at 650°C has a 95% confidence level that strongly overlaps with the input KBLS data. The other two runs (i.e., P6 and P8) give some evidence of sodium loss. In run P6, the 95% confidence level for the char and KBLS do not overlap at all. In run P8 at 700°C, the sodium content of char is 78-96 wt% compared to an input KBLS sodium content of 95-105 wt%. In this case only a very small overlap in the 95% confidence level is observed.

Recent literature data suggests that sodium volatilizes during pyrolysis at low temperatures. Li and van Heiningen (1990a) pyrolysed dry KBLS in a TGA with a heating rate of 20°C·min^{-1} in helium to final temperatures between 675-800°C. They found that during the heat-up phase, the sodium loss was between 8-12 wt% for 675-700°C. Frederick and Hupa (1991) found the sodium loss to be about 15 wt% during pyrolysis. Their experiments involved exposing single-drops of 60% solids KBL (i.e., hardwood and softwood kraft) in a gas mixture consisting of 5%CO/95%N_2 at 700°C. They also noted, without explanation, that sodium loss during gasification in CO_2/CO and combustion in air were at least an order of magnitude lower than for pyrolysis.

After pyrolysis is completed, sodium emission from char at low temperature has been explained by Li and van Heiningen (1990a) by the following reactions:

$$Na_2CO_{3\,(s)} + 2\,C_{char} \rightarrow 2\,Na_{(v)} + 3\,CO \qquad (34)$$

$$Na_2CO_{3\,(s)} \rightarrow Na_2O_{(s)} + CO_2 \qquad (35)$$

$$Na_2O_{(s)} + C_{char} \rightarrow 2\,Na_{(v)} + CO \qquad (36)$$

Experimental evidence shows that the presence of CO and CO_2 can suppress the decomposition of Na_2CO_3. However, even at low CO/CO_2 pressures the decomposition may be minimized if sufficient oxygen is present on the carbon surface. As an example, Saber et al. (1986) give data

for K_2CO_3/carbon mixtures at 1050°C which show that as the molar ratio of potassium metal to organic oxygen (i.e., $K:O_{org}$) decreases from 38 to 1, the potassium volatilization decreases from 40 wt% to 7 wt%. This is because potassium vapour forms from K_2CO_3 decomposition and can bind with surface oxygen on the carbon. In Appendix A, the $Na:O_{org}$ molar ratio for char in run P8 (i.e., 700°C) was estimated as 1.3.

Applying this information to the present work, this can be stated. The sodium losses between 600-700°C are expected to be between 8-15 wt% and occur during the rapid pyrolysis reactions of KBLS. Also, the prolonged exposure of char in the fluidized bed should not lead to significant further volatilization of Na. This is because CO/CO_2 gases from pyrolysis are always present in the fluidized bed during a run, and the amount of surface oxygen on carbon is sufficient to bind about 80% of the sodium as surface complexes.

Fixed Gases

The production of gases during pyrolysis can be better understood from a knowledge of the structural units comprising the KBLS. Avni et al. (1985) took the approach used for coal pyrolysis (Smoot and Smith, 1985) and applied it to the study of alkali lignin pyrolysis. At lower temperatures (say 300-500°C), decomposition of the substituted groups and aliphatic structures occurs. This results in the release of CO_2 from carboxyl groups, H_2O from hydroxyl groups, hydrocarbon gases from aliphatic and methoxy groups, and CO from weakly-bound oxygen groups such as aldehydes. Late in the pyrolysis, the rearrangement of the lignin subunits permits H_2 to be evolved from the aromatic hydrogen. Also, additional CO is evolved from tightly-bound oxygen functionalities, such as diaryl ethers and phenols. As this process continues, the char gradually becomes more graphitic.

Results

Time-samples of fixed gases were taken during each run. The molar flow rates of H_2, CO, CO_2, and CH_4 were calculated as the product of the total volumetric flow rate of gases and the concentration of each gas. Figure 16 shows the change in gas compositions as a function of time for pyrolysis run P1. During the first 20 minutes the gas compositions increased rapidly, followed by a period of gradual stabilization. The sudden decrease of gas concentrations after 80 minutes was due to cessation of KBLS feeding. Although the hydrogen concentration appeared to increase further, up to 1 h, this behaviour was more a function of difficulties in

obtaining leak-tight gas samples. In general, the gas compositions tended to be constant after ~0.5 h. Therefore, an average gas flow rate was calculated for each gas in every experiment. The calculation is given in Appendix A for the gas data shown in Figure 40 - Figure 51.

Figure 17 gives the experimental and equilibrium molar yield of H_2, CO, CO_2, and CH_4 for the pyrolysis experiments in the temperature range 500-700°C. Below 650°C, the kinetics of H_2 production are slow and therefore equilibrium is not achieved. At 700°C, an abrupt jump is observed and the experimental data comes to within 3% of the equilibrium value. Bhattacharya et al. (1986) studied the pyrolysis of dry KBLS and also found that the H_2 concentration increased with temperature.

The yield of CO increases with temperature for both equilibrium predictions and fluidized-bed experiments. Experimentally, the CO yield doubles between 500-650°C, but is far from equilibrium. Although the experimental data approaches the equilibrium calculations at higher temperatures, at 700°C the data are still about 30% below the equilibrium yield.

The yield of CO_2 does not vary significantly over the experimental temperature range. However, equilibrium calculations indicate that the CO_2 yield should decrease gradually to ~0.4 mol·kg KBLS^{-1} at 700°C. At this temperature, the observed yield is ~2.5 mol·kg KBLS^{-1} or about 5 times the equilibrium prediction. The CO_2 released during pyrolysis originates mostly from a rapid, irreversible decomposition of carboxyl groups in KBLS. Once formed, the CO_2 may react with H_2 via the water-gas-shift reaction (i.e., $CO + H_2O \Leftrightarrow CO_2 + H_2$) to produce CO and steam. Meijer et al. (1989b) studied the catalytic effect of alkali carbonate in the water-gas-shift reaction. They found that the rate of the forward reaction (i.e., $CO\text{-}H_2O$ ->) is reduced significantly by the presence of CO_2. It was found by experiment that the rate of the reverse reaction (i.e., $CO_2 + H_2$ ->) was several times slower than the rate of the forward reaction. Also, it should be noted that CO_2 will only spend a short time within the fluidized-bed reactor. Based on the above considerations, it is proposed that the reaction between CO_2 and H_2 is too slow to establish equilibrium. This also explains to some extent why the H_2 and CO are lower than the equilibrium predictions.

The pyrolysis of KBLS leads to the production of low-molecular-weight gaseous hydrocarbons, the most prominent being methane (Jones, 1968). Equilibrium and experimental yields for CH_4 show good agreement.

STEAM GASIFICATION OF CHAR CARBON

Total Mass Balance

In this series of experiments, steam was added to the fluidized-bed reactor with an inlet H_2O:solids weight ratio of 1.75:1 (p_{H_2O} = 22 kPa) for temperatures between 500-700°C. The amount of steam was in excess of the stoichiometric requirement for complete gasification of char carbon. At the highest operating temperature of 700°C, run SG1 was performed with half the steam addition, that is a H_2O:solids ratio of 0.87 or $p_{H_2O} \cong$ 10 kPa. The results of these experiments were needed to verify the effect of steam on carbon gasification and the results are plotted in Figure 22. From these data, it is seen that the fixed gas compositions at the intermediate steam pressure are consistent with the other experiments.

Table 13 gives the elemental balance for sodium and carbon between 500-650°C for steam gasification runs SG2, SG4, and SG5. The data for runs SG1 and SG6 at 700°C were not included because bed agglomeration prevented char sampling. It was found that, within experimental error, the sodium in KBLS reported to the char. For the runs at 600-650°C, the mean sodium content in char is also larger than the pyrolysis runs. The reason for this behaviour is not entirely clear. However, it is possible that the addition of steam may lead to the recombination of metallic Na via the reactions:

$$2\,Na + 2\,H_2O_{(v)} \rightarrow 2\,NaOH + H_2 \qquad (37)$$

$$2\,NaOH + CO \rightarrow Na_2CO_3 + H_2 \qquad (38)$$

These reactions were originally proposed by McKee and Chatterji (1978) to explain the catalytic behaviour of alkali carbonates in steam gasification of carbon. An alternate explanation is that the larger H_2O/H_2 ratio in the gas phase, due to steam addition, increases the adsorbed oxygen content near the alkali active sites (Chapter 2). Similar to pyrolysis at 700°C, the $Na:O_{org}$ molar ratio indicates an excess of Na over organic oxygen. By increasing the O_{org} on the char during gasification, more of the excess Na would be bound as surface complexes.

The carbon content in char and gases between 500-600°C is similar to the pyrolysis runs and the addition of steam has little effect. At 650°C, steam gasification of carbon is evident. Comparison between pyrolysis run P7 and steam gasification run SG5 shows a decrease in char

carbon of about 25 wt%. The maximum amount of carbon that reports to the condensables (i.e., mass balance closure) is lower that during pyrolysis for the entire temperature range.

Hydrodynamics and Equilibrium Calculations

The two-phase theory of fluidization (Davidson and Harrison, 1963) has been the basis for many models describing the mixing behaviour of gas and solids in fluidized beds (Yates, 1983). The theory states that the flow of gas in the particulate phase is equal to that at minimum fluidization, and the bubble phase carries the excess flow of gas. This is expressed as,

$$\frac{Q_b}{A} = U - U_{mf} \tag{39}$$

where Q_b is the visible-bubble volumetric flow rate ($m^3 \cdot s^{-1}$), A, the cross-sectional area of the fluidized bed (m^2), U, the superficial gas velocity ($m \cdot s^{-1}$), and U_{mf}, the minimum fluidization velocity ($m \cdot s^{-1}$). In practice, the bubble flow rate is somewhat smaller than predicted by Eq. 39. This is due to a greater flow in the particulate phase and gas flow-through in the bubble phase. Baeyens and Geldart (1986) have given data for a fluidized bed with similar physical properties as that used in the present study. It was found that the ratio of Q_b/A to U-U_{mf} was 0.8. At 650°C, for the fluidized bed in this study, the variables U, U_{mf}, and A are 0.33 $m \cdot s^{-1}$, 0.025 $m \cdot s^{-1}$ and $7.85 \cdot 10^{-3}$ m^2; this gives a Q_b/A ratio of 0.24 $m \cdot s^{-1}$. Therefore, the flow rate through the bubble phase is estimated as 73% (i.e., $\{0.24/0.33\} \cdot 100$) of the total superficial gas flow rate. For 600°C the corresponding flow rate through the bubble phase is calculated as 72%.

Equilibrium calculations were performed with the F*A*C*T program (Thompson et al., 1988) using the feed rates of KBLS and steam (H_2O:solids =1.75) for each run given in Table 30 - Table 35. Examination of Figure 18 - Figure 21 shows that the equilibrium yield for a H_2O: solids ratio of 1.75 is significantly different from the fluidized-bed data. However, based on fluidized-bed hydrodynamics, only about 27% of the input steam enters the dense phase, the remainder by-passes the char particles without contact. Also, the fluidized bed operates as a semi-batch reactor with continuous removal of gases and accumulation of char. Therefore, the apparent H_2O:solids ratio within the particulate phase of the fluidized bed is lower than the inlet value. However, the thermodynamic calculations assume a closed system in which the mixing between inlet steam and KBLS is perfect, and the reactions are allowed to reach equilibrium.

To show the effect of a lower H_2O:solids ratio on the equilibrium predictions, the gas yields for H_2O:solids ratios of 0.73 and 0.39 are also shown in Figure 18 - Figure 21.

Fixed Gases Production

Reaction Stoichiometry

Calculations were performed to estimate the steam conversion in the fluidized bed. The main reactions that describe the stoichiometry for steam gasification are the carbon gasification reaction, Eq. 40, and the water-gas shift, Eq. 41:

$$C_{char} + H_2O_{(v)} \Leftrightarrow CO_{(g)} + H_{2\,(g)} \tag{40}$$

$$CO + H_2O_{\,(v)} \Leftrightarrow CO_2 + H_2 \tag{41}$$

The reaction rates for Eqs. 40, 41, defined as the reaction extents per unit time (Hill, 1977) are ξ_{40} and ξ_{41}, respectively. The effect of added steam at a particular temperature can be quantified by comparing pyrolysis and steam gasification data.

As an example, at 650°C the stoichiometry with or without steam added is shown in Table 14. The change in yield of CO, CO_2 and H_2 between steam gasification run SG5 and the pyrolysis run P7 is taken to be the result of Eqs. 40-41. The average yield (mol i·kg KBLS fed^{-1}) of fixed gas i, Y^{prod}_{i}, for SG5 and P7 were taken from Table 40 - Table 42. The gas production yields are then converted to molar flow rates (mol·min^{-1}) by normalizing with respect to the KBLS feed rate for SG5 (i.e., 0.343 kg·h^{-1}). This was necessary since the actual KBLS feed rates were different for the two runs. In effect, the gas products of pyrolysis run P7 were adjusted to the KBLS feed rate of run SG5. Differences in the gas composition between SG5 and P7 could then be attributed solely to the addition of steam. The measured average molar flow rates of H_2 and CO for SG5 are equated to the stoichiometric products in Table 14, and the reaction rates, ξ_{40} and ξ_{41}, are found to be 0.068 ±0.005 and 0.064 ±0.009 mol·min^{-1}, respectively. The calculated CO_2 flow rate can then be estimated by inserting ξ_{41} into the stoichiometric equation for CO_2 in Table 14.

A comparison of the calculated and measured CO_2 flow rate is shown in Table 15. For SG4 the 95% confidence intervals overlap between calculated and measured CO_2, and for SG5 the difference is within 5%. Therefore, it is concluded that the gas production data are consistent with the stoichiometry given by Eqs. 40, 41.

The steam conversion in the fluidized bed can be determined by summing the reaction rates, ξ_{40} and ξ_{41}, and dividing by the amount of steam added to the fluidized bed. Table 15 gives the results for the steam gasification runs at 600°C and 650°C. It is seen that the steam conversion increases threefold from 7.1 ±3.2% at 600°C to 23.5 ±1.9% at 650°C.

Hydrogen Production

The experimental H_2 yield as a function of temperature is shown in Figure 18 for an inlet H_2O:solids ratio of 1.75:1 (p_{H_2O} = 22 kPa). The yield increased throughout the experimental temperature range. Comparison with pyrolysis (Figure 17) suggests a significant increase in H_2 production starting at around 650°C, from 4.5 ±1.4 to 27.4 ±0.8 mol·kg KBLS^{-1}. Wood et al. (1984) also observed that the alkali-carbonate C-H_2O reaction occurred rapidly above 625°C leading to a higher H_2 yield.

For comparison, results from a batch study by Feuerstein (1966) with a H_2O:solids ratio of 0.55 showed that the yield of H_2 increased from 1 to 3.5 mol·kg KBLS^{-1} between 500-700°C. Jones (1968) continuously injected KBL at a H_2O:solids ratio of 1.22 and found that the H_2 yield at 700°C was 10 mol·kg KBLS^{-1}. Data from a continuous pilot plant using an atomized suspension technique for pyrolysis (Brink, 1976) showed H_2 yields increasing from 1.8 to 12 mol·kg KBLS^{-1} between 500-700°C.

In Figure 18 the calculated equilibrium H_2 yield is given as a function of reactor temperature for various effective H_2O:solids ratios. The equilibrium H_2 content increases only 5-25% at any particular H_2O:solids ratio between 500-700°C. This small increase is due to offsetting effects of the endothermic (ΔH°_{298}= +90.1 kJ·mol^{-1}) carbon-steam reaction, Eq. 40, and the exothermic (ΔH°_{298}= -41.2 kJ·mol^{-1}) water-gas shift reaction, Eq. 41. Between 500-600°C the measured yield is much lower than any of the equilibrium results. Above 650°C the experimental data overlap with equilibrium predictions for H_2O:solids ratios between 0.39-0.73.

Carbon Monoxide Production

The molar yield of CO increased from 1.27 ±0.05 to 4.78 ±1.1 mol·kg KBLS^{-1} between 500-700°C (Figure 19). Compared to pyrolysis in N_2 (Figure 17), adding steam resulted in a CO decrease of about 50% starting at 650°C. By comparison, Feuerstein et al. (1967) found that the yield of carbon monoxide increased slightly from 0.6 at 500°C to 1.0 mol·kg KBLS^{-1} at 700°C. In the range 500-700°C, Jones (1968) reported a constant CO yield of about 1.9 mol·kg KBLS^{-1}

while Brink (1976) presented data in which the CO yield doubled from 1.2 to 2.6 mol·kg $KBLS^{-1}$. In each of these studies the CO production at 700°C was significantly less than in the fluidized bed.

Comparison of the CO data with equilibrium calculations shows that the agreement is poor for all H_2O:solids ratios. An examination of Table 15 shows that the reaction rates, ξ_{40} and ξ_{41}, of the carbon gasification and water-gas shift reactions are identical within experimental error. This implies that most of the CO formed by the carbon gasification, Eq. 40, is converted to CO_2 and H_2 by reaction with steam, Eq. 41. A lower-than-expected production of CO was also observed by Hashimoto et al. (1986) using a TGA system to study the alkali carbonate catalysed C-H_2O reaction (Chapter 2). They found that the rate of CO formation was only 20-30% that of the carbon gasification and much lower than CO_2 formation.

Carbon Dioxide Production

In contrast to the somewhat constant CO_2 production during pyrolysis (Figure 17), the addition of steam shows a sharp increase in CO_2 concentration as a function of temperature (Figure 20). The work of Jones (1968) and Brink (1976) also showed a large increase from 0.2 to 5.0 mol·kg $KBLS^{-1}$ in this temperature range. For the fluidized-bed runs at 700°C, the CO_2 yield for steam and pyrolysis are 12.0 ±0.5 and 2.3 ±0.5 mol·kg $KBLS^{-1}$, respectively.

The increase in CO_2 yield with temperature is contrary to the equilibrium predictions. A high rate of CO_2 production has been observed by Hashimoto et al. (1986) and Wigmans et al. (1983b) for coal and activated carbons, and by Li (1989) for KBL (kraft black liquor) char. Carbon dioxide is produced by two routes during steam gasification. First, CO_2 is a primary product of the heterogenous C-H_2O reaction via Eq. 33 given in the new mechanism proposed in Chapter 2. Therefore, primary CO_2 production should increase with temperature. Second, CO_2 is a product of the water-gas shift, Eq. 41. As noted in the previous section, the reaction rate of the water-gas shift is comparable to that of the carbon gasification. Therefore, since the CO production increases with temperature owing to the C-H_2O reaction, the CO_2 production will in turn increase with temperature due to the rapid kinetics of the water-gas shift.

Water-Gas Shift Reaction

The water-gas shift reaction, Eq. 41, is catalysed by alkali carbonate as discussed in Chapter 2. Figure 23 shows a plot of the equilibrium constant for Eq. 41, $K_{g\prime}$ as a function of

temperature. The equilibrium line was calculated using the F*A*C*T program "EQUILIB". The results compared favourably with data from Smith and van Ness (1975). KBL pyrolysis data from Jones (1968) were included for comparison. The concentrations of H_2, CO, and CO_2 are based on the analyses of the off-gases. The average molar flow rate of each gas (Figure 40 - Figure 51) and the total volumetric flow rate of gases (Table 22 - Table 35) are used to estimate the concentration. For pyrolysis, the steam production rate was taken as 20 wt% of the KBLS feed rate in the range 500-700°C (Feuerstein, 1966), and this varied from 0.055-0.066 mol·min^{-1}. For steam gasification, $[H_2O]$ was calculated from the inlet flow rate (0.55 mol·min^{-1}) after adjusting for the steam consumption, ξ_{40} and ξ_{41}, due to Eqs. 40, 41.

The experimental curves for K_{gs} display a similar trend with respect to temperature. In all cases, K_{gs} increases sharply with temperature between 500-600°C and then remains somewhat constant. It is seen that an increase in the steam partial pressure also leads to an increase in K_{gs}. For both the fluidized-bed pyrolysis runs and Jones' experiments, the experimental K_{gs} curves remain well below the equilibrium predictions between 500-700°C. However, for the fluidized-bed experiments with the addition of steam, the measured K_{gs} approaches the equilibrium predictions between 650-700°C.

Methane Production

The yield of methane was unaffected by either temperature or steam and averaged 1.0 ±0.5 mol·kg KBLS^{-1} (Figure 17 and Figure 21). By comparison, Feuerstein (1966), Jones (1968) and Brink (1976) showed results varying from 0.7 to 1.2 mol·kg KBLS^{-1}.

The calculated equilibrium yield of CH_4 decreases throughout the range 500-700°C (Figure 21). The principal reactions that are known to affect methane formation are:

$$C_{char} + H_2O_{(v)} \Leftrightarrow 1/2\ CO_2 + 1/2\ CH_4 \qquad \Delta H^\circ_{298} = +7.7\ kJ \cdot mol^{-1} \qquad (42)$$

$$C_{char} + 2\ H_2 \Leftrightarrow CH_4 \qquad \Delta H^\circ_{298} = -74.8\ kJ \cdot mol^{-1} \qquad (43)$$

$$CH_4 + H_2O_{(v)} \Leftrightarrow 3H_2 + CO \qquad \Delta H^\circ_{298} = +206.1\ kJ \cdot mol^{-1} \qquad (44)$$

Reaction 42 is thermoneutral and therefore not a strong function of temperature. However, this reaction was found to be catalysed by alkali hydroxide and carbonate at lower temperatures of 200-400°C (Cabrera et al., 1982). The hydrogasification reaction, Eq. 43, and steam reforming, Eq. 44, explain the decrease in methane equilibrium yields with temperature. However, based

on the fluidized-bed data for pyrolysis and steam gasification runs, the influence of these reactions is negligible due to slow kinetics. For example, at 800°C the rate of Eq. 43 is about 1000 times slower than the carbon-steam reaction (Smoot and Smith, 1985). This reaction is catalysed by transition metals (Wood and Sancier, 1984) and not by alkali carbonate (Huttinger et al., 1986). The steam reforming of methane was also not observed in the work of Jones (1968). In fact, catalysis of Eq. 44 is achieved on an industrial scale by using nickel catalysts (Probstein and Hicks, 1982). It is concluded from the results shown that the production of methane is controlled by the pyrolysis of organic matter in KBLS and Eqs. 42-44 are too slow to influence the product distribution.

Carbon Gasification with Steam

Figure 24 gives the yield of organic carbon as a function of temperature and the H_2O:solids ratio for the fluidized-bed experiments and equilibrium predictions. The experimental data show a decrease in organic carbon with increasing temperature between 500-650°C that is well above any of the equilibrium predictions. The gasification rate data for 700°C is not included since the fluidized bed agglomerated and char samples could not be removed immediately after the run.

The global carbon gasification rate in the fluidized bed can be obtained from the experimental data as follows. From the stoichiometric analysis presented in Table 14, the reaction rate, ξ_{40}, is obtained for steam gasification experiments at 600°C and 650°C. Dividing the reaction rate by the total amount of carbon present in the fluidized bed at the end of a run gives an estimate of the specific carbon consumption according to Eq. 40. As an example, at 650°C the total amount of organic carbon in the fluidized bed near the end of run SG5 (i.e., 5.12 ±0.35 mol C) can be obtained as the product: 18.9 ±1.1 g C/100 g char · 330 ±13 g char · 1/12 mol C·g C^{-1} (Table 18, Table 36). Dividing the reaction rate ξ_{40} for SG5 in Table 15 by the total organic carbon gives a global carbon gasification rate of 0.013 ±0.001 min^{-1}. Similarly, the global gasification rate at 600°C is found to be 0.003 ±0.002 min^{-1}.

In a fluidized-bed study by Durai-Swamy et al. (1989), using steam at 101 kPa and 600 μm particles of Na_2CO_3, a carbon gasification rate of 0.01 min^{-1} at 630°C was reported. It should be noted that their rate data include the contribution of both pyrolysis and steam gasification to

the consumption of carbon. Nevertheless, their results are within the range reported for the C-H_2O gasification in this study.

The global carbon gasification rate measured in the fluidized bed can be compared to predictions based on the rate law given by Eq. 28 in Chapter 2. It is assumed that the influence of the C-CO_2 reaction is small since the C-H_2O reaction is over six times faster. The use of Eq. 28 requires the value of the H_2/H_2O ratio in the particulate phase at the surface of the char. A calculation presented in Appendix D shows that the mass transfer of steam to the char surface is several orders of magnitude greater than the gasification rate. Hence, it is reasonable to approximate the ratio of H_2/H_2O at the char surface by that in the bulk fluid of the particulate phase. In addition, based on the results of several studies on laboratory-scale fluidized beds (Yates, 1983), it will be assumed that the gas in the particulate phase is well-mixed. Therefore, the ratio of H_2/H_2O at the exit of the particulate phase may be used in the rate law to calculate the intrinsic carbon gasification rate.

The steam gasification run SG5 at 650°C will be used as an example. The exit H_2 molar flow rate is equal to 0.157 ±0.005 mol·min^{-1} (i.e., 27.44 ±0.83 mol H_2·kg KBLS^{-1} · 0.343 kg KBLS·h^{-1} · 1/60 h·min^{-1}, Table 34 and Table 42). The exit molar flow rate of steam from the particulate phase can be obtained from a steady-state mole balance as follows. The inlet steam flow rate to the particulate phase is taken as 0.151 ±0.005 mol·min^{-1} (i.e., 27% of 0.56 ±0.02 mol·min^{-1}). This results from the division of flow of gases as given by the two-phase theory of fluidization, and ignores the contribution of interphase transport of steam from the bubbles. The consumption of steam (i.e., 0.132 ±0.010 mol·min^{-1}) is given by the sum of ξ_{40} and ξ_{41} in Table 15. Hence, the steady-state exit steam flow rate is calculated as 0.019 ±0.011 mol·min^{-1}. From this information, the exit H_2/H_2O ratio is found to be 8.2 ±4.7, and therefore the intrinsic carbon gasification rate for run SG5 ranges from 0.017 to 0.057 min^{-1}. The low-end of this range is within 20 percent of the measured gasification rate. A similar analysis at 600°C for run SG4 gives a H_2/H_2O ratio of 0.66 ±0.23 at the exit of the particulate phase and an intrinsic rate of 0.004 ±0.001 min^{-1}. This is in excellent agreement with the measured rate of 0.003 ±0.002 min^{-1}.

The above analysis indicates that the carbon gasification with steam is kinetic-controlled between 600-650°C in the fluidized bed used in this study. To provide further support for this

finding, a calculation is included in Appendix D which shows that the mass transfer of steam to the char is several orders of magnitude larger than the gasification rate at these temperatures.

CHAR BED DEFLUIDIZATION

Introduction

Experimental results showed that defluidization occurred at 700°C for experiments in which steam was added to the reactor. Visual examination of the reactor at room temperature showed that channels had formed within an agglomerated bed. Interestingly, defluidization has also been observed commercially in a fluidized-bed combustor at the Domtar Fine Paper mill in Cornwall, Ontario. Niderost (1977) reported that agglomeration could be prevented if the operating temperature was kept below 685°C. This fluidized bed operated in the combustion mode and produced Na_2SO_4-Na_2CO_3 pellets containing no carbon and an off-gas consisting of CO_2, steam and SO_2.

To properly scale-up the fluidized-bed process, it appears useful to better understand the factors that promote defluidization. In the following sections it is shown that the degree of carbon gasification is a critical variable in the performance of a fluidized bed at 700°C.

Factors Influencing Agglomeration

A brief overview on the topic of particle agglomeration can be found in Klinzing (1981). Agglomeration can be defined as an irreversible combination of particles by chemical forces varying from 40-400 kJ/mol. Some factors that influence this behaviour in particle systems are: the type of particle-particle interactions, shape, size, surface morphology, and stickiness. For sticky particles, the mechanisms that lead to agglomeration are usually either solid bridging or liquid bridging. Solid bridging is a direct fusion of the particles at contact points due to melting, solid diffusion, chemical reaction or crystallization. Liquid bridging involves a continuous liquid film contact between particles.

Particles in the dense phase of a fluidized bed are close to each other since the void fraction is typically only about 20% greater than the fixed bed case. Therefore, the frequent collisions among particles lead to the excellent heat transfer characteristics of a fluidized bed. Unfortunately, this property also limits the utility of fluidized beds for processing particles that

have sticky surfaces (Gluckman et al., 1976). A knowledge of the factors that lead to sticky behaviour in such systems is crucial.

A detailed examination of the char particle surface using a scanning electron microscope (SEM) was initiated to determine whether solid or liquid bridging was responsible for agglomeration.

Surface Morphology of Char-Alumina

Figure 25a shows an example of the surface texture of an uncoated alumina particle at 1100X magnification. The surface appears smooth and non-porous and is typical of the particles examined.

Figure 25(b-c) show two characteristic regions of alumina particles coated with char for pyrolysis experiments at 500°C. A needle-like char structure is present in micrograph (b). The surface in micrograph (c) contains clumps of char about 10 μm in diameter. Interspersed among these are circular patterns with shiny edges that may represent regions of gas evolution. These two surface patterns are typical for most of the samples examined.

Figure 25d shows an example of a char-alumina surface for a pyrolysis experiment at 600°C. The needle-like structure is more pervasive and the needles are generally both thicker and longer than at the lower temperature. At the highest temperature of 700°C (Figure 25e-f) the surface of the particles is more uneven and some localized fusion of the needles seems to have occurred.

Figure 26a shows a portion of a char-alumina particle for steam gasification at 600°C. The needle-like structure is again very evident. At 650°C, two separate surface textures are apparent. In Figure 26b the needle-like structure has collapsed and certain regions appear fused. For the region in Figure 26c, the needles are absent but definite localized melting of small char clumps has occurred. At 700°C, the surface texture is seen to be composed of a matrix of rod-shaped char fragments with varying degrees of surface melting (Figure 26d). Comparison of particle surfaces at 700°C for pyrolysis and steam gasification (Figure 25d versus Figure 26d) shows a significantly different surface texture. The latter has a smoother surface and the char appears as a well-defined series of partially-melted rods.

It is evident from the micrographs presented that the surface of the char-alumina was not completely molten for any of the experiments at 700°C. Therefore the agglomeration was likely

due to solid bridging. The following sections will discuss the effect of composition on the stickiness of the char, and propose an explanation for the difference between the surface textures at 700°C for pyrolysis and steam gasification.

Char Composition

Table 16 gives the composition of the inorganic fraction of the char for both pyrolysis and steam gasification runs. The data for sulphur ions were not included in run SG6 because proper quenching of these reactive species was not possible due to bed agglomeration.

For the runs P1, P8, and SG6, the char was analyzed for inorganic-bound hydrogen as OH^- and the data included as a footnote to the table. Grace et al. (1985) and Li (1989) gave data on the total elemental hydrogen content of char in the range 0.5-0.7 wt%. The present study found that between 0.04-0.2 wt% hydrogen reported as OH^- in char. The organic hydrogen content of char is the difference between these two quantities and is difficult to measure directly. Qualitative identification of this hydrogen was made with GC-MS by Alberta Sulphur Research (Lesage, 1991). Five grams of char-alumina were extracted with 10 mL methylene chloride and concentrated to a volume of 100 µL. A 5 µL sample was analyzed by GC-MS. The mass spectra showed aliphatic hydrocarbons (i.e., pentacene, decane, 6-ethyl-2-methyl octane), aromatics (i.e., ethyl benzene, 1,2- dimethyl benzene), and phenolic groups (i.e., 4-phenoxy phenol).

Within the precision of the analytical technique, the potassium concentration remains constant for all runs. Potassium originates from the wood. The chloride concentration is generally below 2 mol% in all runs. The chloride content of KBLS is a function of the Cl^- content from water used in the digesters and dissolving tanks in the kraft mill. Coastal mills have larger Cl^- content in KBLS because of this. The amount of OH^- is in the same range as K^+ and Cl^- and therefore needs to be considered in the following analysis. The inorganic sulphur ions SO_4^{2-} and S^{2-} vary as a function of reactor temperature. At 700°C, where agglomeration was observed, the sulphide form was predominant.

The inorganic ions form an array of compounds including: Na_2CO_3, K_2CO_3, Na_2SO_4, K_2SO_4, Na_2S, K_2S, NaCl, KCl, NaOH and KOH. However, over 90 mol% of this mixture is Na_2CO_3. X-ray diffraction analysis was attempted to try to resolve the various compound concentrations but interference from the alumina substrate prevented quantification. Also, Tran et al. (1989) observed that x-ray diffraction analysis of recovery boiler deposits (not containing alumina) does

not yield useful results for the compounds of minor elements, such as chloride and potassium. This is due partly to their tendency to form solid solutions.

Influence of Melting of Inorganic Salts

The type and quantity of inorganic compound present in the char affects the melting properties of the mixture. Table 17 shows the temperature, T_{first}, at which liquid first appears for binary and ternary systems containing the major inorganic ions in char. Systems that do not contain either Cl^- or K^+, generally begin to melt at 715°C or above. Noting that the amount of SO_4^{2-} in the char is negligible at 700°C, then the addition of Cl^+ and K^- lowers T_{first} to between 588-598°C. These temperatures correspond to the eutectic of the K_2Cl_2-Na_2CO_3 binary and Na_2S-Na_2CO_3-NaCl ternary system, respectively. The presence of NaOH further decreases the first melting temperature to 280°C. As a first approximation, these diagrams illustrate the significant effect of Cl^-, K^+ and OH^-.

Isaak et al. (1985) studied the ternary system Na_2SO_4-Na_2CO_3-Na_2Cl_2 and found that T_{first} determines the beginning of particle adhesion but the amount of liquid phase controls the stickiness. The amount of liquid phase present is a function of mixture composition and temperature. At a molar ratio Na_2SO_4:Na_2CO_3 between 1.5-4.0, they observed that the addition of Na_2Cl_2 lowered T_{first} by 200°C. Also, as the concentration increased from 2-15 mol%, the amount of liquid increased to about 50 wt%.

For inorganic deposits in recovery boilers, Tran (1986) proposed that a minimum amount of liquid phase (typically 10-20 wt%) was necessary to cause stickiness. Also, he constructed a sticky-temperature diagram for Na_2CO_3:Na_2SO_4 mixtures with added K^+ and Cl^-. For Na_2SO_4-Na_2CO_3-Na_2Cl_2, as the Cl^- increases from 0-5 mol% the sticky temperature decreases from 812°C to 600°C. It was found that once the concentration of Cl^- reached 1 mol% then T_{first} was not lowered further. However, for $T>T_{first}$ the Cl^- content changed the amount of liquid present. The K^+ content also lowered T_{first} but its effect on the amount of liquid was small. The concentration units used above follow the terminology of Tran et al. (1989) as Cl/(Na+K) or K/(Na+K) in mol%.

Backman et al. (1986) performed thermodynamic calculations for a system containing Na_2SO_4-Na_2CO_3-Na_2S-NaCl. He found that as the Na_2S content increased from 0-10 wt%, the amount of liquid increased from 8-25 wt%: assuming equal proportions of Na_2SO_4 and Na_2CO_3.

For the present work the amount of K^+ and Cl^- was recalculated in the units suggested by Tran et al. (1989) and is shown in Table 18. The amount of these minor elements is high enough to lower T_{first} to below 700°C. The amount of liquid present is difficult to estimate but is apparently sufficient to cause catastrophic defluidization. However, it is not obvious from this analysis why the pyrolysis run P8 did not exhibit defluidization compared to SG6 and SG1, since the amounts of Cl^- and K^+ were similar in these runs.

Effect of Organic Carbon

Table 18 includes data for the organic carbon content of the char for various runs. The data for those runs where defluidization occurred (SG1 and SG6) are estimated. It is seen that the two experiments that were performed at 700°C with steam addition led to chars with organic carbon contents of 12.8 ±5.5 and 19.0 ±2.4 wt%. The comparable organic carbon content for a non-agglomerating pyrolysis run P8 was 24.3 ±1.8 wt%. It is postulated that a minimum carbon content in the char of about 25 wt% is required to keep the bed from agglomerating.

The carbon may decrease the proportion of exposed surface occupied by sticky inorganic salts, or change the surface tension. The latter property would reduce the spreading of salts over the char surface. However, it is seen that the surface texture of char will be greatly changed by the quantity of organic carbon present as seen by comparing Figure 25e,f and Figure 26d. The pyrolysis sample has a higher carbon content and the surface is more porous, while that of the steam gasification run seems smoother and with more noticeable melting. Based on this information, it is probable that agglomeration was a result of bridging due to localized melting of inorganic salts on the char surface.

It is also of interest to note that as the amount of steam added to the reactor increased, the time to defluidization decreased. For the H_2O:solids weight ratio of 1.75:1 (run SG6), the defluidization occurred at 65 min of operation. At a ratio of 0.7:1 (run SG1) the time increased to 90 min. Finally, for no steam addition the operation ran without defluidization and a planned shut-down was made after 2 h. These results suggest that the time to defluidization is also a function of the carbon gasification rate.

CONCLUSION

From the total mass balance of sodium for the processing of KBLS in N_2, there is evidence of an 8-15 wt% volatilization between 600-700°C. The volatilization occurs only during the initial rapid pyrolysis of the particles and is similar to the sodium loss reported by Li and van Heiningen (1990a) during the heat-up period of KBLS in a TGA. However, the prolonged exposure of KBLS char in the fluidized bed does not appear to lead to further significant volatilization of sodium. This is due to the presence of CO/CO_2 gases in the reactor and to the high oxygen content on the carbon that binds about 80% of the sodium as surface complexes.

The addition of steam to the fluidized bed suppresses the volatilization of sodium metal between 600-650°C. Two explanations are proposed to account for this behaviour. First, the steam could combine with sodium to form NaOH that subsequently reacts with CO to form Na_2CO_3. Second, the larger H_2O/H_2 ratio in the gas increases the adsorbed oxygen on the char thereby binding more sodium to the surface.

The increase in CO_2 production with temperature during steam gasification is contrary to equilibrium predictions. This temperature dependency could be explained by the fact that CO_2 is produced by two routes during steam gasification. First, CO_2 is a primary product of the heterogenous C-H_2O reaction via Eq. 33 given in the new mechanism proposed in Chapter 2. Therefore, primary CO_2 production should increase with temperature. Second, CO_2 is also a product of the water-gas shift, Eq. 41, which has a reaction rate comparable to that of the carbon gasification. Therefore, since the CO production increases with temperature owing to the C-H_2O reaction, the CO_2 production will in turn increase with temperature due to the rapid kinetics of the water-gas shift.

The global gasification rate of carbon using steam in a fluidized bed is similar in magnitude to that predicted by a known intrinsic rate law for the gasification of KBLS char. It is proposed that the surface reaction between C-H_2O controls the overall gasification for the conditions in this work. However, using a kinetic rate law for the prediction of reactor performance in an industrial plant is difficult. This is because the laboratory scale mixing patterns of gas/solids cannot be scaled-up with sufficient confidence to a commercial unit (Bolthrunis, 1989). Therefore assumptions would need to be made about the mixing behaviour of the gas in the large-scale

fluidized bed. Hence, further pilot plant work will be necessary to successfully commercialize the low-temperature fluidized-bed recovery process.

The defluidization behaviour at 700°C indicates the practical limitations of fluidized beds for processing KBLS. Localized melting of the inorganic salts is the main cause of char agglomeration. However, if an organic carbon concentration above 25 wt% is maintained in the char, catastrophic defluidization may be avoided. In commercial plant operation it is further recommended that larger particles and higher fluidization velocities be used to further reduce the agglomeration tendencies of sticky particles, as mentioned by Gluckman et al. (1976). This would necessitate the use of a fast-fluidized bed for processing KBLS.

CHAPTER 5

SULPHUR DISTRIBUTION DURING FLUIDIZED-BED PROCESSING OF DRY KRAFT BLACK LIQUOR SOLIDS

ABSTRACT

This chapter presents the results of an original study dealing with the pyrolysis and gasification of dry kraft black liquor solids in a fluidized bed of alumina particles. For pyrolysis in N_2, a total mass balance over the temperature range 500-700°C showed that (a) the retention of sulphur in the solid char product increased from 60 ±11 wt% to 91 ±8 wt%, (b) the production of sulphurous gases (H_2S, CH_3SH, and $(CH_3)_2S$) decreased gradually from 34 ±2 wt% to 4 ±1 wt%, (c) the maximum amount of sulphur in the condensables was in the range ±10 wt%.

Between 500-550°C, the major sulphur compounds in the char were Na_2SO_4, Na_2SO_3, and Na_2S, in decreasing order. The quantity of Na_2SO_3 in the char was attributed to the decomposition of sodium thiosulphate, which was present in the kraft black liquor solids. Between 600 and 700°C, the reduction of Na_2SO_4 and Na_2SO_3 by carbon and CO/H_2 lead to an increase in the production of sodium sulphide. The reduction efficiency in the fluidized bed was 99.1 ±11.4% at 700°C, and comparable to the conventional recovery boiler efficiency of over 90%.

The addition of steam was responsible for the increase in volatilization of H_2S above 600°C, due to reaction between Na_2S and steam/CO_2. The emission rate of H_2S was estimated for the fluidized-bed runs and compared to TGA work in the literature. Between 650-700°C, it was found that the H_2S emission in the particulate phase of the fluidized bed was in equilibrium with the product gases. The results imply that sulphur volatilization could reach unacceptable levels in commercial gasification systems employing steam as part of the fluidizing medium.

INTRODUCTION

The recovery of the pulping chemical sodium sulphide is a key step in the commercial success of kraft pulping. To displace the conventional recovery boiler, an alternative fluidized-bed recovery process must therefore accomplish this objective in a more reliable and economic manner. As mentioned in Chapter 1, patents and process flowsheets for alternative recovery methods have appeared in the literature yet no commercial operation presently exists. An adequate assessment of fluidized-bed alternatives is difficult due to the lack of reliable data on the recovery of sulphur in such systems. A key objective of this study was to evaluate the feasibility of using a low-temperature fluidized bed to recover sulphur as Na_2S.

The sulphur distribution in the fluidized-bed pilot plant is a complex function of several variables. The most important are the initial forms of sulphur and organics in kraft black liquor solids (Strohbeen, 1981), the steam content in the reactor (Fallavollita et al., 1987), the heating rate and particle size of kraft black liquor solids (Cantrell, 1988), the particle temperature, and gas-solids mixing (Bjorkman, 1968). In this work the temperature and steam:solids weight ratio were the principal parameters investigated.

TOTAL SULPHUR MASS BALANCE

Introduction

The pilot plant fluidized bed was operated continuously with respect to gas flow while the char product accumulated during a run. To obtain a total sulphur balance, one needs to know the input sulphur content of kraft black liquor solids (KBLS), the total sulphur content of the char after an experiment, and that of the gases produced during an experiment. The results are listed in Table 19, in terms of sulphur content of the total input of KBLS. The raw data and calculation details for the total sulphur balance can be found in Table 22 - Table 35 and Appendix A, respectively.

As can be seen from Table 19, for all eight runs except P4, the total sulphur mass balance is closed within an experimental error of about 10% absolute. This is good considering the complicated nature of the char-alumina product and the necessity to have a complete analysis of the volatile sulphur species. As noted in Chapter 4, the pyrolysis condensables were not measured directly. The calculated "mass balance closure" values shown in Table 19 implicitly

include the total sulphur in the condensables. The data show that the maximum sulphur content in the condensables varies only slightly with temperature and steam addition for the conditions of this study. Pyrolysis of dry KBLS in N_2 resulted in a maximum sulphur yield in the condensables of 1 ±11 wt% at 500°C and 5 ±8 wt% at 700°C. With steam addition, the range was -3 ±6 wt% at 500°C to 0 ±8 wt% at 650°C. These data are consistent with direct measurement of the condensables from several other studies. Feuerstein (1966) reported that the condensables sulphur was constant at 5 wt% of input sulphur between 500-700°C. Brink et al. (1967) presented data which showed that sulphur in the condensables was about 3% of input sulphur. Jones (1968) found that the sulphur in pyrolysis liquids did not exceed 1 wt%.

Distribution of Total Sulphur in the Char and Product Gas

For pyrolysis of dry KBLS in N_2, the total amount of sulphur that reported to the char increased from 60 ±11 wt% at 500°C to 91 ±8 wt% at 700°C (i.e., runs P1 and P8, respectively, in Table 19). Between 500-550°C, approximately 40 wt% of the sulphur present in KBLS reported to the gas phase. For each successive increase of 50°C between 600-700°C, the amount of gaseous sulphur was roughly halved. At 700°C, the gas contained 4 ±1 wt% of the input sulphur.

Experiments were also performed with the addition of steam to the fluidizing N_2 at an inlet H_2O:solids weight ratio of 1.75 (p_{H_2O} = 22 kPa). For runs at 500, 600 and 650°C, Table 19 shows that the total yield of sulphur in the char increased from 49 ±3 to 67 ±8 wt%. In comparison with pyrolysis runs, the addition of steam showed a decrease in total sulphur retention in the char throughout the temperature range. Specifically, for the runs at 600 and 650°C the char sulphur decreased by 30%. Correspondingly, about 55 wt% sulphur was volatilized at 500°C, decreasing to 33 ±2 wt% at 650°C. Since the fluidized bed agglomerated at 700°C, char samples could not be obtained immediately after an experiment to allow a sulphur mass balance. However, time-sampled sulphur gas analyses were obtained and are reported in a later section.

Several studies dealing with pyrolysis of kraft black liquor (KBL) in N_2 atmospheres have been published. Using a strong black liquor (65 wt% solids), Grace (1987) showed data for a single-particle reactor operating in the range 300-1100°C. The total sulphur in the gas peaked within the interval 550-650°C and then decreased steadily with increasing temperature. The volatilized sulphur decreased from 27 to 15 wt% of the input KBL sulphur, as the temperature

increased from 600 to 750°C. Jones (1968) continuously injected a weak black liquor (40 wt% solids) into a heated cylindrical vessel over the temperature range 450-1100°C. The char sulphur yield was 26 wt% at 580°C and increased to 40 wt% at 700°C while sulphur in the gases showed a corresponding decrease from about 80 wt% to 55 wt% of input sulphur. Feuerstein et al. (1967) gave sulphur balance results for batch pyrolysis using slow heating (5°C/min) of a strong black liquor (60 wt% solids). The sulphur yield in char decreased slightly from 26 wt% at 500°C to about 20 wt% at a final temperature of 700°C. Correspondingly, the sulphur in the gases increased from 56 to 63 wt%. A recent study by Harper (1989) examined the volatilization of sulphur from mixtures of soda liquor and the major inorganic sulphur compounds; Na_2S, $Na_2S_2O_3$, Na_2SO_3, and Na_2SO_4. For the compounds that released sulphur during pyrolysis, namely Na_2S and $Na_2S_2O_3$, it was found that 40 wt% sulphur volatilization occurred at 450-500°C, decreasing to 7-13 wt% at 700°C.

Except for Harper's data, the amount of sulphur retention in char for these studies was lower than the present work. This may be the result of differences in black liquor composition and the gas-solids mixing pattern in the reactor. No systematic study exists on the effect of black liquor composition on the recovery of sulphur in char. However, the initial form of sulphur in KBLS is a major factor in determining the distribution of sulphur during pyrolysis and steam gasification. Also, with adequate mixing of char and gases, the sulphur released as H_2S during pyrolysis can recombine with Na_2CO_3 in the char to form Na_2S. This reaction is favoured at higher temperatures. The intimate mixing of product gases and char in the particulate phase of the fluidized bed would enhance this recombination reaction. In the other studies, the KBL char and product gases were quickly separated after pyrolysis, and the recombination of H_2S was not as favourable as in the fluidized bed.

DISTRIBUTION OF SULPHUR SPECIES IN KBLS CHAR

A principal objective of this work was to explain the sulphur product distribution in the fluidized bed. This was done by considering the chemical transformations of sulphur in the KBLS due to pyrolysis and steam gasification. Specifically, the transformations of the various forms of sulphur are considered as a function of the operating temperature, inlet H_2O:solids weight ratio, and char residence time. To assist in the interpretation of the experimental data,

it is useful to summarize the sulphur composition of KBLS. About 80 wt% of the sulphur was accounted for by the sodium salts of $S_2O_3^{2-}$ (50.89 ±3.36 wt%), SO_4^{2-} (23.95 ±1.40 wt%), and S^{2-} (5.98 ±0.62 wt%). Less than 0.06 wt% was bound as elemental sulphur, while SO_3^{2-} and S_x^{2-} were not quantifiable. The remaining 20 wt% of sulphur was bound to the organic matrix of KBLS.

Decomposition of Sodium Thiosulphate

Sodium thiosulphate ($Na_2S_2O_3$) accounts for over 50 wt% of the sulphur in KBLS. This compound is formed during the mill practise of weak black liquor oxidation (Grace, 1977). Analyses of fluidized-bed char samples showed that $S_2O_3^{2-}$ was not detected between 500-600°C (runs P1-P6, SG2 and SG4 in Table 39). At the higher operating temperatures of 650-700°C (runs P7, P8, and SG5 in Table 39) about 4 wt% of the input sulphur in KBLS reported as $S_2O_3^{2-}$ in the char.

It is not likely that thiosulphate exists in the char at 650-700°C. This is because thiosulphate decomposes completely below 500°C (McAmish and Johnston, 1976: Ahlgren et al., 1967: Kubelka and Votoupal, 1957). Instead, it is suggested that the source of $S_2O_3^{2-}$ was the air oxidation of S^{2-} during analysis of aqueous char samples at room temperature, according to the reaction:

$$Na_2S_{(aq)} + O_2 + 1/2\ H_2O \rightarrow 1/2\ Na_2S_2O_{3\ (aq)} + NaOH_{(aq)} \qquad (45)$$

Supporting evidence comes from the observation that the thiosulphate level increased with storage time before injection to the ion chromatograph. Therefore, the sulphur data for the runs P7, P8 and SG5, displayed in Table 20 and Figure 29, include both the measured S^{2-}, and the amount of S^{2-} that was oxidized to $S_2O_3^{2-}$.

The reactions that lead to the disappearance of $S_2O_3^{2-}$ during low-temperature fluidized-bed processing of KBLS are complex and not completely understood. For pure $Na_2S_2O_3$ in an inert atmosphere, McAmish and Johnston (1976) have found that the reaction half-life was 8 s at 450°C with a stoichiometry given by:

$$4\ Na_2S_2O_3 \rightarrow 3\ Na_2SO_4 + Na_2S_5 \qquad (46)$$

with the individual reaction steps (Ahlgren et al., 1967);

$$4\ Na_2S_2O_3 \rightarrow 4\ S^{\circ} + 4\ Na_2SO_3 \qquad (47)$$

$$4\ Na_2SO_3 \rightarrow 3\ Na_2SO_4 + Na_2S \qquad (48)$$

The alkali polysulphide, Na_2S_5, is formed by the reaction of elemental sulphur and sodium sulphide. With a melting point of 252°C (Blackwell and King, 1985) this compound would be a liquid at the temperatures used in this study.

The reaction products from pyrolysis of $Na_2S_2O_3$, whether in KBL or mixed with model organic compounds, are more varied than shown by Eq. 46. Clay et al. (1987) noted the formation of elemental sulphur and Na_2SO_3 from the pyrolysis of KBL droplets in inert and oxygen-bearing atmospheres. Strohbeen (1981) studied the slow pyrolysis (10°C/min) of mixtures of KBL model organic compounds with pure $Na_2S_2O_3$ below 500°C in nitrogen. Reaction with sodium gluconate and vanillic acid resulted in chars containing a wide concentration variation for the sulphur species. For example, one of the experiments gave these results: 45-60 wt% S^{2-}, 17-45 wt% S_x^{2-}, 5-20 wt% bound sulphur, and 3-5 wt% SO_4^{2-}. In addition, between 25-40 wt% of the KBLS sulphur was volatilized as reduced sulphur gases including H_2S, SO_2, CH_3SH and $(CH_3)_2S$. Harper (1989) also observed a maximum sulphur release of 40 wt% at 450°C, decreasing to 13 wt% at 730°C.

Reduction of Sodium Sulphate

The feed kraft black liquor solids (KBLS) contained sodium sulphate that originated mostly from recycled precipitator dust and make-up sulphur in the kraft process. Approximately 25 wt% of the total sulphur in KBLS was bound as SO_4^{2-}.

The yield of SO_4^{2-} in the char product is plotted in Figure 27a as a function of temperature for pyrolysis (H_2O:solids = 0.05) and steam gasification (H_2O:solids = 1.75). The SO_4^{2-} content (95% confidence interval) of KBLS is denoted by the dashed horizontal band. Thermodynamic calculations performed with the F*A*C*T program predict that Na_2SO_4 would not be present at equilibrium in either pyrolysis or steam gasification. The experimental data therefore suggest that the presence of sulphate between 500-650°C is due to slow reduction kinetics. Figure 27b shows a plot of the wt% SO_4^{2-} reduced versus temperature together with the mean residence time of the char.

Pyrolysis in Nitrogen

The SO_4^{2-} yield at 500°C is within 5% of the input sulphate content of KBLS. Duplicate runs at 550°C show that the experimental data overlap with the input SO_4^{2-}. At 600°C, the yield of sulphur as SO_4^{2-} drops sharply to between 5-9 wt% based on duplicate runs. For these

experiments, the mean char residence times are 63 and 70 min, with SO_4^{2-} reduction in the range 57-81 wt% (95% confidence interval). A further large decrease in yield to 1.0 ±0.4 wt% is observed at 650°C. In this run the mean residence time is slightly lower (i.e., 56 min) and the sulphate reduction is 95 ±8 wt%. With an operating temperature of 700°C, only 0.3 ±0.2 wt% of the input sulphur reports as sulphate in the char. The corresponding sulphate reduction is 98 ±8 wt%, for a mean char residence time of 62 min.

From these results, it is seen that SO_4^{2-} is stable during pyrolysis in the temperature range 500-550°C. This supports the data of Harper (1989) for the rapid pyrolysis of a mixture of Na_2SO_4 and soda liquor in a nitrogen atmosphere. However, in interpreting the results it is important to note that some SO_4^{2-} could be formed due to thiosulphate decomposition. For example, the pyrolysis of model compounds with sodium thiosulphate showed that about 2.5 wt% of the input sulphur reported as SO_4^{2-} in the char (Strohbeen, 1981). Also, the work of Ahlgren et al. (1967) with pure sodium thiosulphate showed that ~38 wt% of the sulphur was found as SO_4^{2-}, with the remainder as sodium polysulphide (Eq. 46). Recalling that about half the sulphur in the feed KBLS is $S_2O_3^{2-}$, the yield of SO_4^{2-} owing to $S_2O_3^{2-}$ decomposition would be, respectively, 1 wt% (Strohbeen, 1981) and 19 wt% (Ahlgren et al., 1967). Clearly, the yield change predicted by Strohbeen is within the range of experimental error in this work and cannot be confirmed. However, the large SO_4^{2-} increase predicted by Ahlgren's work is not observed. Therefore, it is concluded that the stoichiometry of Eq. 46 does not describe the decomposition of thiosulphate for the pyrolysis of KBLS in a fluidized bed of alumina particles.

The decrease in sulphate yield at 600°C coincides with a large increase in S^{2-} yield as shown in Figure 29. This indicates that Na_2SO_4 is at least partly converted to Na_2S during pyrolysis. The onset of sulphate reduction at this temperature confirms the data of Li (1986) for KBLS char (i.e., 610°C), and Kubelka and Hojnos (1956) for pure Na_2SO_4 mixed with carbon (i.e., 600-630°C). The reduction of Na_2SO_4 to Na_2S can be accomplished by reaction with carbon, H_2 or CO (Li, 1989: Li and van Heiningen, 1988: Nguyen, 1984: Kubelka and Hojnos, 1956: Nyman and O'Brien, 1947). The overall reactions are as follows:

$$Na_2SO_{4\,(s)} + 4C \rightarrow Na_2S_{(s)} + 4CO \quad (49)$$

$$Na_2SO_{4\,(s)} + 2C \rightarrow Na_2S_{(s)} + 2CO_2 \quad (50)$$

$$Na_2SO_{4\,(s)} + 4H_2 \rightarrow Na_2S_{(s)} + 4H_2O_{(v)} \quad (51)$$

$$Na_2SO_{4\,(s)} + 4CO \rightarrow Na_2S_{(s)} + 4CO_2 \qquad (52)$$

The magnitude of the sulphate reduction between 600-700°C was compared with the predictions of a kinetic rate law for sodium sulphate reduction by carbon reported in Li (1989). For reaction times ranging from 40-70 min, the calculated sulphate reductions at 600°C, 650°C, and 700°C are 0-0.2 wt%, 3-10 wt%, and 79-99 wt%, respectively. The results for 700°C agree well with the fluidized-bed data. However, at 650 and 600°C, the fluidized-bed reduction data are one and two orders of magnitude higher, respectively, than predicted by Li's rate law (Figure 27a, b).

The higher reduction rates in the fluidized bed at 600-650°C are due to several factors. First, Li's reduction rate data did not include experiments where Na_2S was present at the start of reduction. The fluidized-bed char contained Na_2S at the start of sulphate reduction at 600°C since 10-15 wt% S^{2-} yield was found at the lower temperatures of 500-550°C (Figure 29). It is known that sodium sulphate reduction by either carbon or the fixed gases CO/H_2 is autocatalytic in Na_2S (Li, 1989). Also, the rate determining step is thought to be the reaction between Na_2SO_4 and Na_2S to form a reactive intermediate, possibly a liquid polysulphide (Birk et al., 1971). The initial amount of Na_2S in the char would therefore lead to a higher sulphate reduction. Second, the C/SO_4^{2-} molar ratio in the char strongly influences the reduction rate. Data from Li (1989) showed that the reduction half-life decreased from 27 min to 9 min for an increase in the molar ratio C/SO_4^{2-} from 2.8 to 17. The rate law used by Li is only valid for a C/SO_4^{2-} of 2.8. In the fluidized-bed char, this ratio is ~22, based on the data for char at 550°C. Third, the presence of CO (1-5 vol%) and H_2 (5-20 vol%) in the fluidized bed increases the reduction rate according to Eqs. 51, 52. However, the effect will be minor compared to carbon reduction. For example, at 700°C, a 95 wt% reduction of Na_2SO_4 was obtained with carbon (C/SO_4^{2-} = 17 mol/mol) within 0.5 h. This compares to 10 wt% reduction with a 50 vol% CO mixture (Li, 1989) and 15 wt% reduction with 100 vol% H_2 (Kunin and Kirillov, 1968).

Gasification in Steam/Nitrogen

With the addition of steam to the reactor (H_2O:solids = 1.75) the Na_2SO_4 yield also decreased with temperature. However, the data for 600-650°C were higher than for the pyrolysis runs (Figure 27a). The sulphate reduction was 12-25% at 600°C and 82-85% at 650°C (Figure 27b).

The decrease in sulphate reduction with the addition of steam at 600°C, and to some extent at 650°C, was due to several factors. First, the residence time for steam gasification (43 min) at 600°C was 50% shorter than for the pyrolysis case (~67 min). Second, the lower Na_2S content at 600 and 650°C during steam gasification, compared to pyrolysis (Figure 29). Third, the effect of steam addition in lowering the H_2/H_2O and CO/CO_2 ratios in the fluidized bed, and thereby influencing Eqs. 49-52. Some supporting evidence for this is the retarding effect of CO_2 on Eq. 52 as noted by Li (1989).

Formation and Decomposition of Sodium Sulphite

In Figure 28 the yield of SO_3^{2-} in the char is plotted as a function of temperature and the inlet H_2O:solids ratio. The mean residence time (min) of the char for each run is shown in brackets. Since the amount of sulphite in the feed KBLS is negligible (Table 10), it is concluded that sulphite is a major product of low-temperature processing of KBLS.

The magnitude of the sodium sulphite yield is unexpected. The only other work in which any sodium sulphite formation was reported was that of Clay et al. (1987). They studied the early in-flight processes of KBL droplets during pyrolysis and combustion with O_2 (i.e., 0, 10, 21% in N_2). A sodium sulphite increase of 52 ±32 wt% was observed, based on the Na_2SO_3 content of input KBLS. The sulphite formation varied inversely with the water content in KBL and reactor temperature, but O_2 had no effect. The authors did not provide explanations for the sodium sulphite formation.

For pyrolysis (H_2O:solids = 0.05), the quantity of sulphite in the char decreased markedly with temperature. It ranged from a high of 23 ±2 wt% at 500°C, down to less than 0.1 wt% at 700°C. For experiments at 550°C and 600°C, duplicate runs indicated that an increase in mean residence time of about 16% led to a decrease in the SO_3^{2-} yield. For steam gasification runs (H_2O:solids = 1.75) at 500°C and 650°C, the sulphite yield was the same as the pyrolysis runs. However, at 600°C, the SO_3^{2-} yield was several percent lower than for pyrolysis, though the char mean residence time was shorter by 30-40%. By comparison with Clay et al. (1987), the results of the present study confirmed that the yield of sulphite increased as the temperature was decreased. However, the effect of lower water content was not observed.

Equilibrium predictions using the F*A*C*T program are also shown in Figure 28. The results suggest that sodium sulphite is not a thermodynamically favoured compound under these

conditions. Therefore, sodium sulphite formation and subsequent reduction are kinetics-controlled below 650°C.

Formation Reactions

The formation of sodium sulphite during pyrolysis and steam gasification of KBLS could be explained by the decomposition of sodium thiosulphate according to:

$$Na_2S_2O_3 \rightarrow Na_2SO_3 + S^\circ \tag{53}$$

It was previously shown that the frequently-cited thiosulphate decomposition reaction for pure $Na_2S_2O_3$ (Eq. 46) could not account for the fluidized-bed results. However, Dearnaley et al. (1983) showed that Eq. 53 accounted for the stoichiometry of solid $Na_2S_2O_3$ decomposition in a mixture of alkali salts that were exposed to between 330-600°C with inert and oxidizing atmospheres. Without experimental evidence, Li and van Heiningen (1991a) also suggested this reaction as a first step in the production of sulphurous gases from thiosulphate decomposition.

In the present study, the stoichiometry of Eq. 53 suggests that half of the sulphur present as $Na_2S_2O_3$ in KBLS (i.e., 50.89 ±3.36 wt%) would be converted to Na_2SO_3. This is in agreement with the experimental sulphur yield as SO_3^{2-} of 23 ±2 wt% at the lowest temperature of 500°C, before any sulphite decomposition occurs. In addition, elemental sulphur analyses were performed on char samples for pyrolysis and steam gasification runs P2, P4-P8, SG1, and SG4-SG6 shown in Table 23 - Table 35. It was found that the elemental sulphur was less than 0.02 wt% of the total sulphur in the char in each of these runs.

Although some information is available in the literature, the behaviour of elemental sulphur during pyrolysis and steam gasification of KBLS is not well understood. Li and van Heiningen (1991a) hypothesized that elemental sulphur in KBLS char could be volatilized according to:

$$S^\circ + H_2O + CO \rightarrow H_2S + CO_2 \tag{54}$$

The work of Douglass and Price (1968) provides some evidence for this reaction. In their experiments, elemental sulphur was pyrolysed with model compounds of KBL, namely soda lignin and glucose, to yield 75 mol% and 35 mol% H_2S, respectively. If the volatilization occurs via Eq. 54, then about 25 wt% of the input sulphur would report to the gas phase as H_2S. This is comparable to the yield of sulphur as H_2S shown in Figure 31. Strohbeen and Grace (1982) postulated that, for T > 500°C, the elemental sulphur can react with the organic substrate or

pyrolysis products. The products are volatile and nonvolatile organic sulphur compounds and S^{2-}. Lastly, elemental sulphur may react in different proportions with Na_2S according to (Ahlgren et al., 1967):

$$Na_2S + x\,S^\circ \rightarrow Na_2S_x \tag{55}$$

Several char samples (runs P2, P4-P5, SG5) were analyzed for S_x^{2-} and it was found that less than 0.3 wt% of the sulphur was in this form. It is concluded that most of the elemental sulphur formed by thiosulphate decomposition was volatilized as either H_2S or organo-sulphur gases. As the operating temperature is increased from 500 to 700°C the amount of sulphurous gases decreases. A contributing factor to this decrease is the recombination reaction between H_2S and Na_2CO_3 to produce Na_2S, which is favoured at higher temperature.

Decomposition Reactions

In Figure 28, the fluidized bed SO_3^{2-} yield for pyrolysis (H_2O:solids = 0.05) shows a decrease of 20-40% between 500-550°C. By comparison, in the data of Dearnaley et al. (1983) for pure Na_2SO_3 mixed with alkali salts, the decomposition began at 550°C with 6-11% conversion. At 600°C, the experimental SO_3^{2-} yield decreased 70% due to decomposition. This compares favourably with data from Dearnaley et al. of 75% conversion. Without a reductant, the decomposition of pure Na_2SO_3 above 600°C has the following stoichiometry (Rosén, 1960; 1981):

$$4\,Na_2SO_{3\,(s)} \rightarrow Na_2S_{\,(s)} + 3\,Na_2SO_{4\,(s)} \tag{56}$$

Recent work by Li (1989) gives data showing that in the presence of graphite and CO gas at 600°C, only 12 wt% of the sodium sulphite reacts according to Eq. 56. The remainder is rapidly converted by carbon and CO as follows:

$$Na_2SO_{3\,(s)} + 3C \rightarrow Na_2S_{\,(s)} + 3\,CO \tag{57}$$

$$Na_2SO_{3\,(s)} + 3\,CO \rightarrow Na_2S_{\,(s)} + 3\,CO_2 \tag{58}$$

In the present experiments, hydrogen is also present and may reduce Na_2SO_4 as follows:

$$Na_2SO_{3\,(s)} + 3\,H_2 \rightarrow Na_2S_{\,(s)} + 3\,H_2O \tag{59}$$

This increase in Na_2S production at 600°C supports the experimental results shown in Figure 29, and these are discussed in the next section.

The effect of steam on the sulphite yield is not apparent at 500°C since no decomposition occurs. Also, at 650°C the rate of decomposition is too fast to observe a significant difference. However, at 600°C the reduction of Na_2SO_3 is apparently accelerated by the presence of steam. It is possible that the decrease in Na_2S at this temperature (Figure 29) may shift Eqs. 57-59 significantly to the right and therefore increase the Na_2SO_3 reduced.

Yield of Sodium Sulphide

Pyrolysis in Nitrogen

Figure 29 shows the total yield of S^{2-} in char as a function of the fluidized-bed temperature and H_2O:solids weight ratio. The amount of sulphide in the input dry KBLS is 6-8 wt% of the total sulphur content. For pyrolysis in N_2 (H_2O:solids = 0.05), the amount of S^{2-} in the char was in the range 8-12 wt% between 500-550°C. Based on duplicate runs at 600°C, the sulphide yield increased to between 28-45 wt%. As the temperature was increased further to 650 and 700°C, the sulphide content appeared to stabilize between 60-85 wt%.

For comparison, the equilibrium S^{2-} content as calculated using the F*A*C*T program is also plotted in Figure 29. Both experimental and equilibrium results for pyrolysis in N_2 show an increasing S^{2-} content with temperature. The equilibrium yield is much larger than the actual fluidized-bed data between 500-600°C. However, between 650-700°C the difference is reduced to about 15 wt% between equilibrium and measured values.

Between 500-550°C, the slight increase in Na_2S in the char compared to the input KBLS may be attributable to organic sulphur degradation reactions (van Heiningen, Li, and Fallavollita, 1989;1991) and sodium thiosulphate decomposition (Strohbeen, 1981). For $T \geq 600$°C, the large increase in Na_2S is due to the reduction of sodium sulphate and sodium sulphite, as well as the sulphur recombination reaction between H_2S and Na_2CO_3 (May, 1952). Evidence for this can be found in the decrease in Na_2SO_4, Na_2SO_3, and H_2S above 600°C as shown in Figure 27, Figure 28, and Figure 31. The increased stability of Na_2S in this temperature range has also been observed by Harper (1989). In his work, the fast pyrolysis of Na_2S-soda liquor mixtures showed a maximum sulphur release of 35-40 wt% at ~470°C, decreasing to ~7 wt% at 680°C.

Gasification in Steam/Nitrogen

Figure 29 also shows data for runs where steam was added to the fluidizing N_2 stream with an inlet H_2O:solids weight ratio of 1.75 (p_{H_2O} = 22 kPa). For experiments at 500 and 600°C,

almost all the input S^{2-} in KBLS was removed. At 650°C, the sulphide content rose abruptly to 28-38 wt%. Experiments at 700°C could not be analyzed for Na_2S in the char due to agglomeration of the fluidized bed.

For comparison, the equilibrium S^{2-} content is also shown in Figure 29 for steam gasification with an inlet H_2O:solids ratio of 1.75. Two additional yield curves are plotted for lower ratios of 0.39 and 0.73 to account for the fact that some of the steam by-passes the particulate phase as bubbles. The equilibrium predictions using a ratio of 1.75 show that sulphide formation is not favoured between 500-700°C. This does not agree with the measured value at 650°C. However, noting that the effective H_2O:solids ratio is less than 1.75 then the equilibrium predictions do indicate that S^{2-} increases above 600°C.

The Na_2S content during steam gasification was consistently lower than during pyrolysis. With the addition of steam, the Na_2S yield is not only a function of Na_2SO_4 and Na_2SO_3 reduction kinetics, but also the rate of Na_2S decomposition according to the reaction (May, 1952):

$$Na_2S_{(s)} + CO_2 + H_2O_{(v)} \Leftrightarrow Na_2CO_{3\,(s)} + H_2S \qquad (60)$$

At a fixed temperature, this reaction predicts an increase in H_2S with increasing steam concentration in the fluidized bed. The kinetics of H_2S formation are discussed in detail in a later section.

A useful measure of recovery boiler performance in the pulp and paper industry is the so-called reduction efficiency. The reduction efficiency is expressed as the wt% of sodium sulphide to the total weight of Na-S compounds in the char (Appendix A). Reduction efficiencies over 90% are typical for commercial recovery boilers. Table 20 gives the reduction efficiency as a function of the mean residence time of the char particles and reactor temperature. For pyrolysis in the fluidized bed, the reduction efficiency increased from 10% to over 90% between 500-700°C. Most of this increase was due to an increase in temperature, since the residence time increased only marginally from 55 to 62 minutes. When steam was added to the fluidized bed, the highest reduction efficiency was 80.8 ±10.1%, observed at 650°C.

It can be concluded that, in the pyrolysis case, reduction efficiencies comparable to conventional recovery boilers are achievable between 650-700°C. For steam gasification runs it is seen that a significant decrease in reduction efficiency is observed that could lead to problems at the commercial scale.

Fate of Organic Sulphur

The KBLS used in this study contained 19 ±4 wt% organic sulphur. All the organic sulphur compounds resulted from reactions between lignin and sodium sulphide during pulping (Avni et al., 1985). The amount of organic sulphur left in the char after pyrolysis and steam gasification was likely to be minor. An attempt was made to identify the type of organo-sulphur compounds present in char with the assistance of Alberta Sulphur Research Inc. (Calgary, AB). Samples of char were extracted with methyl chloride and analyzed by GC-MS. The mass spectra revealed that unsaturated aliphatic hydrocarbons were the most prevalent surface groups in char. Furthermore, only two organo-sulphur species were found: thio-butyric acid, and 4-hydroxy, benzenesulfonic acid.

Most of the sulphur was volatilized as H_2S and organo-sulphur gases such as CH_3SH and $(CH_3)_2S$. Experimental evidence to support this is given by van Heiningen, Li and Fallavollita (1989; 1991) for slow pyrolysis of dry KBLS in a TGA apparatus. At 650°C, it was found that 20 wt% of the organo-sulphur reported as Na_2S while the remainder was volatilized.

SULPHUR-BEARING GASEOUS PRODUCTS

Introduction

Sulphur appears in the gas phase because of a complex series of reactions during pyrolysis and steam gasification. These reactions can be divided into several categories: the degradation of organic sulphur in KBLS; interactions between inorganic sulphur compounds and the organic matrix (Strohbeen, 1981: Douglass and Price, 1968); stripping reactions between Na_2S and CO_2/H_2O (Li, 1986; 1989); and, homogeneous reactions among the various sulphur and/or non-sulphur gases (Feuerstein, 1966: Jones, 1968). The rate of sulphur volatilization may be also influenced by heat and mass transfer processes. Thus, it has been observed that the heating rate, KBL particle size, and the final temperature can affect the concentration of sulphur species in the gas (Strohbeen, 1981: Cantrell et al., 1988).

Gaseous sulphur exists in various forms. Feuerstein (1966) and Jones (1968) performed extensive gas analyses on the products of KBL pyrolysis and found that the predominant species were methyl mercaptan, dimethyl sulphide, and hydrogen sulphide. Li and van Heiningen (1991a) analyzed the gas phase composition during slow pyrolysis of dry KBLS below 500°C.

They found that the concentration of species followed the order: $(CH_3)_2S > CH_3SH > H_2S$. No SO_2 was detected in the gas and the concentrations of COS and $(CH_3)_2S_2$ were negligible.

In the present study, gas samples were taken at regular intervals from the off-gases of a fluidized bed. Sulphur dioxide was not detected during any experiment. This gave a very good indication that oxygen did not leak into the reactor system. The organo-sulphur gas dimethyl disulphide, $(CH_3)_2S_2$, was detected but the signal was neither reproducible nor quantifiable. Figure 30 gives the molar flow rate of the sulphur gases H_2S, CH_3SH, $(CH_3)_2S$, and COS for pyrolysis run P1 at 500°C. Similar graphs for all the runs are shown in Figure 40 - Figure 51. The molar flow rate is calculated as the product of the total gas flow rate (Table 22 - Table 35) and the concentration of the sulphur gas species measured by gas chromatography. The graph shows that the gas flow rates are somewhat constant during the time frame of the experiment. In this case an *average* molar flow rate for the run is easily calculated. However, in several other runs the data show greater scatter. Therefore, in Appendix A, a standard method is adopted for all the runs to determine the *average* molar flow rate of sulphurous gas (mmol/min) and the sulphur yield (g S in gas/ g S in KBLS). The latter quantity is plotted as the ordinate in Figure 31 - Figure 34.

Yield of Hydrogen Sulphide

Pyrolysis in Nitrogen

The average sulphur yield as H_2S is plotted in Figure 31 as a function of the fluidized-bed temperature and H_2O:solids weight ratio. For pyrolysis of dry KBLS (H_2O:solids = 0.05), the H_2S yield is in the range 20-30 wt% of the input sulphur between 500-550°C. At 600°C, a large decrease occurred and duplicate runs gave an average yield of 6-12 wt%. Further decreases are observed at higher temperatures, and at 700°C only 1-4 wt% of the input sulphur reported as H_2S. Equilibrium predictions using the F*A*C*T program are plotted for comparison. In the temperature range 500-700°C, the experimental yield was generally larger than the equilibrium prediction. The exception was 500°C, where an abrupt increase in the equilibrium H_2S yield was noted.

Hydrogen sulphide is released during pyrolysis of KBLS by the direct degradation of organic sulphur, and the interaction of inorganic sulphur compounds with the organic components of char. As previously observed, most of the organic sulphur in the KBLS was volatilized during

pyrolysis between 500-700°C, and the products included H_2S, CH_3SH, and other organo-sulphur species.

At 550°C or lower, the previous sections have shown that Na_2SO_4 and Na_2SO_3 are somewhat stable and therefore do not contribute to H_2S formation. However, both $Na_2S_2O_3$ and Na_2S react with the degradation products of the organics to form some hydrogen sulphide. For example, Strohbeen (1981) gave results of experiments with model organic compounds and sodium thiosulphate which showed that between 17-25 wt% H_2S was produced. The behaviour of sodium sulphide showed that between 85-97 wt% of the sulphur volatilized as H_2S.

A larger equilibrium H_2S yield is predicted at 500°C because Na_2S is the only stable inorganic sulphur-bearing compound used in the equilibrium calculations, and the equilibrium of Eq. 60 is far to the right. The lower H_2S measured in the fluidized bed is due to kinetic limitations imposed by the reduction of sodium sulphate and sodium sulphite at this temperature. Between 600-700°C, the reduction kinetics of sodium sulphate and sodium sulphite are significant, leading to Na_2S formation (Figure 29). The larger H_2S yield compared to equilibrium predictions at these temperatures is explained as follows. The equilibrium calculations assume a closed system whereas the fluidized bed is operated in a semi-batch mode. Therefore, the Na_2S product was retained in the bed and H_2S was continuously removed. The removal of H_2S from the reactor resulted in a larger decomposition of Na_2S (Figure 29) than predicted by equilibrium calculations, and consequently a larger H_2S yield.

Gasification in Steam/Nitrogen

Steam gasification experiments using an inlet H_2O:solids weight ratio of 1.75 (p_{H_2O} = 22 kPa) showed that, at 500°C, the H_2S yield was similar to that of pyrolysis in N_2 (Figure 31). At 600°C the H_2S yield was twice that of the pyrolysis runs. At even higher temperatures, the yield curve remained flat. For 700°C, the H_2S yield was 7 times greater than the runs without added steam. Another run was performed at 700°C with half of the steam input (H_2O:solids = 0.87), and the results are included in Figure 34, together with data for pyrolysis, steam gasification at H_2O:solids = 1.75, and the equilibrium predictions. The H_2S yield at the intermediate steam concentration is consistent with the other results and highlights the increase of H_2S with steam. Equilibrium predictions at a H_2O:solids ratio of 1.75 show very poor agreement with the experimental data. However, as noted previously, the amount of steam by-passing as bubbles

is significant. This leads to an effective H_2O:solids ratio in the particulate phase that is lower than the inlet value. The H_2S yield curves for H_2O:solids ratios of 0.39 and 0.73 are included in Figure 31 to better illustrate this effect of steam by-passing on the equilibrium predictions.

The addition of steam to the fluidized bed did not significantly increase the H_2S yield between 500-550°C. This is due to the small increase in H_2S production via Eq. 60, since the amount of Na_2S available at these temperatures is low (Figure 29). Above 600°C, Na_2S is present in large concentrations and therefore Eq. 60 becomes more significant.

The H_2S emission rate in the particulate phase, $r^p_{H_2S}$ (g H_2S·(g S^{2-}·min)$^{-1}$), due to the H_2S stripping reaction, Eq. 60, can be calculated for steam gasification runs SG4 and SG5 at 600 and 650°C. Because the char-alumina agglomerated for the steam gasification runs at 700°C, the measurement of the S^{2-} content was not possible and therefore the H_2S emission cannot be obtained. To calculate the H_2S emission it is assumed that the increase in average H_2S yield for steam gasification runs (SG4 and SG5) was due primarily to Eq. 60, compared to the pyrolysis runs (P5 and P7). For example, at 650°C the average yields of H_2S, $Y^{ave}_{H_2S}$, for steam gasification run SG5 and the pyrolysis run P7 were 0.132 ±0.022 and 0.023 ±0.002 mol H_2S·kg KBLS^{-1}, respectively. Normalizing the yields to the feed rate of KBLS (0.343 kg·h^{-1}) for the steam gasification run SG5 gives $7.55 \cdot 10^{-4}$ ±$0.34 \cdot 10^{-4}$ and $1.31 \cdot 10^{-4}$ ±$0.11 \cdot 10^{-1}$ mol·min^{-1}, or on a mass basis, 0.0242 and 0.0042 g H_2S·min^{-1}, respectively. Subtracting these and dividing by the amount of sulphide present in the fluidized bed after a run (i.e., 3.03 g; Table 34, Table 36) gives an average H_2S emission rate in the fluidized bed of 0.007 min^{-1}. Similarly, at 600°C the H_2S emission for steam gasification is 0.129 ±0.09 min^{-1}.

Li (1989) studied Eq. 60 for KBLS char gasification using a TGA apparatus and argued that the measured H_2S production between 600-700°C was similar to that predicted from thermodynamic equilibrium. In view of Li's findings, the gas composition data from steam gasification runs between 600-700°C were used to determine if the H_2S stripping reaction was also in equilibrium in the present study. The equilibrium constant for Eq. 60 was correlated as a function of temperature as follows (Li, 1989):

$$\log K^{eq}_{60} = \log\left(\frac{y^{eq}_{H_2S}}{y^{eq}_{H_2O} \cdot y^{eq}_{CO_2}}\right) = -7.210 + \frac{6.42 \cdot 10^{-3}}{T\,(K)} \qquad (61)$$

The predicted equilibrium constant, K^{eq}_{60}, is given in Table 21 for 600, 650, and 700°C along with the measured product gases ratio from the particulate phase, K^{p}_{60}.

To calculate K^{p}_{60} the mole fractions of H_2S, H_2O, and CO_2 in the exit of the particulate phase (i.e., $y^{p}_{H_2S}$, $y^{p}_{H_2O}$, and $y^{p}_{CO_2}$) need to be quantified. Run SG4 will be used with an example of the calculation method. The gas species considered are N_2, H_2O, H_2, CO, CO_2, CH_4, and H_2S. The molar flow rates at the exit of the particulate phase are obtained as follows. The two-phase theory of fluidization has been used in Chapter 4 to determine the division of flow in the fluidized bed. That analysis ignores the interphase transport of gas from the bubble phase into the particulate phase. The exit N_2 flow rate from the particulate phase (i.e., 0.60 ±0.04 mol·min^{-1}) is taken as 27% of the inlet to the fluidized bed (i.e., 2.23 ±0.13 mol·min^{-1}). The exit steam flow rate from the particulate phase (i.e., 0.11 ±0.02 mol·min^{-1}) is found by a steady-state mole balance. It is the difference between the inlet flow rate to the particulate phase (i.e., 27% · 0.56 ±0.02 mol·min^{-1}) and the consumption rate of steam given by the sum of ξ_{40} and ξ_{41} in Table 15. The production of CO_2, CO, H_2, and CH_4 occurs primarily in the particulate phase and therefore the exit molar flow rates (mol·min^{-1}) are 0.028 ±0.003, 0.0080 ±0.0003, 0.073 ±0.023, and 0.0056 ±0.0009, respectively (Table 40-Table 43). The exit molar flow rate of H_2S due to Eq. 60 (i.e., 0.00047 ±0.00029 mol·min^{-1}) is obtained by subtracting the value for SG4 (i.e., 0.00075 ±0.00029 mol·min^{-1}) by the amount due to pyrolysis. The latter quantity can be taken as the average H_2S flow rate for runs P5 and P6 at 600°C (i.e., 0.052 ±0.006 mol/kg KBLS · 0.342 kg KBLS/h · 1/60 h/min = 0.00029 ±0.00003 mol·min^{-1}). From the above information the exit mole fraction from the particulate phase is calculated for H_2S, H_2O, and CO_2 and is included in Table 21 along with K^{p}_{60}.

The equilibrium constant for Eq. 60 at 600°C is an order of magnitude larger than that measured in the fluidized bed. This implies that the H_2S production is smaller than predicted by equilibrium and likely limited by kinetics. At this temperature the reduction rate of Na_2SO_4 to Na_2S (Figure 27) is smaller than $r^{p}_{H_2S}$ and therefore the amount of Na_2S in the fluidized bed is negligible as shown in Figure 29. In effect, the H_2S stripping reaction is limited by the reduction kinetics of solid Na_2SO_4. As the temperature increases the reduction rate of sodium sulphate increases (Figure 27) whereas $r^{p}_{H_2S}$ decreases sharply (i.e., from 0.129 min^{-1} at 600°C to 0.007 min^{-1} at 650°C). Therefore, at 650 and 700°C the amount of Na_2S in the fluidized bed is

large (Figure 29) and the sulphate reduction does not limit Eq. 60. Table 21 shows that K^{eq}_{60} is within the 95% confidence interval for the measured K^{p}_{60} between 650-700°C, indicating that the H_2S stripping reaction is in equilibrium.

From Figure 31 it is seen that the H_2S emission increases with increasing steam concentration. For low-temperature processing it may therefore be possible to decompose completely the Na_2S if sufficient H_2O is added. This was observed by Durai-Swamy et al. (1989) who used a higher steam partial pressure (101 kPa) and a 65% solids KBL in a fluidized bed of sodium carbonate. They found that at 627°C the sulphur recovery in char was only 3 wt% as Na_2S and the remainder was presumably volatilized as H_2S.

Yield of Methyl Mercaptan

Figure 32 shows that the average yield of CH_3SH decreases steadily between 500-700°C for pyrolysis in N_2 (H_2O:solids = 0.05). Between 500-550°C, it varies between 12-18 wt%. This is about one-half of the H_2S yield at these temperatures. The data at 600-650°C are nearly identical with those of H_2S. At 700°C, the yield drops to only 0.05 ±0.02 wt%. Equilibrium calculations predict that negligible amounts of CH_3SH would be present in the off-gases for all pyrolysis runs.

During pyrolytic decomposition of KBLS, the formation of methyl mercaptan may be due to several processes. Plausible routes include direct organic sulphur emission via free radical reactions (Thomas et al., 1969), interaction of inorganic $Na_2S_2O_3$ or Na_2S with the organic matrix (Strohbeen, 1981: Jones, 1968), and reactions between H_2S and an olefin or alcohol (Attar, 1978: Attar and Corcoran, 1977).

Adding steam to the fluidized bed shows a small increase in CH_3SH emission over the entire temperature range studied. In Figure 34 the methyl mercaptan yield is plotted as a function of the equivalent wt% solids at 700°C. The CH_3SH yield decreased from 1.77 ±0.02 wt% to 0.05 ±0.02 wt% as the equivalent wt% solids increased from 35 to 95 wt%. The small increase in CH_3SH yield with steam above 600°C shown in Figure 34 is explained by the reaction sequence,

$$Na_2S_{(s)} + CO_2 + H_2O_{(v)} \Leftrightarrow Na_2CO_{3\,(s)} + H_2S \qquad (60)$$

$$C_2H_4 + 2\,H_2S \Leftrightarrow 2\,CH_3SH \qquad (62)$$

At a fixed temperature, the increase in H_2S formation due to the addition of steam via Eq. 60 will also lead to a shift to the right in Eq. 62, thereby increasing the methyl mercaptan yield. The olefin-H_2S reaction given in Eq. 62 has been previously given by Attar (1978) in connection with sulphur volatilization from coal. Also, Jones (1968) previously reported the existence of light hydrocarbon gases, such as C_2H_4, during the pyrolysis of KBL. The standard heat of reaction, $\Delta H°_{298}$, for Eq. 62 is -56.9 kJ/mol. Therefore, as the temperature increases the yield of methyl mercaptan is expected to decrease, which is observed experimentally.

Yield of Dimethyl Sulphide and Carbonyl Sulphide

The average yield of $(CH_3)_2S$ for pyrolysis in N_2 (H_2O:solids=0.05) decreased from 2.9 ±0.3 to 0.7 ±0.1 wt% of the input sulphur between 500-700°C (Figure 33). The addition of steam did not significantly affect the yield (Figure 33 and Figure 34). Over the entire temperature range, the $(CH_3)_2S$ emission is about 1/5 that of methyl mercaptan. For comparison, Jones (1968) reported that the dimethyl sulphide yield decreased from 21 to 4 wt% of the input sulphur between 500-700°C. It was also suggested that dimethyl sulphide was formed by gas-phase reactions between an olefin and methyl mercaptan according to,

$$C_2H_{4\,(g)} + 2\,CH_3SH_{(g)} \Leftrightarrow 2\,(CH_3)_2S_{(g)} \qquad (63)$$

This reaction explains the temperature dependency of the $(CH_3)_2S$ yield. The standard heat of reaction for Eq. 63 at 298 K, $\Delta H°_{298}$, is -82.0 kJ/mol. Therefore, as the temperature increases the reaction is expected to shift to the left thereby producing less dimethyl sulphide.

Carbonyl sulphide (COS) production did not vary significantly for both pyrolysis and steam gasification runs (Table 47), and averaged 0.16 ±0.08 wt% of input sulphur. Figure 34 shows the COS production as a function of equivalent wt% solids for 700°C. Except for the data at high solids, the actual COS production is well below equilibrium values. It is proposed that the COS emission results primarily from irreversible pyrolysis of organo-sulphur compounds in KBLS.

SUMMARY

Sodium thiosulphate decomposes completely during pyrolysis and steam gasification, with the key reaction being Eq. 53. The liquid elemental sulphur subsequently reacts almost completely with volatiles to produce various sulphur gases. Below 650°C, sodium sulphite is

a major product of the pyrolysis of KBLS containing sodium thiosulphate. The reduction of sodium sulphite proceeds via several reactions. About 10 wt% decomposes according to Eq. 56, and the remaining 80 wt% is reduced by carbon, CO, and H_2 according to Eqs. 57 - 59. Sodium sulphate is stable between 500-550°C during pyrolysis and steam gasification. In a nitrogen atmosphere, sulphate reductions of 50-75% and 95% were measured at 600 and 650°C, respectively. These are higher than the predictions of 0.2% and 10% for these temperatures given by a kinetic rate law in Li (1989). The higher reductions are explained by the autocatalytic effect of the sodium sulphide that is initially present in char, and the higher C/SO_4^{2-} molar ratio. For pyrolysis, sodium sulphide increases significantly between 600-700°C, from 65 to 85 wt% of the input sulphur. This is attributed to the reduction of sodium sulphate and sodium sulphite, and the sulphur recombination via the reverse of Eq. 60. At isothermal conditions, the addition of steam lowers the sodium sulphide yield due to its effect on the H_2S stripping Eq. 60.

The hydrogen sulphide yield decreases with temperature during pyrolysis. The addition of steam increases the hydrogen sulphide yield for temperatures above 600°C. By considering the composition of gases in the particulate phase, estimates were made between measured and predicted equilibrium constants for the H_2S stripping reaction, Eq. 60. It was found that the emission of H_2S was in equilibrium between 650 and 700°C. This agrees with the earlier work of Li (1989) using a TGA. The yield of methyl mercaptan decreases with increasing temperature. With the addition of steam, a small increase in the methyl mercaptan yield is observed that can be explained by Eqs. 60, 62. Dimethyl sulphide decreases with temperature but no effect is seen with the addition of steam. The temperature dependency of the yield is explained by the gas-phase reaction, Eq 63.

CONCLUSION

A large variation in the quantity and type of sulphur products during the pyrolysis and steam gasification of KBLS were observed from 500 to 700°C. To minimize the emission of sulphurous gases, both a high temperature of 700°C and a low-moisture atmosphere were needed. The persistence of methyl mercaptan and dimethyl sulphide in the off-gas at 700°C will require a cleaning step prior to combustion of the gases for heat recovery. A process is described in Chapter 6 to deal with this aspect.

With the addition of steam, the emission of H_2S increases for temperatures above 600°C. The effect of higher steam partial pressures than those used in this work could lead to near-complete volatilization of sulphur as H_2S. An example of this is given by the work of Durai-Swamy et al. (1989) using steam at 100 kPa pressure. An approach to avoid this problem would be to operate the reactor at 500°C, below the start of the reduction reactions. Also, most of the inorganic sulphur (typically ~80-90 wt% of total S) should be in the sulphate form. This may be done by wet-air oxidation of black liquor using strong oxidants, higher air pressures or catalysts.

CHAPTER 6

IMPLICATIONS FOR A COMMERCIAL PLANT DESIGN

ABSTRACT

The key results of the experimental work are extended by means of a thermodynamic analysis for the case of lower solids content KBL and O_2 gasification. It is shown that excessive amounts of sulphur can be lost to the gas phase under these conditions. To reduce the amount of sulphur volatilized during pyrolysis, Fallavollita et al. (1987) proposed the following: the inorganic sulphur in KBL should be converted to sulphate by wet oxidation, and the pyrolysis should be performed below about 600°C to prevent sulphate reduction. Because organo-sulphur compounds such as CH_3SH and $(CH_3)_2S$ are volatilized during pyrolysis, a separate recovery step is needed downstream of the pyrolyser. A fluidized bed containing particles of Na_2CO_3 and operated in the combustion mode is proposed to recover this sulphur. A basic flowsheet for a low-temperature fluidized-bed process (van Heiningen, Li, and Fallavollita, 1989; 1991) that incorporates these ideas is outlined. This process would satisfy the objectives of chemical and energy recovery in an industrial plant.

WATER CONTENT IN KRAFT BLACK LIQUOR

Over the past ten years, an increasing energy efficiency in the kraft recovery boiler has been achieved by increasing the solids content of kraft black liquor (KBL) fired (Ahonen et al., 1982). Multiple effect evaporators have traditionally been used to increase the solids content of black liquor. Unfortunately they are limited to producing 65% solids due to viscosity problems and fouling of heat exchanger tubes.

Technological developments have been increasing rapidly in the area of black liquor concentration. Methods for increasing the solids content from 75% to 95% in KBL can be found in the papers by Sell and Clay (1991), Nakamura (1989), Oshen et al. (1989), Ryham (1989), and Clay and Karnofski (1981). An economic comparison was made by Harrison et al. (1988) between the state-of-the-art dry solids processes (prilling and drum drying) and methods capable of firing 80% solids. It was concluded that drum drying was the most economical and proven technology.

The kraft black liquor solids (KBLS) that were used as feed material to the fluidized bed contained less than 5 wt% moisture. This represents the ideal case for minimizing the water content and thereby reducing the production of sulphur gases as discussed by Fallavollita et al. (1987). In the near term, a commercial fluidized-bed process must contend with a black liquor feed containing 65-80 wt% solids. The results in Chapter 5 give evidence to support the ideas of Fallavollita et al. (1987). They proposed that the negative impact of higher water content could be minimized if the inorganic sulphur in KBL is in the SO_4^{2-} form. Also, by operating the pyrolysis step below 600°C, sulphate reduction can be avoided and the inorganic sulphur will be retained in the char.

At present, oxidation of inorganic sulphur in KBLS using air (BLOX) is performed industrially. However, the product of oxidation is $Na_2S_2O_3$; very little Na_2SO_4 is formed. Sodium thiosulphate is not desirable since it has been shown in this study to decompose during pyrolysis into volatile and reactive sulphur compounds in the char. Recent research in BLOX has centred on two different approaches. A system using high-intensity BLOX with high solids content KBL, high pressure and temperature (Hermans, 1984); and, the low-severity catalytic system using a low solids content KBL at ambient pressure and 100°C (Sen Gupta, 1987). The high-intensity method converts all inorganic sulphur forms to SO_4^{2-}. However, the black liquor

product has a very high viscosity which makes it difficult to transport. The low-intensity method produces 65-75 wt% SO_4^{2-} and the remainder is trithionate, $S_3O_6^{2-}$. The liquor is easily pumped and between 10-20% of the thermal value is removed. However, the behaviour of trithionate during pyrolysis has not been studied.

GASIFICATION IN AN OXYGEN-BEARING ATMOSPHERE

All the fluidized-bed data presented thus far are for non-oxidative atmospheres. In commercial practice it is likely that some O_2 will be added to the fluidized bed. The reactions between KBLS and steam are slightly endothermic, as observed in the present experiments. Oxygen in the air provides a source of heat from the exothermic reactions with carbon and thereby maintains reactor temperature.

Exploratory fluidized-bed experiments conducted with added O_2 showed uneven temperature control. Modifications incorporating cooling coils would have been required to correct this problem. Due to lack of sufficient time it was decided not to include this as part of the present investigation. Instead, the effect of O_2 was studied by thermodynamic calculations using the F*A*C*T program (Thompson et al., 1988), and the results published in Fallavollita et al. (1987).

Consider KBLS with an ultimate analysis as given in Table 2. This material is reacted with oxygen in different ratios and allowed to reach equilibrium at 700°C. The equilibrium gas composition would be as shown in Figure 35 and Figure 36. In Figure 36, if the oxygen concentration is further increased then the amount of H_2S will begin to decrease until combustion conditions are reached. With excess oxygen, the predominant sulphur compound is Na_2SO_4. For pyrolysis and gasification conditions, the solid product would consist of char containing carbon, Na_2S and Na_2CO_3. Since the quantity of sodium carbonate does not change materially in the analysis, it is not considered further. Figure 37 shows how the quantity of carbon and Na_2S varies with oxygen fed to the reactor. Figure 38 indicates that the Na_2S content in the char is a strong function of both temperature and the O_2/solids weight ratio between 650-700°C.

Some important conclusions that can be drawn from these figures for pyrolysis and gasification conditions are:

- The main combustible gas products are CO and H_2;
- The volatilization of H_2S increases with oxygen added to the reactor and decreasing temperature.

A brief explanation is warranted for the second conclusion. When the oxygen content in the gasifier is less than the stoichiometric requirement then the formation of Na_2SO_4 is not favoured. Under these conditions, an increase in oxygen content results in an increase in carbon dioxide content as shown in Figure 35. This increase in carbon dioxide shifts the equilibrium for the H_2S stripping reaction Eq. 60 (Chapter 5) to the left, thereby increasing the hydrogen sulphide content in the reactor.

$$Na_2CO_3(s) + H_2S \Leftrightarrow Na_2S(s) + CO_2 + H_2O \quad (5)$$

In the fluidized-bed gasifier, the O_2 reactions would occur rapidly near the distributor. This is because the C-O_2 reaction is several orders of magnitude greater than either the C-H_2O or C-CO_2 rate (Walker et. al., 1959). The rapid depletion of the O_2 would result in a steep gradient of O_2 concentration near the reactor inlet. Hence, the steam and CO_2 gasification would become important further along the fluidized bed. The O_2 gasification would therefore be limited by C-H_2O and C-CO_2 gasification in the present reactor system.

As noted above, the addition of O_2 results in temperature control problems when feeding dry KBLS in the pilot plant. The Domtar-Copeland combustor operated with a 30% solids feed. The large water content acts as a heat sink and allows an easier control of the temperature without the need for internal cooling coils (Tomlinson et al., 1976). The disadvantage of this approach is the lowering of overall energy efficiency. Kleinau (1976) pointed out that O_2 gasification of dry KBLS would be very difficult due to temperature control, and suggested that in commercial systems the use of internal heat transfer surfaces would be essential.

RECOVERY OF SULPHUR FROM PYROLYSIS GASES

Even if complete oxidation of the inorganic sulphur to Na_2SO_4 was practised, it would still be necessary to provide for a secondary recovery of the organic sulphur in KBLS. In this work, about 20 wt% organic sulphur is present in KBLS. Most of this is volatilized during pyrolysis, thereby increasing the organo-sulphur gas emission.

Various scrubbing techniques using liquid solutions have been proposed in the patent literature concerning fluidized-bed systems (see Chapter 1). None of these systems can adequately collect the complex organo-sulphur species and allow conversion to the Na_2S form. Instead, a proposal is made by the author to use a fluidized-bed combustor to convert all the gaseous sulphur to SO_2 and react it with Na_2CO_3 between 600-650°C. This approach has been incorporated into a patent application (van Heiningen, Li and Fallavollita, 1989; 1991

This fluidized-bed reactor concept is based on the sulphation reaction between sodium carbonate and SO_2 in an oxygen-bearing atmosphere,

$$Na_2CO_3(s) + SO_2 + 1/2\ O_2 \Leftrightarrow Na_2SO_4(s) + CO_2 \qquad (64)$$

Backman et al.(1985) found that this reaction was rapid with an initial intrinsic reaction rate of SO_2 at 650°C of 0.035 mol SO_2·mol $Na_2CO_3^{-1}$·min^{-1}. An important aspect of the sulphation reaction is that the reaction rate slows due to the formation of a solid Na_2SO_4 layer over the particle. To keep the reaction rates high, it would be necessary to keep the residence time of carbonate particles to a minimum.

The limitation on the operating temperature of this reactor would be the stickiness of Na_2CO_3-Na_2SO_4 particles. In coastal mills where the Cl^- content would be higher, this could represent a major problem. In this case it may be appropriate to use a bed operating in the turbulent flow regime (i.e., fast-fluidized bed) with large sodium carbonate particles. This combination of operating parameters would provide better fluidization stability when processing agglomerating particles (Gluckman et al. 1976). However, the major advantage of this method for scrubbing sulphur is that the sulphation reaction allows the recombination of gaseous sulphur with sodium in a single step. It also avoids introducing any undesirable chemicals into the pulp mill that could adversely affect other unit operations.

PROPOSED LOW-TEMPERATURE FLUIDIZED-BED PROCESS

Fluidized-Bed Pyrolyser

A low-temperature recovery process using fluidized beds must accommodate the variability in KBL composition. Some important variables are the water content, sulphur species, and the minor elements Cl and K. Figure 39 gives a general flowsheet for accomplishing both energy and chemical recovery in a kraft pulp mill.

Kraft black liquor, at 65-80 % dry solids, is sprayed into a fluidized bed containing alumina and char. The inorganic sulphur in KBL will be mostly SO_4^{2-} if an advanced BLOX method is used, or may contain large quantities of $S_2O_3^{2-}$. The main difference in these systems will be the degree of volatilization of sulphur. As the quantity of sulphate in KBL increases, so does the amount reporting to the char stream of the pyrolyser.

The temperature should be maintained around 600°C to prevent reduction of sulphate to sulphide and the residence time should be short. The fluidizing medium will be the recycled combustion gases, CO_2 and steam, and trace amounts of SO_2. It is expected that this gas also will contain unreacted O_2 from the fluidized-bed combustor. A steam-air mixture may be added to control temperature and increase the flow rates in this vessel.

The product streams from the pyrolyser are volatiles (containing some elutriated solids) and the char-alumina bed particles. A cyclone is required in the volatiles stream to recycle any elutriated fines.

Char Reducer

The char-alumina bed particles are transported to a reducer in which the temperature is kept between 700-750°C using indirect heating and mechanical agitation to prevent agglomeration. The agitation may be accomplished by a kiln or screw conveyer. Nitrogen is added to maintain a positive pressure in the system and prevent the introduction of air into the vessel. Some H_2 may be added to increase the reaction rates, but this would be at the expense of a greater safety hazard. Residence time in the order of 30 minutes are sufficient to achieve over 90% reduction of sodium sulphate at these temperatures.

The reduced char-alumina particles are then cooled to recover heat and then immersed in a water leaching vessel to dissolve most of the inorganics. Because the inorganics in the char are distributed throughout the bulk, incomplete leaching is expected due to diffusion limitations. The undissolved char-alumina is then filtered and transported to the fluidized-bed combustor.

Fluidized-Bed Combustor

In the fluidized-bed combustor, the hydrocarbon volatiles from the pyrolyser are combusted with excess O_2 to produce CO_2/steam, and the complex array of sulphur gases is converted to SO_2. With an appropriate design, turbulent mixing of the volatiles and air stream could be

achieved in the entry section of the windbox. This would ensure complete combustion of the gases upstream of the distributor plate.

The input bed material consists of char-alumina from the leaching step and fluidized-bed pyrolyser. The bleed stream from the pyrolyser is used primarily for Na_2CO_3 make-up. Carbon in the char will be rapidly combusted and the steady state concentration in the bed will be very low. The SO_2 in the fluidizing gas will react with the solid Na_2CO_3 to form Na_2SO_4. The temperature is kept below the fusion point of the inorganic salts mixture to prevent agglomeration. To control temperature and recover the exothermic heat of combustion, heat exchanger tubes are necessary either on the walls or within the fluidized bed.

Bed material consisting of alumina, coated with Na_2CO_3-Na_2SO_4, is withdrawn and transported to a tank containing water. Complete dissolution of the inorganics is easily achieved, and the pH is adjusted to control the viscosity of KBL. Alumina is filtered and returned to the fluidized-bed pyrolyser.

CONCLUSION

The alternative kraft recovery process using two fluidized beds is technically capable of recovering both the energy in the KBL organics, and sulphur as sodium sulphide. The process steps are based on fundamental data acquired either in this work (i.e., pyrolysis and steam gasification), or in the literature (i.e., sulphation reaction).

The next stage of development work for the novel low-temperature recovery process would be to study the performance of the pyrolyser using kraft black liquor obtained by low-severity oxidation. In particular, this would give information on the pyrolytic behaviour of trithionate. Also, the efficiency of sulphur recovery from the fluidized-bed combustor will need to be investigated to provide adequate scale-up information of this step.

CONTRIBUTIONS TO KNOWLEDGE

1. Dry kraft black liquor solids of about 50 micron size were pyrolysed and gasified with steam in a pilot plant fluidized-bed reactor containing solid alumina as the inert bed material.
2. Analytical methods were developed for the complete quantification of sodium, sulphur and total carbon in the char-alumina product. In particular, a novel technique which combined an oxygen bomb combustion followed by ion chromatographic analysis of SO_4^{2-} was successfully employed to determine total sulphur in char.
3. Overall mass balances for the pilot plant gasification of KBLS were obtained for carbon, sulphur and sodium. This information has not previously been available in order to assess the low-temperature recovery of KBLS.
4. A significant loss of sodium was found during processing in N_2 between 600-700°C. The volatilization was thought to occur only during the initial rapid pyrolysis of KBLS particles. After the particles reached reactor temperature, the concentrations of CO and CO_2 were sufficiently large to suppress further volatilization. The addition of steam suppressed the sodium volatilization. Two recombination reactions involving steam, CO, and the intermediate NaOH, may bind the sodium as Na_2CO_3. Alternatively, the higher H_2O/H_2 ratio could also increase the adsorbed oxygen on the char thereby binding more sodium as surface complexes.
5. The global rate of carbon gasification was found to be kinetic-controlled between 600-650°C. Theoretical estimates of the mass transfer rate of steam to the char surface support this observation.
6. The average yields of fixed gases as well as sulphur species were obtained in the temperature range 500-700°C. The production rate of CO_2 was found to increase with temperature, contrary to thermodynamic prediction. The difference has been explained by assuming the direct production of CO_2 during the Na_2CO_3-catalysed gasification of carbon, and the rapid forward rate of the water-gas shift reaction. The production of H_2S and CH_3SH were similar between 500-600°C for pyrolysis and steam gasification. At 700°C the major sulphur gas was H_2S. Between 650-700°C, the addition of steam resulted in an emission of H_2S in the particulate phase that was in equilibrium with the product gases from the H_2S stripping reaction.

7. Sodium thiosulphate in KBLS decomposed readily below 600°C to form sodium sulphite and elemental sulphur. The elemental sulphur subsequently reacted almost completely with volatiles to produce various sulphur gases. Below 650°C, sodium sulphite was a major product of the pyrolysis of KBLS containing sodium thiosulphate. The sodium sulphate in KBLS was essentially inert during pyrolysis below 600°C, confirming earlier TGA results in the literature. The reduction rate of solid sodium sulphate between 600-650°C was at least an order of magnitude higher than data given in the literature. This was explained mainly by the presence of Na_2S at the start of reduction and the higher C/SO_4^{2-} ratio in the char, and to a lesser extent by the reducing power of the gaseous atmosphere containing CO, CO_2, H_2O, and H_2. Sodium sulphide was not stable below 600°C and was volatilized as H_2S. However, the production of Na_2S increased with temperature for pyrolysis and steam gasification experiments. At 700°C, the recovery of sulphur as sodium sulphide was above 90 wt%, and comparable to commercial recovery boiler performance.
8. Application of the results of this study to the situation where higher steam contents are present along with O_2 suggest that most of the Na_2S may be converted to H_2S between 650-700°C.
9. A proposal was made (Fallavollita et al., 1987) to reduce the sulphur emission during pyrolysis by converting most of the inorganic sulphur in KBL to the SO_4^{2-} form. This can be achieved by high-intensity or low-severity BLOX systems.
10. A contribution to the patent by van Heiningen, Li, and Fallavollita (1989;1991) was made. This involved the suggestion that the recovery of volatilized sulphur from the pyrolyser be accomplished by means of a fluidized-bed combustor wherein the solid Na_2CO_3 from char would participate in the sulphation reaction with SO_2 to recover sulphur as Na_2SO_4.
11. The temperature limit of operation of a fluidized-bed reactor processing KBLS can be extended by controlling the stickiness of the particles. A major variable was found to be the amount of amorphous carbon present on the char. A minimum amount of carbon of about 25 wt% is necessary to prevent defluidization at the highest temperature of 700°C.
12. A mechanism was proposed for the alkali-catalysed steam gasification of carbon that accounted for the primary production of CO_2, the inhibition of CO and H_2 on gasification sites, and resulted in the proper form of the rate law.

REFERENCES

Adjorlolo, A.A. and Y.K. Rao, "Effect of Potassium and Sodium Carbonate Catalysts on the Rate of Gasification of Metallurgical Coke," *Carbon 22(2)*, 173-6 (1984).

Ahlgren, P. et al., "Preparation of Sodium Polysulphides by Solid and Molten State Reactions," *Acta Chem. Scand. 21(4)*, 1119-1120 (1967).

Ahonen, A. et al., "Latest Developments in Black Liquor Evaporation," *Black Liquor Recovery Symp.*, Helsinki, B5:1-6 (1982).

American Society for Testing and Materials (ASTM), "Total Sulphur in the Analysis Sample of Coal and Coke," Standard D 3177-84 (1984).

Andersson, S., "Studies on Phase Diagrams Na_2S-Na_2SO_4, Na_2CO_3-Na_2S-Na_2SO_4, Na_2CO_3-Na_2SO_4-NaOH, and Na_2CO_3-Na_2S-NaOH," *Chemica Scripta. 20*, 164-170 (1982).

Anthony, D.B., and J.B. Howard, "Coal Devolatilization and Hydrogasification," *AICHE J. 22(4)*, 625-656 (1976).

Attar, A., "Chemistry, Thermodynamics and Kinetics of Reactions of Sulphur in Coal-Gas Reactions: A Review," *Fuel 57(4)*, 201-212 (1978).

Attar, A. and W.H. Corcoran, "Sulphur Compounds in Coal," *Ind. Eng. Chem., Prod. Res. Dev., 16(2)*, 168-170 (1977).

Avedesian, M.M. and Davidson, J.F., "Combustion of Carbon Particles in a Fluidised Bed," *Trans. Inst. Chem. Eng. 51*, 121-131 (1973).

Avni, E., et al., "Mathematical Modelling of Lignin Pyrolysis," *Fuel 64(11)*, 1495-1501, (1985).

Backman, R., et al., "Kinetics of Sulphation of Sodium Carbonate in Flue Gases," *Proc. Intl. Chem. Recovery Conf., Book 3*, TAPPI, New Orleans, 445-450 (1985).

___, "Fouling and Corrosion Mechanisms in Recovery Boiler Superheater Area," *5th Intl. Corrosion Symp. Pulp Paper Ind.*, Co-sponsored by TAPPI/CPPA/NACE, Vancouver, 243-9 (1986).

Baeyens, J. and D. Geldart, in *Gas Fluidization Technology*, (Ed. D. Geldart), John Wiley, 97-122 (1986).

Barin, I., et al., *Thermochemical Properties of Inorganic Substances*, Springer-Verlag, Berlin (1977).

Bergman, A.G. and A.K. Sementsova, "An Inner Section Across the Prism of the Quaternary Reciprocal System Na,K‖Cl,SO_4,CO_3," *Zh. Neorg. Khim. 3(12)*, 187-200 (1958a).

___, " Ternary Systems Na‖Cl,SO_4,CO_3 and K‖Cl,SO_4,CO_3," *Zh. Neorg. Khim. 3(2)*, 201-212 (1958b).

___, " Ternary Systems K_2Cl_2-Na_2SO_4-Na_2CO_3 and Na_2Cl_2-K_2SO_4-K_2CO_3," *Zh. Neorg. Khim. 3(2)*, 213-224 (1958c).

Bernhard, R. and J. Martenson, "Plasma Gasification of Kraft Thick Liquor," *Proc. Intl. Chem. Recovery Conf., Book 2*, TAPPI, New Orleans, 245-7 (1985).

Bhattacharya, P.H., et al., "Pyrolysis of Black Liquor Solids," *Ind. Eng. Chem., Proc. Des. Dev. 25(2)*, 420-6 (1986).

Birk, J.R., et al., "Hydrogen Reduction of Alkali Sulphate," *Ind. Eng. Chem., Proc. Des. Dev. 10(1)*, 7-13, (1971).

Bjorklund, H., et al., "The NSP Cyclone Furnace for Black Liquor Reductive Combustion - Status Report," *Proc. Intl. Chem. Recovery Conf., Book 2*, TAPPI, New Orleans, 221-5 (1985).

Bjorkman, A., "Pyrolysis of Spent Liquors," *Proc. Symp. Recovery Pulp. Chem.*, Helsinki, 235-264 (1968).

Bjorkman, A. and B. Warnqvist, "Basic Processes in Kraft Liquor Reductive Gasification and Burning," *Proc. Intl. Chem. Recovery Conf., Book 1*, TAPPI, New Orleans, 13-23 (1985).

Blackwell, B. and T. King, "Technology Review: Exploring Kraft Recovery Boiler Chemical Reactions," *Pulp Paper Mag. 11*, 122-4 (1985).

___, *Chemical Reactions in Kraft Recovery Boilers*, Sandwell and Co., Vancouver (1985).

Bliek, A., *Mathematical Modelling of a Co-Current Fixed Bed Coal Gasifier*, Ph.D. Thesis, Twente University, The Netherlands (1984).

Bolthrunis, C.O., "An Industrial Perspective on Fluid Bed Reactor Models," *Chem. Eng. Progr. 85(5)*, 51-4 (1989).

Borchardt, L.G. and D.B. Easty, "Gas Chromatographic Determination of Elemental and Polysulphide Sulphur in Kraft Pulping Liquors," *J. Chromatogr. 299*, 471-6 (1984).

Brink, D.L., "Pyrolysis-Gasification-Combustion: A Process for Utilization of Plant Material," *Applied Polymer Symp. 28*, 1377-1391 (1976).

Brink, D.L., et al., "Malodorous Products from the Combustion of Kraft Black Liquor. II. Analytical Aspects," *Tappi J. 50(6)*, 276-285 (1967).

Bryce, J.R.G., in *Pulp and Paper Chemistry and Technology- Vol. 1, 3rd. ed.*, (Ed. Casey, J.), Wiley and Sons, 377-492 (1980).

Cabrera, A.L., et al., "Methane Production from the Catalysed Reaction of Graphite and Water Vapour at Low Temperatures (500-600 K)," *J. Catal. 75*, 7-22 (1982).

Cameron, J.H., et al., "Oxidative Fuming - The Phenomenon and Possible Interpretations," *Proc. Intl. Chem. Recovery Conf., Book 3*, TAPPI, New Orleans, 435-444 (1985).

Canadian Pulp and Paper Association, Technical Section (CPPA), "Analysis of Sulphate Process Black Liquors," Standard J.15P (1981).

Cantrell, J.G., et al., "Sulphur Release and Retention During Combustion of Kraft Black Liquor," *Chem. Eng. Technol. Forest Prod. Process. Vol. 2*, (Ed., Crowell, B.), 31-9 (1988).

Cerfontain, M.B., et al., "The Difference in Reactivity of the Alkali Carbonates for the Catalysed Carbon Gasification Interpreted with Transient Kinetics Measurements," *Proc. Intl. Conf. Coal Science*, Sydney, Australia, 277-80 (1985a).

___, "The Mechanism of the Potassium Catalysed Carbon Gasification: A Study by Transient Techniques," *Proc. 8th Intl. Conf. Catal.* 3, 593-603 (1985b).

___, "CO_2 Step-Response Experiments During Alkali Catalysed Carbon Gasification: Evaluation of the So-Called CO Overshoot," *Carbon 25(3)*, 351-9 (1987a).

___, "Alkali-Catalysed Carbon Gasification in CO/CO_2 Mixtures: An Extended Model for the Oxygen Exchange and Gasification Reaction," *J. Catal. 107(1)*, 173-180 (1987b).

___, "Characterization of Alkali Carbonate Catalysts for Carbon Gasification with 18-Labelled CO_2," *Carbon 26(1)*, 41-8 (1988).

Clark, P.D. and K.L Lesage, "Quantitative Determination of Elemental Sulphur in Hydrocarbons, Solids, and Other Materials," *J. Chromatogr. Sci. 27(5)*, 259-261 (1989).

Clay, D.T. and M.A. Karnofski, "Black Liquor Solids Formation During Oil-Flash Evaporation," *Intl. Conf. Recovery Pulp. Chem.*, Vancouver, B.C., 13 (1981).

Clay, D.T., et al., "Black Liquor Combustion in a Laboratory Flow Reactor -Status Report One," *Proc. Tappi Eng. Conf.*, 41-8 (1987).

Cook, W.H., "Black Liquor Recovery," Canadian Patent No. 1,104,764. Issued July 14 (1981).

Davidson, J.F. and D. Harrison, *Fluidised Particles*, Cambridge University Press (1963).

Dearnaley, R.I., et al., "Molten Lithium Sulphate-Sodium Sulphate-Potassium Sulphate Eutectic: Reactions of Some Sulphur Compounds," *Inorg. Chem.* 22, 3242-7 (1983).

DeHaas, G.G., et al., "Dry Pyrolysis Approach to Chemical Recovery," *Intl. Forum on Kraft Recovery Alternatives*, Inst. Paper Chem., Appleton, Wisc., 103-123 (1976).

DeSouza, T.L.C., et al., "Analysis of Sulphur-Containing Gases by Gas-Solid Chromatography on a Specially-Treated Porapak QS Column," *Anal. Chem.* 45, 543-5 (1975).

DiNovo, S.T. and W.E. Ballantyne, "Process and Apparatus for Recovery of Spent Pulping Liquors," U.S. Patent No. 4,303,469. Issued Dec. 1 (1981).

Dionex Corporation, "Determination of Sulphur Compounds and Oxalate in Kraft Liquors Using Ion Chromatography," Application Note 30R, November, Sunnyvale, CA, 1-5 (1984).

Douglass, I.B. and L. Price, "Sources of Odour in the Kraft Process. II. Reactions Forming Hydrogen Sulphide in the Recovery Furnace," *Tappi J. 51(10)*, 465-7 (1968).

Durai-Swamy, K., et al., "Pulse-Enhanced Indirect Gasification for Kraft Liquor Recovery," *Proc. Intl. Chem. Recovery Conf.*, Ottawa, 217-221 (1989).

Easty, D.B. and J.E. Johnson, "Recent Progress in Ion Chromatographic Analysis of Pulping Liquors: Determination of Sulphide and Sulphate," *TAPPI J.*, March, 109-111 (1987).

Empie, H.J., "Alternative Kraft Recovery Processes," *Tappi J. 5*, 272-6 (1991).

Ergun, S., "Kinetics of the Reaction of Carbon Dioxide with Carbon," *J. Phys. Chem. 60(4)*, 480-5 (1956).

___, "Kinetics of the Reactions of Carbon Dioxide and Steam with Coke," *US Bureau of Mines Bulletin 598* (1961).

Ergun, S. and M. Mentser, "Reactions of Carbon with Carbon Dioxide and Steam," *Chem. Phys. Carbon 1*, 203-63 (1965).

Eriksson, G., "Thermodynamic Studies of High Temperature Equilibria," *Chemica Scripta 8*, 100-3 (1975).

Eriksson, G. and E. Rosén, "Thermodynamic Studies of High Temperature Equilibria: VIII. General Equations for the Calculation of Equilibria in Multiphase Systems," *Chemica Scripta 4*, 193-4 (1973).

Fallavollita, J.A., *Pyrolysis and Gasification of Kraft Black Liquor Solids in a Fluidized Bed Reactor*, Ph.D. Research Proposal, Dept. of Chem. Eng., McGill University (1984).

Fallavollita, J.A., et al., "Kraft Black Liquor Recovery in a Fluidized Bed: Part I - A Review," *Can. J. Chem. Eng. 65*, October, 812-7 (1987).

Ferguson, E., et al.,"Gasification of Potassium -Intercalated and Impregnated Natural Graphites," *Fuel 63(8)*, 1048-1058 (1984).

Feuerstein, D.L., *A Study of Malodorous Products from Thermal Decomposition of Kraft Black Liquor*, Ph.D. Thesis, University of California, Berkeley (1966).

Feuerstein, D.L., et al., "Malodorous Products from the Combustion of Kraft Black Liquor. I. Pyrolysis and Combustion Aspects," *TAPPI 50(6)*, 258-262 (1967).

Flood, H. W., "Kraft Black Liquor Recovery," U. S. Patent No. 3,322,492. Issued May 30 (1967).

Fogler, H.S., *Elements of Chemical Reaction Engineering*, Prentice-Hall, N.J. (1986).

Fox D.A. and A.H. White, "Effect of Sodium Carbonate Upon Gasification of Carbon and Production of Producer Gas," *Ind. Eng. Chem. 23(3)*, 259-266 (1931).

Freriks, I.L.C., et al., "Potassium - Catalysed Gasification of Carbon with Steam: A Temperature -Programmed Desorption and Fourier Transform Infrared Study," *Fuel 60(6)*, 463-70 (1981).

Frederick, W.J., "Combustion Parameters for Black Liquor," *Black Liquor Chemical Recovery Research- DOE Program Review Meeting*, Tacoma Washington, April 8-9, paper M:1-27 (1991).

Frederick, W.J. and M. Hupa, "Evidence of Sodium Fuming During Pyrolysis of Black Liquor," *Tappi J. 11*, 192-4 (1991).

Freund, H., "Kinetics of Carbon Gasification by CO_2," *Fuel 64(5)*, 657-660 (1985).

___, "Gasification of Carbon by CO_2: A Transient Kinetics Experiment," *Fuel 65(1)*, 63-6 (1986).

Gaskell, D.R., *Introduction to Metallurgical Thermodynamics, 2nd Ed.*, Hemisphere Publ. Co., 241-4 (1981).

Gitlesen, G. and K. Motzfeldt, "Phase Diagram by the Conductance Method. The System Na_2SO_4-Na_2CO_3," *Acta Chem. Scand. 18(2)*, 488-494 (1964).

Gluckman, M.J., et al., "Defluidization Characteristics of Sticky or Agglomerating Beds," *Fluidization Technology Vol. II*, (Ed., Keairns, D.L.), Hemisphere Publ., 395-422 (1976).

Grace, T.M., "The Impact of Black Liquor Oxidation on Total Energy Recovery," *Tappi J. 60(11)*, 132-5 (1977).

___, "Improved Energy Efficiency, Safety Likely in Future Recovery Systems," *Pulp and Paper Mag.*, October, 90-94 (1981).

___, "Black Liquor Combustion," *Intl. Colloquium High Temp. Res.- Black Liquor Combust.*, Univ. of Toronto, Ontario, paper 2:1-11 (1987).

Grace, T.M., et al., "Role of the Sulphate/Sulphide Cycle in Char Burning - Experimental Results and Implications," *Proc. Intl. Chem. Recovery Conf., Book 3*, TAPPI, New Orleans, 371-9 (1985).

Gundersby, P., "Keynote Address: Outlook for the Pulp Industry During the Second Half of the 1980's," *Proc. Intl. Chem. Recovery Conf., Book 1*, TAPPI, New Orleans, 1-5 (1985).

Harper, F.D., *Sulphur Release During the Pyrolysis of Kraft Black Liquor*, Ph.D. Thesis, Lawrence University, Appleton, Wisc. (1989).

Harrison, R.E., et al., "Ultra-High-Solids Evaporation of Black Liquor," *Tappi J. 2*, 61-6 (1988).

Hashimoto, K., et al., "Steam Gasification of Carbon: Effect of Several Metals on the Rate of Gasification and Rates of CO and CO_2 Formation," *Fuel 65(3)*, 407-411 (1986).

Hermans, M.A., *High Intensity Black Liquor Oxidation*, Ph.D. Dissertation, Inst. of Paper Chem., Appleton, Wisc. (1984).

Hill, C.G., *An Introduction to Chemical Engineering Kinetics and Reactor Design*, John Wiley and Sons (1977).

Hough, G.W., (Ed.), *Chemical Recovery in the Alkaline Pulping Processes*, TAPPI Press, Atlanta (1985).

Huhn, F., et al., "Investigations of the Alkali-Catalysed Steam Gasification of Coal: Kinetics and Interactions of Alkali Catalyst with Carbon," *Fuel 62(2)*, 196-9 (1983).

Hupa, M., et al., "Combustion Behaviour of Black Liquor Droplets," *Proc. Intl. Chem. Recovery Conf., Book 3*, TAPPI, New Orleans, 335-344 (1985).

Huttinger, K.J. and R. Minges, "Water Vapour Gasification of Carbon. Improved Catalytic Activity of Potassium Chloride Using Anion Exchange," *Fuel 64(4)*, 486-490 (1985a).

___, "Catalytic Water Vapour Gasification of Carbon: Importance of Melting and Wetting Behaviour of the Catalyst," *Fuel 64(4)*, 491-4 (1985b).

___, "Water Vapour Gasification of Carbon: Improved Catalytic Activity of Potassium Chloride Using Anion Exchange," *Fuel 64(4)*, 486-9 (1985c).

Huttinger, K.J., et al., "Catalytic Activity of Carbon Supported Potassium in the Carbon Monoxide Shift Reaction," *Fuel 65(7)*, 932-6 (1986).

Institute of Paper Chemistry (IPC), "Forum on Kraft Recovery Alternatives," Appleton, Wisc., (1976).

Isaak, P., et al., "Stickiness of Fireside Deposits in Kraft Recovery Units," *Proc. Intl. Chem. Recovery Conf. Book 3*, Tappi Press, 427-434 (1985).

Johnson, J.L, *Kinetics of Coal Gasification*, John Wiley and Sons, (1979).

Jones, K.H., *Control of Malodors from Kraft Recovery Operations by Pyrolysis*, Ph.D. Thesis, University of California, Berkeley (1968).

Juntgen, H., "Application of Catalysts to Coal Gasification Processes. Incentives and Perspectives," *Fuel 62(2)*, 234-8 (1983).

Kamyr AB, "Chemrec Technology: Chemicals and Energy Recovery from Kraft Spent Liquor," Technical Bulletin, Box 1033, S-651 15 Karlstad, Sweden (1990).

Kapteijn, F. and J.A. Moulijn, "Kinetics of the Potassium Carbonate-Catalysed CO_2 Gasification of Activated Carbon," *Fuel 62(2)*, 221-5 (1983).

___, in *Carbon and Coal Gasification: Science and Technology* (Eds. J.L. Figueiredo and J.A. Moulijn), NATO ASI Series E. No. 105, Martinus Nijhoff Publ., 291-360 (1986).

Kapteijn, F., et al.,"Kinetics of the Alkali Carbonate Catalysed Gasification of Carbon: 1. CO_2 Gasification," *Fuel 65(10)*, 1371-6 (1986).

Kelleher, E. G., "Feasibility Study: Black Liquor Gasification and Use of the Products in Combined Cycle Cogeneration," *TAPPI 67(4)*, 114-7 (1984).

___, "Black Liquor Gasification and Use of the Product Gases in Combined-Cycle Cogeneration," *Proc. Intl. Chem. Recovery Conf., Book 2*, TAPPI, New Orleans, 241-4 (1985a).

___, "Potential Replacement for Recovery Furnace Shows Promise," *TAPPI 68(12)*, p. 17 (1985b).

Kignell, J.E., "Process for Chemicals and Energy Recovery from Waste Liquors," U.S. Patent No. 4,808,264. Issued February 8 (1989).

Kleinau, J.H., "Addendum- Incremental Kraft Recovery with a Fluidized Bed System," *Forum on Kraft Recovery Alternatives*, Inst. Paper Chem., Appleton, Wisc., 148 (1976).

Klinzing, G.E., *Gas-Solid Transport*, McGraw-Hill (1981).

Kohl, A.L., "Black Liquor Gasification," *Can. J. Chem. Eng. 64(4)*, 299-304 (1986).

Krishnagopalan, J., et al., "Chromatographic Analysis of Kraft Liquor Anions," *TAPPI J. 10*, 108-112 (1985).

Kubaschewski, O., et al., *Metallurgical Thermochemistry, 5th Edition*, London (1977).

Kubelka, K.J. and J. Hojnos, "Dynamics of Reduction Reactions in Kraft Pulp Mill Recovery Units," *Collection Czech. Pulp and Paper Ind. Res. Works 1*, 113-131 (1956).

Kubelka, V. and J. Votoupal, *Sbornik Vyzkum. Praci z Oburu Celulozy a Papiru* 2, 49-73 (1957).

Kunii, D. and O. Levenspiel, *Fluidization Engineering*, Krieger Publ. Co., Huntington, N.Y. (1977).

Kunin, V.T. and J.P. Kirillov, "Reduction of Na_2SO_4 with Gaseous Reagents," *Khimia i Khimicheskaia Tekhnologia 11(5)*, 569-572 (1968).

Lang, R.L., "Anion Effects in Alkali-Catalysed Steam Gasification," *Fuel 65(10)*, 1324-9 (1986).

La Nauze, R.D. and K. Jung, "Mass Transfer Relationships in Fluidized-Bed Combustors," *Chem. Eng. Commun.* 43, 275-286 (1986).

Laurendeau, N.M., "Heterogeneous Kinetics of Coal Char Gasification and Combustion," *Progr. Energy Combust. Sci.* 4, 221-270 (1978).

Lesage, K.L., private communication with Alberta Sulphur Research Inc. (1991).

Li, J., *Pyrolysis and CO_2 Gasification of Black Liquor Char*, M.Eng. Thesis, Dept. of Chem. Eng., McGill University (1986).

___, *Rate Processes During Gasification and Reduction of Black Liquor Char*, Ph.D. Thesis, Dept. of Chem. Eng., McGill University (1989).

Li, J. and A.R.P. van Heiningen, "Kinetics of Sodium Sulphate Reduction in the Solid State by Carbon Monoxide," *Chem. Eng. Sci. 43(8)*, 2079-2085 (1988).

___, "Reaction Kinetics of Gasification of Black Liquor Char," *Can. J. Chem. Eng. 67(8)*, 693-7 (1989).

___, "Sodium Emission During Pyrolysis and Gasification of Black Liquor Char," *Tappi J. 12*, 213-9 (1990a).

___, "Kinetics of CO_2 Gasification of Fast Pyrolysis Black Liquor Char," *Ind. Eng. Chem. Res. 29(9)*, 1776-1785 (1990b).

___, "Sulphur Emission During Slow Pyrolysis of Kraft Black Liquor," *Tappi J. 3*, 237-9 (1991a).

___, "Kinetics of Gasification of Black Liquor Char by Steam," *Ind. Eng. Chem. Res. 30(7)*, 1594-1601 (1991b).

Magnusson, H. and B. Warnqvist, "Properties of Sodium Sulphide- Sodium Carbonate Melts," *Svensk Papperstidning 17*, 614-6 (1975).

Matsumoto, S. and P.L. Walker Jr., "Char Gasification in Steam at 1123 K Catalysed by K, Na, Ca and Fe-Effect of H_2, H_2S and COS," *Carbon 24(3)*, 277-285 (1986).

May, M.N., "Chemical Reaction Equilibrium in the Combustion of Sodium-Base Pulping Liquors," *Tappi J. 35(11)*, 511-7 (1952).

McAmish, L.H. and F.J. Johnston, "Sulphur Exchange and Decomposition Kinetics in Solid $Na_2S_2O_3$," *J. Inorg. Nucl. Chem. 30*, 537-540 (1976).

McKee, D.W., "The Catalysed Gasification Reactions of Carbon," *Chem. Phys. Carbon 16*, 1-118 (1981).

___, "Gasification of Graphite in Carbon Dioxide and Water Vapour -the Catalytic Effects of Alkali Metal Salts," *Carbon 20(1)*, 59-66 (1982).

McKee, D.W. and D. Chatterji, "The Catalytic Behaviour of Alkali Metal Carbonates and Oxides in Graphite Oxidation Reactions," *Carbon 13(5)*, 381-390 (1975).

___, "The Catalysed Reaction of Graphite with Water Vapour," *Carbon 16(1)*, 53-7 (1978).

McKee, D.W., et al., "Eutectic Salt Catalysts for Graphite and Coal Char Gasification," *Fuel 64(6)*, 805-8 (1985).

McKeough, P. and K. Saviharju, "Novel Energy Production Processes for Pulp Mills," *Kemia-Kemi 18(2)*, 102-6 (1991).

Meijer, R. et al., "Catalyst Loss and Retention During Alkali Catalysed Carbon Gasification in CO_2," *Am. Chem. Soc., Div. Fuel Chem., Prepr. 34(1)*, 36-43 (1989a).

___, "A Kinetic Mechanism of the Water-Gas Shift Reaction Over K_2CO_3/Carbon," *Prepr. Pap. - Am. Chem Soc., Div. Fuel Chem. 34(1)*, 130-5 (1989b).

Mentser, M. and S. Ergun, "Kinetics of Oxygen Exchange Between CO_2 and CO on Carbon," *Carbon 5*, 331-7 (1967).

Milanova, E. and G.J. Kubes, "The Combustion of Kraft Liquor Chars," *Proc. Intl. Chem. Recovery Conf.*, Book 3, TAPPI, New Orleans, 363-370 (1985).

Miller, P.T., et al., "The Influence of Composition on the Swelling of Kraft Black Liquor During Pyrolysis," *Proc. Tappi Eng. Conf.*, 225-234 (1986).

Mills, A.F., et al., "Analysis of Coal Particles Undergoing Rapid Pyrolysis," *Future Energy Production Systems, Vol. II*, (Eds. Denton, J.C. and N.H. Afgan), Academic Press, 537-547 (1976).

Mills, K.C., *Thermodynamic Data for Inorganic Sulphides, Selenides and Tellurides*, Butterworths, London (1974).

Mims, C.A. and J.K. Pabst, "Alkali Catalysed Carbon Gasification I. Nature of the Catalytic Sites," *Am. Chem. Soc., Div. Fuel Chem., Prepr. 25(3)*, 258-262 (1980a).

___, "Alkali Catalysed Carbon Gasification II. Kinetics and Mechanism," *Am. Chem. Soc., Div. Fuel Chem., Prepr. 25(3)*, 263-8 (1980b).

___, "Chemical Characterization of Active Sites in Alkali Catalysed Gasification", *Proc. Intl. Conf. Coal Science*, Verlag Gluckauf GmbH, Essen, 730-5 (1981).

___, "Role of Surface Salt Complexes in Alkali Catalysed Carbon Gasification," *Fuel 62(2)*, 176-9 (1983).

___, "Alkali Catalysed Carbon Gasification Kinetics: Unification of H_2O, D_2O and CO_2 Reactivities," *J. Catal. 107*, 209-220 (1987).

Miura, K. et al., "Steam Gasification of Carbon: Effect of Several Metals on the Rate of Gasification and the Rates of CO and CO_2 Formation," *Fuel 65(3)*, 407-411 (1986).

Moulijn, J.A. and F. Kapteijn," in *Carbon and Coal Gasification*, (Eds., Figueiredo, J.L. and J.A. Moulijn), NATO ASI Series E, No. 105, Martinus Nijhoff Publ., 181-95 (1986).

___, "The Mechanism of the Alkali Metal Catalysed Gasification of Carbon," *Erdoel Kohle Erdgas Petrochem 40(1)*, 15-21 (1987).

Moulijn, J.A., et al., "Mechanism of the Potassium Catalysed Gasification of Carbon in CO_2," *Fuel 63(8)*, 1043-7 (1984).

Nahas, N.C., "Exxon Catalytic Coal Gasification Process," *Fuel 62(2)*, 239-241 (1983).

Nakamura, N. "The Global Evaporator: A New Technology for Black Liquor Heating and High Solids Evaporation," *Proc. Intl. Chem. Recovery Conf.*, Ottawa, 183-8 (1989).

Newman, S.A., (Ed.), *Acid and Sour Gas Treating Processes*, Gulf Publ. (1985).

Nguyen, X.T., "Pulp Mill Residual Liquor Recovery System," Canadian Patent No.1,174,014. Issued September 11 (1984).

___, "Process to Regenerate Kraft Liquor," Canadian Patent No. 1,193,406. Issued Sept. 17 (1985).

Niderost, A.C., "Operation of an Incremental Kraft Recovery Boiler with a Fluid Bed System," *Pulp Industry 11*, 28-30 (1977).

Noopila, T., et al., "Combustion Properties of Laboratory-Made Cooking Liquors," *Intl. Chem. Recovery Conf.*, Ottawa, 75-80 (1989).

Nyman, C.J. and T.D. O'Brien, "Catalytic Reduction of Sodium Sulphate," *Ind. Eng. Chem. 39(8)*, 1019-1021 (1947).

Oshen, S. et al., "Ultra-High Solids Concentration of Black Liquor Using the HPD High-Solids Crystallizer," *Proc. Intl. Chem. Recovery Conf.*, Ottawa, 161-8 (1989).

Osterman, J. and H.E. Klei, "Paper Pulping Chemical Recovery System", U. S. Patent No. 3,523,864. Issued Aug. 11 (1970).

Ovechkin, E.K., et al., "Equilibrium Diagram of the Na_2CO_3-Na_2S System," *Zh. Neorg. Khim. 16(11)*, 1672-4 (1971).

Pejryd, L. and M. Hupa, "Bed and Furnace Gas Composition in Recovery Boilers - Advanced Equilibrium Calculations," *Proc. TAPPI Pulping Conf.*, 579-590 (1984).

Prahacs, S., in *Forum on Kraft Recovery Alternatives*, Inst. Paper Chem., Appleton, Wisc., 219-227 (1976).

Probstein, R.F. and R.E. Hicks, *Synthetic Fuels*, McGraw - Hill, New York (1982).

Rao, Y.K., et al., "On the Mechanism of Catalysis of the Boudouard Reaction by Alkali - Metal Compounds," *Carbon 20(3)*, 207-212, (1982).

Reid, R.C., et al., *The Properties of Gases and Liquids, 3rd Ed.*, McGraw-Hill, N.Y. (1977).

Reif, A.E., "The Mechanism of the Carbon Dioxide - Carbon Reaction," *J. Phys. Chem. 56*, 785-8 (1952).

Rosén, E., "Data and Calculations for the Gasification of Spent Cooking Liquors from the Pulp Industry. Part I. Fundamental Thermodynamic Quantities," *Trans. Roy. Inst. Techn. 159*, Stockholm (1960).

___, "Data and Calculations for the Gasification of Spent Cooking Liquors from the Pulp Industry. Part IV: The Behaviour of the Elements Sulphur and Sodium," *Trans. Roy. Inst. Tech. Stockholm 187*, 1-47 (1961).

___, "Study of Sulphide-Sulphate Equilibria Occurring in Recovery Boilers," *Intl. Conf. on Recovery of Pulp. Chem.*, Vancouver, 71-4 (1981).

Ryham, R., "High Solids Evaporation Through Thermal Depolymerization of Black Liquor," *Proc. Intl. Chem. Recovery Conf.*, Ottawa, 157-160 (1989).

Saber, J.M., et al., "Carbon Dioxide Gasification of Carbon Black: Isotope Study of Carbonate Catalysis," *J. Catal. 90*, 65-74 (1984).

___, "Interaction of Potassium Carbonate with Surface Oxides of Carbon," *Fuel 65(10)*, 1356-9 (1986).

___, "A Mechanism for Sodium Oxide Catalysed CO_2 Gasification of Carbon," *J. Catal. 109*, 329-346 (1988).

Sams, D.A. and F. Shadman, "Catalytic Effect of Potassium on the Rate of Char-CO_2 Gasification," *Fuel 62(8)*, 880-2 (1983).

___, "Mechanism of Potassium-Catalysed Carbon/CO_2 Reaction," *AIChE J. 32(7)*, 1132-7 (1986).

Sams, D.A., et al., "Kinetics of Catalyst Loss During Potassium-Catalysed CO_2 Gasification of Carbon," *Fuel 64(9)*, 1208-1213 (1985).

Sell, N.J. and D.T. Clay, "Computer Modelling and Design of a Fluidized Bed Dryer for Kraft Black Liquor," *Tappi J. 6*, 177-184 (1991).

Sen Gupta, S.K., *Oxidation of Sodium Thiosulphate in Weak Kraft Black Liquor*, M.Eng. Thesis, Dept. of Chem. Eng., McGill University (1987).

Shadman, F., et al., "Significance of the Reduction of Alkali Carbonates in Catalytic Carbon Gasification," *Fuel 66(12)*, 1658-1663 (1987).

Shah, I.S., "Recovery of Black Liquor," U.S. Patent No. 3,574,051. Issued April 6 (1971).

Shivgulam, N., et al., "Sodium Chloride, Potassium: Their Effects on Kraft Smelt," *Pulp Paper Can. 80(9)*, 89-92 (1979).

Skoog, D.A., *Principles of Instrumental Analysis*, 3rd Ed., Saunders College Publ., N.Y., 5-21 (1985).

Smith, J.M. and H.C. van Ness, *Introduction to Chemical Engineering Thermodynamics, 3rd Edition*, McGraw-Hill (1975).

Smoot, L.D. and P.J. Smith, *Coal Combustion and Gasification*, Plenum Press (1985).

So, C.W. and D. Barham, "The System K_2SO_4 - K_2S. A New Experimental Technique," *J. Thermal Anal. 20*, 275-280 (1981).

Spiro, C.L., et al., "Significant Parameters in the Catalysed CO_2 Gasification of Coal Chars," *Fuel 62(3)*, 323-330 (1983).

___, "Observation of Alkali Catalyst Particles during Gasification of Carbonaceous Materials in CO_2 and Steam," *Fuel 63(5)*, 686-691 (1984).

Stigsson, L., "A New Concept for Kraft Recovery," *Proc. Intl. Chem. Recovery Conf.*, Ottawa, 191-4 (1989).

Stigsson, L. "Chemrec Kraft Recovery Technology," *Black Liquor Chemical Recovery Research - Program Review Meeting*, paper N:1-8, Abstract available from DOE, Washington, D.C., April 8-9 (1991).

Strohbeen, D.T., *An Investigation of the Reactions Leading to Volatilization of Inorganic Sulphur During Pyrolysis with Vanillic Acid and Sodium Gluconate*, Ph.D. Thesis, Lawrence University, Appleton, Wisc. (1981).

Strohbeen, D.T. and T.M. Grace, "Production of Volatile Sulphur Compounds During Pyrolysis," *Tappi J. 65(10)*, 125 (1982).

Stull, D.R. and H. Prophet, *JANAF Thermochemical Tables - 2nd ed.*, Natl. Bur. Stand., Washington, (1970).

Thomas, J.F. et al., "A Mechanism to Explain the Production of Malodorous Products in Kraft Recovery Furnaces," *Tappi J. 52(10)*, 1873-5 (1969).

Thompson, W.T., et al., "F*A*C*T User's Guide Supplement 'EQUILIB'," McGill University - Ecole Polytechnique (1988).

Thorman, R.P. and T.S. Macur, "Kinetics of Sodium Sulphate Reduction by Carbon in Molten Sodium Carbonate," *Proc. Intl. Chem. Recovery Conf., Book 3*, TAPPI, New Orleans, 451-8 (1985).

Tomlinson, II, G. H., "Pulp Mill Recovery System," U. S. Patent No. 4,011,129. Issued March 8 (1977).

Tomlinson, II, G.H., et al., "Incremental Kraft Recovery with a Fluidized Bed System," *Proc. from Gunnar Sundblad Seminar at Billingehus*, Skovde, Sweden, STFI Meddelande Serie D, No. 7 (1976).

Tran, H.N., "How Does a Kraft Recovery Boiler Become Plugged," *Tappi J. 11*, 102-6 (1986).

Tran, H.N. and D. Barham, "The System Na_2SO_4-Na_2S," *Can. Pulp Paper Assoc., Tech. Sect. -Intl. Conf. on Recovery of Pulp Chem.*, Vancouver, 67-70 (1981).

Tran, H.N., et al., "Chloride and Potassium in the Kraft Chemical Recovery Cycle," *Proc. Intl. Chem. Recovery Conf.*, Ottawa, 23-8 (1989).

Treybal, R.E., *Mass-Transfer Operations, 3rd Ed.*, McGraw-Hill, N.Y. (1980).

van den Berg, G.J. et al., in *Energy Technology Handbook*, (Ed., Considine, D.M.), McGraw-Hill, 9:165-170 (1977).

van Heiningen, A.R.P., private communication, July (1991).

van Heiningen, A.R.P. and J. Li, private communication, December (1986).

van Heiningen, A.R.P., J. Li and J.A. Fallavollita, *Low-Temperature Recovery of Kraft Black Liquor*, U.S. Patent Application PD-4081 (1989); Reference no. 433604, approved June 5 (1991).

van Krevelen, D.W., *Coal*, Elsevier, New York (1961).

Veraa, M.J., and A.T. Bell, "Effect of Alkali Metal Catalysts on Gasification of Coal Char," *Fuel 57(4)*, 194-200 (1978).

von Fredersdorff, C.G. and M.A. Elliott, in *Chemistry of Coal Utilization*, (Ed., H.H. Lowry) Supplementary Volume, 892-1022 (1963).

Wagman, D. D., et al., "Selected Values of Chemical Thermodynamic Properties," *Natl. Bur. Stand. (U.S.) Series 270*, Washington (1971); revision (1982).

Walker, P.L. Jr., et al., "Gas Reactions of Carbon," *Advan. Catal. 11*, 133-221 (1959).

___, in *Chemistry and Physics of Carbon 4*, (Ed. Walker, P.L. Jr.), Marcel Dekker, N.Y., 287-383 (1968).

Warnqvist, B., "Comments on Thermochemical Data and Fusion Temperature for Pure Sodium Sulphide," *Thermochemica Acta 37*, 343-5 (1980).

___, private communication with M. M. Avedesian, Dec. 4 (1986).

___, "Gasification of Black Liquor - Chemical Equilibrium Considerations," *Intl. Colloquium in High Temp. Res. -Black Liquor Combustion*, Univ. of Toronto, paper 11, 1-6 (1987).

Wen, W.Y., "Mechanisms of Alkali Metal Catalysis in the Gasification of Coal, Char, or Graphite," *Catal. Rev.-Sci. Eng. 22(1)*, 1-28 (1980).

Wigmans, T., et al., "The Influence of Pretreatment Conditions on the Activity and Stability of Sodium and Potassium Catalysts in Carbon - Steam Reactions," *Carbon 21(3)*, 295-301 (1983a).

___, "On the Mechanism of the Potassium Carbonate Catalysed Gasification of Activated Carbon: The Influence of the Catalyst Concentration on the Reactivity and Selectivity at Low Steam Pressures," *Carbon 21(1)*, 1-12 (1983b).

Wood, B.J. and K.M. Sancier, "The Mechanism of the Catalytic Gasification of Coal Char: A Critical Review," *Catal. Rev.- Sci. Eng. 26(2)*, 233-279 (1984).

Wood, B.J., et al., "Reactive Intermediate in the Alkali Carbonate-Catalysed Gasification of Coal Char," *Fuel 63(11)*, 1600-3 (1984).

___, "A Study of the Role of Alkali Metal Salts as Char Gasification Catalysts by Knudsen Cell Mass Spectroscopy," *Carbon 23(1)*, 73-7 (1985).

Yates, J.G., *Fundamentals of Fluidized-Bed Chemical Processes*, Butterworths (1983).

Yuh, S.J., *Kinetics and Mechanistic Studies of the Steam Gasification of Coal Chars Catalysed by Alkali Metal Salts*, Ph.D Thesis, University of Notre Dame (1984).

Yuh, S.J. and E.E. Wolf, "Kinetic and FT-i.r. Studies of the Sodium -Catalysed Steam Gasification of Coal Chars," *Fuel 63(11)*, 1604-9 (1984).

Zou X. et al., "Autocausticizing of Kraft Black Liquor: Process Implications Based on Chemical Equilibrium Calculations," *Proc. TAPPI Pulping Conf.*, 897-903 (1990).

TABLES

Table 1

Inorganic Sulphur Composition of Solid Char Residue for Pyrolysis Experiments Performed with a Final Temperature of 750°C (Li, 1986)

Pyrolysis atmosphere	S^{2-} (wt%)*	SO_4^{2-} (wt%)*	Reduction efficiency **
He	0.96	0.17	90%
He + CO (12 vol%)	1.20	0.17	92%

* Based on dry black liquor solids.
** [(weight Na_2S)/(weight Na_2S + weight Na_2SO_4)] x 100.

Table 2

Typical Ultimate and Proximate Analyses for Dry Kraft Black Liquor Solids

Ultimate analysis (wt%)		Proximate analysis (wt%)	
Carbon	39	Alkali Lignin	41
		Hydroxy acids	26
Hydrogen	4	Extractives	3
		Acetic acid	5
Oxygen	36	Formic acid	3
		Methanol	1
Sodium	18	Sodium	18
Sulphur	3	Sulphur	3

Table 3

Thermodynamic Data for Solid Na_2S

Reference	C_p ($J \cdot K^{-1} \cdot mol^{-1}$)	ΔH°_{298} ($kJ \cdot mol^{-1}$)	S°_{298} ($J \cdot K^{-1} \cdot mol^{-1}$)
Warnqvist (1980) and Rosén (1960)	$81.57 + 9.20 \cdot 10^{-3}$ T	- 386.6	90.3
F*A*C*T database (Mills, 1974)	$82.87 + 6.86 \cdot 10^{-3}$ T	- 374.4	79.5

Table 4

Thermodynamic Properties of Selected Chemical Species from the F*A*C*T Database

Chemical Species	C_p Range (K)	ΔH°_{298} (kJ·mol^{-1})	S°_{298} (J·K^{-1}·mol^{-1})	ΔH_{Trans} (kJ/mol)	$C_p^\dagger$ (J·K^{-1}·mol^{-1})			
					A	B	C	D
GASES								
N_2	298-2500	0.000	191.502	-	27.865	4.268	0.000	0.000
CO	298-2500	-110.515	197.505	-	28.403	4.099	-0.460	0.000
CO_2	298-2500	-393.411	213.609	-	44.131	9.035	-8.533	0.000
CH_4	298-2000	-74.792	186.143	-	12.444	76.670	1.447	-17.999
O_2	298-3000	0.000	204.988	-	29.950	4.183	-1.673	0.000
H_2	298-3000	0.000	130.551	-	27.273	3.263	0.502	0.000
$H_2O_{(v)}$	298-2500	-241.589	189.343	-	29.992	10.708	0.335	0.000
COS	298-1800	-141.804	231.320	-	47.393	9.119	-7.655	0.000
$(CH_3)_2S$	295-300	-37.2	285.85	-	74.099	0.000	0.000	0.000
CH_3SH	295-300	-22.34	255.057	-	50.250	0.000	0.000	0.000
CS_2	298-2000	117.255	238.687	-	49.568	13.276	-7.012	-3.653
H_2S	298-1800	-20.497	205.636	-	29.365	15.393	0.000	0.000
LIQUIDS								
NaOH	593-900	-420.036	74.160	-	89.454	-5.858	0.000	0.000
	900-1663	-418.673	77.013	-	83.680	0.000	0.000	0.000
SOLIDS								
Na_2S	298-1251	-374.378	79.477	-	82.865	6.860	0.000	0.000
Na_2CO_3	298-723	-1130.498	138.750	0.690	11.014	243.978	24.487	0.000
	723-1123	-1116.643	165.367	-	50.071	129.046	0.000	0.000
Na_2SO_4	298-522	-1386.874	149.584	10.809	82.305	154.323	0.000	0.000
	522-980	-1380.942	157.515	0.335	145.016	54.584	0.000	0.000
	980-1157	-1382.816	157.456	-	142.649	59.298	0.000	0.000
Na_2SO_3	298-1000	-1089.430	146.022	-	107.110	43.514	0.000	0.000
Na_2O	298-1023	-417.982	75.061	-	66.216	43.865	-8.134	-14.088
C(graphite)	298-1100	0.0	5.739	-	0.109	38.931	-1.481	-17.380

† $C_p = A + 1{\cdot}10^{-3}{\cdot}B{\cdot}T + 1{\cdot}10^{5}{\cdot}C{\cdot}T^{-2} + 10^{-6}{\cdot}D{\cdot}T^{2}$

Table 5

Reaction Mechanisms and Rate Laws for the Uncatalysed Gasification of Carbon by CO_2 and H_2O

C - CO_2 (Reif, 1952: Ergun, 1956: Walker et al., 1959: Laurendeau, 1978)

$$C_F + CO_2 \underset{i_{-1}}{\overset{i_1}{\Leftrightarrow}} C(O) + CO(g) \qquad (65)$$

$$- r_n = \frac{k_1 p_{CO_2}}{1 + k_2 p_{CO} + k_3 p_{CO_2}} \qquad (66)$$

$$C(O) \xrightarrow{i_2} CO(g) + C_F' \qquad (67)$$

$$- r_n = \frac{i_2 N_T}{1 + \left(\frac{p_{CO}}{p_{CO_2} \cdot K_{CO\text{-}CO_2}} \right)} \qquad (68)$$

where $k_1 = i_1 N_T$; $k_2 = \frac{i_{-1}}{i_2}$; $k_3 = \frac{i_1}{i_2}$; $K_{CO\text{-}CO_2} = \frac{i_1}{i_{-1}}$

C - H_2O (Walker et al., 1959: Kapteijn and Moulijn, 1986)

$$C_F + H_2O \underset{m_{-1}}{\overset{m_1}{\Leftrightarrow}} C(O) + H_2 \qquad (69)$$

$$- r_n = \frac{\ell_1 p_{H_2O}}{1 + \ell_2 p_{H_2} + \ell_3 p_{H_2O}} \qquad (70)$$

$$C(O) \xrightarrow{i_2} CO(g) + C_F' \qquad (67)$$

$$- r_n = \frac{i_2 N_T}{1 + \left(\frac{p_{H_2}}{p_{H_2O} \cdot K_{H_2\text{-}H_2O}} \right)} \qquad (71)$$

where $\ell_1 = m_1 N_T$; $\ell_2 = \frac{m_{-1}}{i_2}$; $\ell_3 = \frac{m_1}{i_2}$; $K_{H_2\text{-}H_2O} = \frac{m_1}{m_{-1}}$

C - H_2O - CO_2 (Ergun, 1961: Laurendeau, 1978: Kapteijn and Moulijn, 1986)

$$C_f + H_2O \underset{m_{-1}}{\overset{m_1}{\Leftrightarrow}} C(O) + H_2 \qquad (69)$$

$$- r_n = \frac{k_1 p_{CO_2} + \ell_1 p_{H_2O}}{1 + k_2 p_{CO} + k_3 p_{CO_2} + \ell_2 p_{H_2} + \ell_3 p_{H_2O}} \qquad (72)$$

$$C(O) \xrightarrow{i_2} CO(g) + C_F' \qquad (67)$$

$$- r_n = \frac{i_2 N_T}{1 + \left(\frac{p_{H_2}}{p_{H_2O} \cdot K_{H_2\text{-}H_2O}} \right)} = \frac{i_2 N_T}{1 + \left(\frac{p_{CO}}{p_{CO_2} \cdot K_{CO\text{-}CO_2}} \right)} \qquad (73)$$

$$C_F + CO_2 \underset{i_{-1}}{\overset{i_1}{\Leftrightarrow}} C(O) + CO(g) \qquad (65)$$

where ℓ_1, ℓ_2, ℓ_3, k_1, k_2, k_3, $K_{CO\text{-}CO_2}$, $K_{H_2\text{-}H_2O}$ are defined in Eqs. 66, 68, 70, 71

Table 6

Mechanisms for CO_2 Gasification of Carbon Catalysed by Alkali Carbonates

Mechanism		References
Alkali Carbonate cycles		
$Na_2CO_3(l) + 2C \Leftrightarrow 2Na(v) + 3CO$	(74)	Fox and White (1931)
$2Na(v) + CO_2 \Leftrightarrow Na_2O(v) + CO$	(75)	
$Na_2O(v) + CO_2 \Leftrightarrow Na_2CO_3(v)$	(76)	
$Na_2CO_3(v) \Leftrightarrow Na_2CO_3(l)$	(77)	
$M_2CO_3(s,l) + 2C \rightarrow 2M(s,l) + 3CO$	(78)	McKee and Chatterji (1975; 1978)
$2M(s,l) + CO_2 \Leftrightarrow M_2O(s,l) + CO$	(79)	
$M_2O(s,l) + CO_2 \Leftrightarrow M_2CO_3(s,l)$	(80)	
$M_2CO_3 + 2C \rightarrow 2M + 3CO$	(78)	Wen (1980)
$2M + 2nC \Leftrightarrow 2C_nM$	(81)	
$2C_nM + CO_2 \Leftrightarrow (2C_nM)\cdot OCO \Leftrightarrow (2nC)\cdot M_2O + CO$	(82)	
$(2nC)\cdot M_2O + CO_2 \Leftrightarrow (2nC)\cdot M_2CO_3 \Leftrightarrow 2nC + M_2CO_3$	(83)	
Alkali Oxide cycles		
$K_xO_y + CO_2 \Leftrightarrow K_xO_{y+1} + CO$	(84)	Kapteijn and Moulijn (1983) Moulijn et al. (1984)
$K_xO_{y+1} + C_f \rightarrow K_xO_y + C(O)$	(85)	
$(-COK) + CO_2 \Leftrightarrow (-CO_2K) + CO$	(86)	Sams and Shadman (1986)
$(-CO_2K) + C_f \rightarrow (-COK) + C(O)$	(87)	
$C_f + CO_2 \Leftrightarrow C(O) + CO$	(65)	Cerfontain et al. (1987b)
$CO_2(*) + CO_2 \underset{k_{-8}}{\overset{k_8}{\Leftrightarrow}} CO_3(*) + CO$	(88)	
$CO_3(*) + C_f \underset{k_{10}}{\overset{CO_2}{\rightarrow}} CO_2(*) + C(O)$	(89)	
$C(O) \xrightarrow{i_2} CO(g) + C_f'$	(67)	

Table 7

Mechanisms for Steam Gasification of Carbon Catalysed by Alkali Carbonates

Mechanism		References
Alkali Carbonate Cycles		
$M_2CO_3 + 2C \rightarrow 2M(g) + 3CO$	(90)	
$2M(g) + 2H_2O \Leftrightarrow 2MOH + H_2$	(91)	McKee and Chatterji (1978)
$2MOH + CO \Leftrightarrow M_2CO_3 + H_2$	(92)	
Alkali Oxide Cycles		
$(*) + H_2O \Leftrightarrow O(*) + H_2$	(93)	Kapteijn and Moulijn (1986)
$O(*) + C_F \rightarrow (*) + CO$	(94)	
$K_{surf} + H_2O \Leftrightarrow K_{surf}(O) + H_2$	(95)	
$K_{surf}(O) + C_F \rightarrow K_{surf} + C(O)$	(96)	Wigmans et al. (1983b)
$C(O) \xrightarrow{i_2} CO(g) + C_F^{\cdot}$	(67)	
$C(O) + K_{surf}(O) \Leftrightarrow K_{surf} + CO_2$	(97)	
$K_xO_y + H_2O \Leftrightarrow K_xO_{y+1} + H_2$	(98)	
$K_xO_{y+1} + C_F \rightarrow K_xO_y + C(O)$	(99)	
$C(O) \xrightarrow{i_2} CO(g) + C_F^{\cdot}$	(67)	Huttinger and Minges (1985a,b)
$C(O) + K_xO_{y+1} \Leftrightarrow K_xO_y + CO_2$	(100)	
$1\cdot[Na_2O\text{-}C + H_2O \Leftrightarrow (NaO)_2\text{-}C + H_2]$	(101)§	
$a\cdot[(NaO)_2\text{-}C + C_F \rightarrow Na_2O\text{-}C + CO]$	(102)§	Saber et al. (1988)
$(1\text{-}a)\cdot[CO + (NaO)_2\text{-}C \Leftrightarrow Na_2O\text{-}C + CO_2]$	(103)§	
Water-Gas Shift		
$K_xO_y + H_2O \Leftrightarrow K_xO_{y+1} + H_2$	(98)	Huttinger et al. (1986)
$CO + K_xO_{y+1} \Leftrightarrow K_xO_y + CO_2$	(104)	
$(*) + H_2O \Leftrightarrow O(*) + H_2$	(105)	
$CO + O(*) \Leftrightarrow CO_2(*)$	(106)	Meijer et al. (1989b)
$CO_2(*) \Leftrightarrow CO_2 + (*)$	(107)	

§ 1, a and (1-a) are multipliers indicating the frequency of each reaction step.

Table 8

Variation in Carbon Reactivity with Carbon Burn-off for Na_2CO_3- and K_2CO_3- Catalysed Gasification with CO_2 or H_2O

Rate Type	Observations	Temp (K)	Catalyst	Mixing	(M/C) initial ($mol \cdot mol^{-1}$)	Pretreatment	Carbon Type	Gas Concentration	Reference
$-r_n$	constant up to ~ 80% burn-off then decrease	1050	K_2CO_3	aqueous impregnation	0.009	He at 1050 K for 30 min	steam-activated peat char	$p_{CO_2} = 140\ kPa$	Kapteijn and Moulijn (1983)
$-r_w$	constant between 20-70% burn-off	973	K_2CO_3	aqueous impregnation	varied	-	coal chars	p_{H_2O} & p_{CO_2} not reported	Mims and Pabst (1980a)
$-r_n$	constant up to 80% burn-off then sharp decrease	1153	K_2CO_3	aqueous impregnation	-	-	bituminous coal char	$p_{H_2O} = 100\ kPa$	Huhn et al. (1983)
$-r_n$	constant up to 90% burn-off	1050-1098	Na_2CO_3 or K_2CO_3	volumetric dispersion	0.0025	-	polymer of coconut char and phenol formaldehyde	p_{CO_2} or $p_{H_2O} = 1\ atm$	Miura et al. (1986)
$-r_w$	maximum observed at 30% burn-off which was 3 times the initial rate	1073	K_2CO_3	incipient wetting	0.025	1 h at 1073 K in N_2	graphitized carbon	15 vol % CO_2 85 vol % N_2	Sams et al. (1985)
$-r_n$	maximum rate at 20-50% burn-off followed by steady decrease	973-1173	K_2CO_3	aqueous impregnation	0.018	-	sub-bituminous coal char	$p_{H_2O} = 0.5\ atm$ $p_{He} = 0.5\ atm$	Veraa and Bell (1978)

Table 9

Langmuir-Hinshelwood Kinetics for CO_2 and Steam Gasification of Various Carbons Catalysed by Alkali Carbonates

Rate Law	Parameters					Carbon Burn-off (%)	Initial M/C (mol/mol)	Catalyst & Carbon	T (K) Pressure (kPa)	Reference
$-r_a = \frac{K'_r N_{cT}}{1 + \frac{p_{CO}}{p_{CO_2} \cdot K'_{ox}}}$	$K'_r N_{ox}$ ($10^{-4} mol \cdot s^{-1} \cdot g^{-1}$)		K'_{ox}				0.018	K_2CO_3 / peat char	T = 1050 p_{CO_2} = 50-2030	Kapteijn and Moulijn (1983)
	0.34 ± 0.02		0.09 ± 0.01			• 20				
	0.32 ± 0.03		0.10 ± 0.03			• 40				
	0.16 ± 0.02		0.10 ± 0.04			• 80				
$-r_a = \frac{K'_r N_{cT}}{1 + \frac{p_{CO}}{p_{CO_2} \cdot K'_{ox}}}$	$-r_a$ (@ 1000 K) ($\mu mol \cdot s^{-1} \cdot mol^{-1}$)	$\ln(N_{ox} A'_r)$ ($\mu mol \cdot s^{-1} \cdot mol^{-1}$)	E'_r (kJ/mol)	$\Delta S'_{ox}$ (J/mol·K)	$\Delta H'_{ox}$ (kJ/mol)	20-60	0.018		T = 750-1000 P_t = 50-3000	Kapteijn et al. (1986)
	35.3	35.8	268	40 ± 22	64 ± 23			• Na_2CO_3		
	75.0	31.5	226	61	85			• K_2CO_3		
	3.1	31.7	254	57	96 ■			• carbon		
$-r_a = \frac{i_2 N_{cT}}{1 + \frac{p_{CO}}{p_{CO_2} \cdot K_{CO-CO_2}}}$	$K_{C-CO_2} = \exp\left[\frac{-1.34 \cdot 10^4}{T} + 10.7\right]$ $i_2 = i_2 N_{cT} = \exp\left[\frac{-2.77 \cdot 10^4}{T} + 25\right]$					-	0.018	K_2CO_3 / Supelco Carbosieve	T = 850-1073 P_t = 10 p_{CO} = 0.5-4 p_{CO_2} = 6-9.5	Freund (1985)
$-r_a = \frac{k_0 p_{H_2O}}{1 + k'_0 p_{H_2O}}$	A_o (10^6 mol/kg·s·kPa)		E_o (kJ·mol^{-1})	A'_o (10^3 kPa^{-1})	E'_o (kJ·mol^{-1})	initial rate	0.005	Na_2CO_3 / carbon black	T = 873-1100 p_{H_2O} = 25-101	Hashimoto et al. (1986)
	3.85		195	1.19	101					

■ value obtained from uncatalysed gasification (Ergun, 1956)

Table 10

Composition of Kraft Black Liquor Solids (wt% moisture-free basis) †

Elemental Analysis		Inorganic Species	
C	37.65 ± 1.95	S^{2-}	0.10 ± 0.01*
O	34.87 ± 2.44	$S_2O_3^{2-}$	0.85 ± 0.05*
Na	18.82 ± 1.01	SO_4^{2-}	0.40 ± 0.02*
H	3.44 ± 0.07	SO_3^{2-}	NQ■
S	1.67 ± 0.05	S_x^{2-}	NQ■
Ca	0.02 ± 0.005	S^0	< 0.001*
K	0.63 ± 0.03	Total	1.35 ± 0.06*
Cl	0.28 ± 0.01		
Total	97.38 ± 3.28	CO_3^{2-}	6.66 ± 0.33
		OH^-	0.90 ± 0.04

† 95% confidence level for the population mean.
* expressed as equivalent sulphur (wt%).
■ not quantifiable.

Table 11

Char Analyses Data for Triplicate Runs at 550°C and Duplicate Runs at 600°C (g /100 g char)

Run No.	T (°C)	Total C	Total S	Na^+	CO_3^{2-}	S^{2-}	SO_3^{2-}	SO_4^{2-}
Pyrolysis								
P4	550	37.0 ± 1.2	1.69 ± 0.11	24.4 ± 1.1	30.4 ± 1.8	0.29 ± 0.04	1.10 ± 0.08	1.69 ± 0.06
P3	550	38.3 ± 5.8	1.51 ± 0.29	23.9 ± 3.8	30.0 ± 4.6	-	-	-
P2	550	33.7 ± 2.0	1.45 ± 0.15	-	-	0.24 ± 0.02	0.76 ± 0.05	1.61 ± 0.32
P5	600	36.2 ± 3.0	1.94 ± 0.19	28.0 ± 4.0	30.2 ± 3.5	1.03 ± 0.09	0.33 ± 0.06	0.48 ± 0.04
P6	600	37.6 ± 2.7	2.00 ± 0.17	22.8 ± 2.1	28.1 ± 2.6	0.84 ± 0.10	0.50 ± 0.12	0.59 ± 0.07

Table 12

Gas Analyses Data for Duplicate Pyrolysis Runs at 550°C, 600°C, and Steam Gasification Runs at 500°C (mol /kg KBLS)

Run No.	T (°C)	CO_2	CO	H_2	CH_4	H_2S	CH_3SH	$(CH_3)_2S$
Pyrolysis								
P3	550	2.02 ± 0.09	1.58 ± 0.05	0.94 ± 0.14	0.76 ± 0.02	0.14 ± 0.03	-	-
P4	550	2.41 ± 0.18	1.90 ± 0.10	0.44 ± 0.06	0.77 ± 0.11	0.15 ± 0.02	-	-
P5	600	2.78 ± 0.23	2.26 ± 0.26	7.98 ± 1.13	0.72 ± 0.39	0.06 ± 0.01	-	-
P6	600	2.65 ± 0.16	2.12 ± 0.19	5.96 ± 1.93	0.77 ± 0.16	0.04 ± 0.01	-	-
Steam Added								
SG3	500	1.36 ± 0.24	0.96 ± 0.27	1.26 ± 0.86	0.98 ± 0.27	0.13 ± 0.02	0.09 ± 0.03	0.02 ± 0.01
SG2	500	2.16 ± 0.34	1.27 ± 0.05	3.73 ± 0.80	1.50 ± 0.26	0.16 ± 0.02	0.10 ± 0.01	0.02 ± 0.01

Table 13

Mass Balances for Sodium and Carbon During Pyrolysis and Steam Gasification

	Carbon $\left(\frac{g}{100\ g\ C\ in\ KBLS}\right)$	Sodium $\left(\frac{g}{100\ g\ Na\ in\ KBLS}\right)$
Input KBLS	100 ± 5	100 ± 5
Pyrolysis		
Run: P1 (500°C)		
Char	71 ± 8	95 ± 28
Gases	14 ± 2	-
Mass Balance Closure[1]	15 ± 8	5 ± 28
Run: P4 (550°C)		
Char	72 ± 5	96 ± 7
Gases	16 ± 1	-
Mass Balance Closure[1]	12 ± 5	4 ± 7
Run: P6 (600°C)		
Char	68 ± 8	82 ± 11
Gases	18 ± 1	-
Mass Balance Closure[1]	14 ± 8	18 ± 11
Run: P7 (650°C)		
Char	61 ± 9	87 ± 15
Gases	19 ± 3	-
Mass Balance Closure[1]	20 ± 9	13 ± 15
Run: P8 (700°C)		
Char	41 ± 4	87 ± 9
Gases	40 ± 3	-
Mass Balance Closure[1]	19 ± 5	13 ± 9
Steam Gasification		
Run: SG2 (500°C)		
Char	75 ± 7	-
Gases	16 ± 2	-
Mass Balance Closure[1]	9 ± 7	-
Run: SG4 (600°C)		
Char	65 ± 7	98 ± 24
Gases	23 ± 2	-
Mass Balance Closure[1]	12 ± 7	2 ± 24
Run: SG5 (650°C)		
Char	46 ± 3	125 ± 10
Gases	45 ± 2	-
Mass Balance Closure[1]	9 ± 3	-25 ± 10 [2]

[1] Calculated by difference and includes the amount of material which was not recovered during maintenance of the unit as well as the condensables.

[2] Indicates that the measured sodium content in the char accounts for more than the total input sodium in KBLS.

Table 14

Stoichiometric Relationships Among Reactants For Steam Gasification at 650°C

	Before Steam Addition (Run P7) ($mol \cdot min^{-1}$)	After Steam Addition (Run SG5) ($mol \cdot min^{-1}$)
Carbon Monoxide	0.020 ± 0.001	(0.020 ± 0.001) + ξ_{40} - ξ_{41}
Carbon Dioxide	0.010 ± 0.004	(0.010 ± 0.004) + ξ_{41}
Hydrogen	0.025 ± 0.008	(0.025 ± 0.008) + ξ_{40} + ξ_{41}
Steam	0	0.56† - ξ_{40} - ξ_{41}

† The inlet H_2O molar feed rate for run SG5.

Table 15

Stoichiometric Predictions of CO_2, Steam, and Reaction Rate for 600°C and 650°C

Run No.	T (°C)	CO_2 (calculated)	CO_2 (measured)	Steam (calculated)	Steam Conversion	ξ_{40}	ξ_{41}
		($mol \cdot min^{-1}$)	($mol \cdot min^{-1}$)	($mol \cdot min^{-1}$)	(wt%)	($mol \cdot min^{-1}$)	($mol \cdot min^{-1}$)
SG5	650	0.074 ± 0.009	0.061 ± 0.001	0.42 ± 0.02	23.5 ± 1.9	0.068 ± 0.005	0.064 ± 0.009
SG4	600	0.037 ± 0.013	0.028 ± 0.003	0.52 ± 0.03	7.1 ± 3.2	0.018 ± 0.013	0.022 ± 0.013

Table 16

Molar Concentration of Major Inorganic Species in the Char (mol %)

Run No.	T (°C)	$[CO_3^{2-}]$	$[Cl^-]$	$[SO_4^{2-}]$	$[S^{2-}]$	$[Na^+]$	$[K^+]$
Pyrolysis							
P1§	500	30.1 ± 6.7	1.1 ± 0.2	0.8 ± 0.2	0.4 ± 0.1	65.7 ± 22.1	1.7 ± 0.3
P4	550	30.9 ± 2.1	1.5 ± 0.1	1.1 ± 0.1	0.5 ± 0.1	64.2 ± 3.8	1.7 ± 0.1
P5	600	27.9 ± 4.0	1.0 ± 0.2	0.3 ± 0.1	1.8 ± 0.3	67.6 ± 11.7	1.6 ± 0.2
P6	600	30.3 ± 3.2	1.6 ± 0.2	0.4 ± 0.1	1.7 ± 0.2	63.9 ± 7.1	1.9 ± 0.2
P7	650	26.5 ± 3.2*	1.8 ± 0.3	< 0.1	3.5 ± 0.5	66.1 ± 10.8	2.0 ± 0.3
P8§	700	25.4 ± 2.0	0.9 ± 0.1	< 0.1	3.4 ± 0.4	68.4 ± 6.0	1.8 ± 0.2
Steam Addition							
SG4	600	35.5 ± 6.0	0.8 ± 0.1	0.7 ± 0.1	0.1 ± 0.05	60.9 ± 16.8	2.0 ± 0.4
SG5	650	29.8 ± 2.0	0.7 ± 0.1	< 0.1	1.2 ± 0.1	66.5 ± 4.2	1.6 ± 0.1
SG6§	700	28.2 ± 1.8	0.6 ± 0.1	N/A	N/A	69.5 ± 3.7	1.5 ± 0.2

* Estimate made by assuming most of the CO_3^{2-} combines as Na_2CO_3. This is valid since $[C_{K^+}] << [C_{Na^+}]$.

§ The OH^- concentrations for P1,P8 and SG6 were 3.0±1.1, 10.2±1.2 and 2.3±0.4 mol%, respectively.

Table 17

Eutectic Melting Point Data for Salts Containing Na^+, K^+, Cl^-, S^{2-}, SO_4^{2-}, CO_3^{2-}, and OH^-

System	T_{first} (°C)	Reference
Binary		
Na_2SO_4-Na_2CO_3	826	Gitlesen and Motzfeldt (1964)
Na_2S-Na_2CO_3	755	Ovechkin et al. (1971)
Na_2S-Na_2SO_4	745	Tran and Barham (1981)
Na_2S-Na_2Cl_2	712	Shivgulam et al. (1979)
	690	Magnusson and Warnqvist (1975)
Na_2Cl_2-K_2Cl_2	652	Bergman and Sementsova (1958a)
Na_2Cl_2-Na_2CO_3	634	Magnusson and Warnqvist (1975)
	~630	Shivgulam et al. (1979)
K_2Cl_2-K_2CO_3	632	Bergman and Sementsova (1958b)
Na_2Cl_2-Na_2SO_4	628	Bergman and Sementsova (1958b)
K_2CO_3-K_2SO_4	622	Bergman and Sementsova (1958b)
K_2S-K_2SO_4	610	So and Barham (1981)
K_2Cl_2-Na_2CO_3	588	Bergman and Sementsova (1958c)
K_2Cl_2-K_2SO_4	588	Bergman and Sementsova (1958b)
K_2Cl_2-Na_2SO_4	528	Bergman and Sementsova (1958c)
Ternary		
Na_2CO_3-Na_2S-Na_2SO_4	715	Andersson (1982)
K_2Cl_2-K_2SO_4-K_2CO_3	622	Bergman and Sementsova (1958b)
Na_2Cl_2-Na_2SO_4-Na_2CO_3	612	Bergman and Sementsova (1958b)
Na_2S-Na_2CO_3-NaCl	598	Shivgulam et al (1979)
Na_2Cl_2-K_2SO_4-K_2CO_3	~570	Bergman and Sementsova (1958c)
K_2Cl_2-Na_2CO_3-Na_2SO_4	544	Bergman and Sementsova (1958c)
Na_2CO_3-Na_2SO_4-NaOH	280	Andersson (1982)
Na_2CO_3-Na_2S-NaOH	280	Andersson (1982)

Table 18

Concentration of Potassium, Chloride, and Organic Carbon in the Char

Run	T (°C)	$K^{\bullet}$ $\left(\frac{mol}{100\ g\ char}\right)$	Cl^{-} $\left(\frac{mol}{100\ g\ char}\right)$	Organic C $\left(\frac{g}{100\ g\ char}\right)$	$\frac{K}{Na+K}$ (mol%)	$\frac{Cl}{Na+K}$ (mol%)
Pyrolysis						
P1	500	0.028 ± 0.002	0.018 ± 0.002	32.2 ± 3.0	2.5 ± 0.7	1.5 ± 0.4
P4	550	0.028 ± 0.002	0.025 ± 0.002	30.9 ± 1.4	2.5 ± 0.2	2.3 ± 0.2
P5	600	0.028 ± 0.003	0.017 ± 0.003	30.1 ± 3.1	2.3 ± 0.4	1.4 ± 0.3
P6	600	0.029 ± 0.003	0.025 ± 0.002	31.9 ± 2.8	2.9 ± 0.4	2.4 ± 0.3
P7	650	0.038 ± 0.004	0.033 ± 0.004	N/A	2.9 ± 0.5	2.6 ± 0.5
P8	700	0.038 ± 0.003	0.020 ± 0.001	24.3 ± 1.8	2.6 ± 0.3	1.4 ± 0.1
Steam Addition						
SG4	600	0.033 ± 0.003	0.014 ± 0.001	23.9 ± 2.3	3.1 ± 0.8	1.3 ± 0.3
SG5	650	0.038 ± 0.003	0.018 ± 0.001	18.9 ± 1.1	2.3 ± 0.2	1.1 ± 0.1
SG6	700	0.045 ± 0.006	0.019 ± 0.001	19.0 ± 2.4[§]	2.2 ± 0.3	1.0 ± 0.1
SG1	700	0.049 ± 0.006	0.023 ± 0.003	12.8 ± 5.5[§]	3.0 ± 0.5[•]	1.4 ± 0.3[•]

[•] Sodium content of 1.58 ± 0.18 $mol \cdot 100^{-1} \cdot g^{-1}_{char}$ was estimated from the CO_3^{2-} and $K^{\bullet}$ data.

[§] Estimates based on mass balance calculations in Appendix A. Actual measurements for these agglomerated samples showed less than 1 wt% organic carbon in char.

Table 19

Mass Balance for Sulphur During Pyrolysis and Steam Gasification

	$\left(\frac{g}{100\ g\ S\ in\ KBLS}\right)$
Input KBLS	100 ± 3
Pyrolysis	
Run: P1 (500°C)	
Char	60 ± 11
Gases	39 ± 2
Mass Balance Closure[†]	1 ± 11
Run: P4 (550°C)	
Char	75 ± 6
Gases	45 ± 4
Mass Balance Closure[†]	-20 ± 7*
Run: P6 (600°C)	
Char	81 ± 9
Gases	21 ± 2
Mass Balance Closure[†]	-2 ± 9*
Run: P7 (650°C)	
Char	100 ± 16
Gases	10 ± 2
Mass Balance Closure[†]	-10 ± 16*
Run: P8 (700°C)	
Char	91 ± 8
Gases	4 ± 1
Mass Balance Closure[†]	5 ± 8
Steam Gasification	
Run: SG2 (500°C)	
Char	49 ± 3
Gases	54 ± 5
Mass Balance Closure[†]	-3 ± 6*
Run: SG4 (600°C)	
Char	56 ± 6
Gases	41 ± 5
Mass Balance Closure[†]	3 ± 8
Run: SG5 (650°C)	
Char	67 ± 8
Gases	33 ± 2
Mass Balance Closure[†]	0 ± 8

* Indicates that the sum of the measured sulphur content in char and gases exceeded the measured input to the fluidized bed.

† Calculated by difference and includes the amount of material which was not recovered during maintenance of the unit and the condensables.

Table 20

Reduction Efficiency as a Function of Temperature and Mean Residence Time of Char

Run No.	Mean Residence Time (min)	Temperature (°C)	Reduction Efficiency (%)
Pyrolysis			
P1	55	500	10.2 ± 0.8
P2	71	550	14.1 ± 1.7
P4	60	550	14.2 ± 1.3
P5	70	600	67.1 ± 4.5
P6	63	600	55.0 ± 5.3
P7	56	650	92.3 ± 10.1*
P8	62	700	99.1 ± 11.4*
Steam Addition			
SG2	54	500	0.9 ± 0.1
SG4	43	600	4.9 ± 0.8
SG5	56	650	80.8 ± 10.1*

* Includes as part of the Na_2S content, the amount oxidized to $Na_2S_2O_3$ by exposure to air during the analytical procedure.

Table 21

Predicted Equilibrium Constant, K^{eq}_{60}, and the Measured Product Gases Ratio in the Particulate Phase, K^{p}_{60}, for the H_2S Stripping Eq. 60

T (°C)	K^{eq}_{60}	K^{p}_{60}	y^{p}_{H1S}	y^{p}_{H2O}	y^{p}_{CO2}
600	1.39	0.13 ± 0.09	0.00057 ± 0.00036	0.13 ± 0.03	0.034 ± 0.005
650	0.57	0.49 ± 0.18	0.00074 ± 0.00016	0.021 ± 0.006	0.072 ± 0.004
700	0.25	0.34 ± 0.11	0.00051 ± 0.00007	0.020 ± 0.006	0.076 ± 0.005

Table 22 - Operating Conditions and Char-Alumina Analyses for Pyrolysis Run - P1

OPERATING CONDITIONS

Fluidized Bed Temp.	: 500 ± 2 °C
Bed Sampling Time	: 100 min
KBLS Feed Time	: 90 min
Total Dry KBLS Fed	: 537 ± 3 g
Dry KBLS Feed Rate	: 0.358 $kg \cdot h^{-1}$
Product Gas Flow Rate§	: 54.3 ± 0.5 $L \cdot min^{-1}$ @ STP
Injector Lance N_2	: 8 $L \cdot min^{-1}$ @ STP
Elutriated Char	: 35 g
Alumina Input	: 6104 g

CHAR-ALUMINA ANALYSES

Measurement (i)	No. of samples	C_i^{c-a} $\left\{\frac{g}{100\ g\ char\text{-}alumina}\right\}_t$	C_i^{char} $\left\{\frac{g}{100\ g\ char}\right\}_t$
Total C	5	2.02 ± 0.03	38.3 ± 2.9
Total S	10	0.0752 ± 0.0109	1.43 ± 0.23
Sodium*	2	1.35 ± 0.36	25.6 ± 7.1
CO_3^{2-}	6	1.62 ± 0.15	30.7 ± 3.7
S^{2-} ##	10	0.0105 ± 0.0008	0.199 ± 0.021
SO_3^{2-}	10	0.0749 ± 0.0026	1.42 ± 0.12
SO_4^{2-}	10	0.0724 ± 0.0035	1.37 ± 0.12
OH^-	3	0.037 ± 0.008	0.70 ± 0.16
Char Content	4	5.27 ± 0.40	

† 95% confidence level for the population mean.
* Analyzed by Norwest Labs, Edmonton.
Determined by potentiometric titration.
§ N_2 for fluidization was about 45 $L \cdot min^{-1}$.

Table 23 - Operating Conditions and Char-Alumina Analyses for Pyrolysis Run - P2

OPERATING CONDITIONS

Fluidized Bed Temp.	: 550 ± 2 °C
Bed Sampling Time	: 120 min
KBLS Feed Time	: 98 min
Total Dry KBLS Fed	: 460 ± 2 g
Dry KBLS Feed Rate	: 0.281 $kg \cdot h^{-1}$
Product Gas Flow Rate	: N/A *
Injector Lance N_2	: 3 $L \cdot min^{-1}$ @ STP
Elutriated Char	: 12 g
Alumina Input	: 4429 g

CHAR-ALUMINA ANALYSES

Measurement (i)	No. of samples	C_i^{c-a} $\left\{\frac{g}{100\ g\ char\text{-}alumina}\right\}$ †	C_i^{char} $\left\{\frac{g}{100\ g\ char}\right\}$ †
Total C	5	2.35 ± 0.12	33.7 ± 2.0
Total S	5	0.101 ± 0.01	1.45 ± 0.15
S^{2-} ##	10	0.0168 ± 0.0014	0.241 ± 0.021
SO_3^{2-}	10	0.0529 ± 0.0031	0.759 ± 0.049
S^0 §	2	< 0.00001	< 0.0003
S_x^{2-} §	2	< 0.0002	< 0.002
SO_4^{2-}	10	0.112 ± 0.022	1.61 ± 0.32
Char Content	6	6.97 ± 0.19	

† 95% confidence level for the population mean.

* Product gas flow rate measurements and gas sampling were not attempted.

Determined by ion chromatography.

§ Analyzed by K. Lesage at the laboratory of Alberta Sulphur Research, Calgary, using the method given in Clark and Lesage (1989).

Table 24 - Operating Conditions and Char-Alumina Analyses for Pyrolysis Run - P3

OPERATING CONDITIONS

Fluidized Bed Temp.	: 550 ± 2 °C
Bed Sampling Time	: 120 min
KBLS Feed Time	: 95 min
Total Dry KBLS Fed	: 517 ± 2 g
Dry KBLS Feed Rate	: 0.326 $kg \cdot h^{-1}$
Product Gas Flow Rate	: 56.2 ± 0.8 $L \cdot min^{-1}$ @ STP
Injector Lance N_2	: 6 $L \cdot min^{-1}$ @ STP
Elutriated Char	: 32 g
Alumina Input	: 4416 g

CHAR-ALUMINA ANALYSES*

Measurement (i)	No. of samples	$C_i^{c\text{-}a}$ $\left\{\frac{g}{100\ g\ char\text{-}alumina}\right\}_t$	C_i^{char} $\left\{\frac{g}{100\ g\ char}\right\}_t$
Total C	10	2.80 ± 0.04	38.3 ± 5.8
Total S	10	0.110 ± 0.013	1.51 ± 0.29
Sodium	5	1.75 ± 0.08	23.9 ± 3.8
CO_3^{2-}	7	2.19 ± 0.04	30.0 ± 4.6
Moisture	3	0.19 ± 0.15	2.6 ± 2.1
Char Content	5	7.31 ± 1.10	

† 95% confidence level for the population mean.

* Problems with ion chromatograph column prevented analysis of sulphur ions.

Table 25 - Operating Conditions and Char-Alumina Analyses for Pyrolysis Run - P4

OPERATING CONDITIONS

Fluidized Bed Temp.	: 550 ± 2 °C
Bed Sampling Time	: 120 min
KBLS Feed Time	: 120 min
Total Dry KBLS Fed	: 590 ± 2 g
Dry KBLS Feed Rate	: 0.295 $kg \cdot h^{-1}$
Product Gas Flow Rate	: 59.2 ± 0.6 $L \cdot min^{-1}$ @ STP
Injector Lance N_2	: 7 $L \cdot min^{-1}$ @ STP
Elutriated Char	: 31 g
Alumina Input	: 4411 g

CHAR-ALUMINA ANALYSES*

Measurement (i)	No. of samples	C_i^{c-a} $\left\{\frac{g}{100\ g\ char\text{-}alumina}\right\}$†	C_i^{char} $\left\{\frac{g}{100\ g\ char}\right\}$†
Total C	8	3.11 ± 0.03	37.0 ± 1.2
Total S	10	0.142 ± 0.008	1.69 ± 0.11
Sodium	5	2.05 ± 0.07	24.4 ± 1.1
CO_3^{2-}	8	2.55 ± 0.13	30.4 ± 1.8
S^{2-} *	5	0.0239 ± 0.0035	0.285 ± 0.043
SO_3^{2-}	10	0.0921 ± 0.0062	1.10 ± 0.08
S^0 §	2	< 0.00001	< 0.0003
S_x^{2-} §	2	< 0.0001	< 0.001
SO_4^{2-}	10	0.142 ± 0.003	1.69 ± 0.06
Moisture	3	0.11 ± 0.07	1.3 ± 0.8
Char Content	10	8.40 ± 0.26	

† 95% confidence level for the population mean.

* Determined by ion chromatography. Second-order fit for calibration.

\# Quenching of fluidized-bed sample took about 10 minutes longer due to insufficient liquid N_2.

§ Analyzed by K. Lesage at the laboratory of Alberta Sulphur Research, Calgary, using the method given in Clark and Lesage (1989).

Table 26 - Operating Conditions and Char-Alumina Analyses for Pyrolysis Run - P5

OPERATING CONDITIONS

Fluidized Bed Temp.	: 600 ± 3 °C
Bed Sampling Time	: 120 min
KBLS Feed Time	: 99 min
Total Dry KBLS Fed	: 436 ± 2 g
Dry KBLS Feed Rate	: 0.265 $kg \cdot h^{-1}$
Product Gas Flow Rate	: 58.5 ± 0.5 $L \cdot min^{-1}$ @ STP
Injector Lance N_2	: 3 $L \cdot min^{-1}$ @ STP
Elutriated Char	: 8 g
Alumina Input	: 4405 g

CHAR-ALUMINA ANALYSES

Measurement (i)	No. of samples	C_i^{c-a} $\left\{\frac{g}{100\ g\ char\text{-}alumina}\right\}_t$	C_i^{char} $\left\{\frac{g}{100\ g\ char}\right\}_t$
Total C	9	2.18 ± 0.04	36.2 ± 3.0
Total S	10	0.117 ± 0.006	1.94 ± 0.19
Sodium	3	1.69 ± 0.20	28.0 ± 4.0
CO_3^{2-}	5	1.82 ± 0.15	30.2 ± 3.5
S^{2-} #	7	0.062 ± 0.002	1.03 ± 0.09
SO_3^{2-} ##	4	0.020 ± 0.003	0.33 ± 0.06
S^o §	2	< 0.00001	< 0.0003
S_x^{2-} §	2	< 0.0004	< 0.006
SO_4^{2-}	8	0.029 ± 0.001	0.48 ± 0.04
Moisture	3	0.185 ± 0.154	3.07 ± 2.57
Char Content	6	6.03 ± 0.49	

† 95% confidence level for the population mean.

Ion chromatographic analysis. Second-order fit of calibration curve.

Ion chromatograph column deterioration resulted in overlap of peaks for SO_3^{2-} and SO_4^{2-}.

§ Analyzed by K. Lesage at the laboratory of Alberta Sulphur Research, Calgary, using the method given in Clark and Lesage (1989).

Table 27 - Operating Conditions and Char-Alumina Analyses for Pyrolysis Run - P6

OPERATING CONDITIONS

Fluidized Bed Temp.	: 600 ± 3 °C
Bed Sampling Time	: 100 min
KBLS Feed Time	: 75 min
Total Dry KBLS Fed	: 359 ± 5 g
Dry KBLS Feed Rate	: 0.287 $kg \cdot h^{-1}$
Product Gas Flow Rate	: 59.5 ± 0.5 $L \cdot min^{-1}$ @ STP
Injector Lance N_2	: 3 $L \cdot min^{-1}$ @ STP
Elutriated Char	: 10 g
Alumina Input	: 4402 g

CHAR-ALUMINA ANALYSES

Measurement (i)	No. of samples	C_i^{c-a} $\left\{\frac{g}{100\ g\ char\text{-}alumina}\right\}$ †	C_i^{char} $\left\{\frac{g}{100\ g\ char}\right\}$ †
Total C	8	1.90 ± 0.03	37.6 ± 2.7
Total S	10	0.101 ± 0.005	2.00 ± 0.17
Sodium	5	1.15 ± 0.07	22.8 ± 2.1
CO_3^{2-}	6	1.42 ± 0.08	28.1 ± 2.6
S^{2-} #	4	0.0423 ± 0.0041	0.838 ± 0.101
SO_3^{2-} ##	3	0.0254 ± 0.0057	0.503 ± 0.118
S^o §	2	< 0.00001	< 0.0003
SO_4^{2-}	3	0.030 ± 0.003	0.594 ± 0.073
Char Content	6	5.05 ± 0.36	

† 95% confidence level for the population mean.
# Determined by ion chromatography.
Chromatogram peaks for SO_3^{2-} and SO_4^{2-} were overlapping.
§ Analyzed by K. Lesage at the laboratory of Alberta Sulphur Research, Calgary, using the method given in Clark and Lesage (1989).

Table 28 - Operating Conditions and Char-Alumina Analyses for Pyrolysis Run - P7

OPERATING CONDITIONS

Fluidized Bed Temp.	: 650 ± 2 °C
Bed Sampling Time	: 90 min
KBLS Feed Time	: 68 min
Total Dry KBLS Fed	: 380 ± 2 g
Dry KBLS Feed Rate	: 0.335 $kg \cdot h^{-1}$
Product Gas Flow Rate	: 61.1 ± 0.5 $L \cdot min^{-1}$ @ STP
Injector Lance N_2	: 7 $L \cdot min^{-1}$ @ STP
Elutriated Char	: 18 g
Alumina Input	: 5652 g

CHAR-ALUMINA ANALYSES *

Measurement (i)	No. of samples	C_i^{c-a} $\left\{\frac{g}{100\ g\ char\text{-}alumina}\right\}$ †	C_i^{char} $\left\{\frac{g}{100\ g\ char}\right\}$ †
Total C	5	1.37 ± 0.03	40.3 ± 4.0
Total S	10	0.100 ± 0.008	2.94 ± 0.37
Sodium	5	0.98 ± 0.09	28.8 ± 3.9
S^{2-} ##	10	0.0716 ± 0.0050	2.11 ± 0.25
SO_3^{2-}	4	0.006 ± 0.003	0.2 ± 0.1
S^o §	2	< 0.00001	< 0.0003
SO_4^{2-}	3	0.003 ± 0.001	0.09 ± 0.03
$S_2O_3^{2-}$	4	0.006 ± 0.002	0.2 ± 0.1
Char Content	5	3.40 ± 0.33	

† 95% confidence level for the population mean.
* Quenching of bed material took about 20 minutes due to insufficient liquid N_2.
Analyzed by potentiometric titration.
§ Analyzed by K. Lesage at the laboratory of Alberta Sulphur Research, Calgary, using the method of Clark and Lesage (1989).

Table 29 - Operating Conditions and Char-Alumina Analyses for Pyrolysis Run - P8

OPERATING CONDITIONS

Fluidized Bed Temp.	: 700 ± 2 °C
Bed Sampling Time	: 113 min
KBLS Feed Time	: 101 min
Total Dry KBLS Fed	: 605 ± 2 g
Dry KBLS Feed Rate	: 0.359 $kg \cdot h^{-1}$
Product Gas Flow Rate	: 60.8 ± 1 $L \cdot min^{-1}$ @ STP
Injector Lance N_2	: 7 $L \cdot min^{-1}$ @ STP
Elutriated Char	: 28 g
Alumina Input	: 6109 g

CHAR-ALUMINA ANALYSES

Measurement (i)	No. of samples	C_i^{c-a} $\left\{\frac{g}{100\ g\ char\text{-}alumina}\right\}_\dagger$	C_i^{char} $\left\{\frac{g}{100\ g\ char}\right\}_\dagger$
Total C	4	1.32 ± 0.02	30.6 ± 1.8
Total S	10	0.131 ± 0.004	3.04 ± 0.19
Sodium	4	1.42 ± 0.06	32.9 ± 2.3
CO_3^{2-}	8	1.36 ± 0.02	31.6 ± 1.8
S^{2-} #	4	0.0976 ± 0.0103	2.26 ± 0.27
S^o §	2	< 0.00001	< 0.0003
SO_4^{2-}	4	0.0014 ± 0.0007	0.033 ± 0.017
$S_2O_3^{2-}$ *	4	0.0108 ± 0.0038	0.251 ± 0.089
OH^-	3	0.144 ± 0.008	3.34 ± 0.26
Char Content	6	4.31 ± 0.24	

† 95% confidence level for the population mean.

* The char-alumina sample was very reactive in solution during analysis. The SO_3^{2-} peak was unreliable due to its low resolution. The $S_2O_3^{2-}$ concentration was changing slightly over time.

\# Determined by potentiometric titration.

§ Analyzed by K. Lesage at the laboratory of Alberta Sulphur Research, Calgary, using the method given in Clark and Lesage (1989).

Table 30 - Operating Conditions and Char-Alumina Analyses for Steam Gasification Run - SG1

OPERATING CONDITIONS

Fluidized Bed Temp.	: 700 ± 3 °C
Feed Rate of H_2O	: 4 mL·min^{-1}
Bed Sampling Time	: 10 h
KBLS Feed Time	: 90 min *
Total Dry KBLS Fed	: 498 ± 2 g
Dry KBLS Feed Rate	: 0.332 kg·h^{-1}
Product Gas Flow Rate	: 62.5 ± 0.5 L·min^{-1} @ STP
Injector Lance N_2	: 7 L·min^{-1} @ STP
Total Elutriated Char	: 31 g
Alumina Input	: 6008 g

CHAR-ALUMINA ANALYSES #

Measurement (i)	No. of samples	C_i^{c-a} $\left\{\frac{g}{100\ g\ char\text{-}alumina}\right\}_t$	C_i^{char} $\left\{\frac{g}{100\ g\ char}\right\}_t$
Total C	5	0.375 ± 0.003	12.2 ± 1.4
Total S	10	0.075 ± 0.004	2.4 ± 0.3
CO_3^{2-}	5	1.46 ± 0.05	47.6 ± 5.5
S^o §	2	< 0.00001	< 0.0003
OH^-	3	0.02 ± 0.007	0.7 ± 0.2
Char Content	5	3.07 ± 0.34	

† 95% confidence level for the population mean.

* Bed agglomerated after 90 min of operation.

\# Sampling of bed material was not feasible immediately after the run. Char data cannot be used for mass balance purposes without incurring a large error for carbon content.

§ Analyzed by K. Lesage at the laboratory of Alberta Sulphur Research, Calgary, using the method given in Clark and Lesage (1989).

Table 31 - Operating Conditions and Char-Alumina Analyses for Steam Gasification Run - SG2

OPERATING CONDITIONS

Fluidized Bed Temp.	: 500 ± 2 °C
Feed Rate of H_2O	: 10 ± 0.5 mL·min^{-1}
Bed Sampling Time	: 99 min
KBLS Feed Time	: 90 min
Total Dry KBLS Fed	: 522 ± 2 g
Dry KBLS Feed Rate	: 0.348 kg·h^{-1}
Product Gas Flow Rate	: 56.4 ± 0.6 L·min^{-1} @ STP
Injector Lance N_2	: 3 L·min^{-1} @ STP
Elutriated Char	: 14 g
Alumina Input	: 4417 g

CHAR-ALUMINA ANALYSES

Measurement (i)	No. of samples	C_i^{c-a} $\left\{\frac{g}{100\ g\ char\text{-}alumina}\right\}$†	C_i^{char} $\left\{\frac{g}{100\ g\ char}\right\}$†
Total C	5	2.99 ± 0.14	38.0 ± 2.3
Total S	10	0.087 ± 0.002	1.11 ± 0.05
CO_3^{2-}	5	3.08 ± 0.07	39.2 ± 1.7
S^{2-} ##	8	0.00129 ± 0.00025	0.016 ± 0.003
SO_3^{2-}	10	0.109 ± 0.003	1.39 ± 0.06
SO_4^{2-}	10	0.104 ± 0.002	1.32 ± 0.06
Char Content	4	7.86 ± 0.29	

† 95% confidence level for the population mean.
Determined by ion chromatography.
§ Analyzed by the method in Clark and Lesage (1989).

Table 32 - Operating Conditions for Steam Gasification Run - SG3

OPERATING CONDITIONS

Fluidized Bed Temp.	: 500 ± 2 °C
Feed Rate of H_2O	: 10 ± 0.5 mL·min^{-1}
KBLS Feed Time	: 35 min
Total Dry KBLS Fed	: 191 g
Dry KBLS Feed Rate	: 0.327 kg·h^{-1}
Product Gas Flow Rate	: 53.4 ± 0.8 L·min^{-1} @ STP

COMMENTS: Pressure drop across distributor was twice the value as that without steam feeding. Fluidized bed could not be emptied because the underflow sampling line was blocked. More KBLS in cyclones than usual. Only gas analyses could be performed.

Table 33 - Operating Conditions and Char-Alumina Analyses for Steam Gasification Run - SG4

OPERATING CONDITIONS

Fluidized Bed Temp.	: 600 ± 5 °C
Feed Rate of H_2O	: 10 ± 0.4 mL·min^{-1}
Bed Sampling Time	: 75 min
KBLS Feed Time	: 64 min
Total Dry KBLS Fed	: 365 ± 2 g
Dry KBLS Feed Rate	: 0.342 kg·h^{-1}
Product Gas Flow Rate	: 56.8 ± 0.4 L·min^{-1} @ STP
Injector Lance N_2	: 4 L·min^{-1} @ STP
Elutriated Char	: 13 g
Alumina Input	: 5504 g

CHAR-ALUMINA ANALYSES

Measurement (i)	No. of samples	C_i^{c-a} $\left\{\frac{g}{100\ g\ char\text{-}alumina}\right\}_t$	C_i^{char} $\left\{\frac{g}{100\ g\ char}\right\}_t$
Total C	5	1.47 ± 0.05	31.1 ± 2.2
Total S	10	0.055 ± 0.004	1.2 ± 0.1
Sodium#	2	1.12 ± 0.25	23.7 ± 5.5
CO_3^{2-}	5	1.69 ± 0.10	35.8 ± 3.1
S^{2-} *	10	0.0020 ± 0.0002	0.04 ± 0.01
SO_3^{2-}	10	0.0080 ± 0.0005	0.17 ± 0.02
S^o §	2	< 0.00001	< 0.0003
SO_4^{2-}	10	0.053 ± 0.002	1.1 ± 0.1
Char Content	6	4.72 ± 0.30	

† 95% confidence level for the population mean.
* An extra peak was observed during analysis by ion chromatography.
\# Analyzed by Norwest Labs, Edmonton.
§ Analyzed by K. Lesage at the laboratory of Alberta Sulphur Research, Calgary, using the method given in Clark and Lesage (1989).

Table 34 - Operating Conditions and Char-Alumina Analyses for Steam Gasification Run - SG5

OPERATING CONDITIONS

Fluidized Bed Temp.	: 650 ± 2 °C
Feed Rate of H_2O	: 10 ± 0.4 mL·min^{-1}
Bed Sampling Time	: 102 min
KBLS Feed Time	: 92 min
Total Dry KBLS Fed	: 526 ± 2 g
Dry KBLS Feed Rate	: 0.343 kg·h^{-1}
Product Gas Flow Rate	: 60.0 ± 0.7 L·min^{-1} @ STP
Injector Lance N_2	: 7 L·min^{-1} @ STP
Elutriated Char	: 31 g
Alumina Input	: 6311 g

CHAR-ALUMINA ANALYSES

Measurement (i)	No. of samples	C_i^{c-a} $\left\{\frac{g}{100\ g\ char\text{-}alumina}\right\}$ †	C_i^{char} $\left\{\frac{g}{100\ g\ char}\right\}$ †
Total C	5	1.25 ± 0.02	27.7 ± 1.0
Total S *	7	0.083 ± 0.008	1.8 ± 0.2
Sodium	5	1.70 ± 0.04	37.6 ± 1.9
CO_3^{2-}	6	1.97 ± 0.04	43.6 ± 2.1
S^{2-} #	6	0.0415 ± 0.0058	0.918 ± 0.135
SO_3^{2-}	5	0.00358 ± 0.00108	0.079 ± 0.024
S^0 §	2	< 0.00001	< 0.0003
S_x^{2-} §	2	< 0.0001	< 0.002
SO_4^{2-}	5	0.0145 ± 0.0007	0.321 ± 0.021
$S_2O_3^{2-}$	6	0.0092 ± 0.0017	0.204 ± 0.039
Char Content	5	4.52 ± 0.20	

† 95% confidence level for the population mean.

* Particles were sieved and the fractions -250 + 150 µm were analyzed. A higher degree of variability was observed for the total sulphur values.

\# Determined by ion chromatography.

§ Analyzed by K. Lesage at the laboratory of Alberta Sulphur Research, Calgary, using the method of Clark and Lesage (1989).

Table 35 - Operating Conditions and Char-Alumina Analyses for Steam Gasification Run - SG6

OPERATING CONDITIONS

Fluidized Bed Temp.	: 700 ± 4 °C
Feed Rate of H_2O	: 10 ± 0.4 mL·min^{-1}
Bed Sampling Time	: 12 h
KBLS Feed Time	: 65 min *
Total Dry KBLS Fed	: 382 ±2 g
Dry KBLS Feed Rate	: 0.352 kg·h^{-1}
Product Gas Flow Rate	: 61.2 ± 0.7 L·min^{-1} @ STP
Injector Lance N_2	: 4 L·min^{-1} @ STP
Elutriated Char	: 15 g
Alumina Input	: 5103 g

CHAR-ALUMINA ANALYSES #

Measurement (i)	No. of samples	C_i^{c-a} $\left\{\frac{g}{100\ g\ char\text{-}alumina}\right\}$ †	C_i^{char} $\left\{\frac{g}{100\ g\ char}\right\}$ †
Total C	5	0.31 ± 0.01	10.4 ± 1.2
Sodium	5	1.38 ± 0.05	46.1 ± 1.7
CO_3^{2-}	5	1.42 ± 0.05	47.5 ± 1.7
S^o §	2	< 0.00001	< 0.0003
OH^-	3	0.034 ± 0.005	1.1 ± 0.2
Char Content	5	2.99 ± 0.34	

† 95% confidence level for the population mean.

* Bed agglomerated after 65 min of operation.

\# Quenching of bed samples was not feasible immediately after the run. The char data cannot be used for mass balance purposes without incurring significant errors for carbon content. Gas analysis data are valid.

§ Analyzed by K. Lesage at the laboratory of Alberta Sulphur Research, Calgary, using the method given in Clark and Lesage (1989).

Table 36 - Experimental Data for the Fluidized Bed and Elutriated Char Product Streams

Run No.	$Total_{bed}$ (g)	$Total_{char}$ (g)	Y_{char} $\left(\frac{g\ char}{100\ g\ KBLS\ fed}\right)$
P1	340 ± 26	375 ± 26	69.8 ± 4.8
P2	331 ± 9	343 ± 9	74.8 ± 2.0
P3	348 ± 53	380 ± 53	73.6 ± 10.2
P4	405 ± 13	436 ± 13	73.8 ± 2.2
P5	283 ± 23	291 ± 23	66.7 ± 5.3
P6	234 ± 17	244 ± 17	68.0 ± 4.8
P7	199 ± 19	217 ± 19	57.1 ± 5.1
P8	275 ± 15	303 ± 15	50.1 ± 2.5
SG1	190 ± 21	221 ± 21	44.4 ± 4.2
SG2	377 ± 14	391 ± 14	74.5 ± 2.7
SG4	273 ± 17	286 ± 17	78.3 ± 4.8
SG5	298 ± 13	330 ± 13	62.7 ± 2.5
SG6	157 ± 18	172 ± 18	45.1 ± 4.7

Table 37 - Amount of Sodium, Total Sulphur, and Total Carbon in the KBLS Feed Reporting to the Char Product

Run No.	$D^{Na,\ KBLS}_{Na,\ char}$ $\left(\frac{g\ Na\ in\ char}{100\ g\ Na\ in\ KBLS}\right)$	$D^{S,\ KBLS}_{S,\ char}$ $\left(\frac{g\ S\ in\ char}{100\ g\ S\ in\ KBLS}\right)$	$D^{C,\ KBLS}_{C,\ char}$ $\left(\frac{g\ C\ in\ char}{100\ g\ C\ in\ KBLS}\right)$
P1	94.9 ± 27.6	59.8 ± 10.6	70.9 ± 8.1
P2	-	64.4 ± 7.2	66.4 ± 5.5
P3	93.2 ± 20.3	66.2 ± 15.8	74.6 ± 15.8
P4	95.5 ± 7.3	74.5 ± 5.7	72.3 ± 4.9
P5	99.1 ± 17.0	77.4 ± 10.0	64.0 ± 8.1
P6	82.3 ± 10.5	81.4 ± 9.3	67.9 ± 7.7
P7	87.3 ± 14.8	100.3 ± 15.6	61.0 ± 8.7
P8	87.4 ± 8.9	90.9 ± 7.3	40.6 ± 3.7
SG1	-	63.8 ± 10.2*	14.4 ± 2.3 (26.4 ±5.2)
SG2	-	49.4 ± 3.2	75.3 ± 6.5
SG4	98.6 ± 24.3	56.2 ± 6.0	64.6 ± 6.9
SG5	125.0 ± 10.4	67.4 ± 8.2	46.1 ± 3.4
SG6	109.8 ± 13.3	-	12.4 ± 2.0 (34.1 ± 5.5)

* The sample was taken after 10 h under a nitrogen purge. The value is likely too low since volatilization as H_2S is expected. Nevertheless, the value for sulphur is similar to that for the run at 650°C (SG5) and gives some confidence to the statement that sulphur in char increased with temperature for the steam runs.

Table 38 - Amount of Organic Carbon in the Feed KBLS Reporting to the Char

Run No.	$D_{OC,\,char}^{C,\,KBLS}$ $\left(\frac{g\ organic\ C\ in\ char}{100\ g\ C\ in\ KBLS}\right)$	$D_{OC,\,char}^{OC,\,KBLS}$ $\left(\frac{g\ organic\ C\ in\ char}{100\ g\ organic\ C\ in\ KBLS}\right)$
P1	59.6 ± 8.5	61.7 ± 8.8
P3	62.9 ± 16.0	65.2 ± 16.7
P4	60.4 ± 4.7	62.6 ± 4.9
P5	53.4 ± 8.2	55.3 ± [illegible]
P6	57.7 ± 7.6	[illegible] ± 8.0
P8	32.5 ± 3.7	33.7 ± 3.9
SG1	3.2 ± 2.9 (15.1 ± 6.7)	3.3 ± 3.1 (15.6 ± 6.9)
SG2	59.8 ± 6.5	61.9 ± 6.7
SG4	49.7 ± 7.0	51.5 ± 7.3
SG5	31.6 ± 2.8	32.8 ± 2.9
SG6	1.1 ± 1.8 (22.8 ± 3.9)	1.1 ± 1.9 (23.6 ± 4.1)

Table 39 - Amount of Sulphur in KBLS Reporting as S^{2-}, SO_4^{2-}, SO_3^{2-}, and $S_2O_3^{2-}$ in the Char

Run	$D_{S^{2-},\,char}^{S,\,KBLS}$ $\left(\frac{g\ S\ as\ S^{2-}}{100\ g\ S\ in\ KBLS}\right)$	$D_{SO_4^{2-},\,char}^{S,\,KBLS}$ $\left(\frac{g\ S\ as\ SO_4^{2-}}{100\ g\ S\ in\ KBLS}\right)$	$D_{SO_3^{2-},\,char}^{S,\,KBLS}$ $\left(\frac{g\ S\ as\ SO_3^{2-}}{100\ g\ S\ in\ KBLS}\right)$	$D_{S_2O_3^{2-},\,char}^{S,\,KBLS}$ $\left(\frac{g\ S\ as\ S_2O_3^{2-}}{100\ g\ S\ in\ KBLS}\right)$
P1	8.3 ± 1.1	19.0 ± 2.2	23.7 ± 2.7	-
P2	10.7 ± 1.0	23.8 ± 4.8	13.5 ± 1.0	-
P4	12.6 ± 2.0	24.8 ± 1.4	19.4 ± 1.6	-
P5	41.1 ± 5.0	6.4 ± 0.8	5.3 ± 1.1	-
P6	34.1 ± 4.9	8.1 ± 1.2	8.1 ± 2.0	-
P7	72.0 ± 10.8	1.0 ± 0.4	2.7 ± 1.4	3.9 ± 2.0
P8	67.6 ± 9.0	0.3 ± 0.2	<0.1	4.3 ± 1.5
SG2	0.7 ± 0.1	19.6 ± 1.3	24.8 ± 1.6	-
SG4	1.9 ± 0.5	17.1 ± 1.9	3.2 ± 0.4	-
SG5	34.4 ± 5.3	4.0 ± 0.3	1.2 ± 0.4	4.4 ± 0.9

Table 40 - Experimental Data for CO_2

Run No.	$Y_{CO_2}^{ave}$ $\left(\frac{mol\ CO_2}{kg\ KBLS}\right)$	$D_{C,CO_2}^{C,KBLS}$ $\left(\frac{g\ C\ as\ CO_2}{100\ g\ C\ in\ KBLS}\right)$
P1	2.26 ± 0.01	7.20 ± 0.48
P3	2.02 ± 0.09	6.56 ± 0.45
P4	2.41 ± 0.18	7.81 ± 0.70
P5	2.78 ± 0.23	8.86 ± 0.87
P6	2.65 ± 0.16	8.43 ± 0.67
P7	1.80 ± 0.71	5.74 ± 2.28
P8	2.27 ± 0.45	7.25 ± 1.48
SG1	10.37 ± 0.96	33.06 ± 3.49
SG2	2.16 ± 0.34	6.89 ± 1.13
SG3	1.36 ± 0.24	4.34 ± 0.80
SG4	4.83 ± 0.54	15.39 ± 1.89
SG5	10.72 ± 0.12	34.17 ± 1.81
SG6	11.96 ± 0.46	38.10 ± 2.46

Table 41 - Experimental Data for CO

Run No.	Y_{CO}^{ave} $\left(\frac{mol\ CO}{kg\ KBLS}\right)$	$D_{C,CO}^{C,KBLS}$ $\left(\frac{g\ C\ as\ CO}{100\ g\ C\ in\ KBLS}\right)$
P1	1.08 ± 0.15	3.44 ± 0.51
P3	1.58 ± 0.05	5.04 ± 0.31
P4	1.90 ± 0.10	6.06 ± 0.45
P5	2.26 ± 0.26	7.20 ± 0.92
P6	2.12 ± 0.19	6.77 ± 0.71
P7	3.66 ± 0.25	11.67 ± 1.00
P8	9.26 ± 0.39	29.51 ± 1.95
SG1	8.83 ± 0.66	28.14 ± 2.56
SG2	1.27 ± 0.05	4.05 ± 0.26
SG3	0.96 ± 0.27	3.06 ± 0.86
SG4	1.40 ± 0.06	4.46 ± 0.28
SG5	2.78 ± 0.01	8.86 ± 0.46
SG6	4.78 ± 1.10	15.24 ± 3.60

Table 42 - Experimental Data for H_2

Run No.	$Y_{H_2}^{ave}$ $\left(\frac{mol\ H_2}{kg\ KBLS}\right)$	$D_{H,H_2}^{H,input}$ $\left(\frac{g\ H\ as\ H_2}{100\ g\ H\ in\ input}\right)$
P1	3.42 ± 0.49	19.88 ± 2.89
P3	0.94 ± 0.14	5.41 ± 0.79
P4	0.44 ± 0.06	2.53 ± 0.34
P5	7.98 ± 1.13	46.43 ± 6.65
P6	5.96 ± 1.93	34.63 ± 11.25
P7	4.50 ± 1.40	26.15 ± 8.13
P8	14.34 ± 2.90	83.35 ± 16.91
SG1	36.98 ± 4.71	64.4 ± 8.34
SG2	3.73 ± 0.80	3.30 ± 0.71
SG3	1.26 ± 0.85	1.06 ± 0.72
SG4	12.88 ± 4.09	11.23 ± 3.57
SG5	27.44 ± 0.83	23.9 ± 0.82
SG6	36.81 ± 3.66	32.9 ± 3.30

Table 43 - Experimental Data for CH_4

Run No.	$Y_{CH_4}^{ave}$ $\left(\frac{mol\ CH_4}{kg\ KBLS}\right)$	$D_{C,CH_4}^{C,KBLS}$ $\left(\frac{g\ C\ as\ CH_4}{100\ g\ C\ in\ KBLS}\right)$
P1	1.18 ± 0.36	3.76 ± 1.16
P3	0.76 ± 0.02	2.25 ± 0.14
P4	0.77 ± 0.11	2.45 ± 0.36
P5	0.72 ± 0.39	2.29 ± 1.25
P6	0.77 ± 0.16	2.45 ± 0.52
P7	0.34 ± 0.19	1.08 ± 0.59
P8	1.09 ± 0.28	3.46 ± 0.92
SG1	1.07 ± 0.19	3.42 ± 0.61
SG2	1.50 ± 0.26	4.78 ± 0.87
SG3	0.98 ± 0.27	3.12 ± 0.88
SG4	0.99 ± 0.16	3.14 ± 0.55
SG5	0.93 ± 0.09	2.97 ± 0.33
SG6	1.12 ± 0.48	3.56 ± 1.53

Table 44 - Experimental Data for H_2S

Run No.	$Y^{ave}_{H_2S}$ $\left(\frac{mol\ H_2S}{kg\ KBLS}\right)$	$D^{S,\ KBLS}_{S,\ H_2S}$ $\left(\frac{g\ S\ as\ H_2S}{100\ g\ S\ in\ KBLS}\right)$
P1	0.113 ± 0.005	21.65 ± 1.31
P3	0.135 ± 0.029	25.07 ± 5.69
P4	0.145 ± 0.016	27.83 ± 3.16
P5	0.063 ± 0.001	12.32 ± 2.03
P6	0.040 ± 0.006	7.83 ± 1.27
P7	0.023 ± 0.002	4.49 ± 0.61
P8	0.016 ± 0.007	3.07 ± 1.32
SG1	0.046 ± 0.008	9.40 ± 1.65
SG2	0.157 ± 0.023	30.22 ± 4.50
SG3	0.129 ± 0.024	24.74 ± 9.88
SG4	0.133 ± 0.051	25.16 ± 4.57
SG5	0.132 ± 0.023	25.43 ± 1.50
SG6	0.097 ± 0.007	18.70 ± 3.76

Table 45 - Experimental Data for CH_3SH

Run No.	$Y^{ave}_{CH_3SH}$ $\left(\frac{mol\ CH_3SH}{kg\ KBLS}\right)$	$D^{S,\ KBLS}_{S,\ CH_3SH}$ $\left(\frac{g\ S\ as\ CH_3SH}{100\ g\ S\ in\ KBLS}\right)$
P1	0.074 ± 0.003	14.31 ± 0.67
P3	-	-
P4	0.089 ± 0.008	17.01 ± 1.58
P5	-	-
P6	0.054 ± 0.002	10.46 ± 0.69
P7	0.019 ± 0.006	3.64 ± 1.15
P8	0.0003± 0.0001	0.05 ± 0.02
SG1	0.002 ± 0.001	0.38 ± 0.15
SG2	0.103 ± 0.009	19.74 ± 1.78
SG3	0.097 ± 0.031	18.54 ± 5.94
SG4	0.068 ± 0.004	12.78 ± 0.86
SG5	0.031 ± 0.003	5.98 ± 0.69
SG6	0.009 ± 0.001	1.77 ± 0.20

Table 46 - Experimental Data for $(CH_3)_2S$

Run No.	$Y^{ave}_{(CH_3)_2S}$ $\left(\frac{mol\ (CH_3)_2S}{kg\ KBLS}\right)$	$D^{S,\ KBLS}_{S,\ (CH_3)_2S}$ $\left(\frac{g\ S\ as\ (CH_3)_2S}{100\ g\ S\ in\ KBLS}\right)$
P1	0.015 ± 0.002	2.87 ± 0.31
P6	0.012 ± 0.001	2.38 ± 0.20
P7	0.009 ± 0.002	1.69 ± 0.38
P8	0.003 ± 0.001	0.65 ± 0.19
SG1	0.004 ± 0.001	0.70 ± 0.08
SG2	0.023 ± 0.002	4.46 ± 0.53
SG3	0.021 ± 0.008	4.12 ± 1.65
SG4	0.016 ± 0.001	2.89 ± 0.41
SG5	0.010 ± 0.001	1.83 ± 0.44
SG6	0.004 ± 0.001	0.77 ± 0.12

Table 47 - Experimental Data for COS

Run No.	Y^{ave}_{COS} $\left(\frac{mol\ COS}{kg\ KBLS}\right)$	$D^{S,\ KBLS}_{S,\ COS}$ $\left(\frac{g\ S\ as\ COS}{100\ g\ S\ in\ KBLS}\right)$
P1	0.0004 ± 0.0001	0.08 ± 0.02
P3	0.0008 ± 0.0001	0.15 ± 0.02
P4	0.0020 ± 0.0002	0.38 ± 0.04
P5	0.0008 ± 0.0001	0.15 ± 0.02
P6	0.0014 ± 0.0001	0.27 ± 0.02
P7	0.0005 ± 0.0001	0.10 ± 0.02
P8	0.0002 ± 0.0001	0.04 ± 0.02
SG4	0.0005 ± 0.0001	0.10 ± 0.02
SG5	0.0008 ± 0.0002	0.15 ± 0.04
SG6	0.0007 ± 0.0001	0.13 ± 0.02

FIGURES

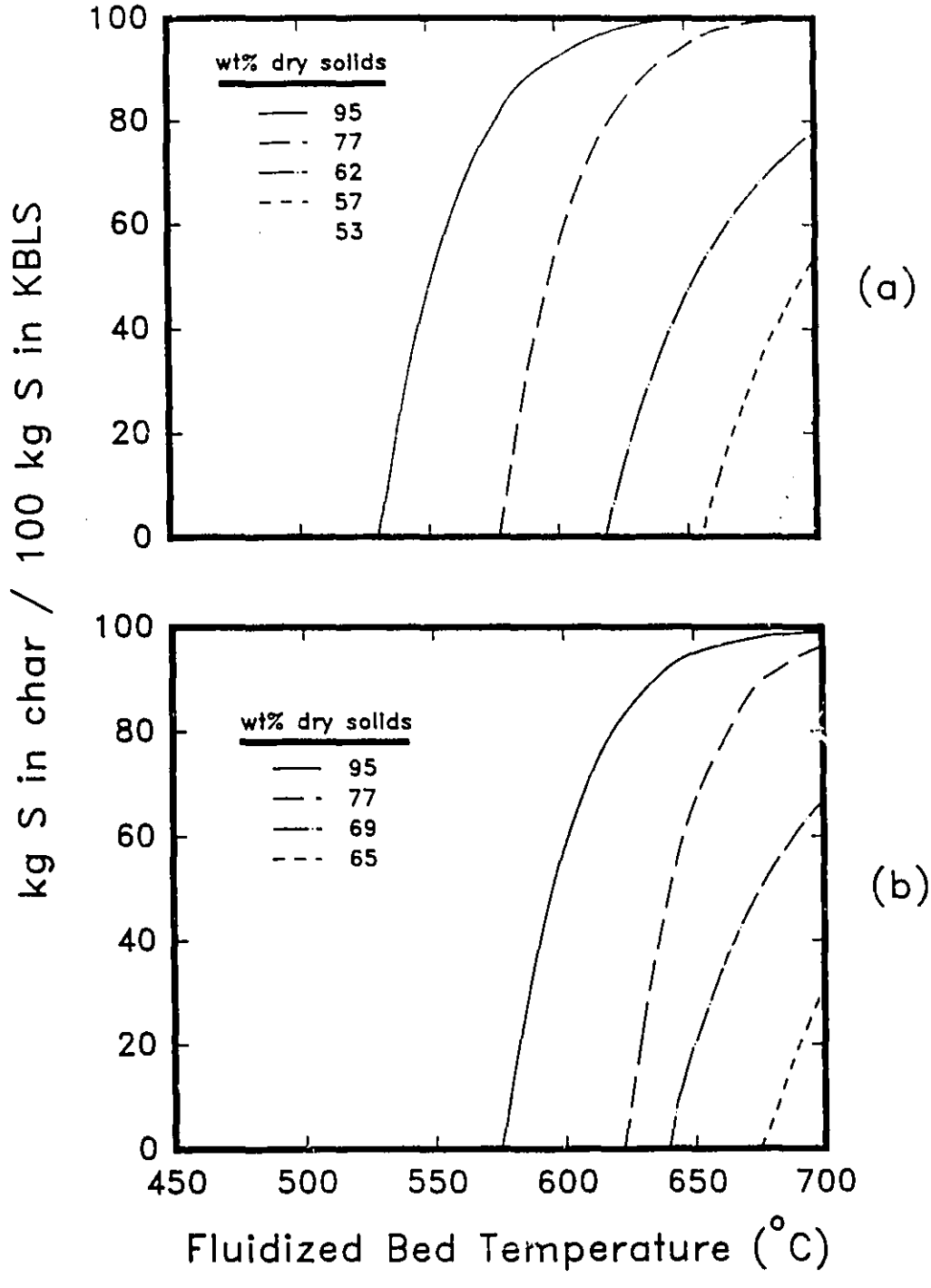

Figure 1 Equilibrium Sulphur C ntent of Char Calculated with Solid Na_2S Data given by (a) Warnqvist and Rosén (b) F*A*C*T database.

Figure 2 Pilot Plant Flowsheet.

Legend: 1) N_2 cylinder manifold; 2) N_2 Rotameter; 3) Compressed air supply; 4) Filter; 5) Silica gel; 6) Air Rotameter; 7) Distilled water reservoir; 8) N_2 purge; 9) Metering pump; 10) Lindberg furnace; 11) Gas preheaters; 12) Fluidized-bed reactor; 13) Char quench vessel; 14) KBLS feeder; 15) Insulation; 16) Cyclones; 17) Receiving vessels; 18) Shell-and-tube exchanger; 19) Cooling Water Inlet; 20) Cooling Water Outlet; 21) Syringe gas sampler; 22) Condensate collector; 23) Primary water scrubber; 24) NaOH soln. holding tank; 25) Packed-bed gas scrubber; 26) Demister; 27) Dry test meter; 28) To fume hood; 29) Natural gas; 30) Combustion air; 31) Burner; 32) Induction fan.

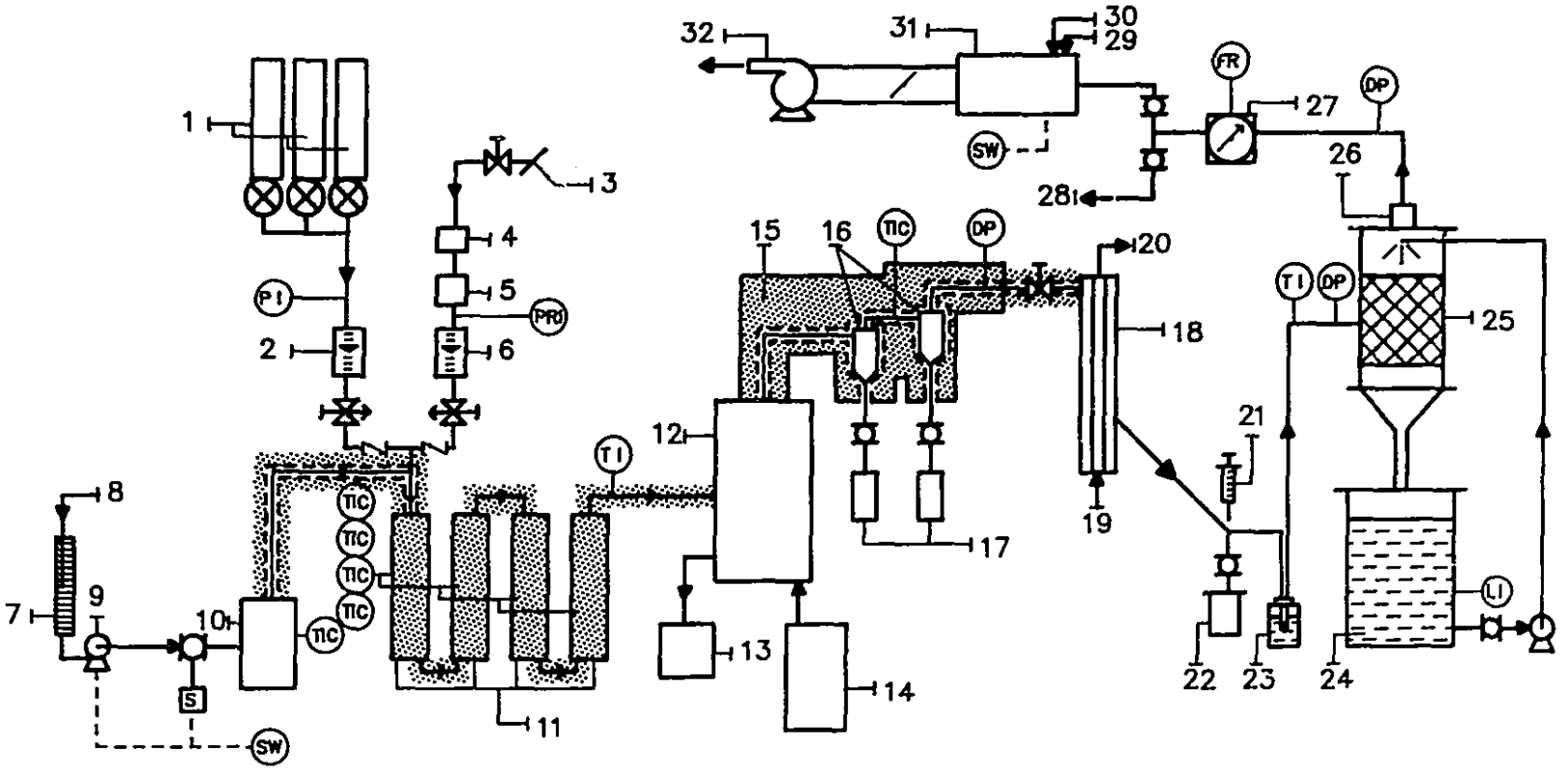

Symbols Legend

- PR — Pressure regulator indicator
- TIC — Temperature indicator/controller
- TI — Temperature indicator
- Ball valve
- SAMOX heat tape
- SW — ON–OFF switch
- DP — Differential pressure (manometer)
- FR — Flow recorder
- Gate valve
- Check valve
- Electrical signal
- LI — Level indicator
- 2–stage pressure regulator
- PI — Pressure indicator
- Needle valve
- S — Solenoid activator

Figure 3 Kraft Black Liquor Solids Feeder.

Legend: 1) Support table; 2) DC horizontal motor; 3) Gear box; 4) Metering auger/overwrap; 5) Kraft Black Liquor Solids; 6) Solids hopper; 7) Mixing blade; 8) Vertical motor; 9) To fume hood; 10) Main pneumatic N_2; 11) Mixing chamber; 12) Vibration mechanism; 13) Injector lance; 14) Auxiliary N_2 purge; 15) Cooling H_2O-in; 16) Cooling H_2O-out; 17) Heat Exchanger; 18) 15.9 mm OD outer shell; 19) 9.5 mm OD inner tube; 20) 5.0 mm ID injector tube; 21) Char-covered Al_2O_3 particles; 22) Kraft Black Liquor Solids in N_2.

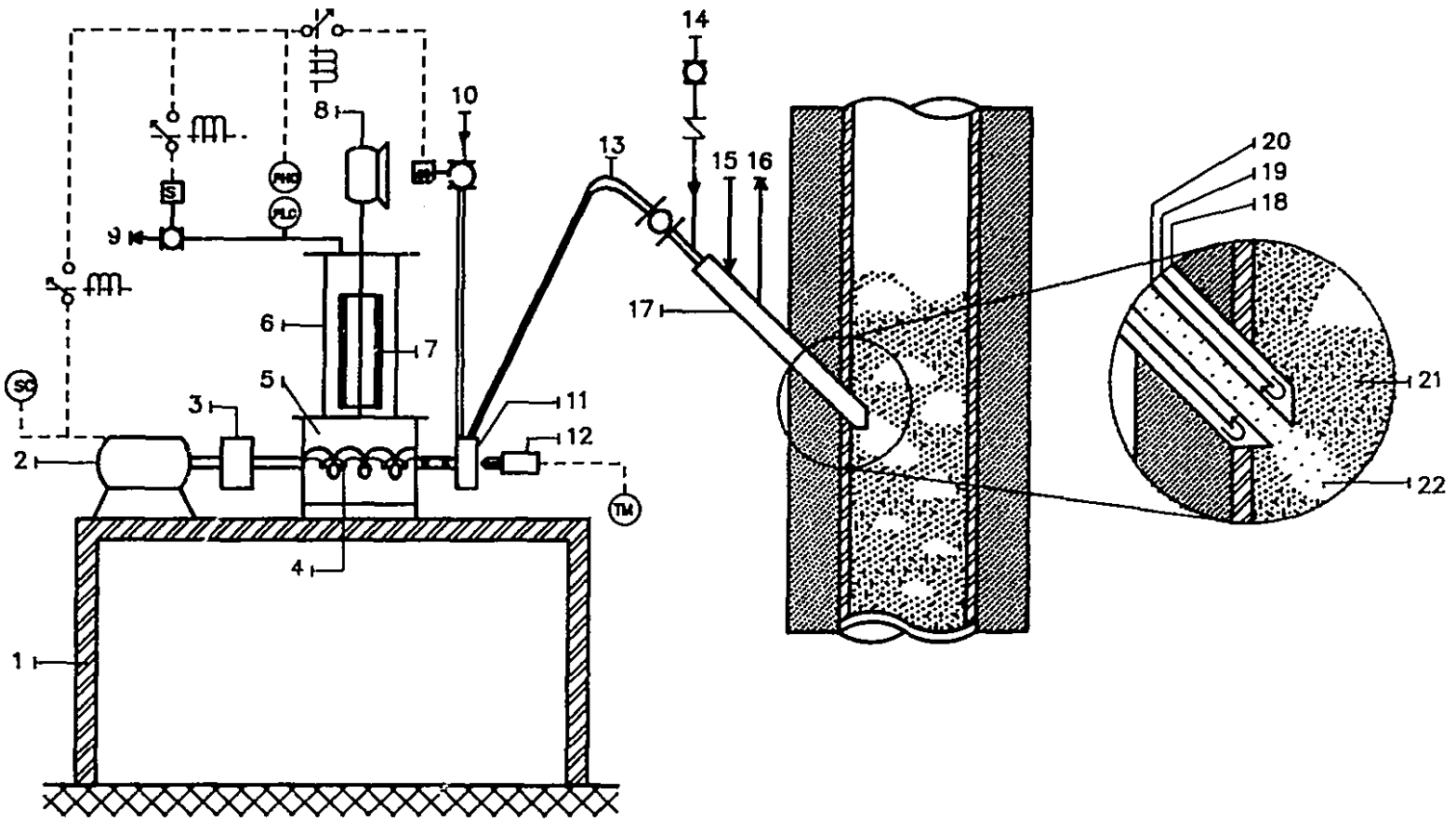

Symbols Legend

--- Electrical line	Relay	PHC High pressure shut-off
S Solenoid activator	TM Timer circuit	PLC Low pressure shut-off
Ball valve	Check valve	SC Speed control

Figure 4 Fluidized-Bed Reactor.

Legend: 1) Fluidizing gas inlet; 2) Multi-orifice plate; 3) Steel enclosure; 4) Resistance heater; 5) Insulation; 6) Reactor shell; 7) Reactor flange gasket; 8) Off-gas to cyclones; 9) Solids injector lance; 10) Fluidized bed; 11) Bed sampling line; 12) N_2 purge; 13) Vacuum line; 14) Quench vessel; 15) Liquid N_2; 16) Holding vessel; 17) Insulation; 18) Wire-mesh screen; 19) Distributor plate gasket.

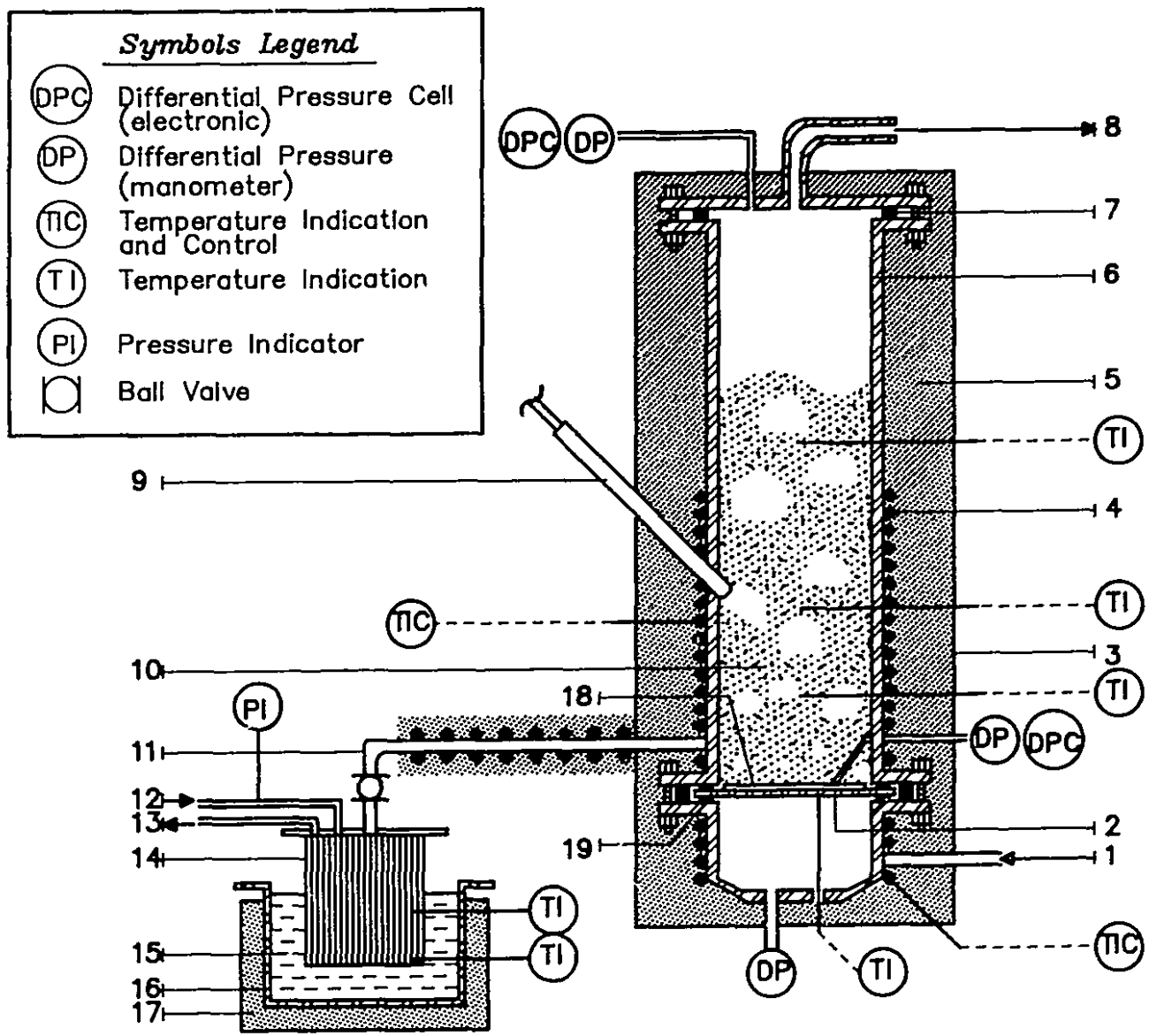
Symbols Legend
DPC Differential Pressure Cell (electronic)
DP Differential Pressure (manometer)
TIC Temperature Indication and Control
TI Temperature Indication
PI Pressure Indicator
Ball Valve
DPC
DP
8
7
6
5
TI
9
4
TIC
TI
10
3
18
TI
PI
DP
DPC
11
12
13
2
14
19
1
TI
TI
TIC
15
16
17
DP
TI

Figure 5 SEM Micrographs of (a) Pure Alumina Particles (b) Char-Coated Alumina for Steam Gasification at 700°C, and (c) Higher Resolution View of the Char Layer.

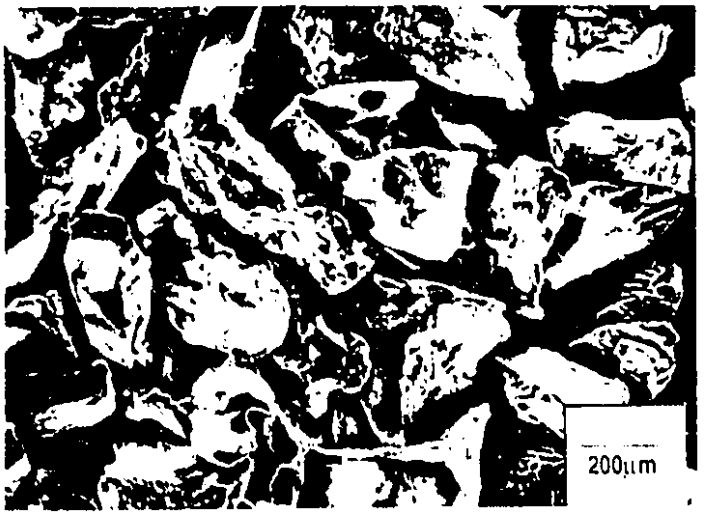

(a)

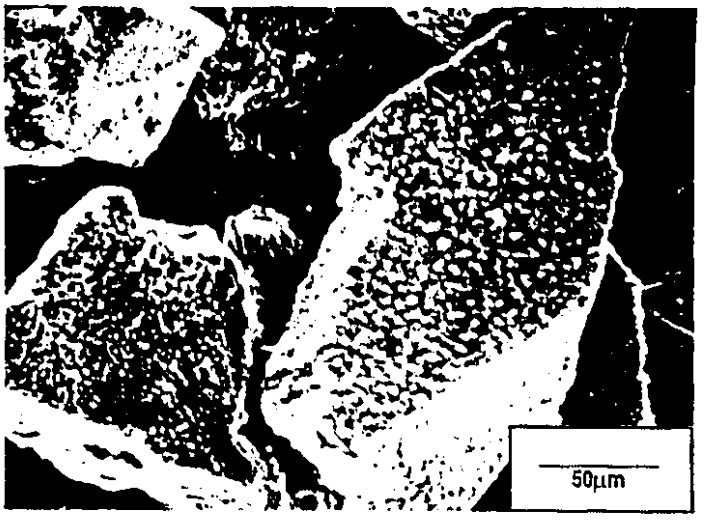

(b)

(c)

Figure 6 SEM Micrographs of Dry Kraft Black Liquor Solids.

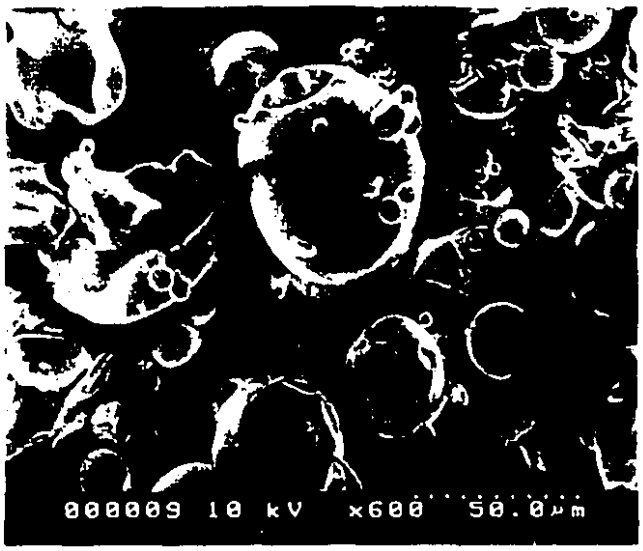

(a)

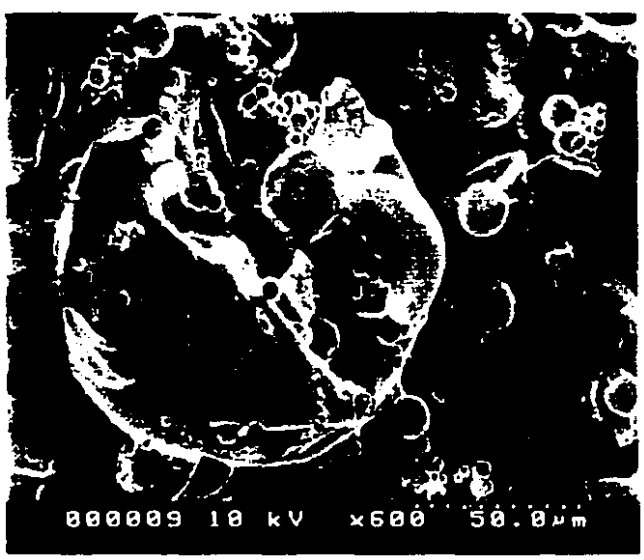

(b)

Figure 7 EDXA maps of (b) Sodium and (c) Sulphur for the Char-Alumina Particles in SEM Micrograph (a). Pyrolysis run P8 at 700°C.

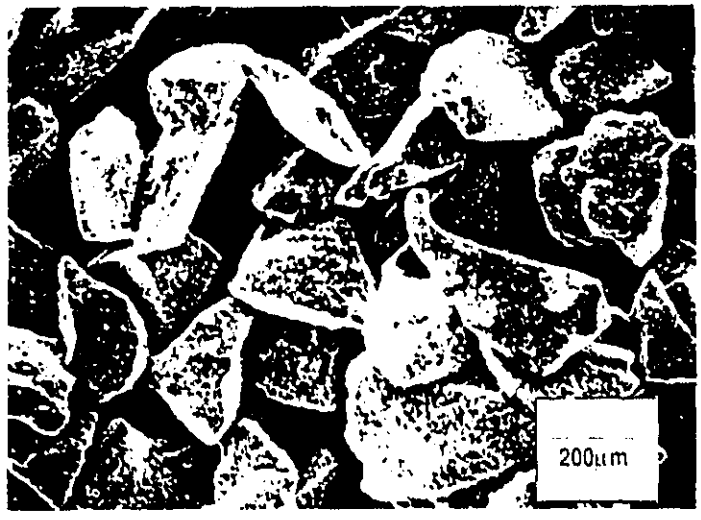

(a)

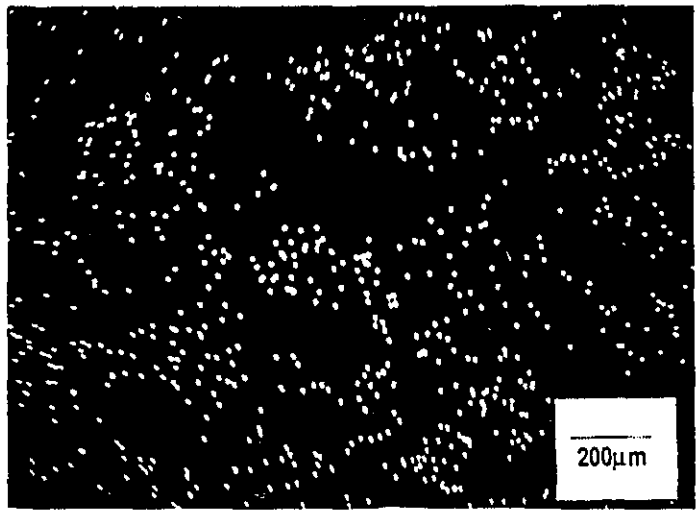

(b)

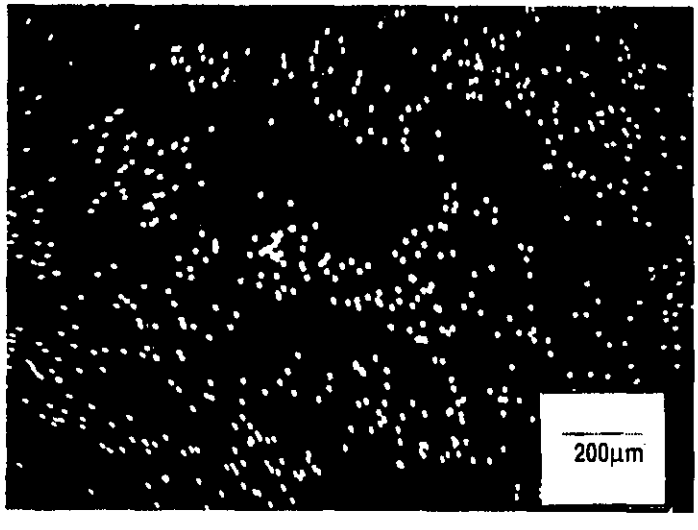

(c)

Figure 8 EDXA maps of (b) Al, (c) S, and (d) Fe for Char-Alumina Particles in SEM Micrograph (a). Steam Gasification Run SG6 at 700°C.

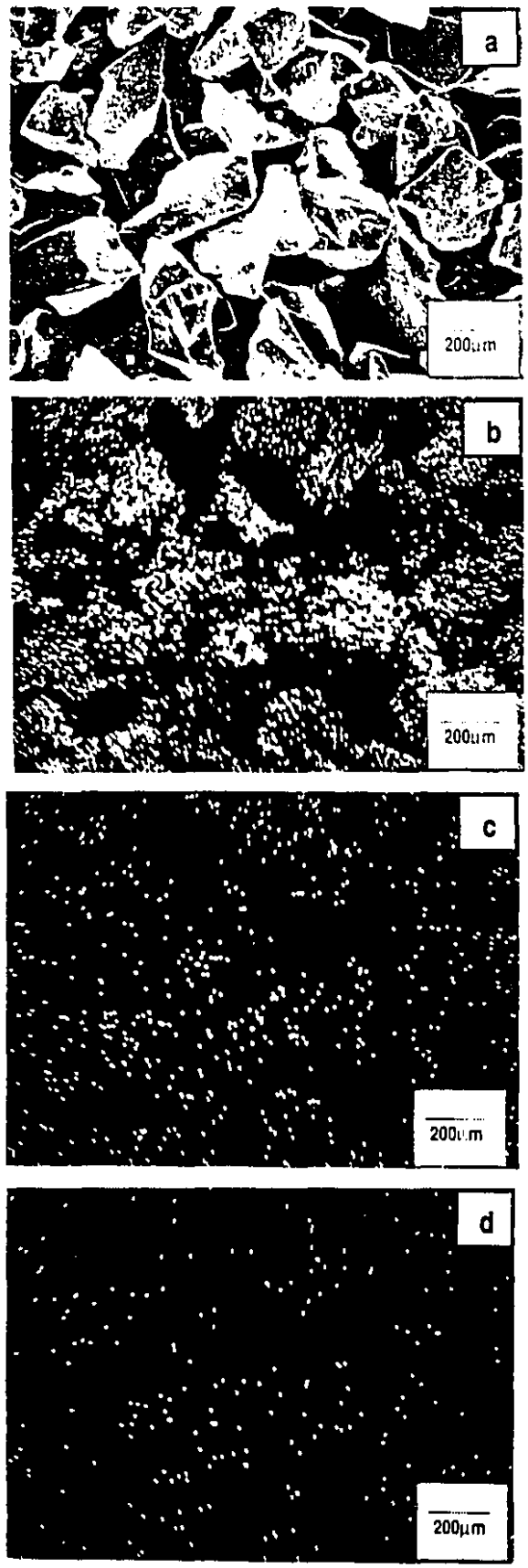
a
200µm
b
200µm
c
200µm
d
200µm

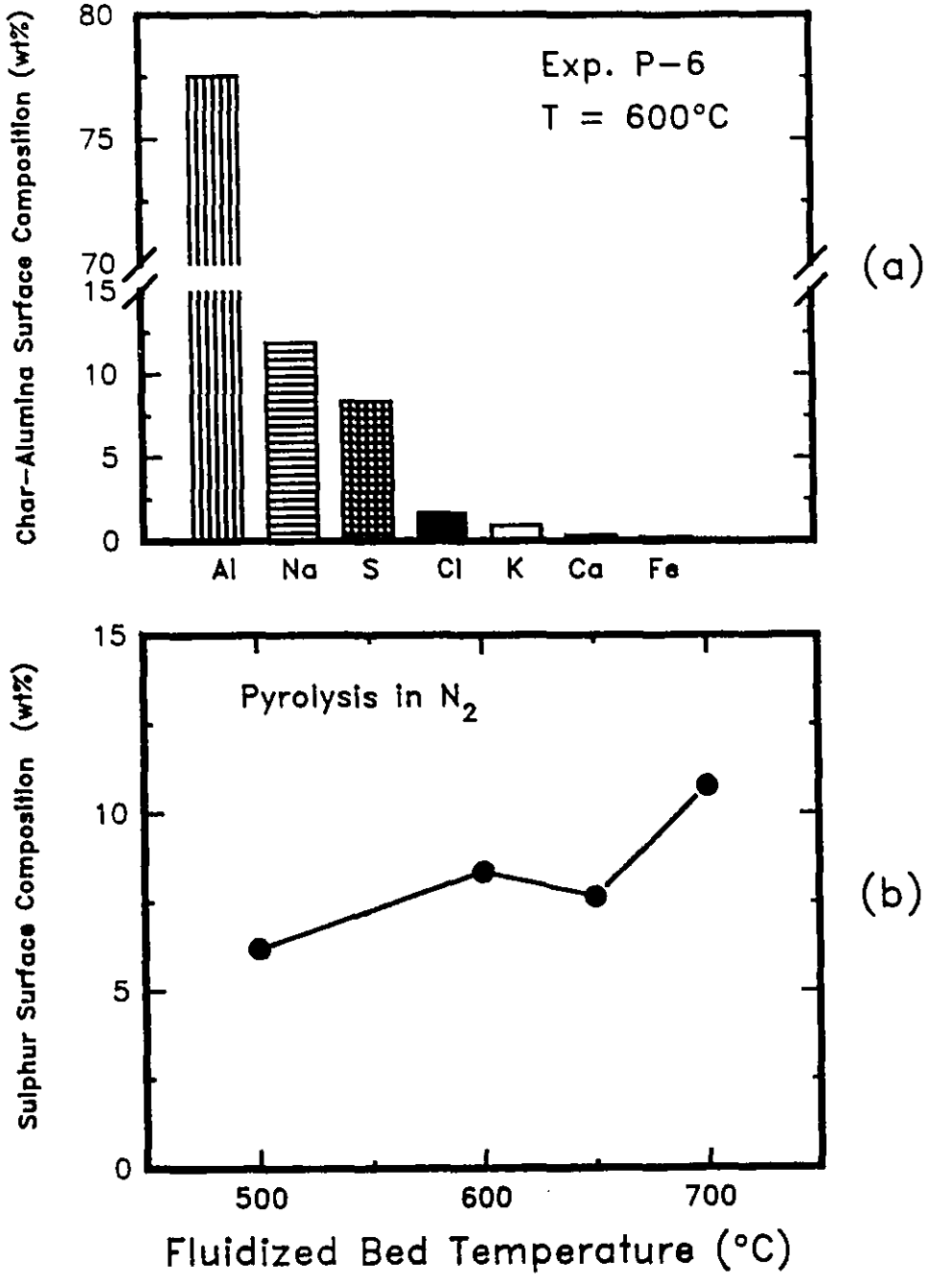

Figure 9 EDXA Surface Composition of Char-Alumina for Pyrolysis in a Nitrogen Atmosphere; (a) Major Elements in Pyrolysis Run P6, and (b) Sulphur as a Function of Reactor Temperature.

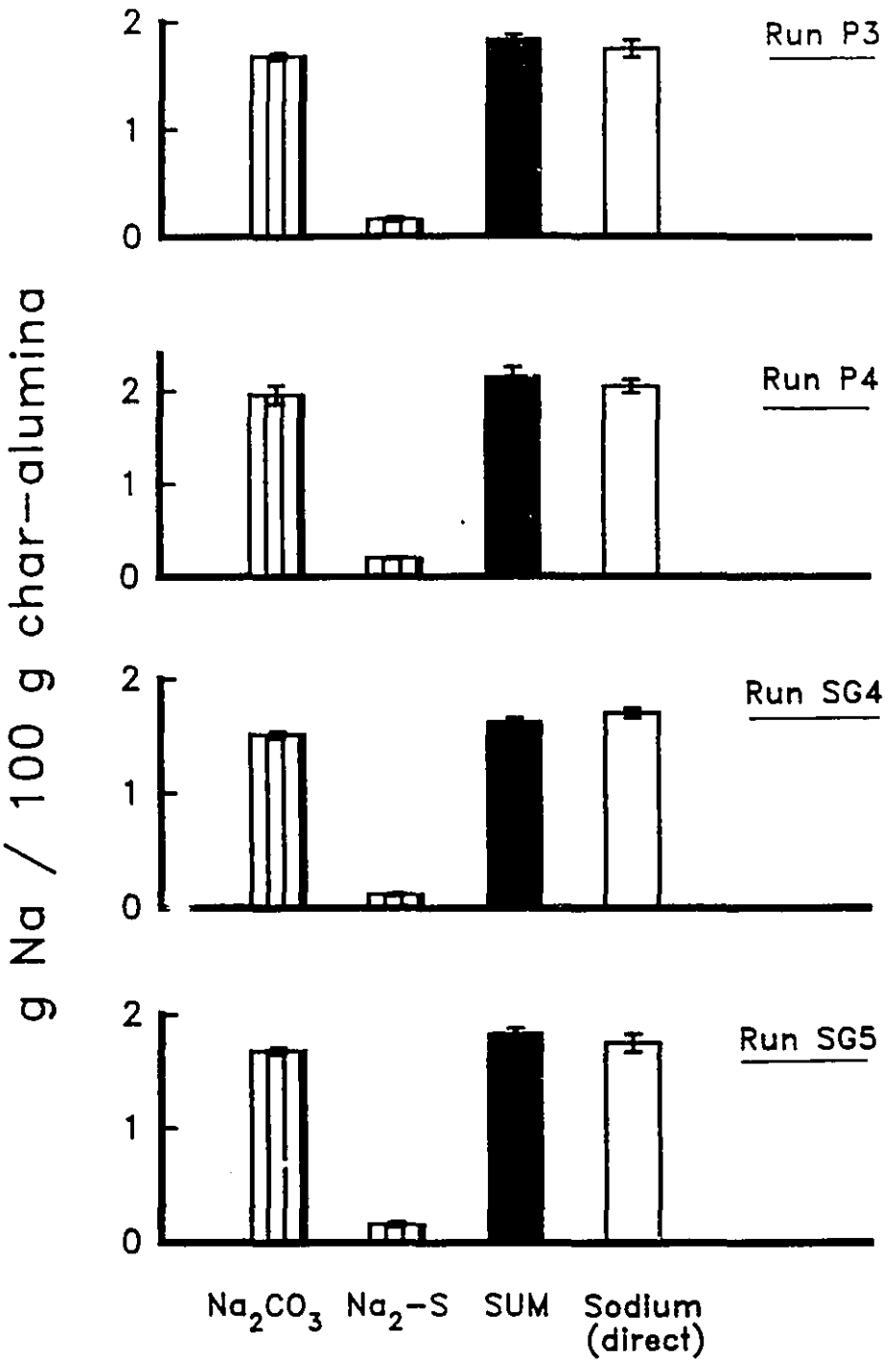

Figure 10 Independent Estimates of the Sodium Content in the Char-Alumina Bed Material for Several Pyrolysis and Steam Gasification Runs.

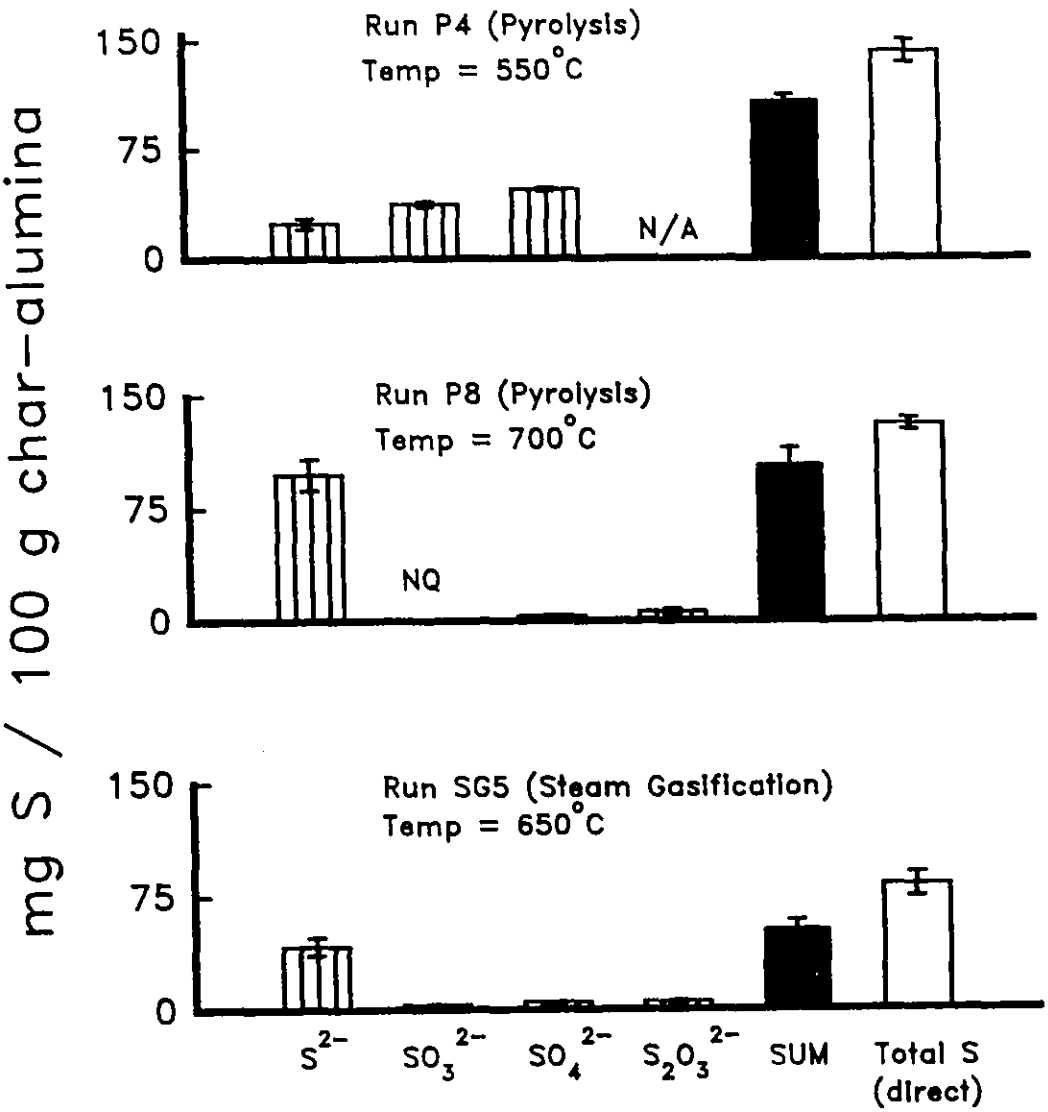

Figure 11 Independent Estimates of the Sulphur Content in Char-Alumina Bed Material for Pyrolysis and Steam Gasification Between 550-700°C.

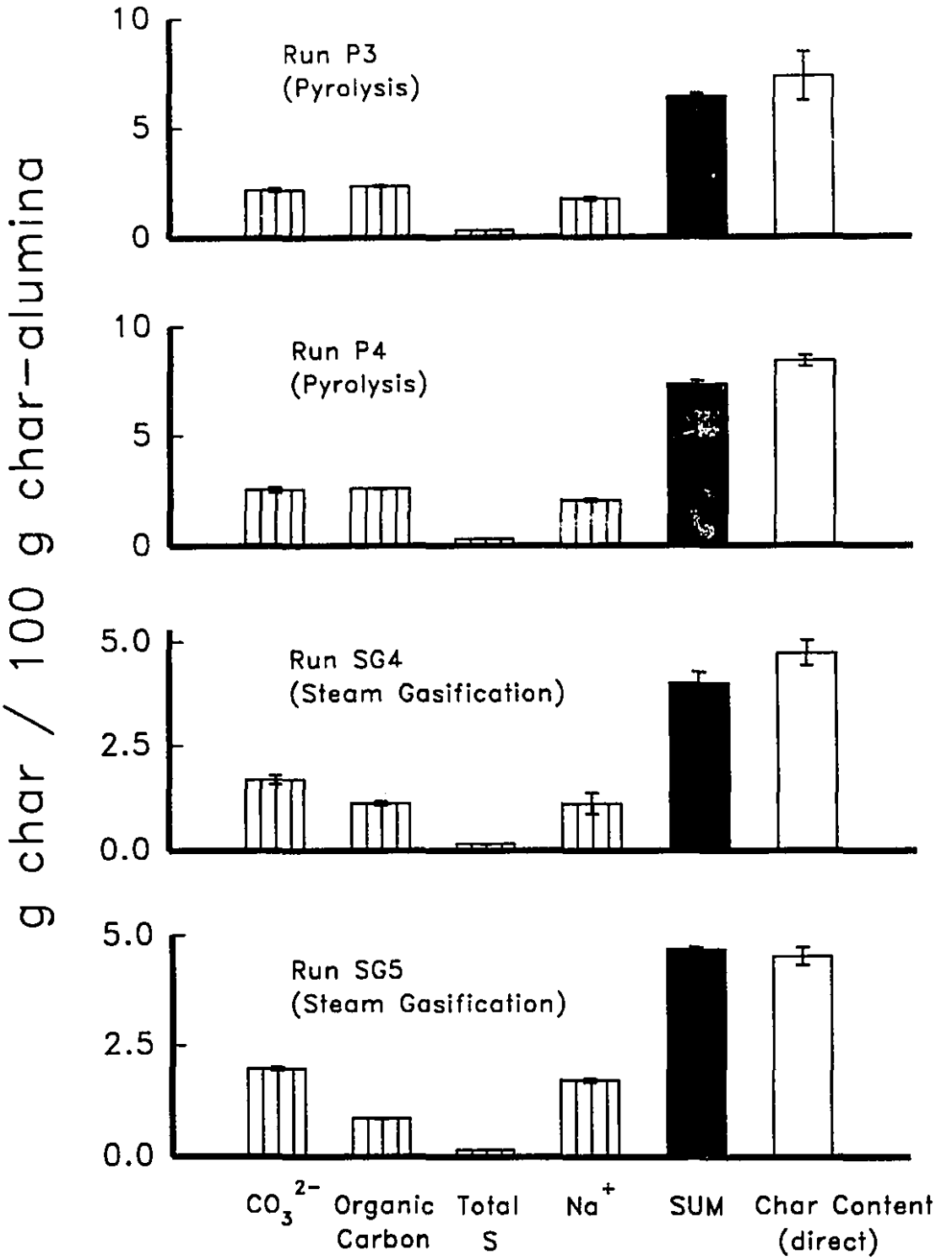

Figure 12 Independent Estimates of the Char Content in Char-Alumina Bed Material for Several Pyrolysis and Steam Gasification Runs.

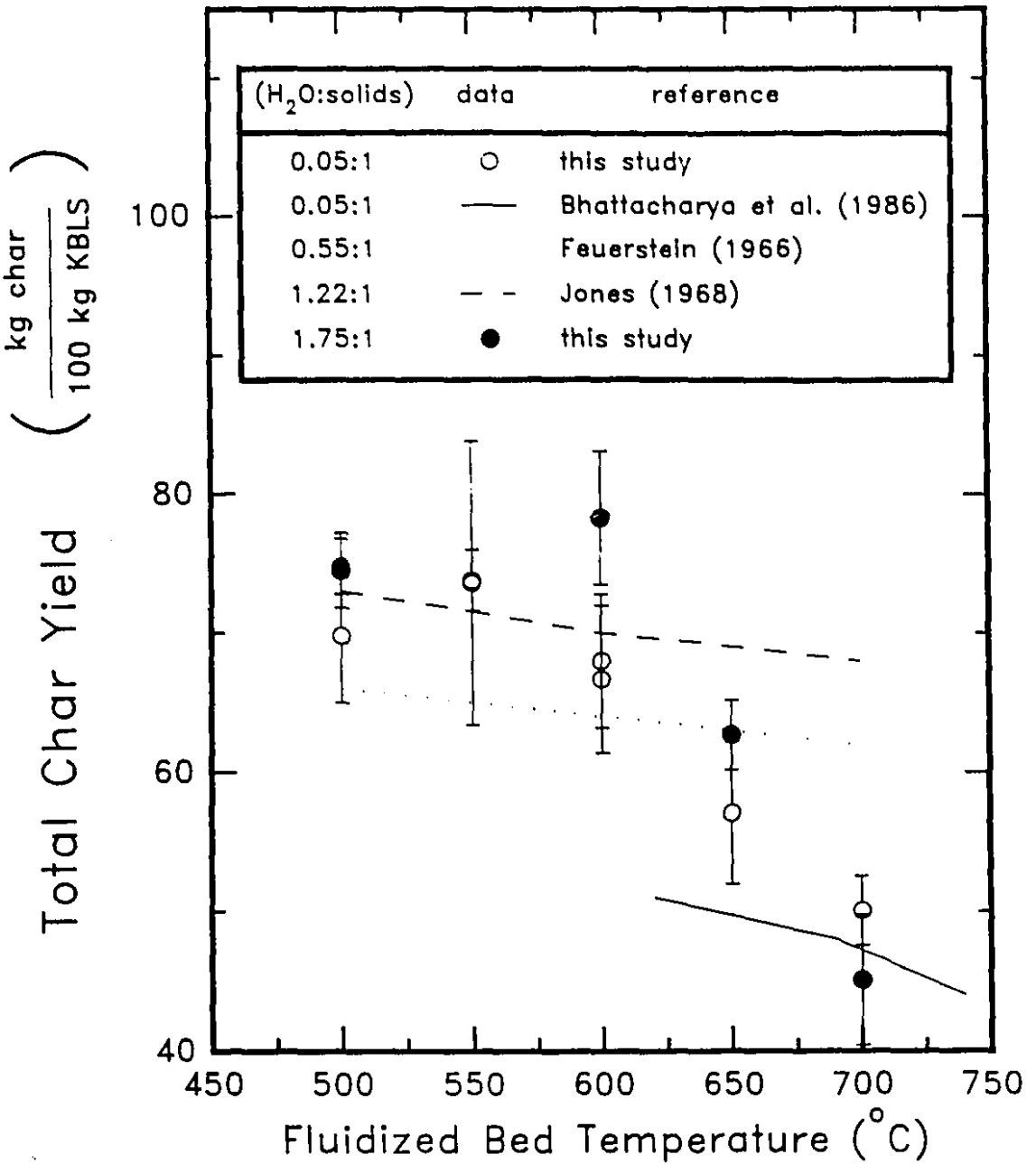

Figure 13 Total Char Yield as a Function of Reactor Temperature and Inlet H_2O:Solids Weight Ratio.

Comparative Data for Different Reactor Types: (●,○) Fluidized Bed, Semi-Batch [this study]; (...) Fixed Bed, Batch, Non-Isothermal [Feuerstein, 1966]; (____) Fixed Bed, Batch [Bhattacharya et al., 1986]; (—) Continuous Droplet Injection into a Heated Cylinder [Jones, 1968].

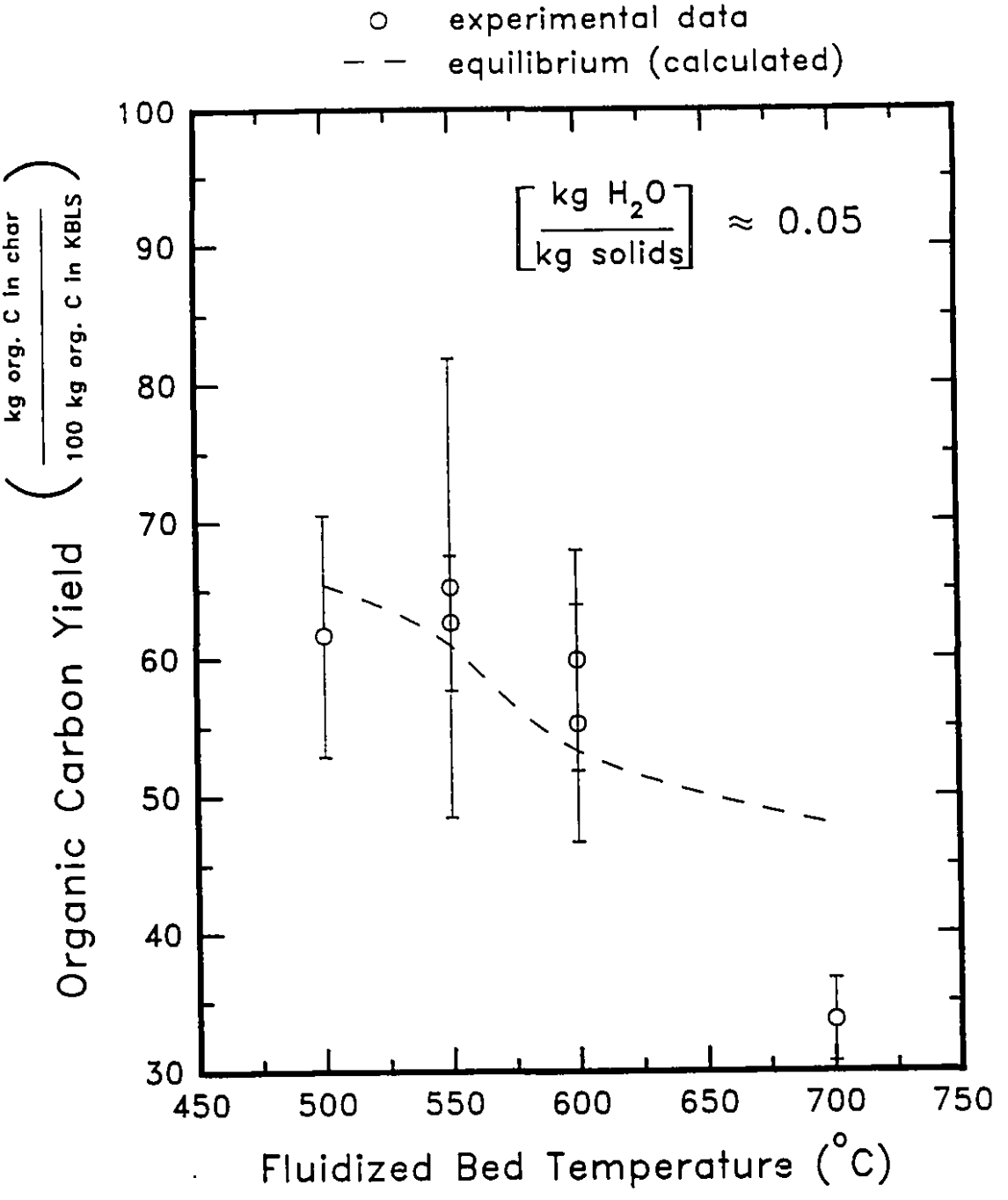

Figure 14 Experimental and Equilibrium Yield of Organic Carbon in the Fluidized-Bed Char During Pyrolysis for T = 500-700°C.

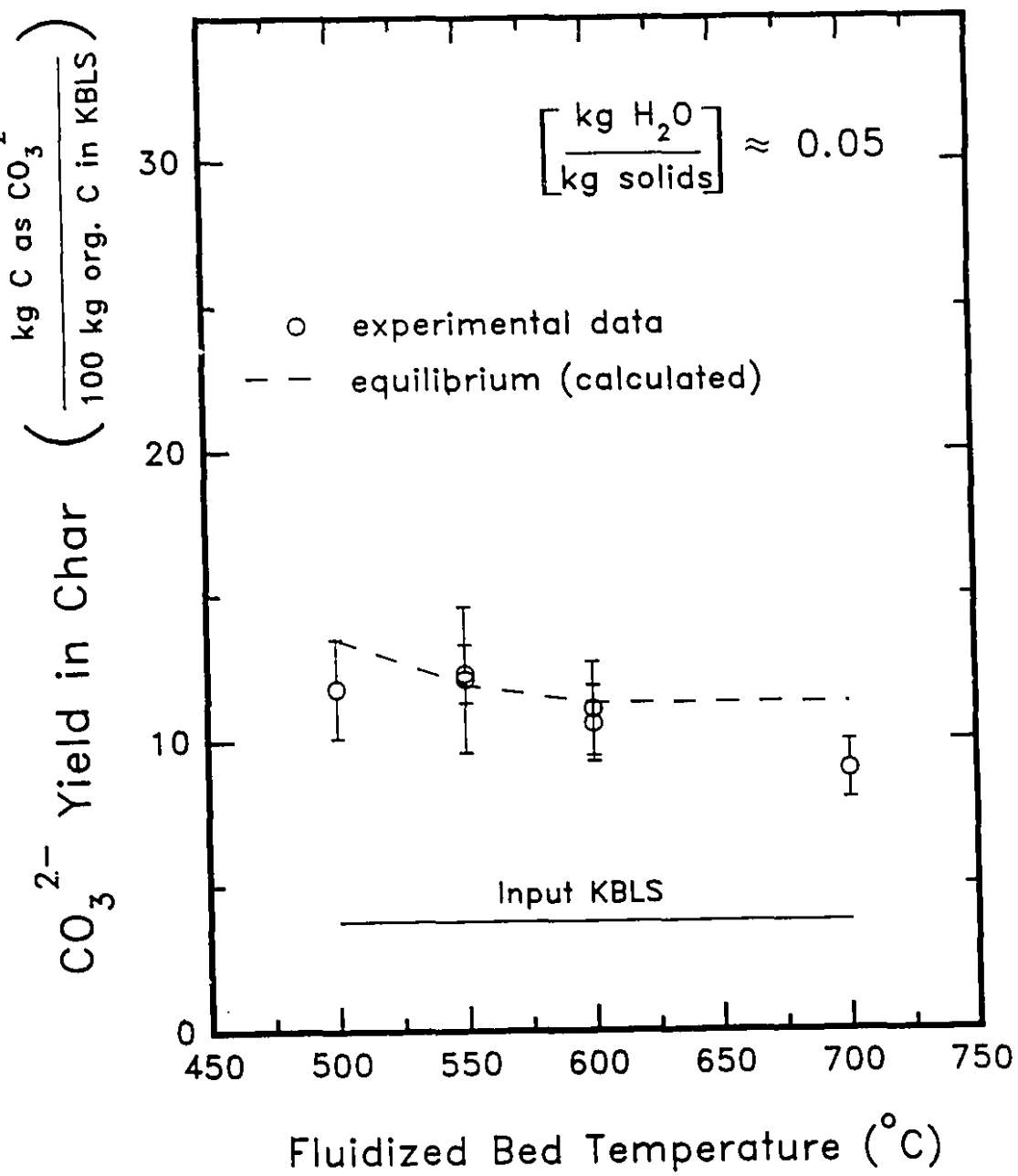

Figure 15 Experimental and Equilibrium Yield of Inorganic Carbon as CO_3^{2-} in Char During Pyrolysis for T = 500-700°C.

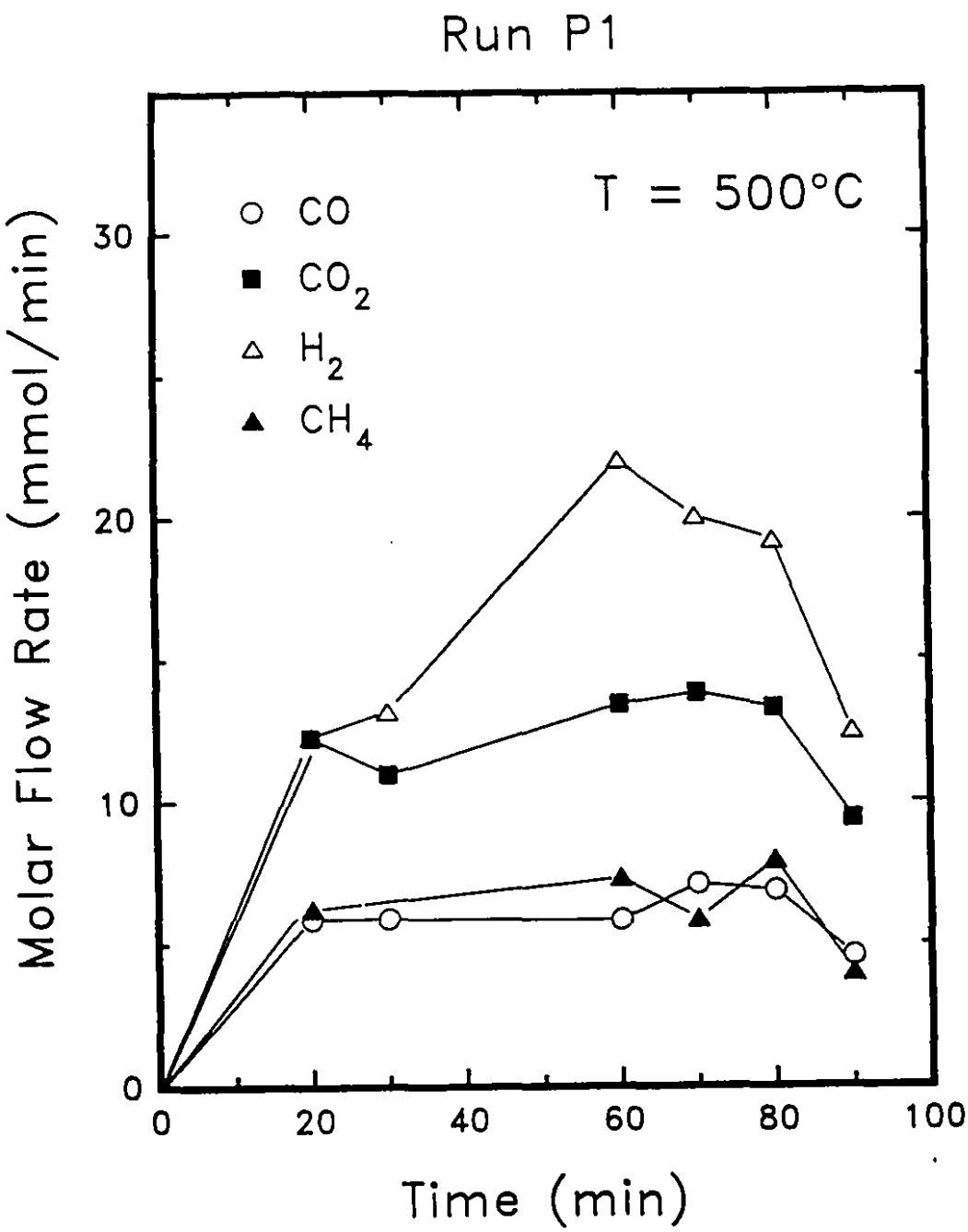

Figure 16 Time-Sampled Molar Flow Rate of Fixed Gases for Pyrolysis Run P1 at 500°C.

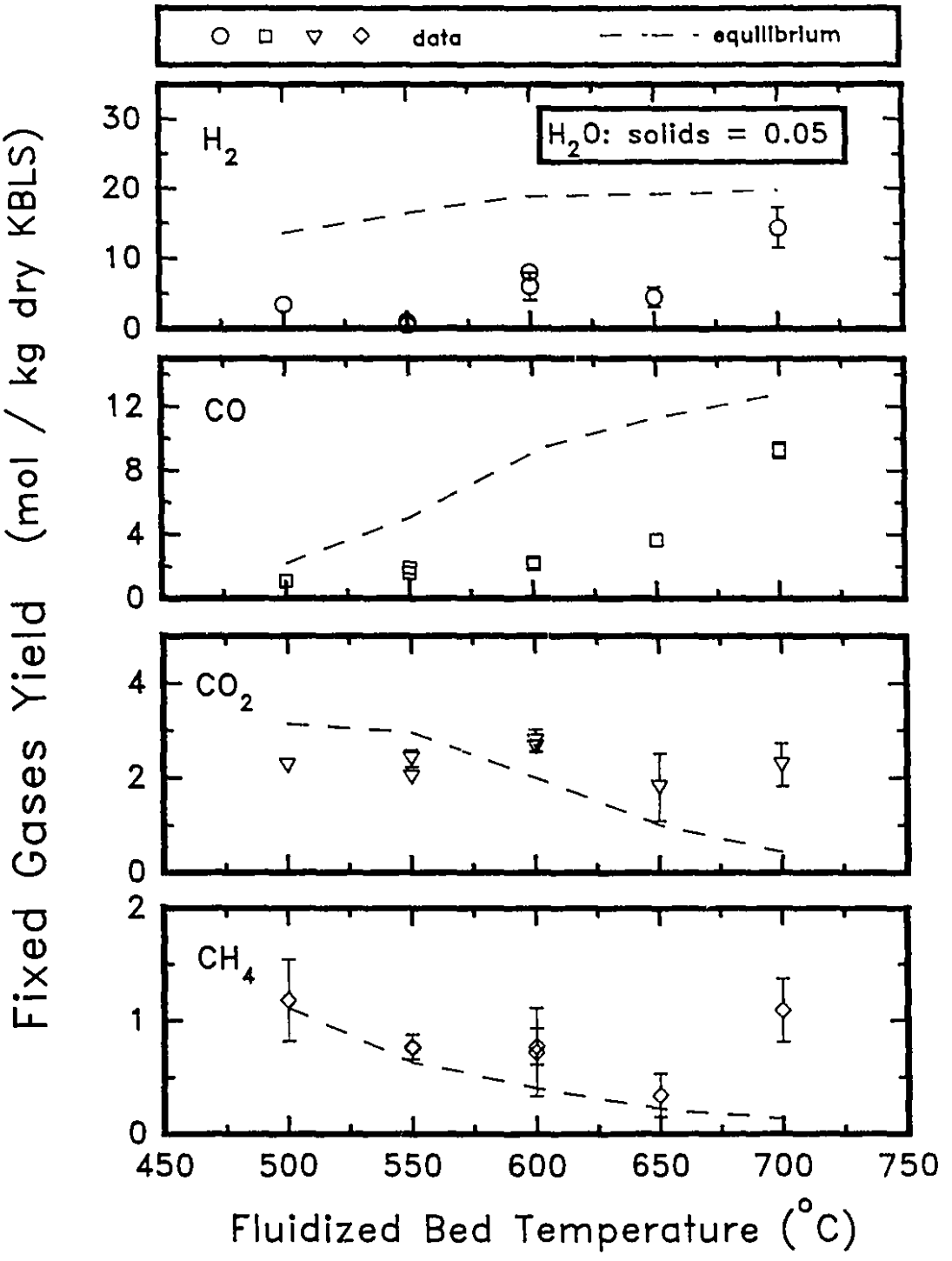

Figure 17 Experimental and Equilibrium Yield of H_2, CO, CO_2, and CH_4 During Fluidized Bed Pyrolysis in N_2 for T = 500-700°C.

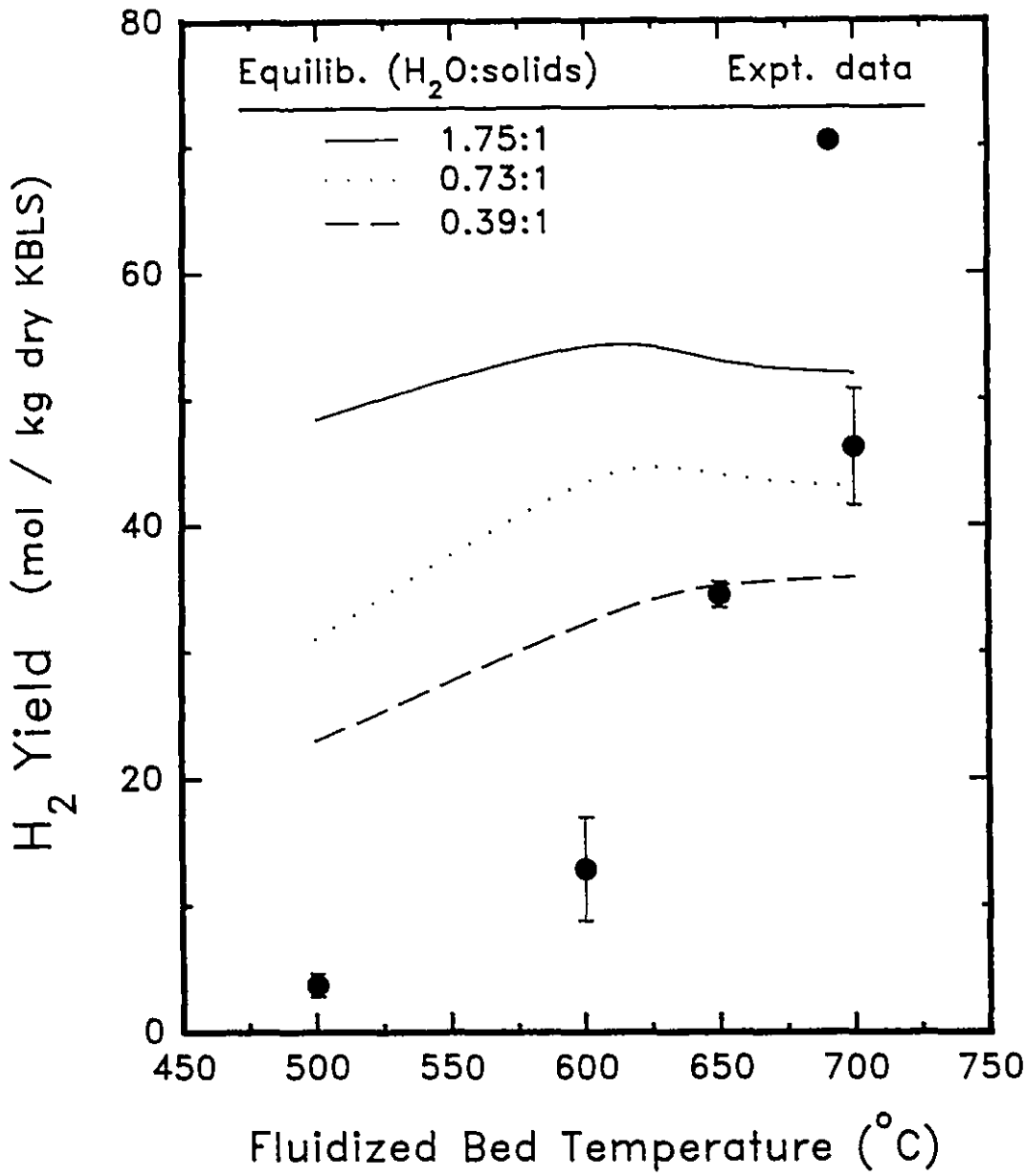

Figure 18 Experimental and Equilibrium Yield of H_2 During Fluidized-Bed Steam Gasification for T = 500-700°C.

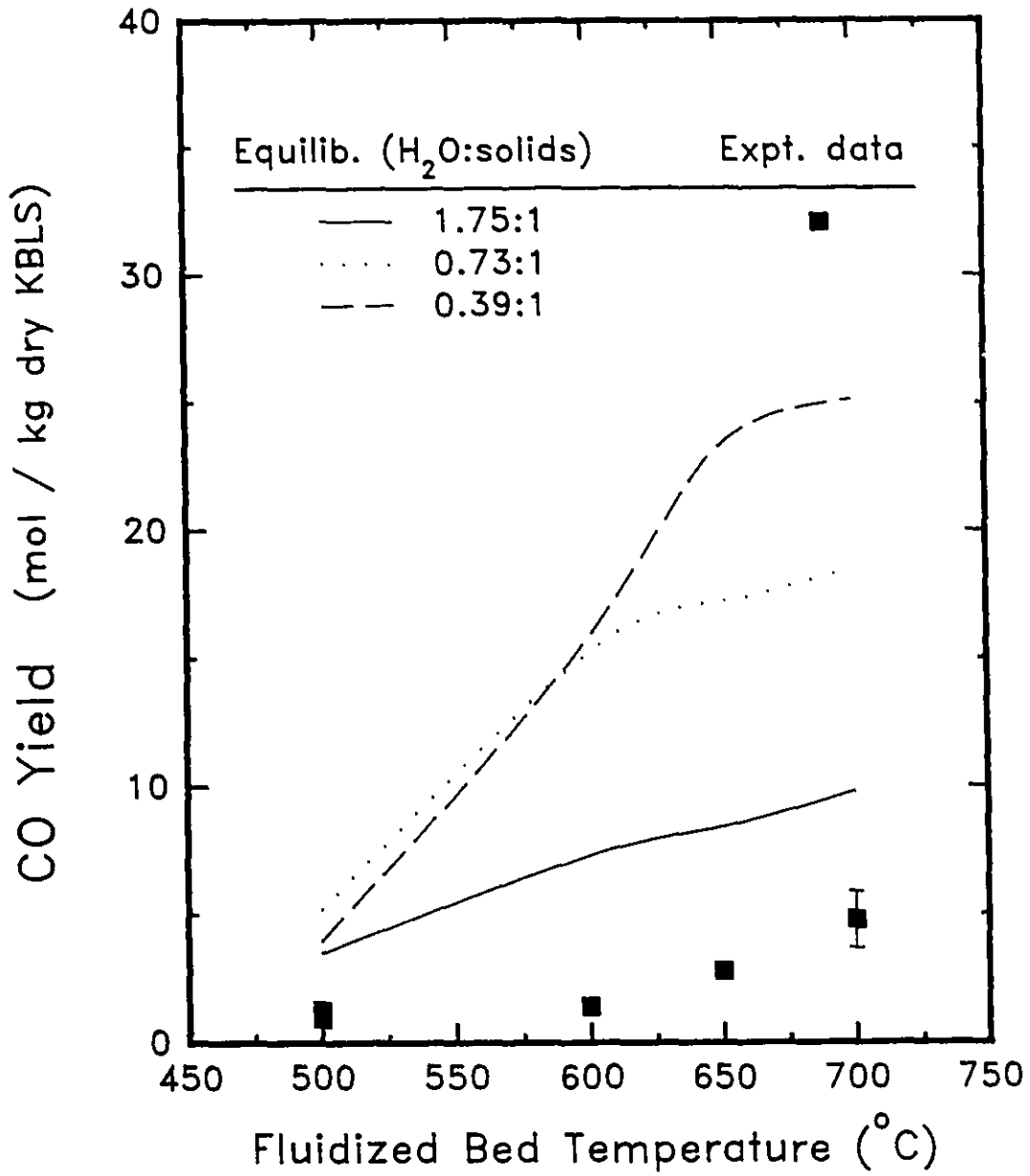

Figure 19 Experimental and Equilibrium Yield of CO During Fluidized-Bed Steam Gasification for T = 500-700°C.

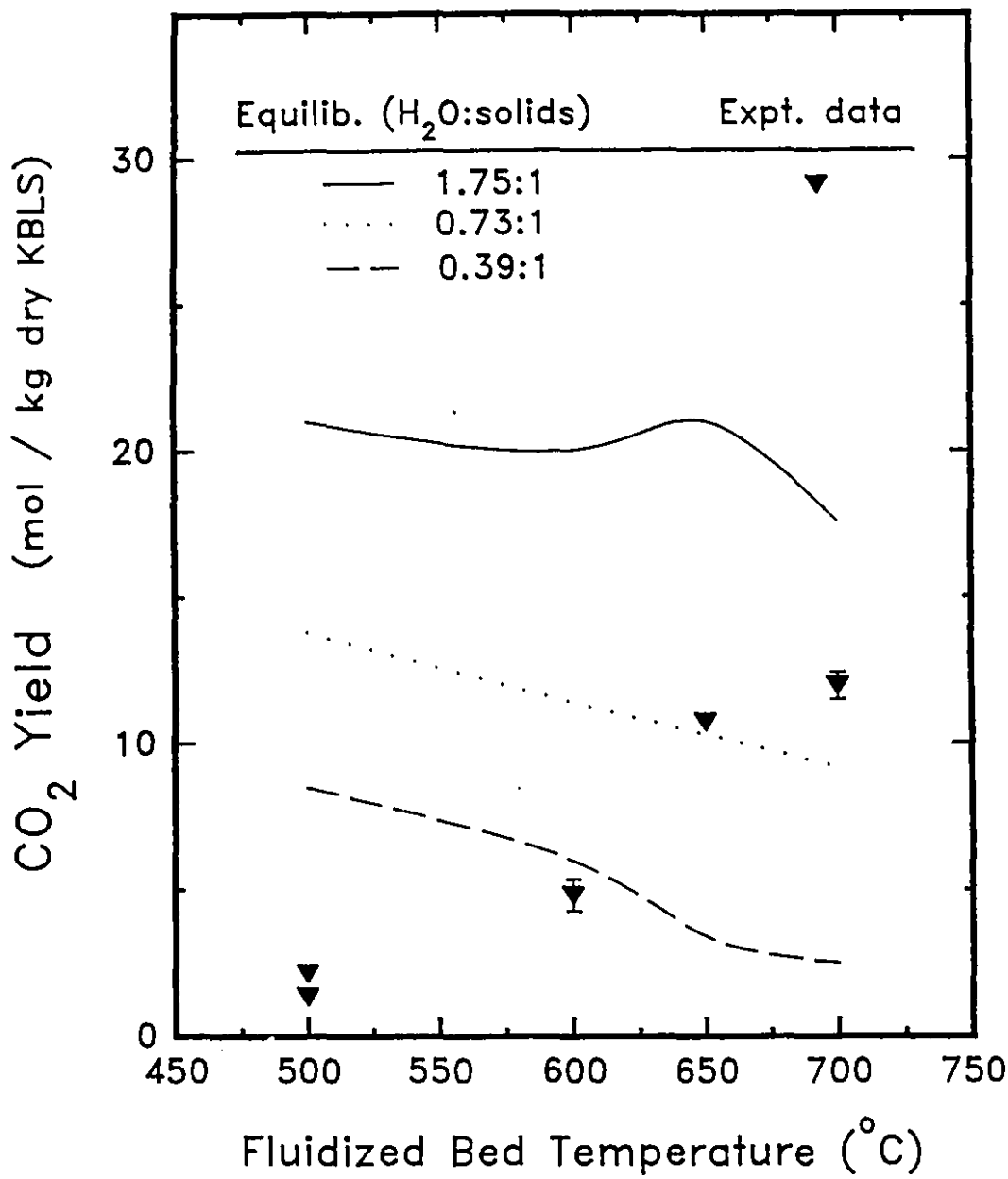

Figure 20 Experimental and Equilibrium Yield of CO_2 During Fluidized-Bed Steam Gasification for T = 500-700°C.

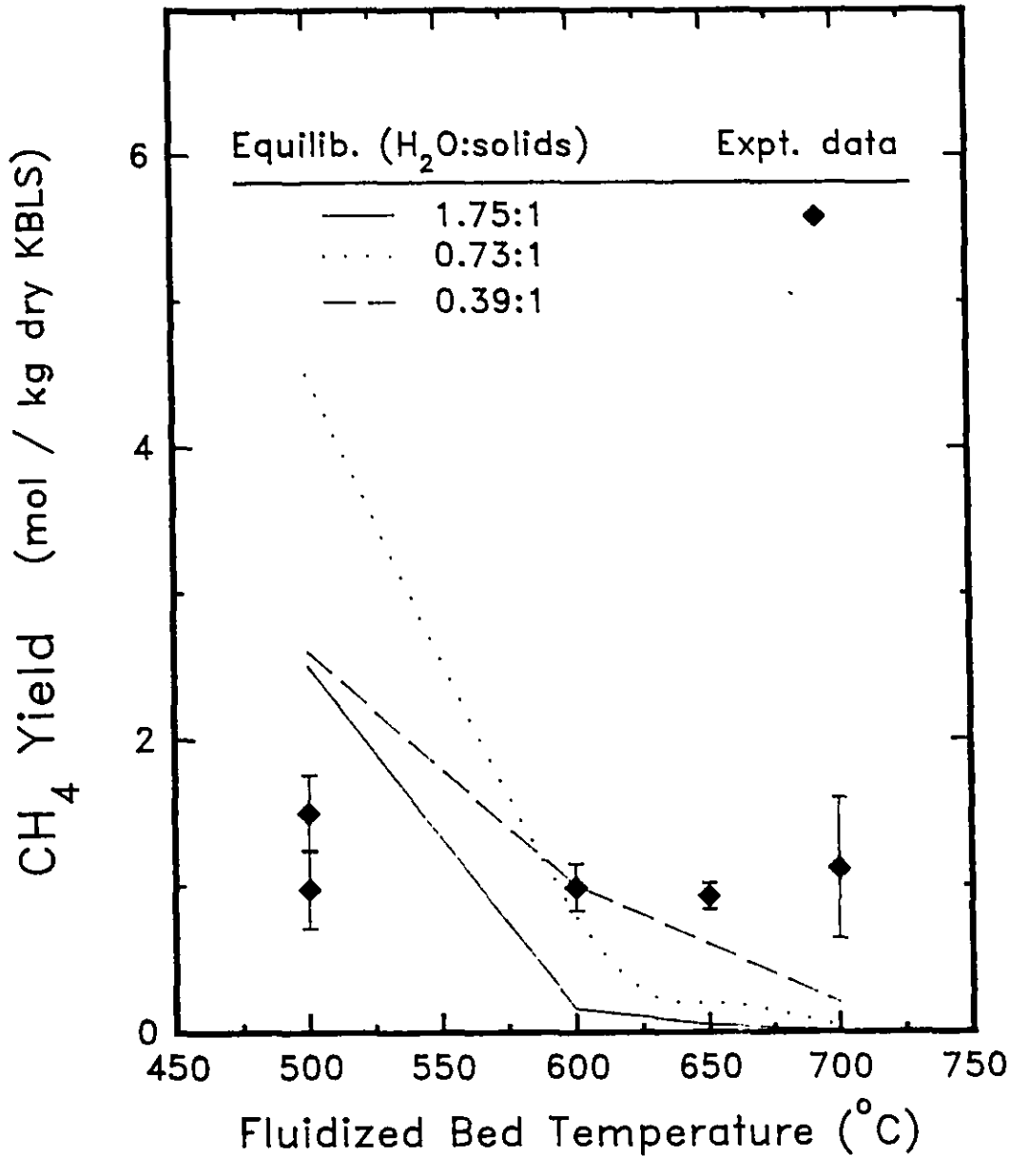

Figure 21 Experimental and Equilibrium Yield of CH_4 During Fluidized-Bed Steam Gasification for T = 500-700°C.

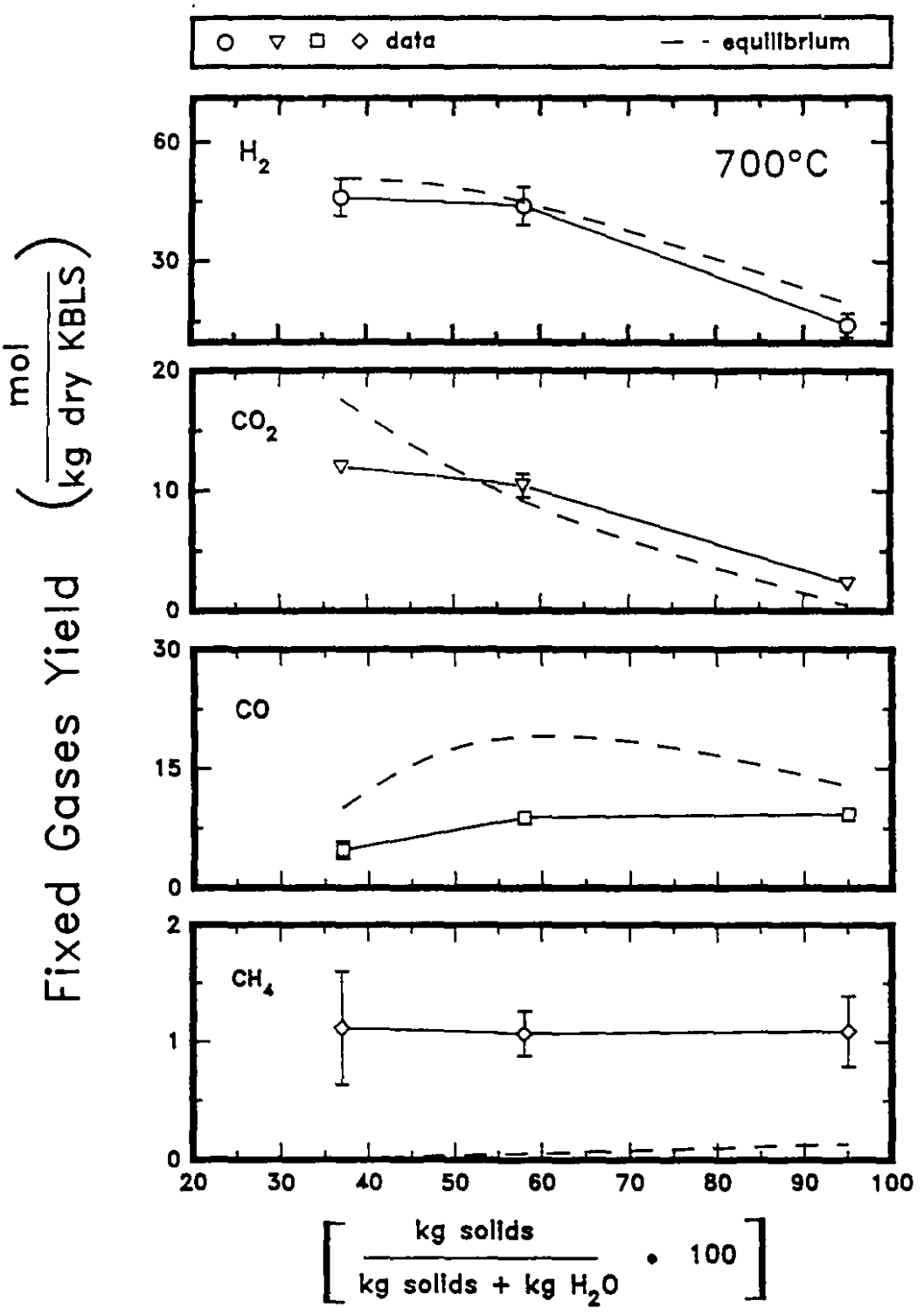

Figure 22 Experimental and Equilibrium Yield of Fixed Gases as a Function of the Equivalent wt% Solids in the Fluidized Bed for T = 700°C.

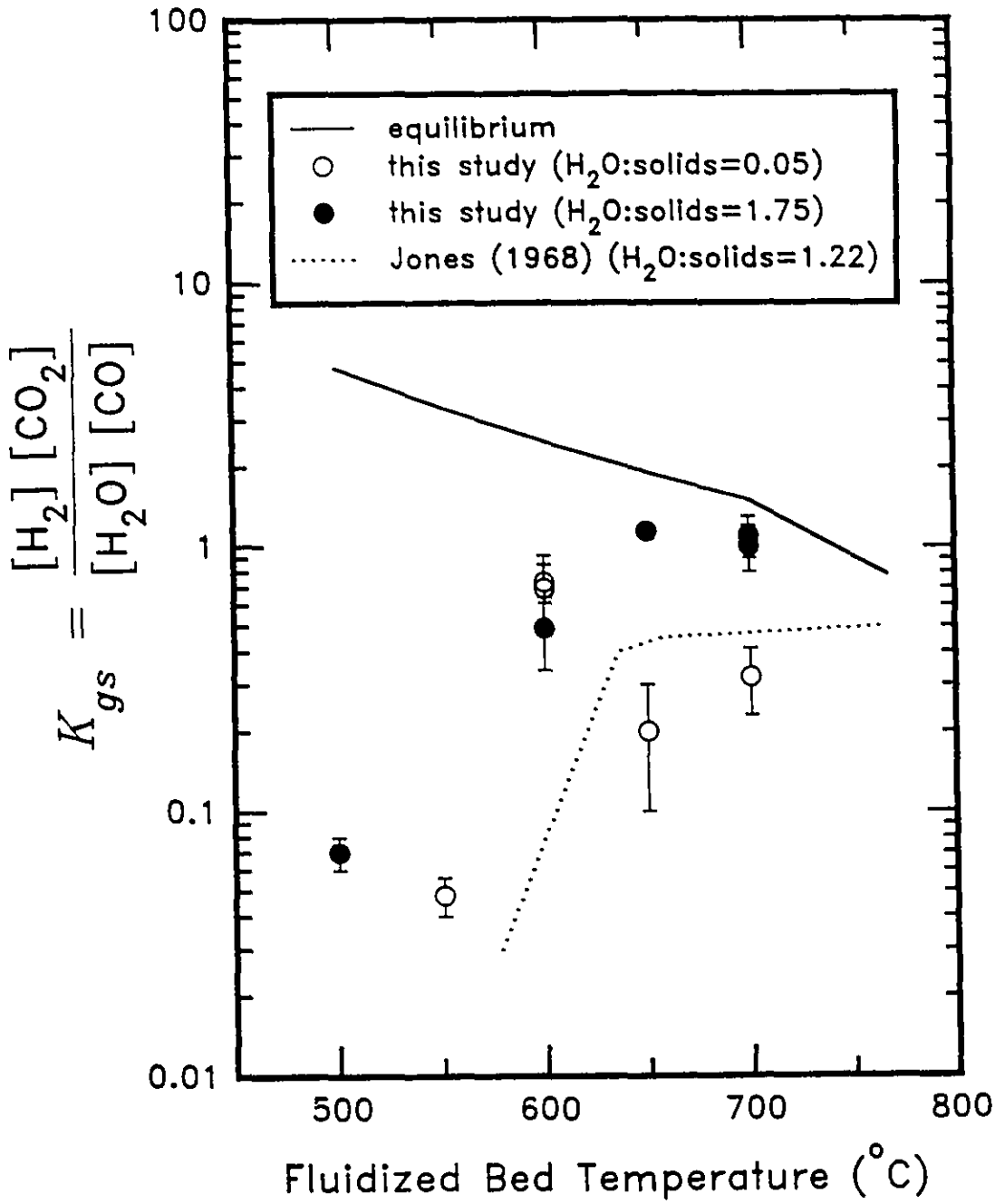

Figure 23 Water-Gas Shift Constant, K_{gs}, as a Function of the Fluidized-Bed Temperature and H_2O:Solids Weight Ratio.

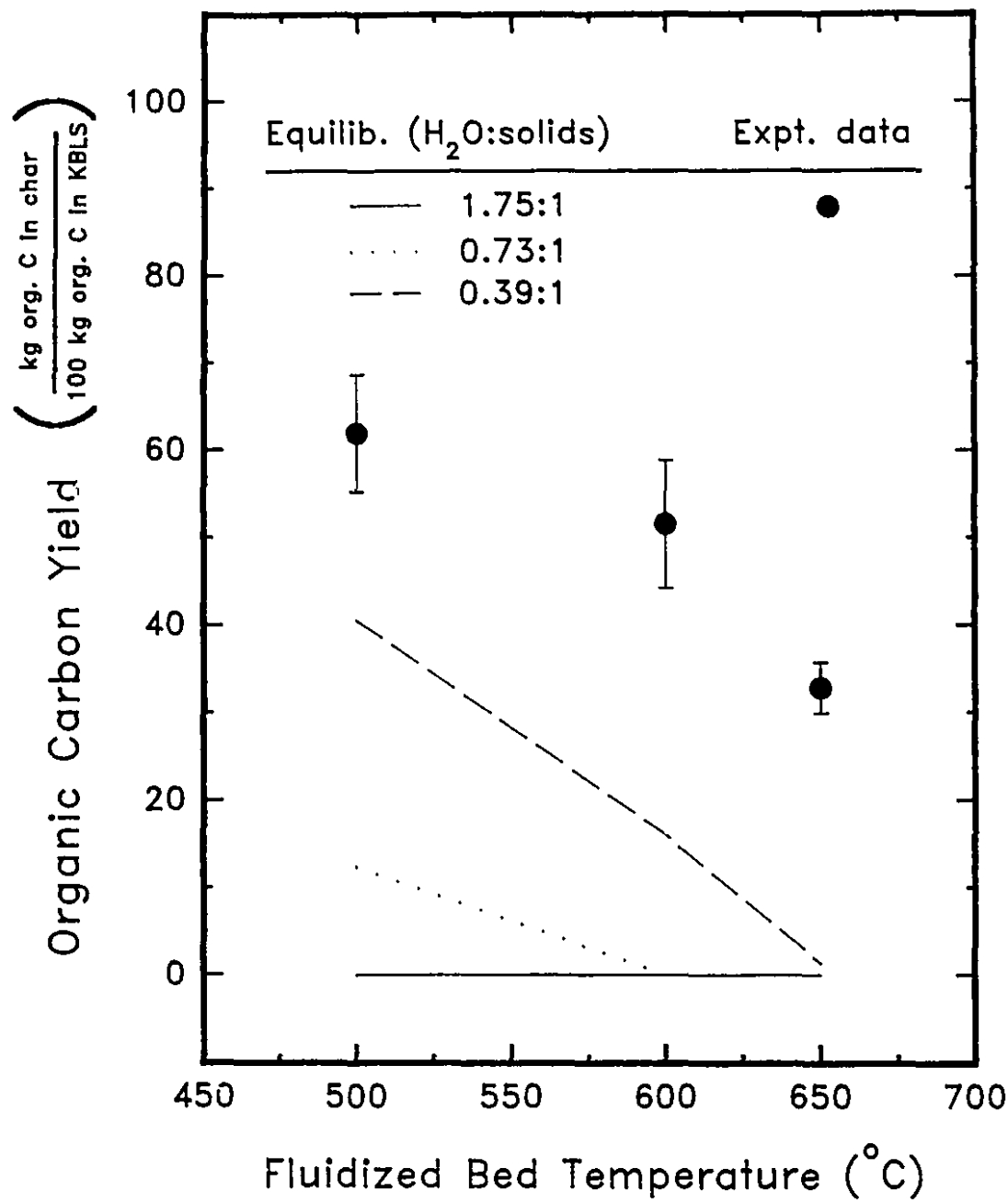

Figure 24 Experimental and Equilibrium Yield of Organic Carbon in Fluidized-Bed Char During Steam Gasification for T = 500-700°C.

Figure 25 SEM Micrographs of an Alumina Particle Surface (a); and Char-Alumina for Pyrolysis Runs at 500°C (b-c), 600°C (d), and 700°C (e-f).

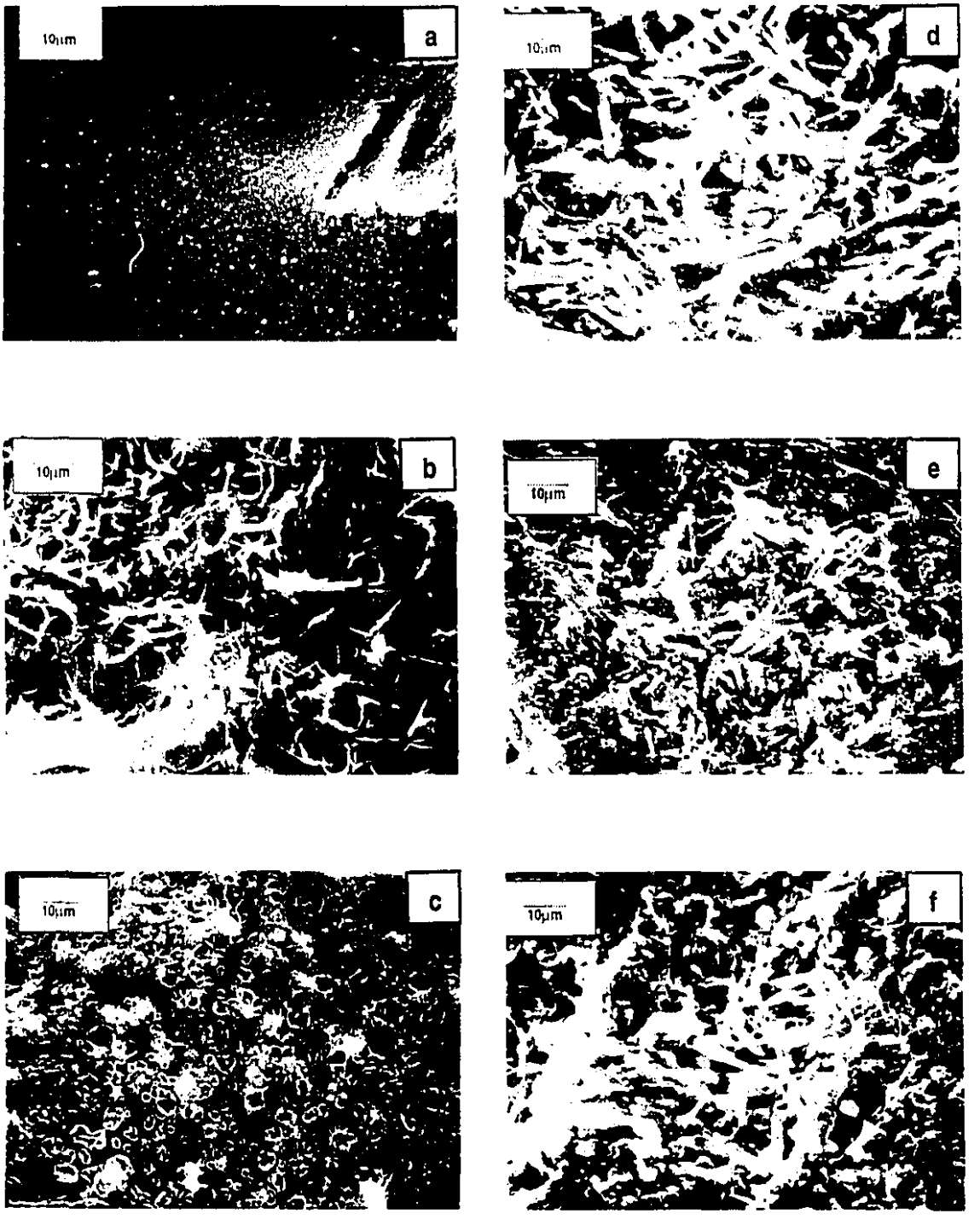
10µm
a
10µm
d
10µm
b
10µm
e
10µm
c
10µm
f

Figure 26 SEM Micrographs of Char-Alumina Particle Surfaces for Steam Gasification at 600°C (a), 650°C (b-c), 700°C (d).

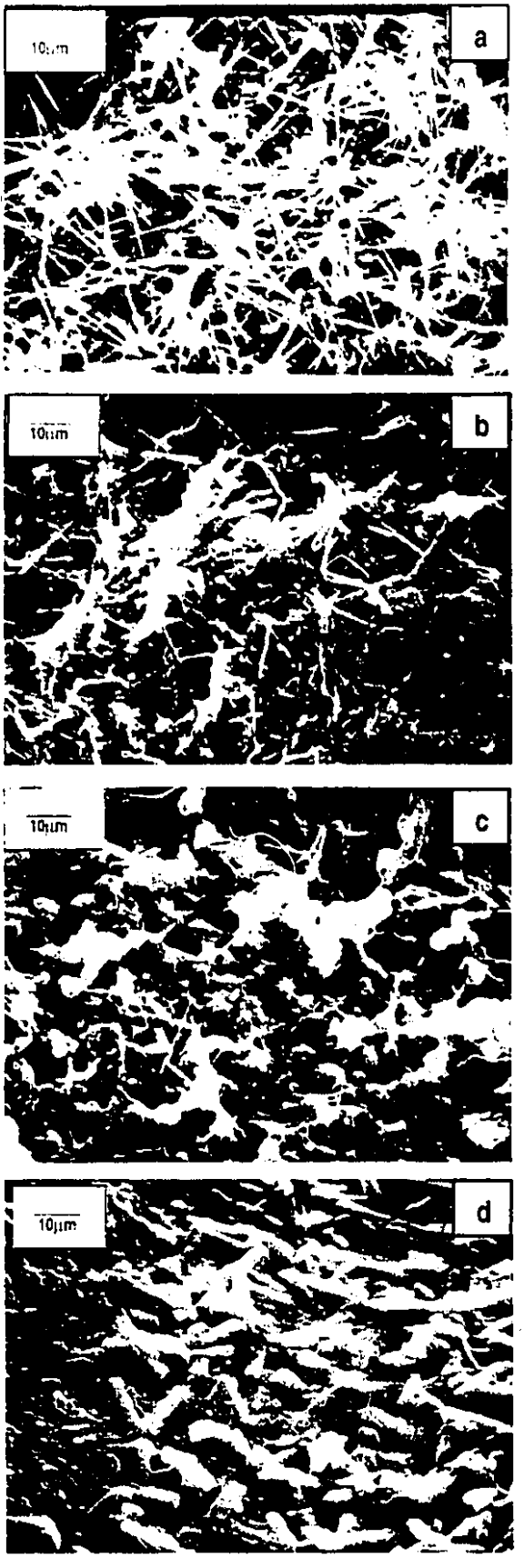
10µm
a
10µm
b
10µm
c
10µm
d

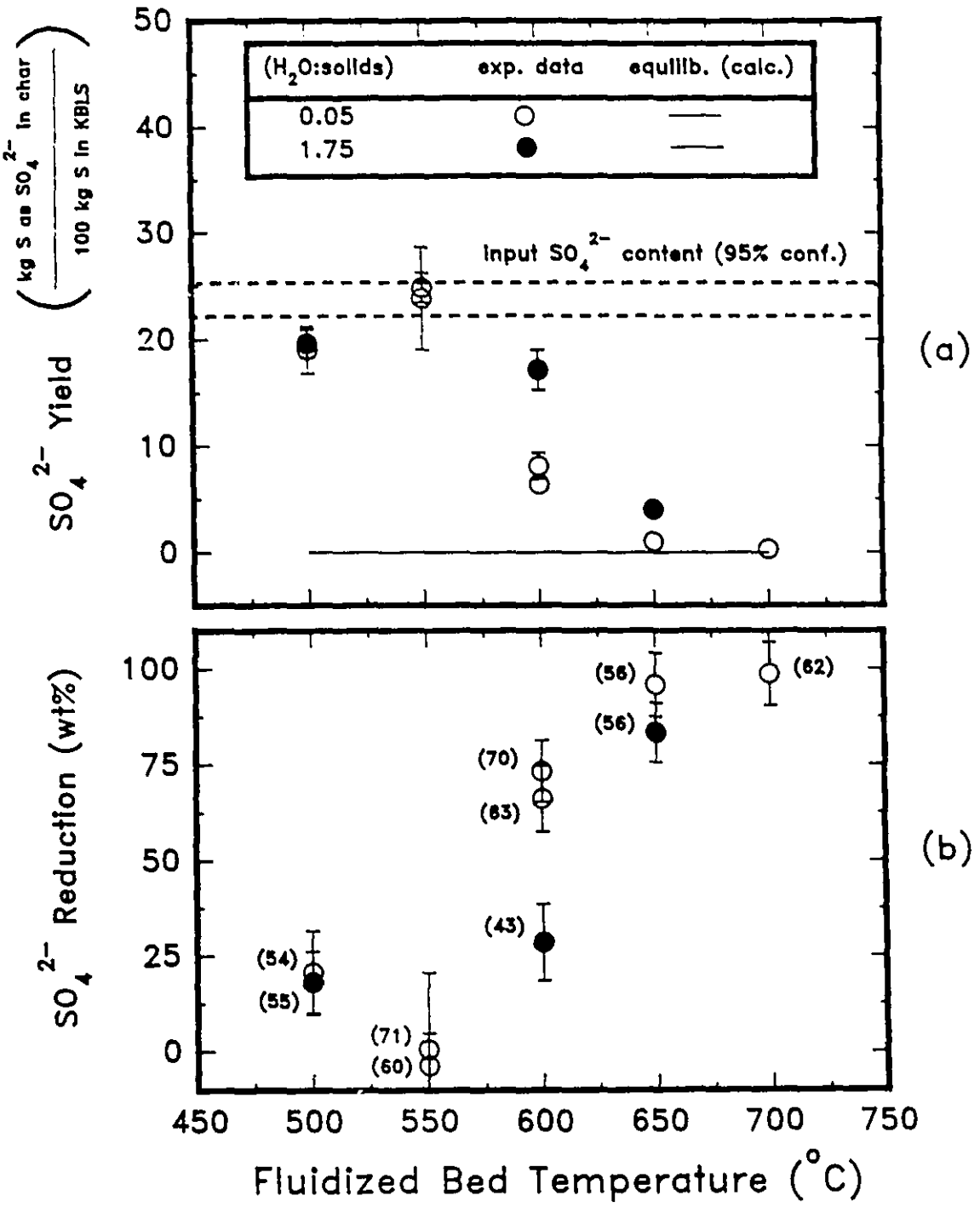

Figure 27 (a) SO_4^{2-} Char Yield and (b) SO_4^{2-} Reduction, as a Function of Temperature for Pyrolysis and Steam Gasification. The mean residence times (min) for char are in brackets.

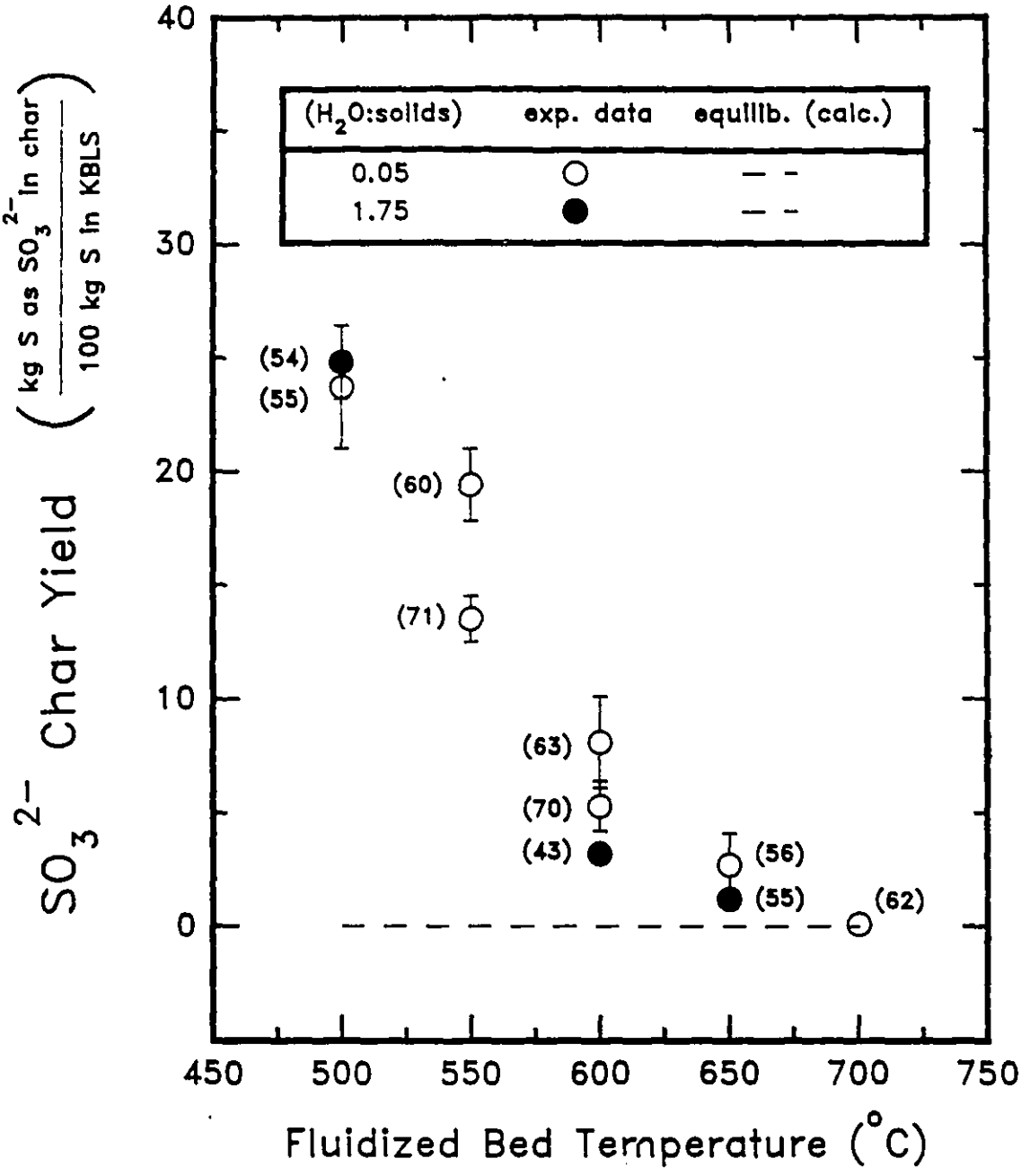

Figure 28 SO_3^{2-} Char Yield as a Function of the Inlet H_2O:Solids Ratio and Fluidized-Bed Temperature. The mean residence times (min) for char are shown in brackets.

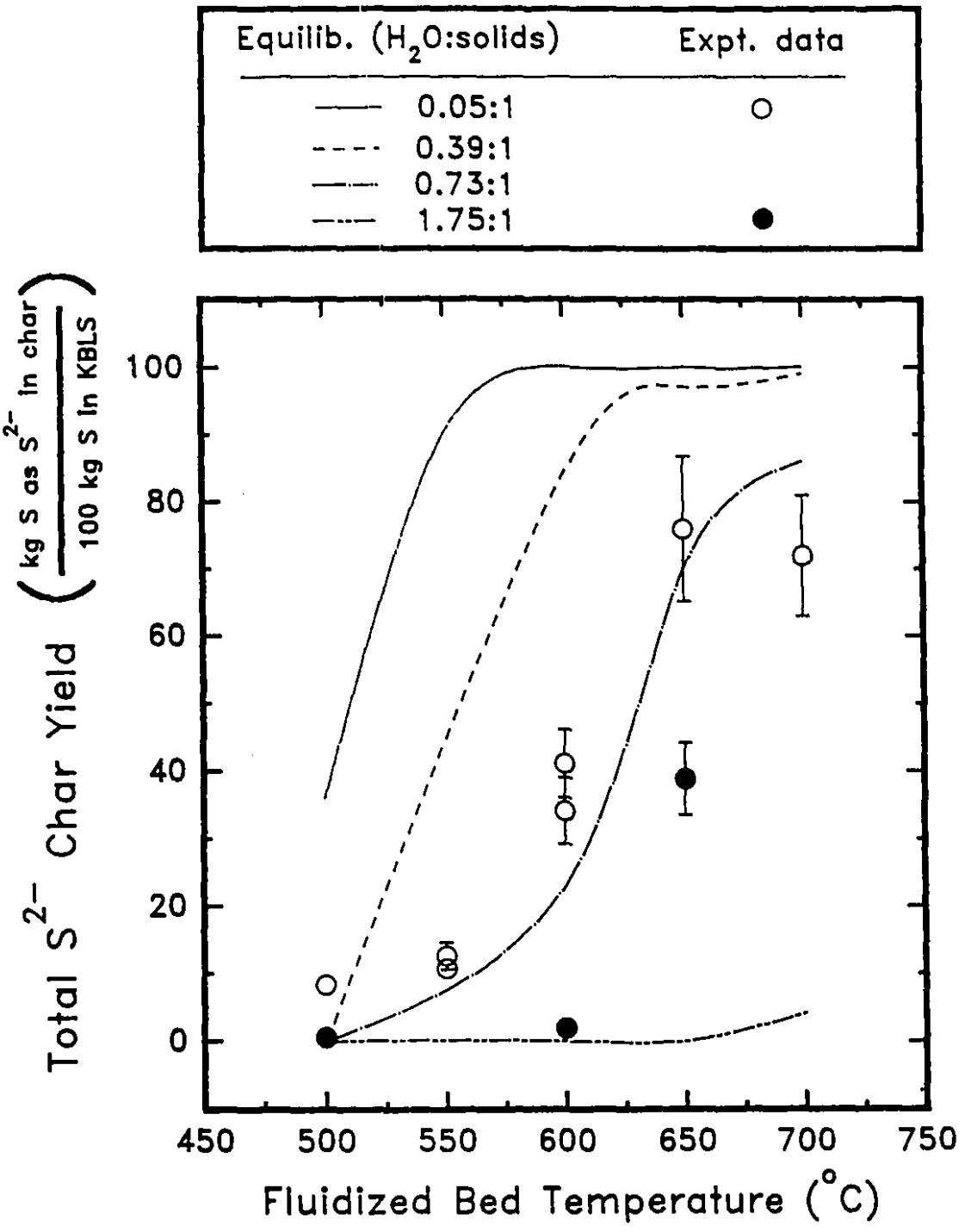

Figure 29 Total S^{2-} Char Yield as a Function of the Inlet H_2O:Solids Ratio and Fluidized-Bed Reactor Temperature.

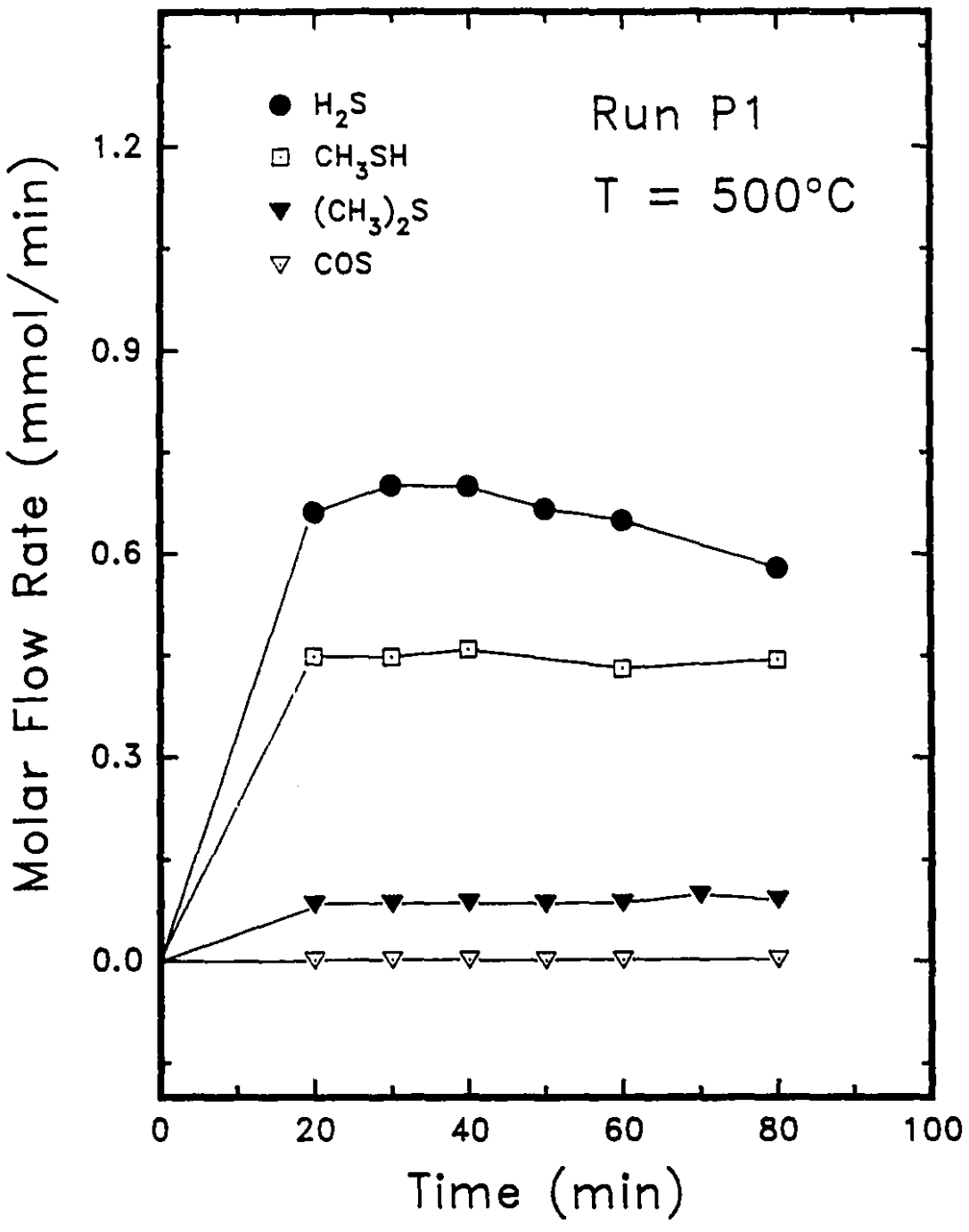

Figure 30 Time-Sampled Molar Flow Rate of Sulphur-Bearing Gases for Pyrolysis Run P1 at 500°C.

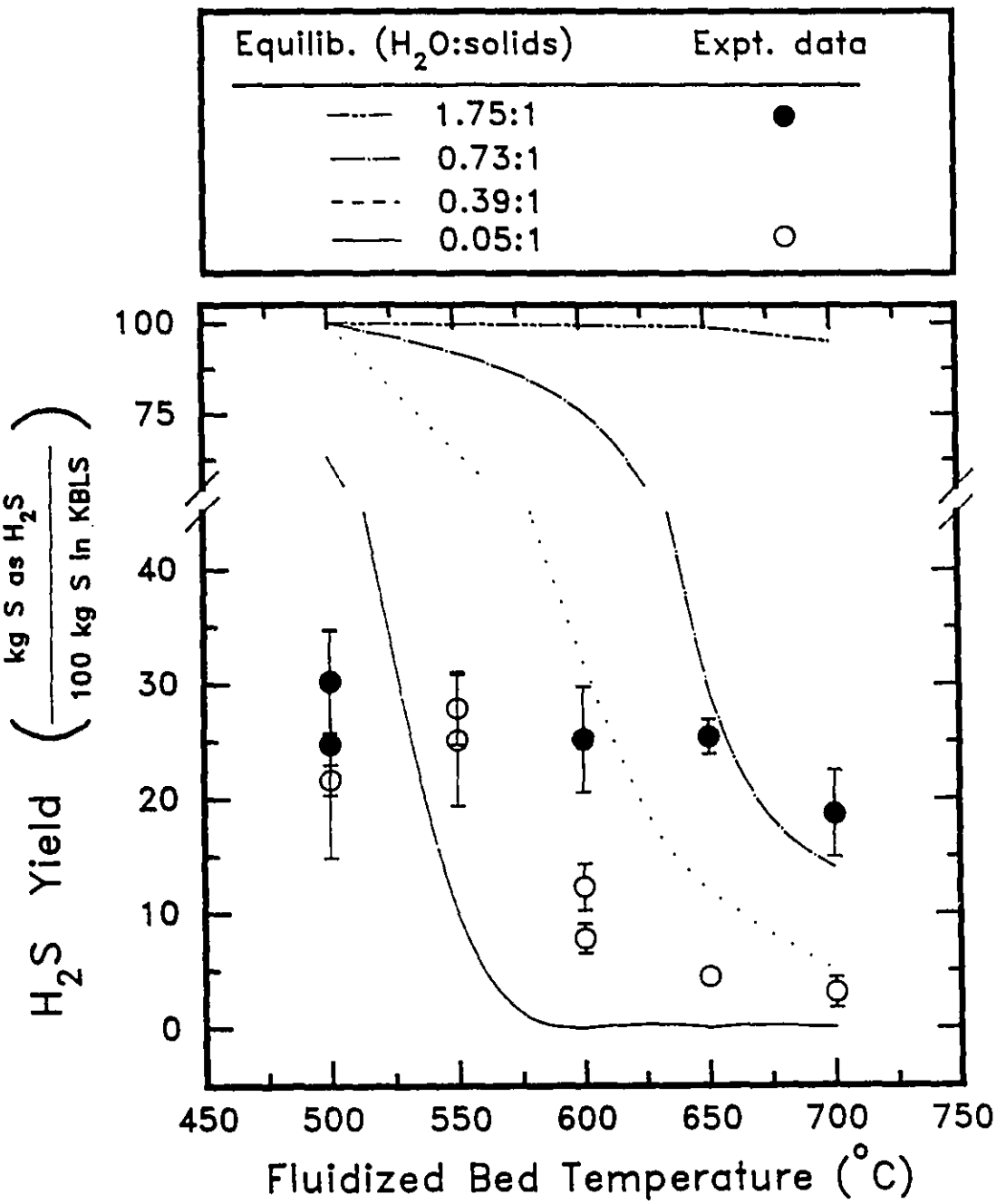

Figure 31 Average Yield of H_2S in the Gas Phase as a Function of the Inlet H_2O:Solids Ratio and Fluidized-Bed Temperature.

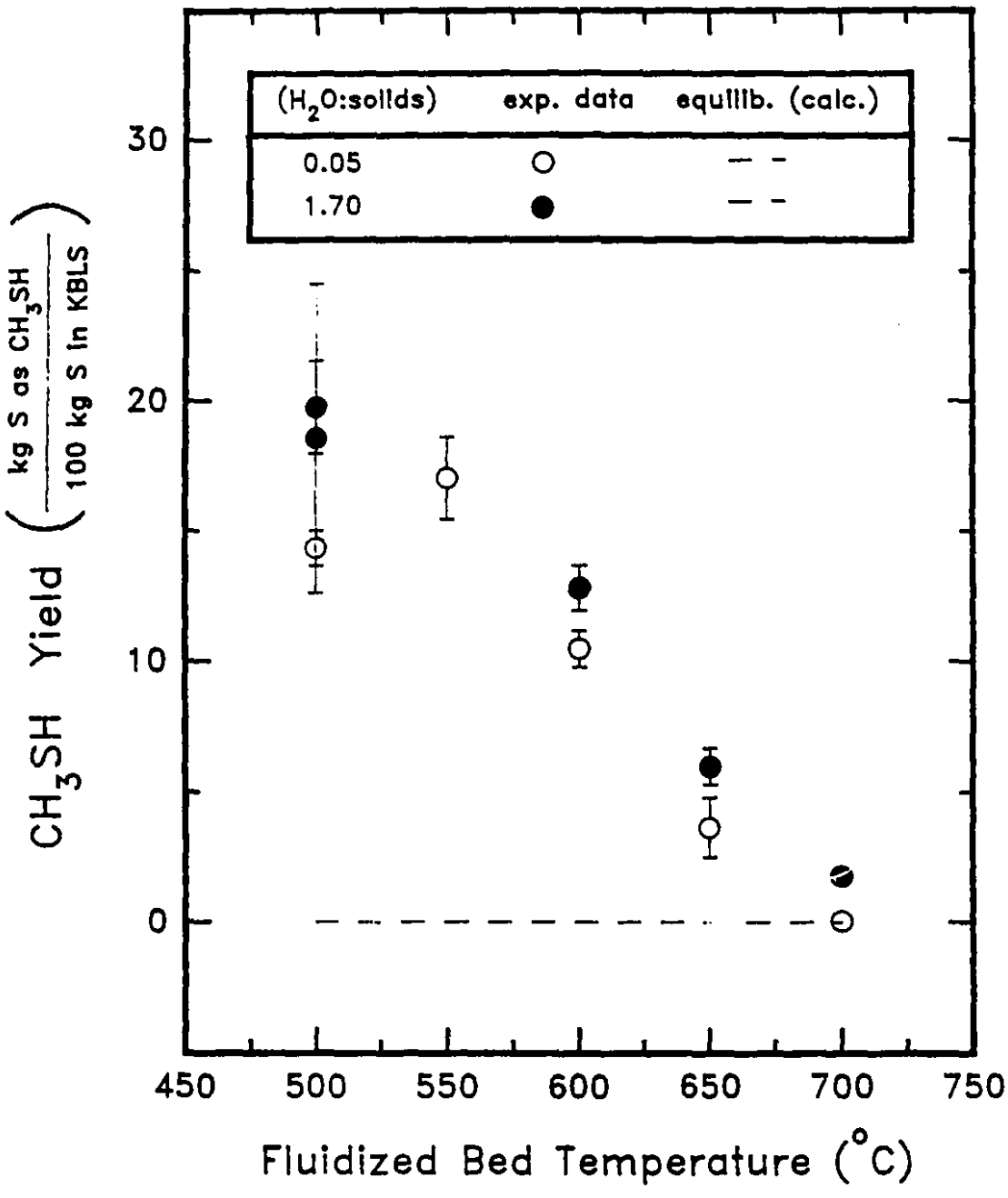

Figure 32 Average Yield of CH_3SH in the Gas Phase as a Function of the Inlet H_2O:Solids Ratio and Fluidized-Bed Temperature.

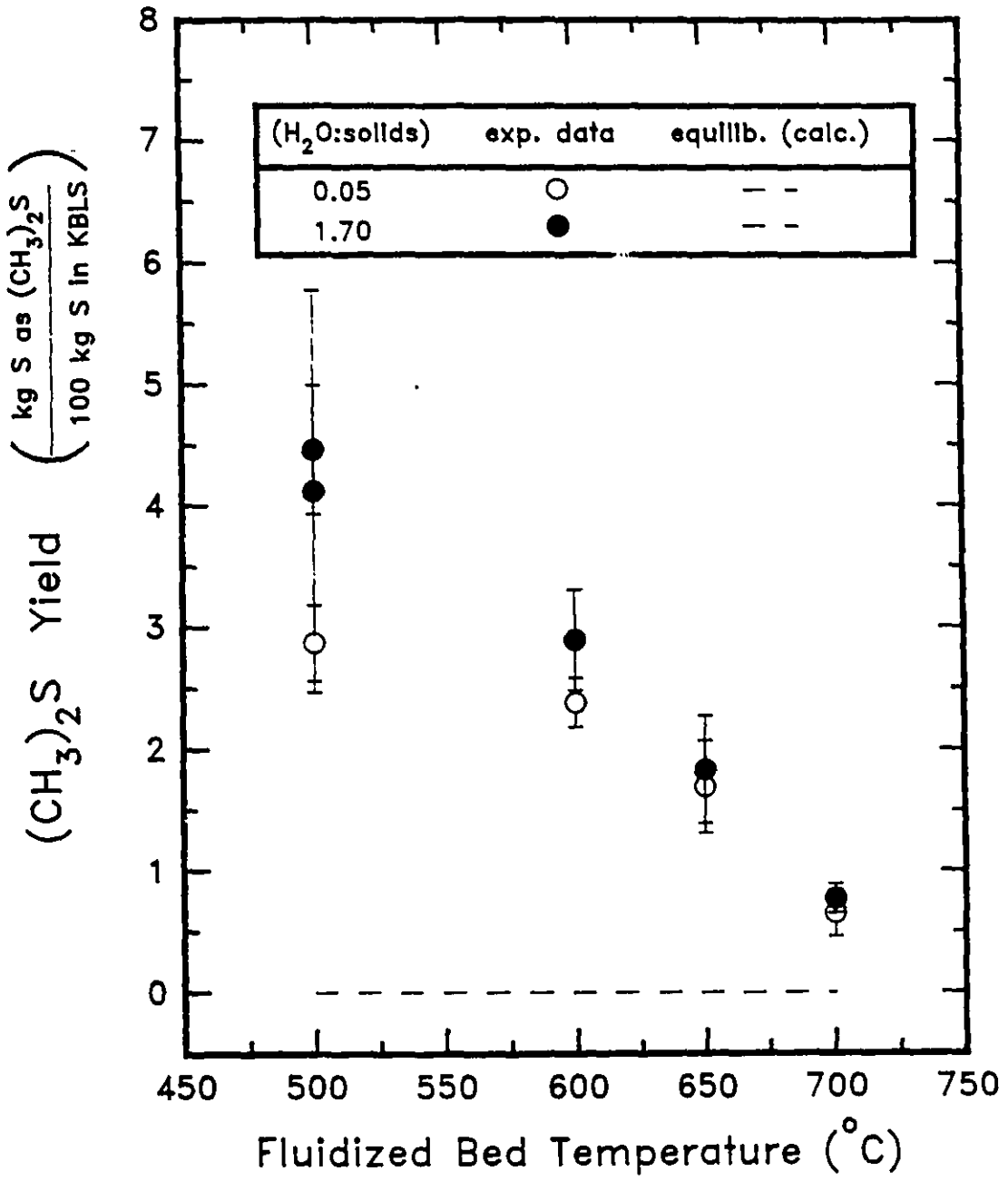

Figure 33 Average Yield of $(CH_3)_2S$ in the Gas Phase as a Function of the Inlet H_2O:Solids Ratio and Fluidized-Bed Temperature.

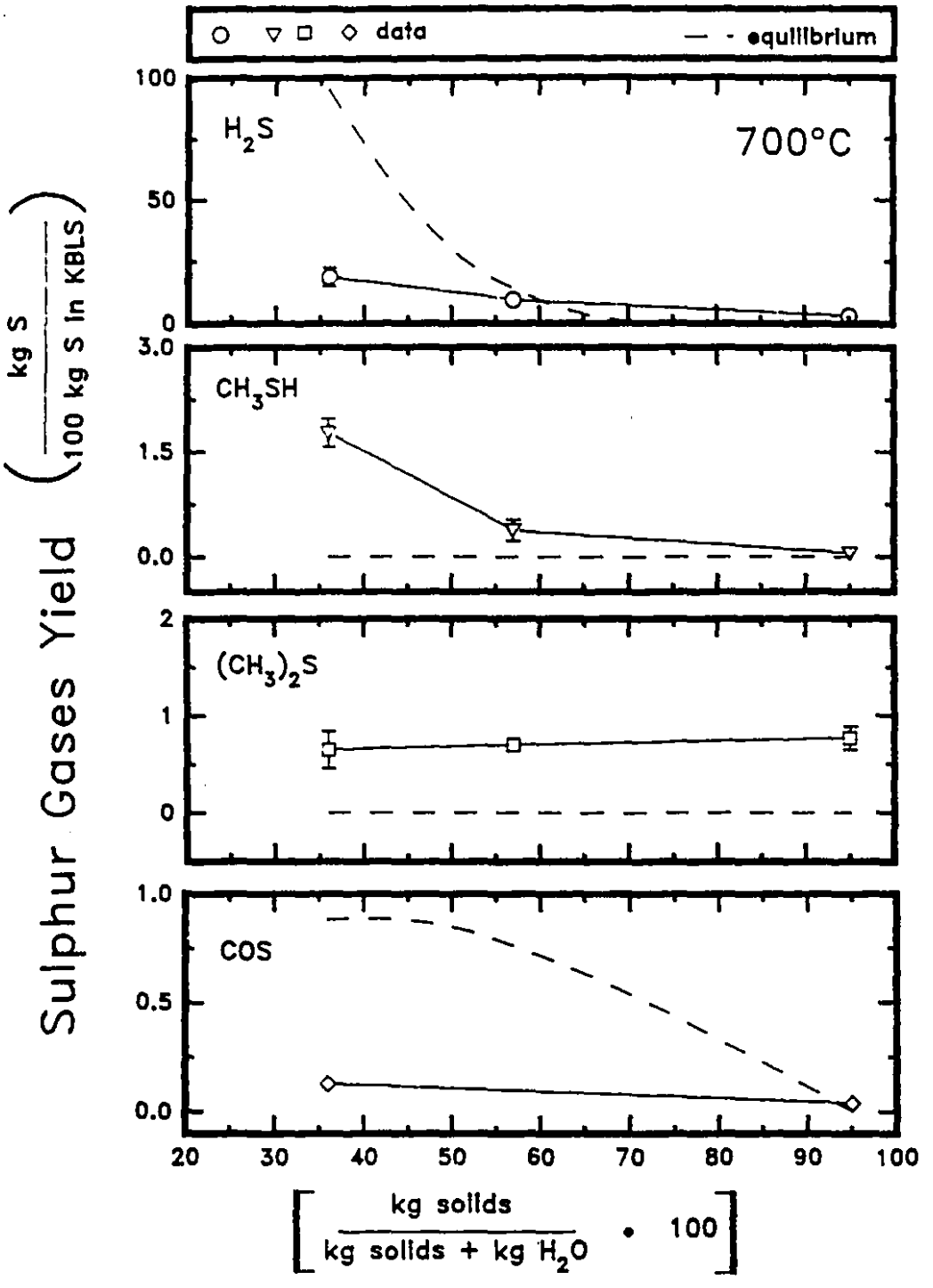

Figure 34 Equilibrium and Experimental Data for Sulphur Gases as a Function of the Equivalent wt% Solids in the Fluidized Bed at T = 700°C.

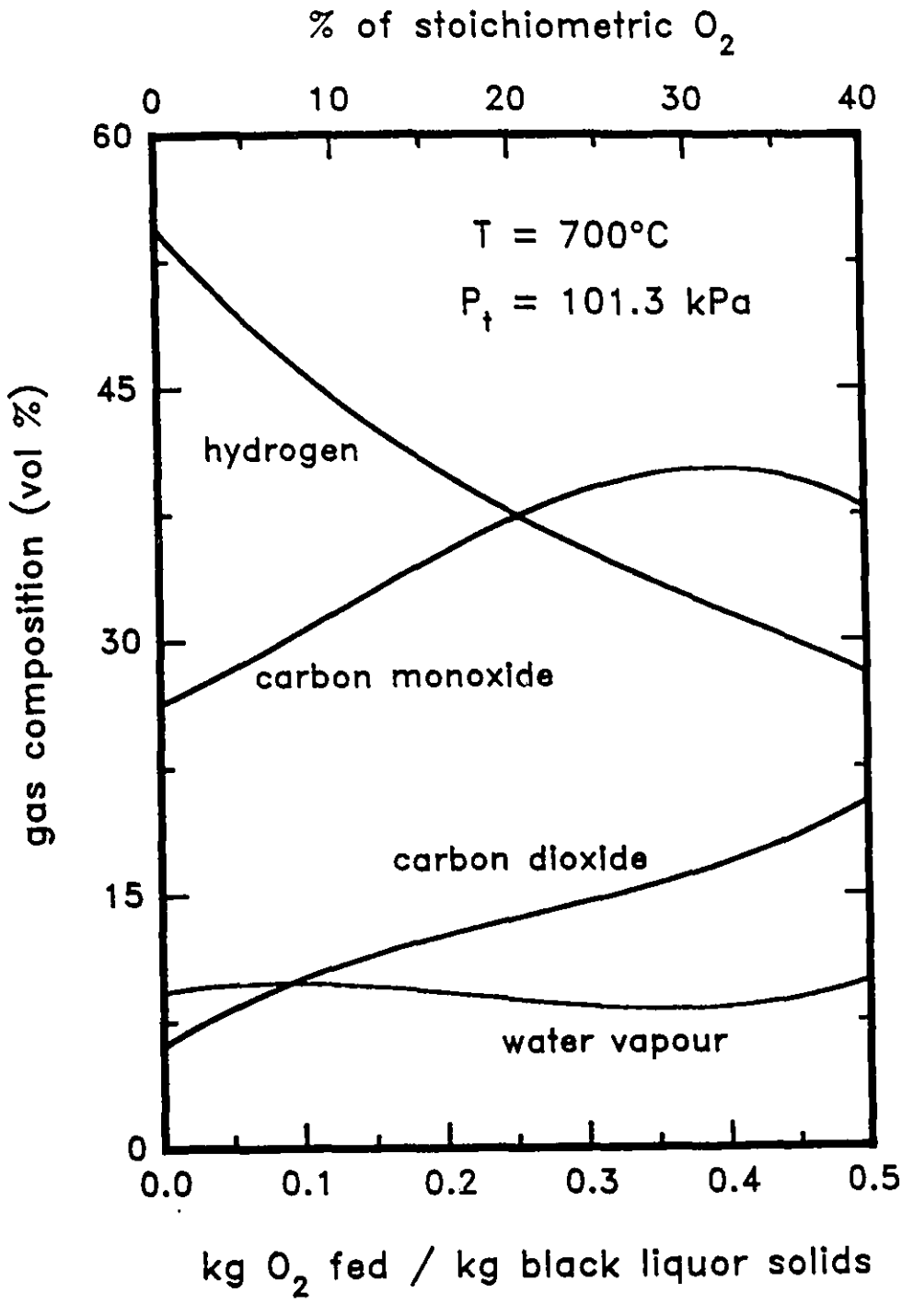

Figure 35 Equilibrium Composition of H_2, CO, CO_2 and H_2O at 700°C for Pyrolysis and O_2 Gasification of Dry Black Liquor Solids.

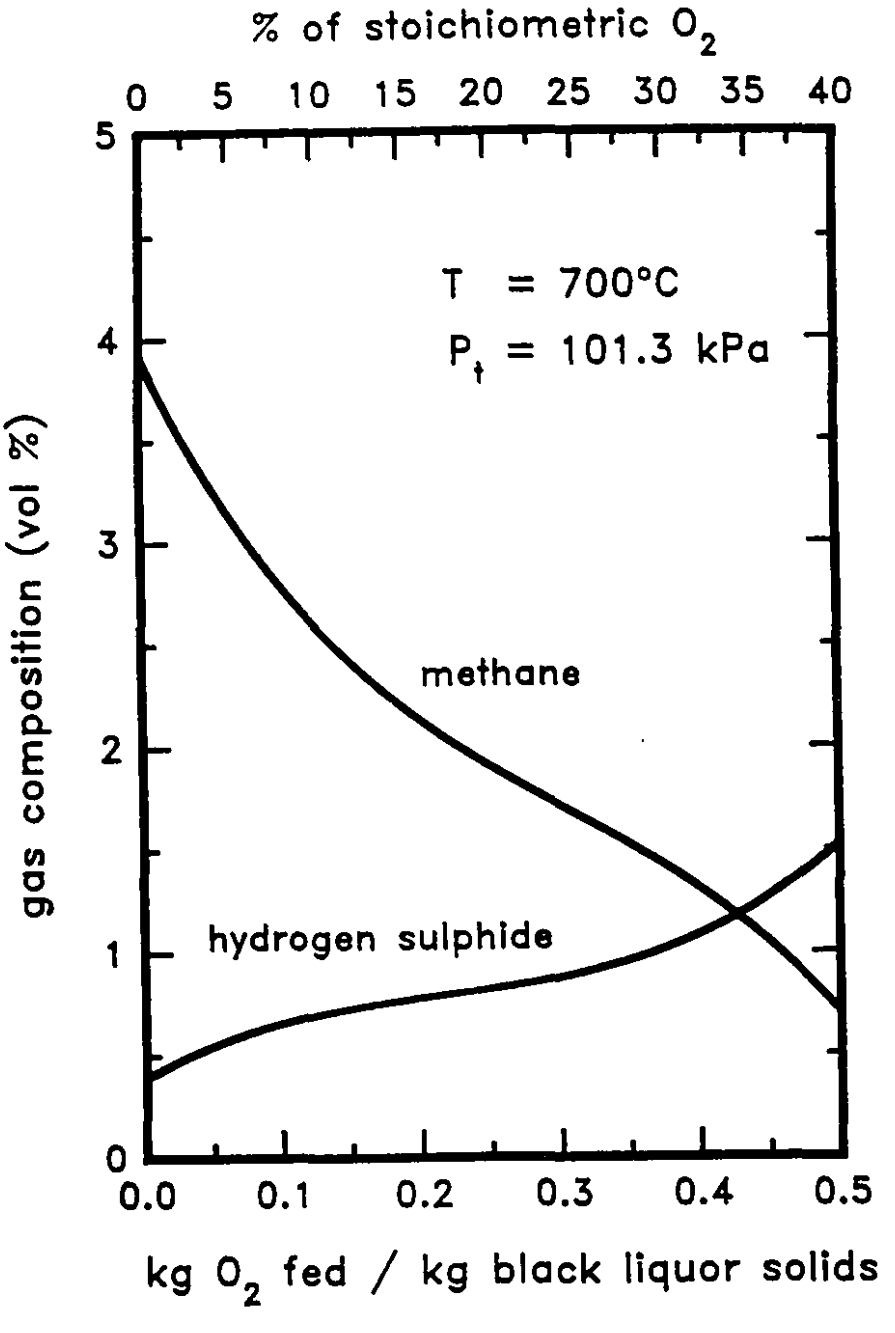

Figure 36 Equilibrium Composition of H_2S and CH_4 at 700°C for Pyrolysis and O_2 Gasification of Dry Black Liquor Solids.

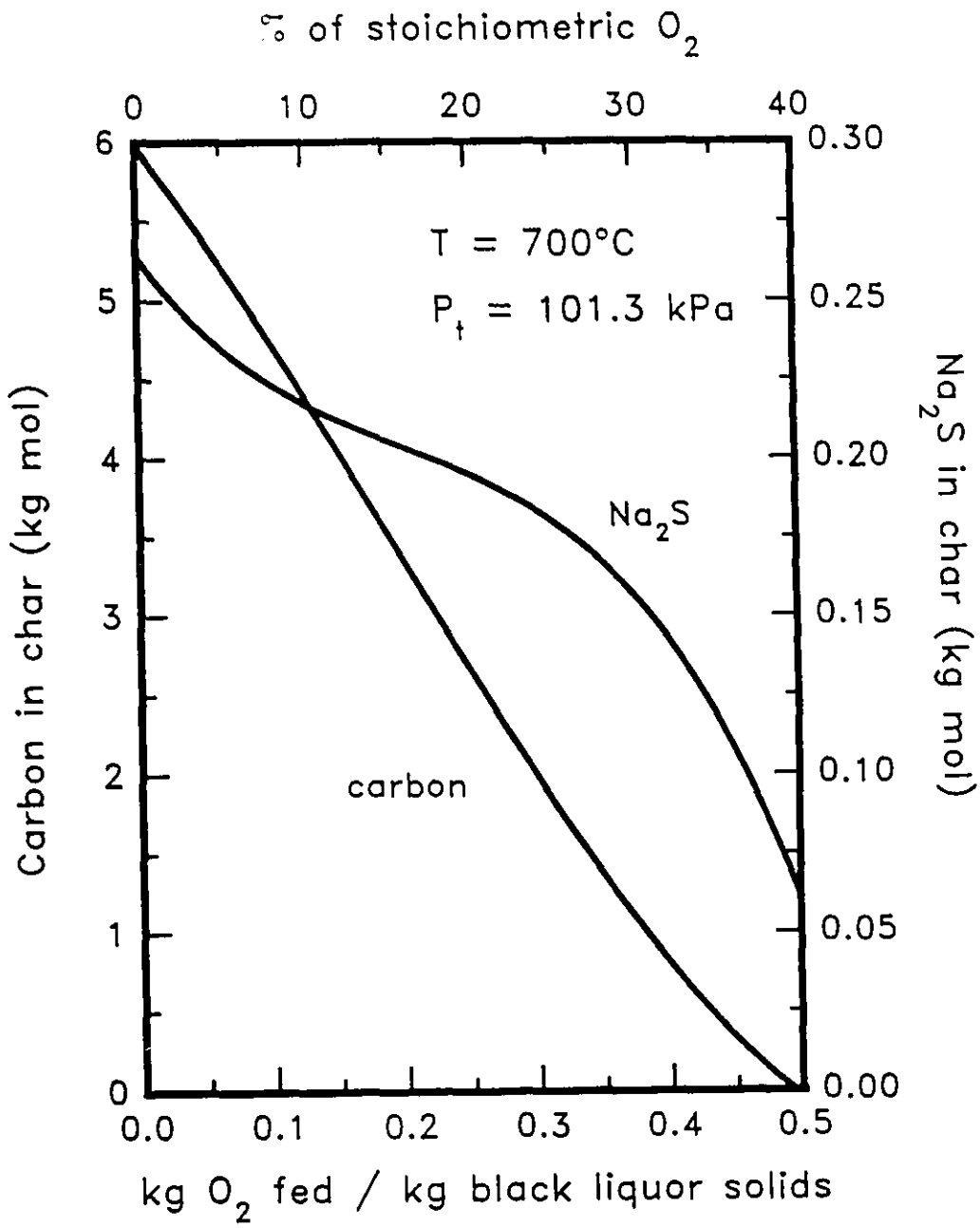

Figure 37 Equilibrium Content of Organic Carbon and Sodium Sulphide in Char for Pyrolysis and O_2 Gasification of Dry Black Liquor Solids.

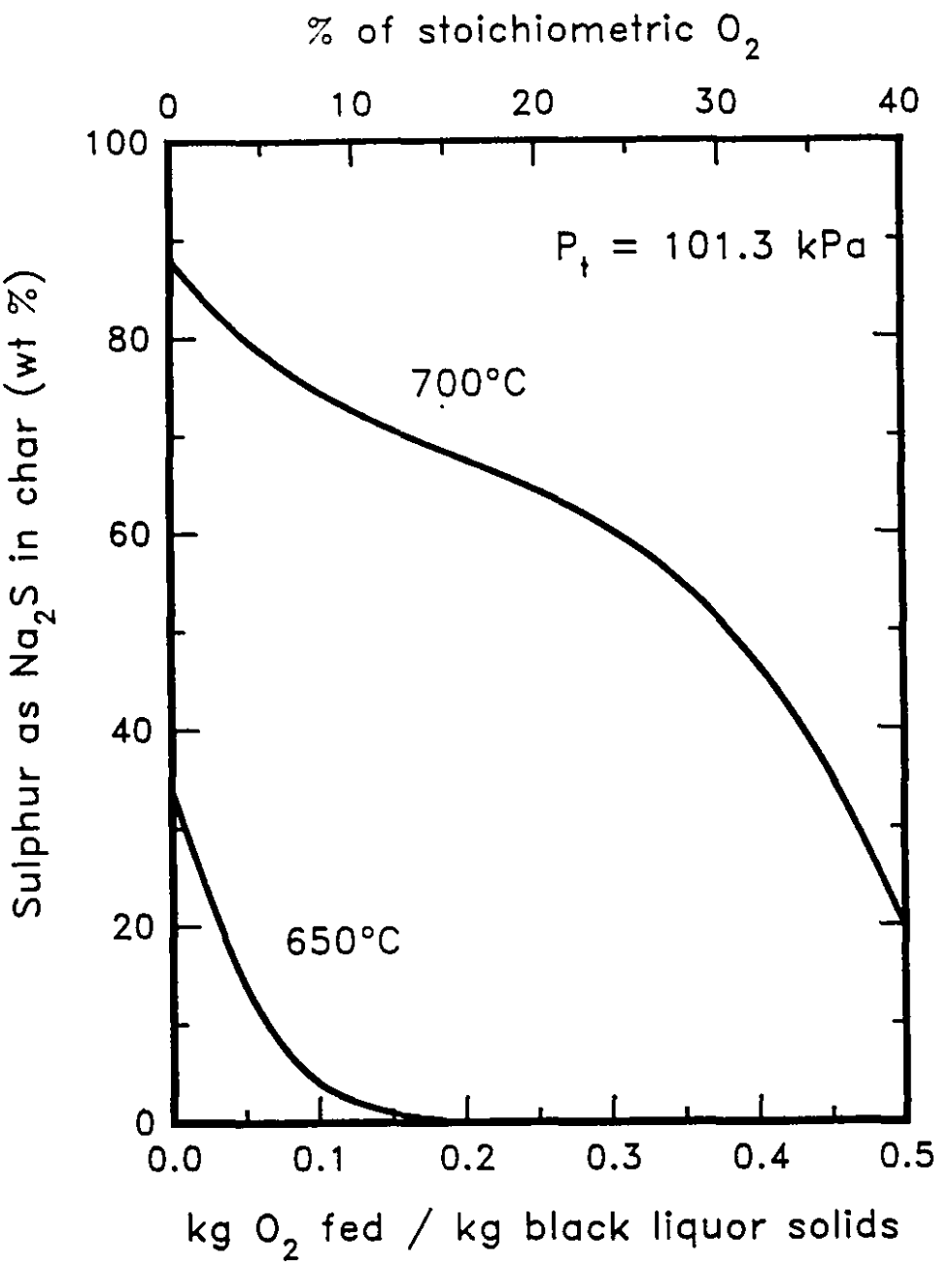

Figure 38 Equilibrium Sulphur Content of Char at 650°C and 700°C for Pyrolysis and O_2 Gasification of Dry Black Liquor Solids.

Figure 39 Flowsheet for an Alternative Low-Temperature Fluidized-Bed Recovery Process (adapted from van Heiningen, Li and Fallavollita, 1989)

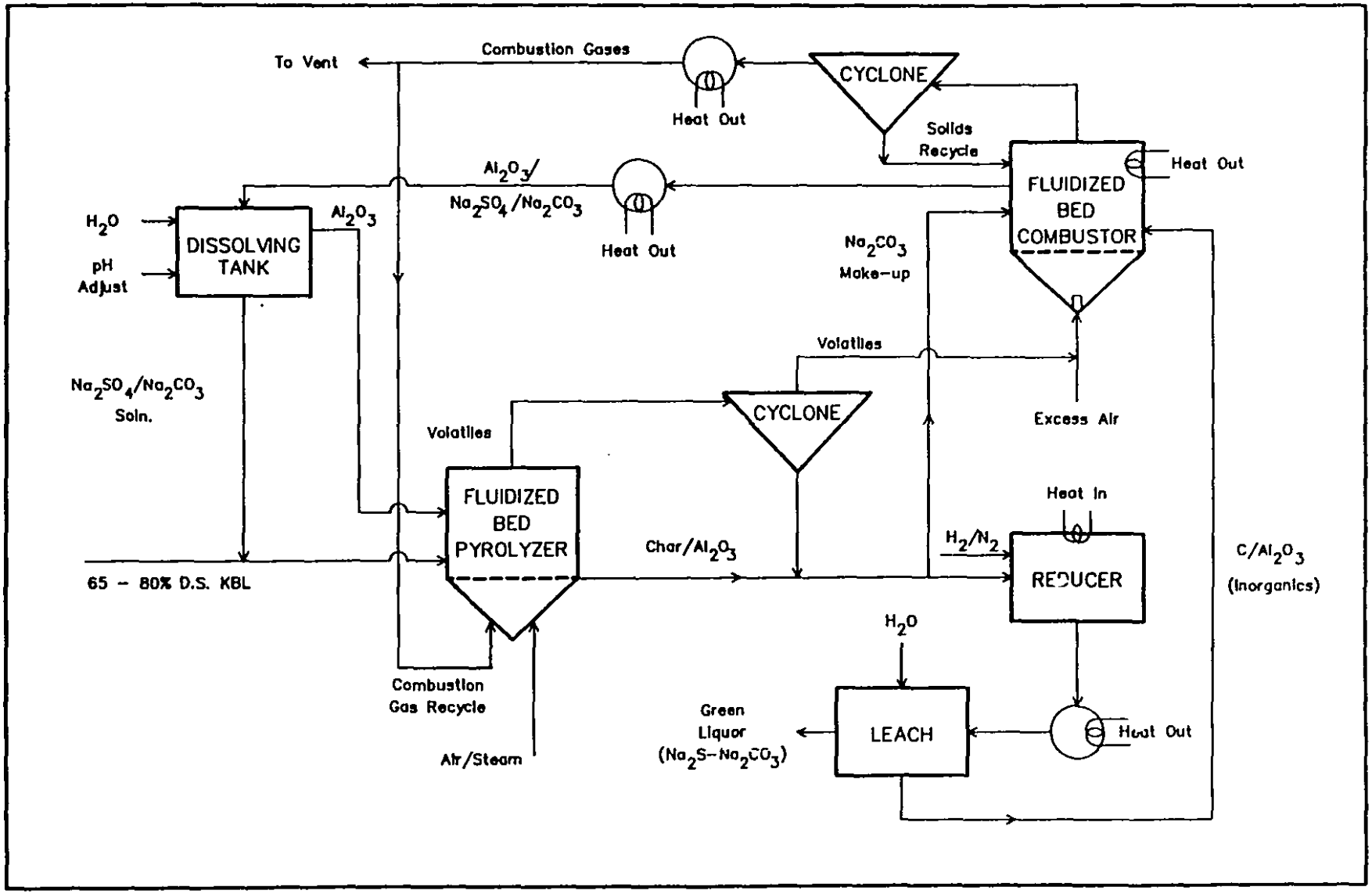
To Vent
Combustion Gases
Heat Out
CYCLONE
Solids
Recycle
FLUIDIZED
BED
COMBUSTOR
Heat Out
Al_2O_3/
Na_2SO_4/Na_2CO_3
Heat Out
H_2O
pH
Adjust
DISSOLVING
TANK
Al_2O_3
Na_2CO_3
Make-up
Volatiles
Na_2SO_4/Na_2CO_3
Soln.
CYCLONE
Excess Air
Volatiles
FLUIDIZED
BED
PYROLYZER
Heat In
H_2/N_2
REDUCER
C/Al_2O_3
(Inorganics)
Char/Al_2O_3
65 - 80% D.S. KBL
H_2O
Combustion
Gas Recycle
Green
Liquor
(Na_2S-Na_2CO_3)
LEACH
Heat Out
Air/Steam

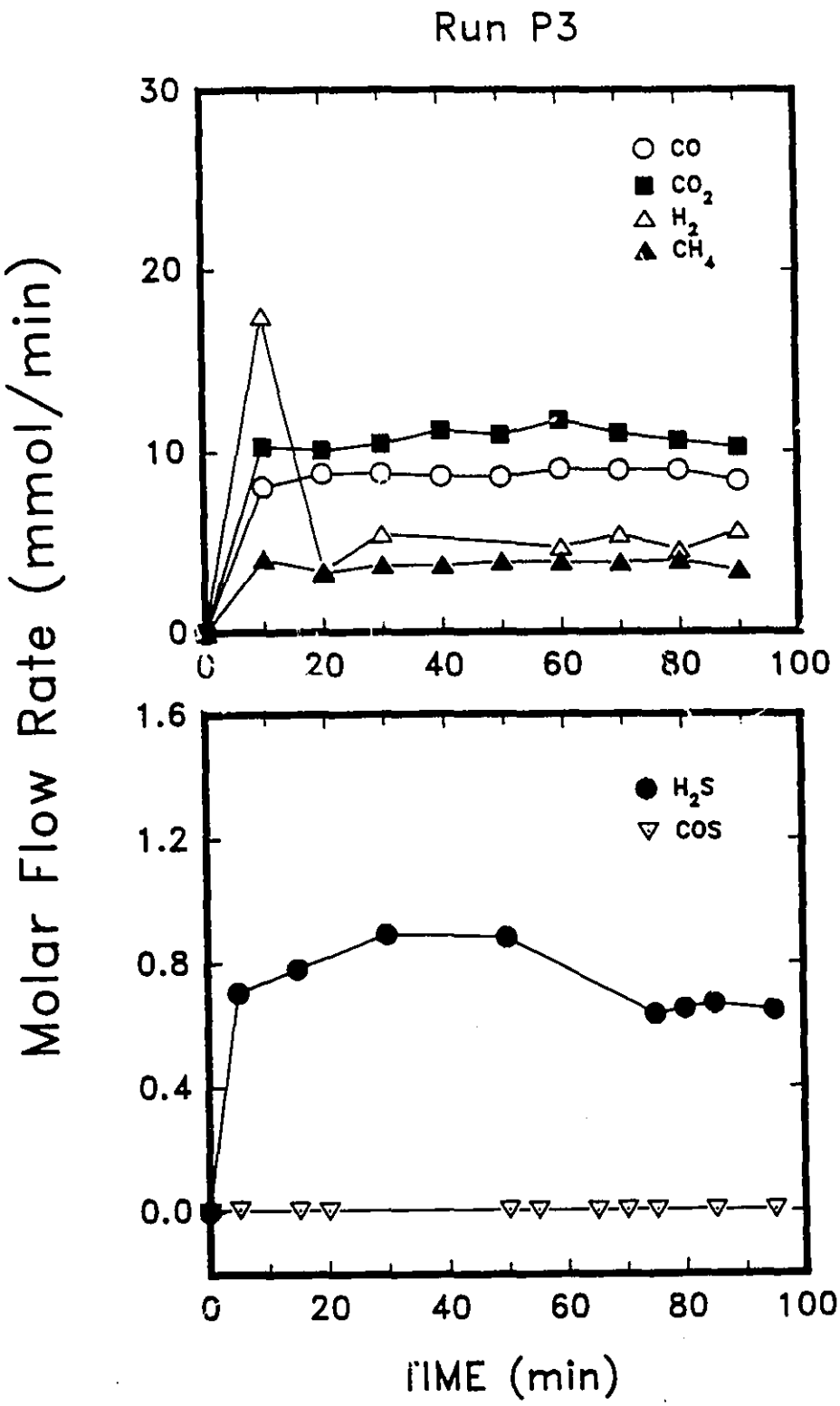

Figure 40 Time-Sampled Molar Flow Rate of Fixed and Sulphurous Gases for Pyrolysis Run P3 at 550°C.

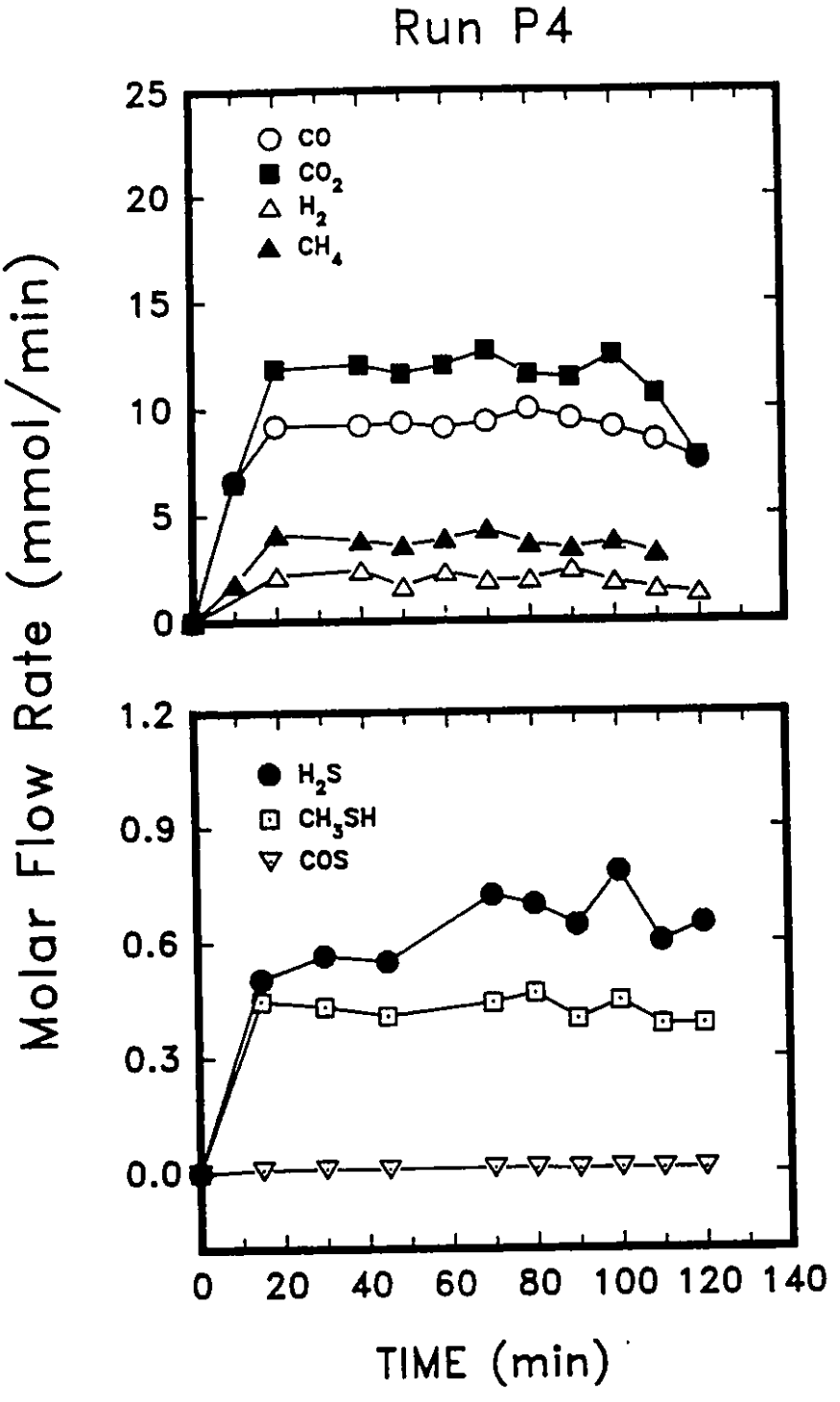

Figure 41 Time-Sampled Molar Flow Rate of Fixed and Sulphurous Gases for Pyrolysis Run P4 at 550°C.

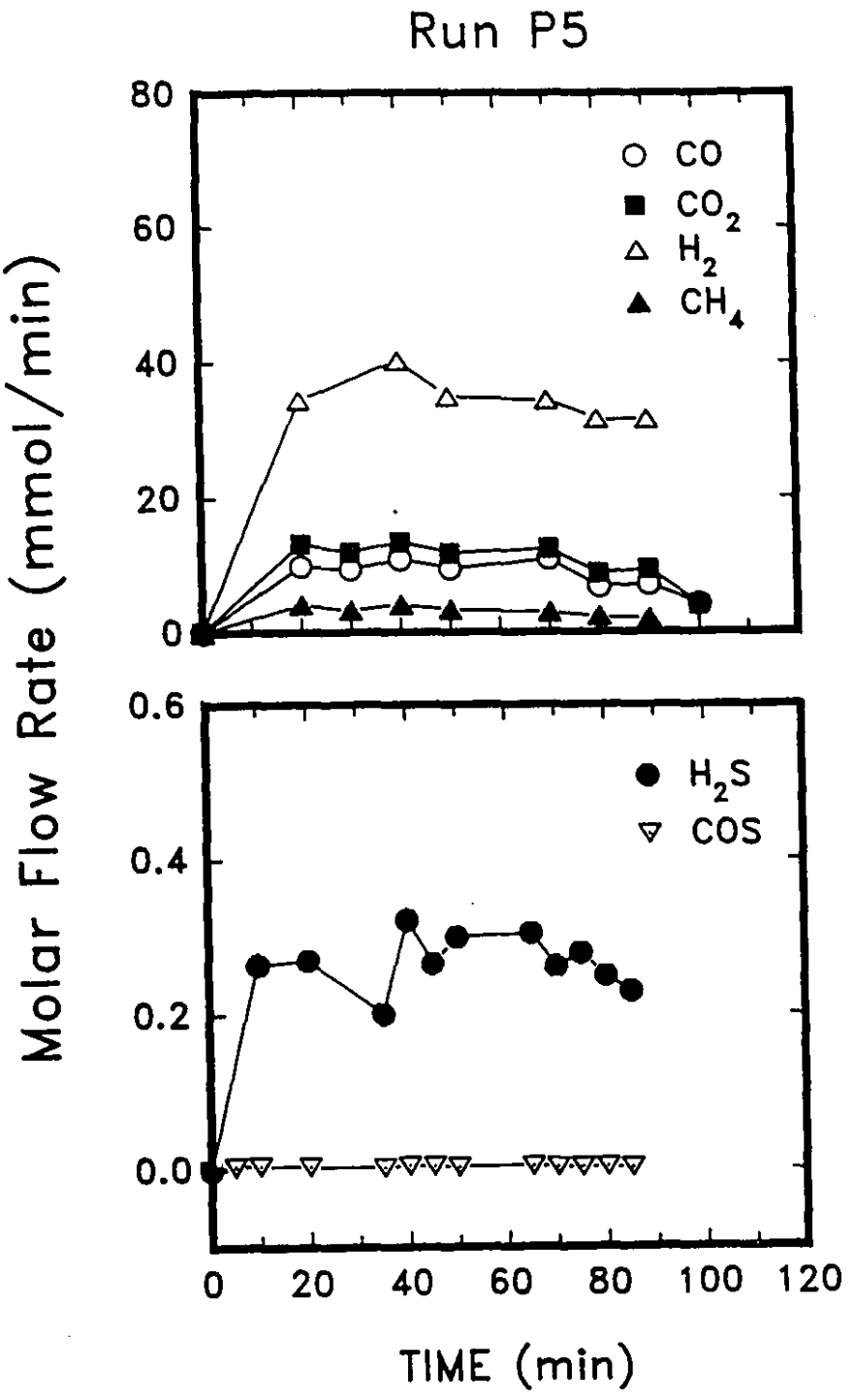

Figure 42 Time-Sampled Molar Flow Rate of Fixed and Sulphurous Gases for Pyrolysis Run P5 at 600°C.

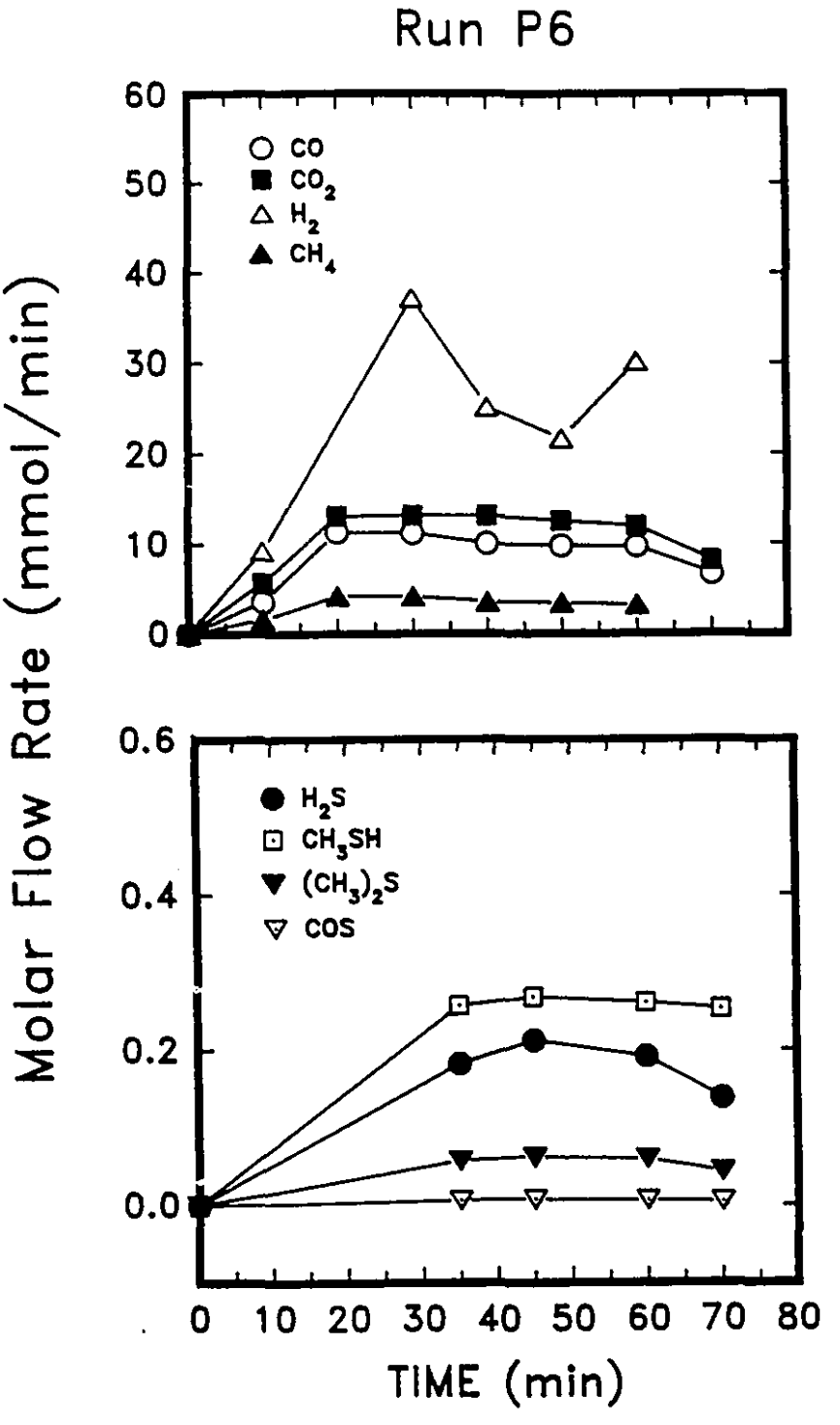

Figure 43 Time-Sampled Molar Flow Rate of Fixed and Sulphurous Gases for Pyrolysis Run P6 at 600°C.

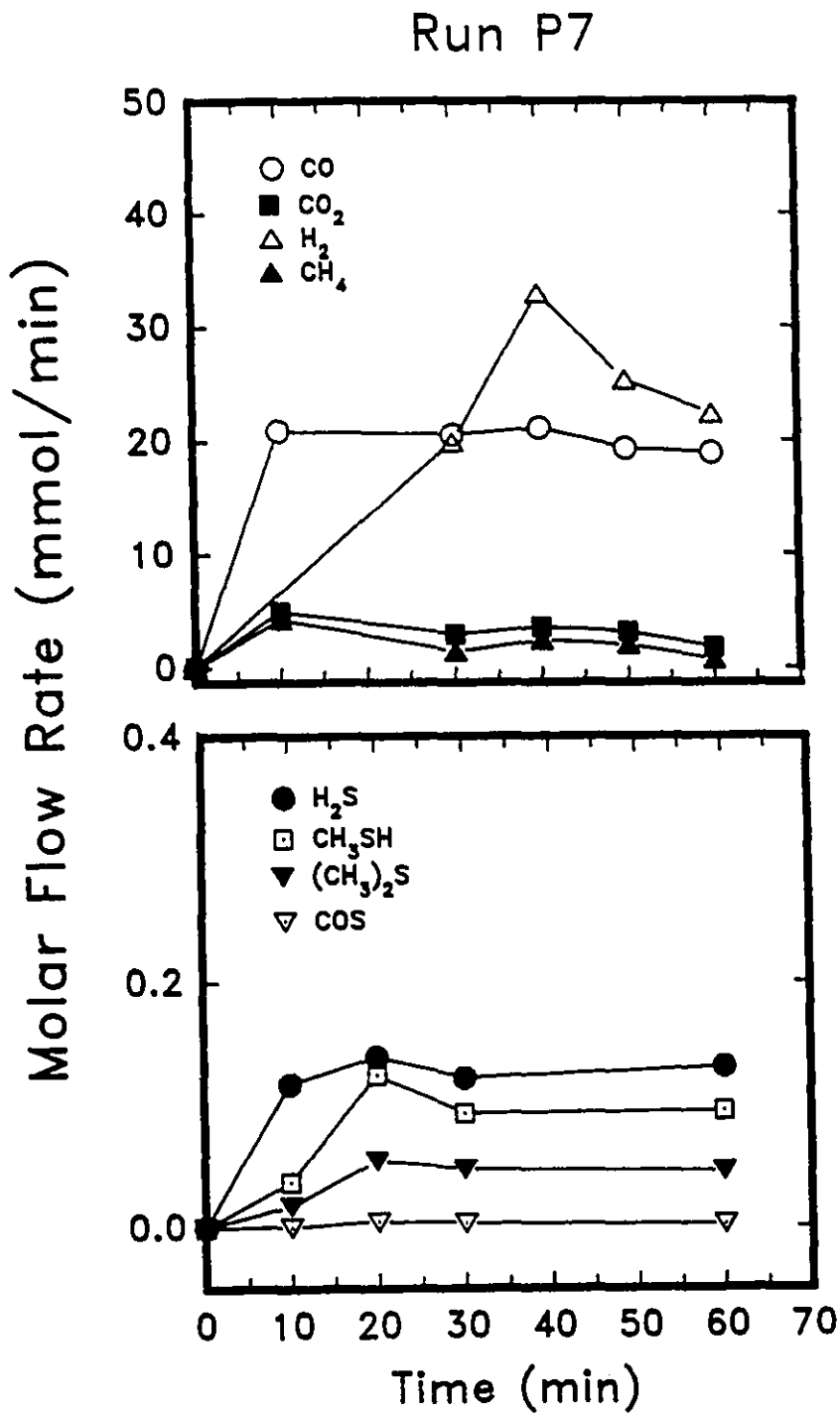

Figure 44 Time-Sampled Molar Flow Rate of Fixed and Sulphurous Gases for Pyrolysis Run P7 at 650°C.

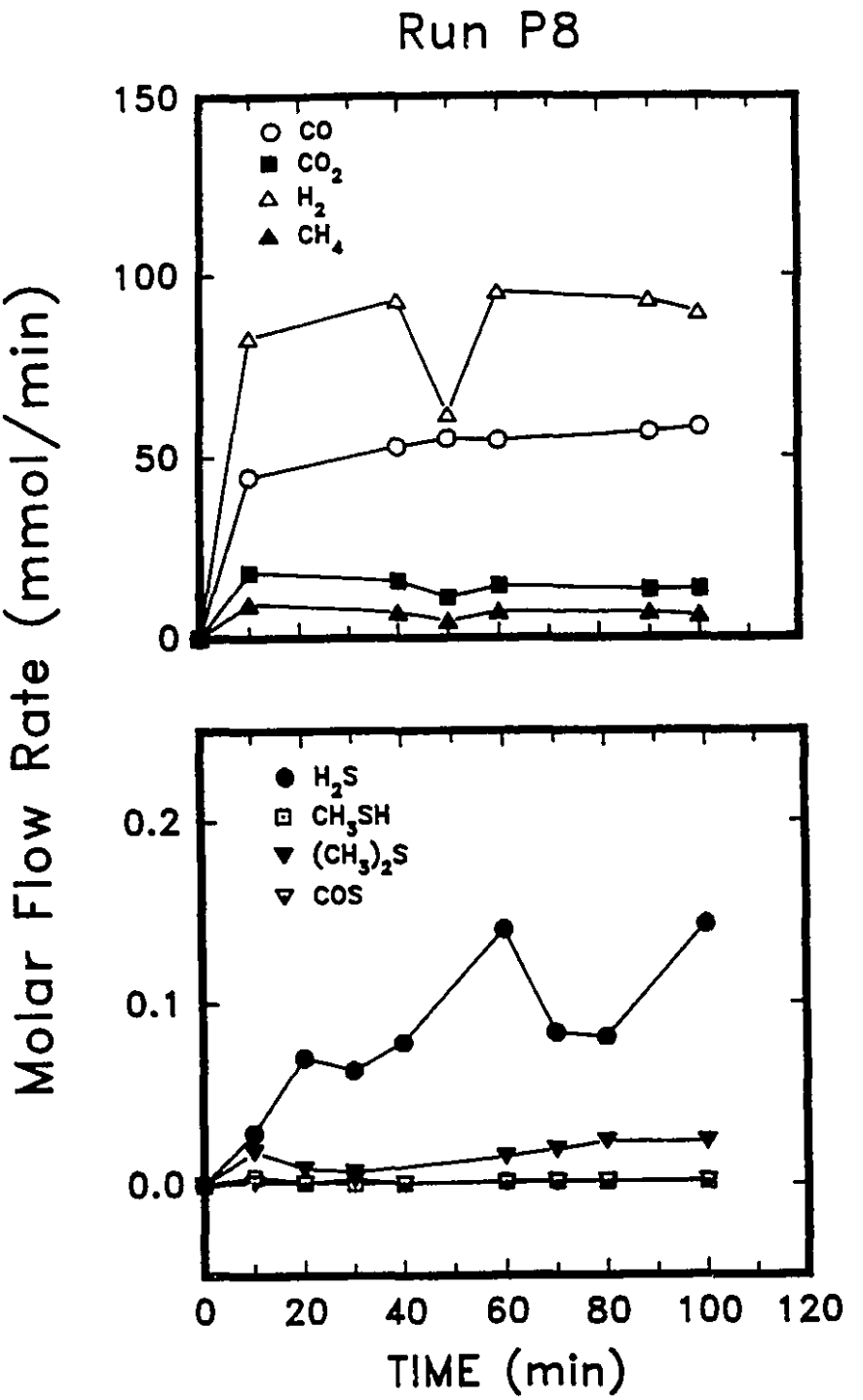

Figure 45 Time-Sampled Molar Flow Rate of Fixed and Sulphurous Gases for Pyrolysis Run P8 at 700°C.

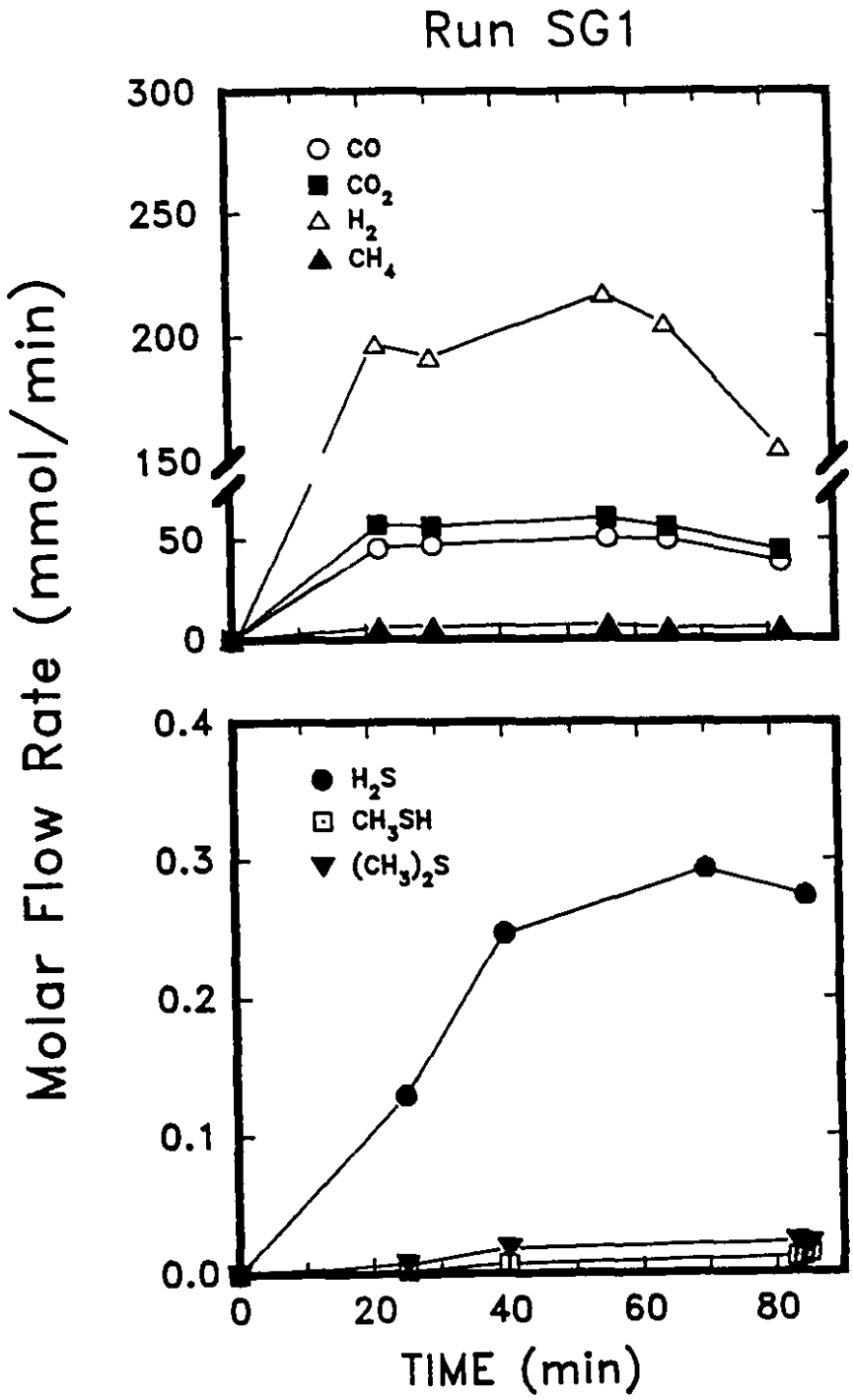

Figure 46 Time-Sampled Molar Flow Rate of Fixed and Sulphurous Gases for Steam Gasification Run SG1 at 700°C.

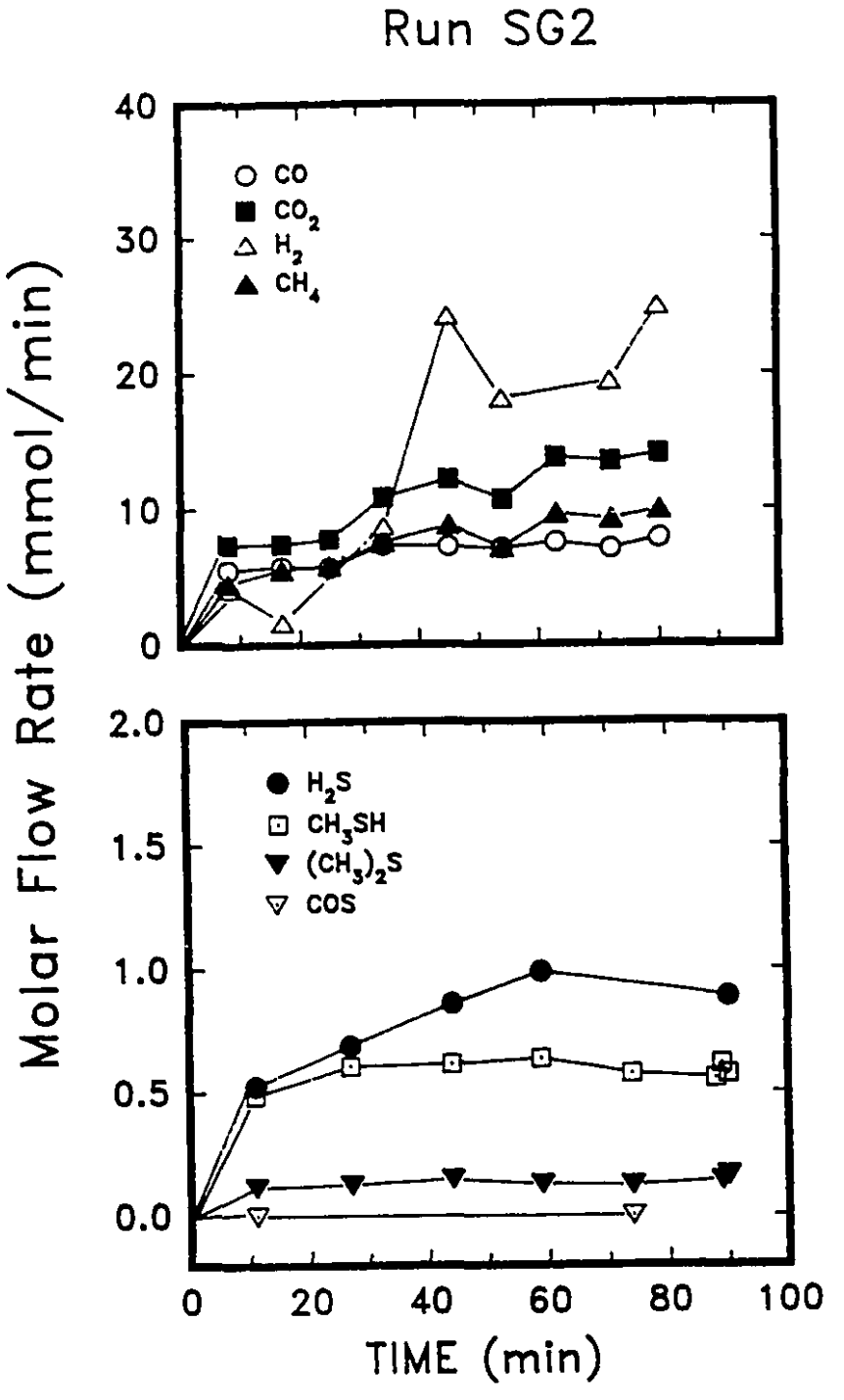

Figure 47 Time-Sampled Molar Flow Rate of Fixed and Sulphurous Gases for Steam Gasification Run SG2 at 500°C.

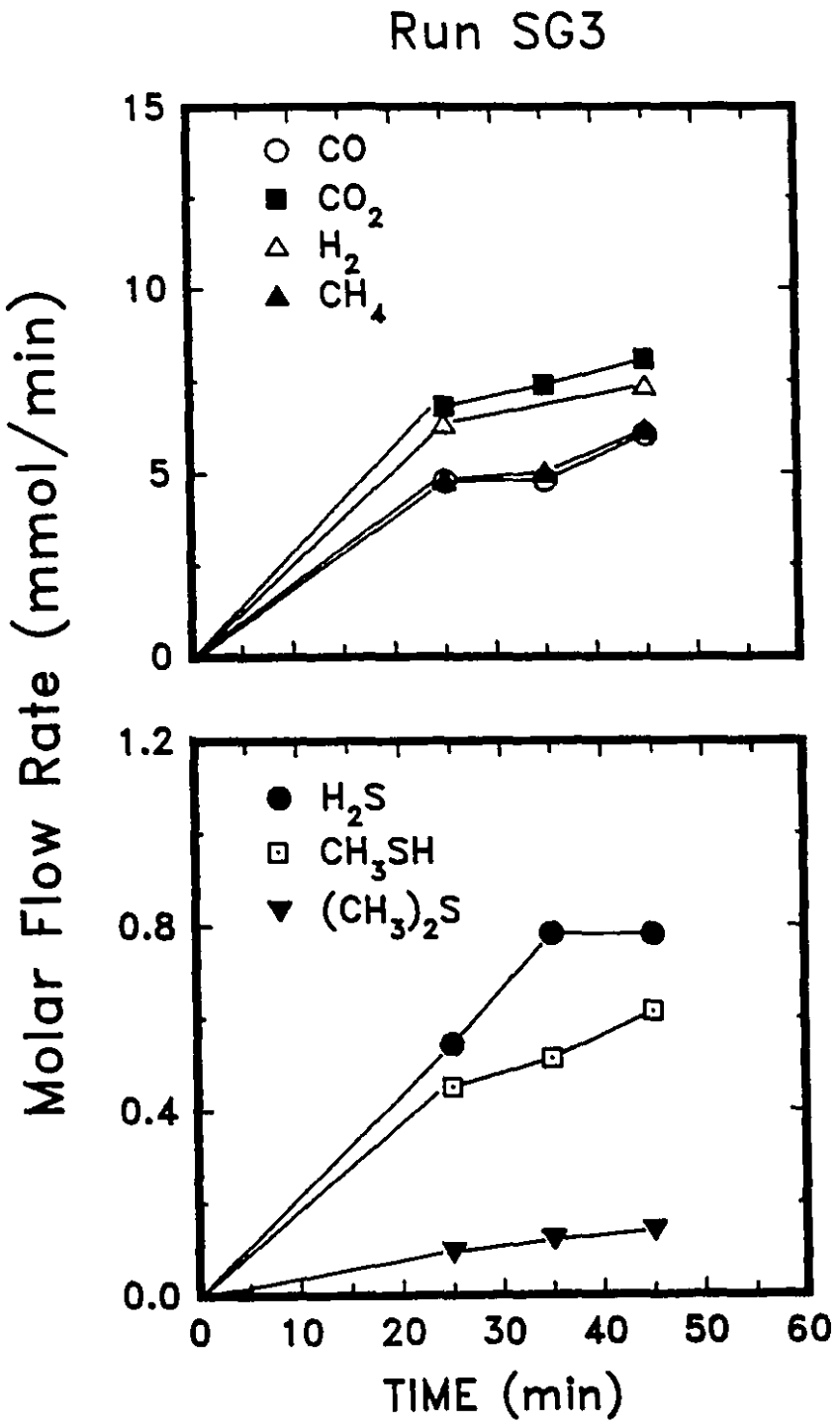

Figure 48 Time-Sampled Molar Flow Rate of Fixed and Sulphurous Gases for Steam Gasification Run SG3 at 500°C.

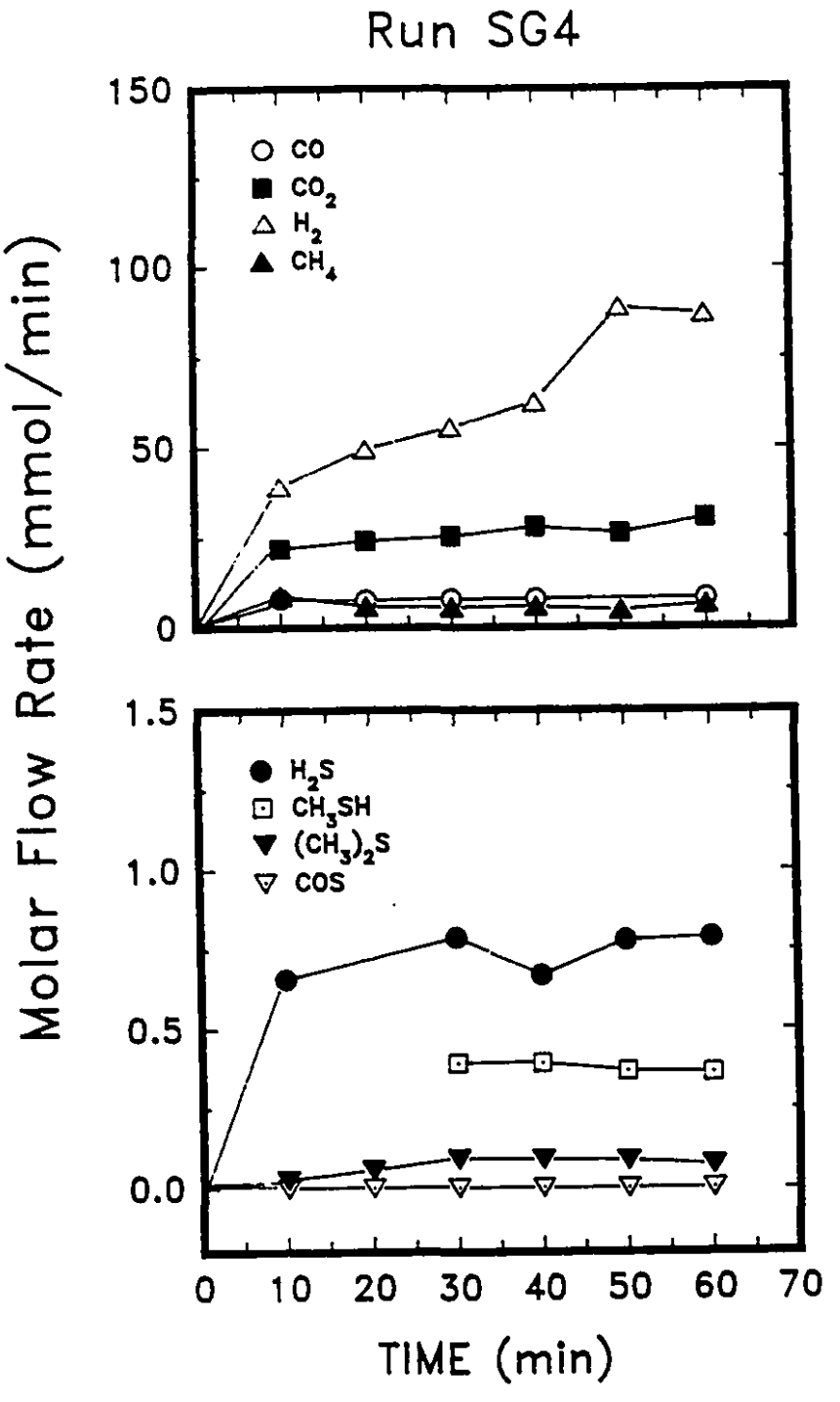

Figure 49 Time-Sampled Molar Flow Rate of Fixed and Sulphurous Gases for Steam Gasification Run SG4 at 600°C.

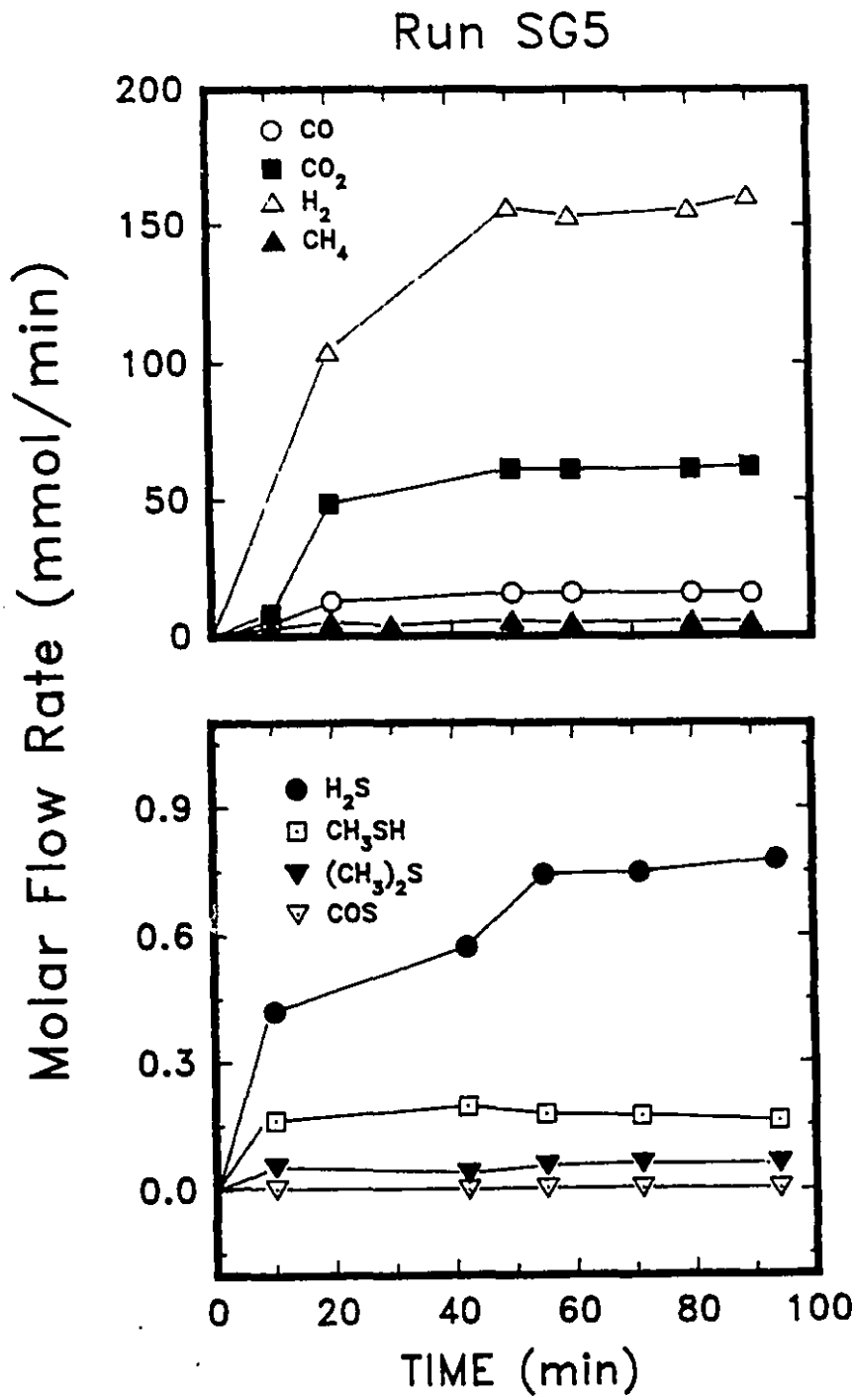

Figure 50 Time-Sampled Molar Flow Rate of Fixed and Sulphurous Gases for Steam Gasification Run SG5 at 650°C.

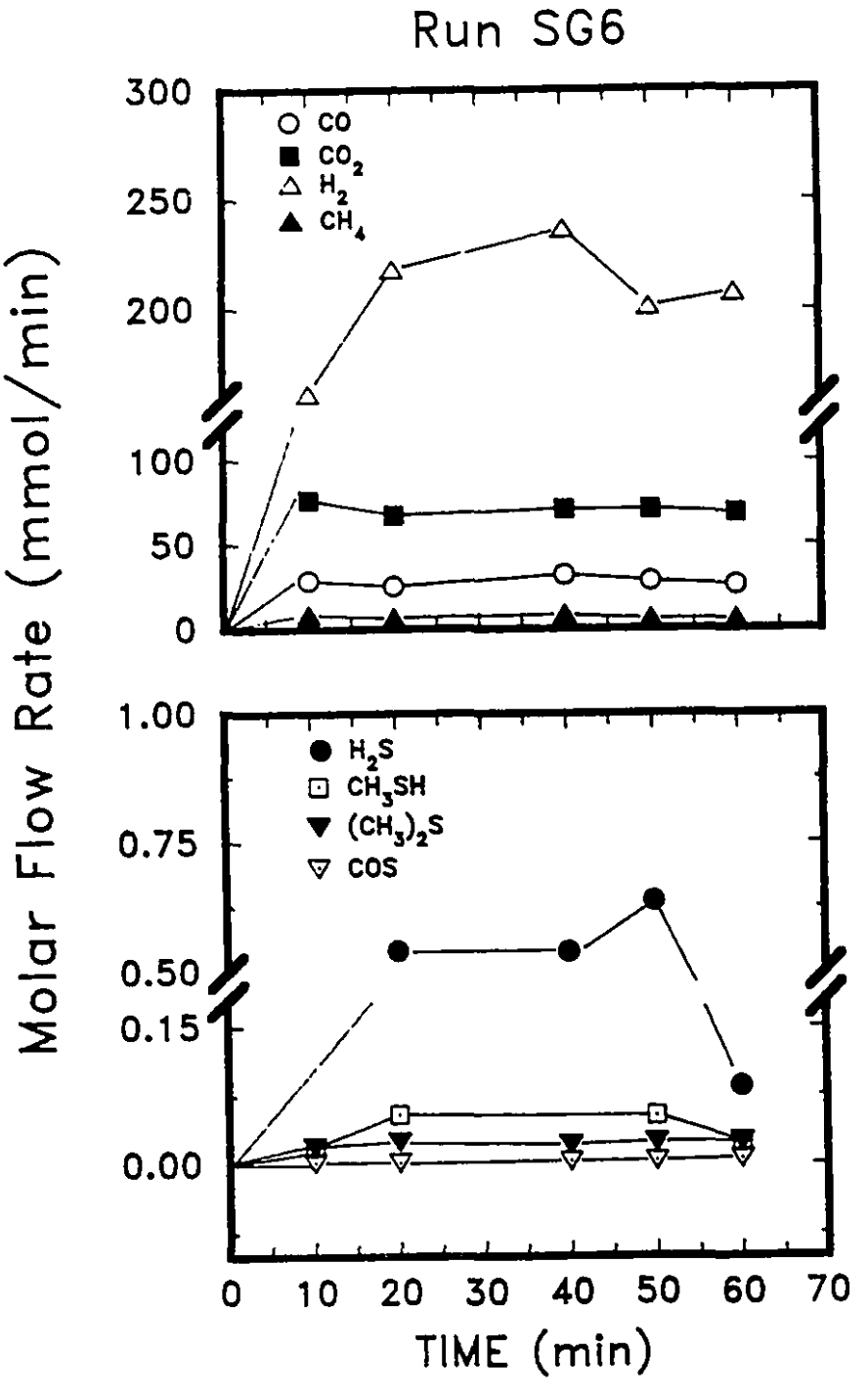

Figure 51 Time-Sampled Molar Flow Rate of Fixed and Sulphurous Gases for Steam Gasification Run SG6 at 700°C.

APPENDICES

APPENDIX A
MASS BALANCE CALCULATIONS

INTRODUCTION

The major elements in kraft black liquor solids (KBLS) which can be considered for mass balance purposes are sodium, oxygen, sulphur, carbon, and hydrogen. At the outset of the investigation it was decided to focus only on sodium, carbon,and sulphur for two reasons. First, from a process development standpoint it was critical to ascertain how the sulphur and carbon compounds behaved during pyrolysis and steam gasification. Second, adequate analytical equipment was not available to measure elemental oxygen and hydrogen in the char product. This appendix gives calculation details for the Na, S, and C mass balances, and other data reduction calculations.

OPERATING CONDITIONS

A brief explanation of the various operating data shown in Table 22 - Table 35 follows. The data recorded for the fluidized bed temperature are average values obtained from several thermocouples located at different heights in the bed. In most runs there was a slight change in the temperature of the bed at the start of feeding. However, these fluctuations dampened out after about 10 minutes.

The feed rate of distilled water into the system was obtained by noting the volume change in a graduated cylinder and dividing by the total time elapsed. Considerable commissioning work on the water pumping system showed that the on-line feed rate was reproducible to within the cited 95% confidence interval. "Bed sampling time" is intended to represent the total time elapsed from the start of KBLS feeding through to removal and quenching of the bed sample. The KBLS feed time refers to the length of time that KBLS were fed into the fluidized bed. In all runs, feeding of KBLS was stopped before a bed sample was actually removed. The amount of KBLS fed was an average value obtained by weighing the feeder before and after a run and dividing by the KBLS feed time. "Product gas flow rate" values were calculated by averaging the volume flow rate of gas passing through the dry test meter after a period of about 15 minutes from the start of KBLS feeding. A strip chart recorder was connected to an optical sensor located on the meter dial face. As the dial completed a rotation (4 L of volume) the strip chart gave an associated time interval elapsed. "Injector lance nitrogen" refers to the flow rate of pneumatic N_2 that was used to transport the KBLS into the fluidized bed via an injector lance (shown in Figure 3). The amount of char collected in the cyclones and shell-and-tube heat exchanger is referred to as "elutriated char". It was found that the amount of elutriated char varied proportionally to the injector lance N_2 flow rate. "Alumina input" refers to the amount of alumina which remained in the fluidized bed

at the end of the run. This was calculated by subtracting the initial alumina placed into the fluidized bed by the amount recovered in the cyclones.

CHAR-ALUMINA ANALYSES

Char Yield

Solid char particles form when kraft black liquor solids are subjected to a thermal treatment between 500-700°C in the fluidized bed. Between 80-90 wt% of the char can be recovered as a thin coating which covers the surface of the fluidized bed alumina particles. This mechanical mixture will be referred to as char-alumina. The rest of the char bypasses the dense phase of the fluidized bed and, from operating experience, it is seen that the majority of this elutriated material is recovered either in the cyclones or the shell-and-tube heat exchanger. The elutriated char was dried and weighed and included in the mass balance. The char particles which passed through to the water scrubber section of the plant were not analyzed. Their contribution to the overall mass balance is implicitly included in the "mass balance closure" product stream of Table 13 and Table 19.

Attempts to analyze the very fine elutriated powder for total sulphur and char content using an oxygen bomb combustion technique were unsuccessful due to explosions. Since the quantity of material was small (typically less than 5-10 wt%) compared to that found in the fluidized bed, it was decided to assign the same composition to the two product streams. Because the elutriated char spends very little time in the reaction zone it is expected that this assumption will have the following impact. The carbon content in char would be underestimated, the sodium content would not be affected, and the sulphur content may be overestimated. Overall, due to the small magnitude of these bias errors, the observed trends remain valid.

The raw data for the solid char-alumina product are presented in Table 22 - Table 35. In most runs the char-alumina product samples were taken from the reactor at the end of an experiment. In run SG1 and SG6 the fluidized bed agglomerated completely. It was therefore necessary to wait for about 10 hours for the bed to cool under a nitrogen blanket before a sample could be removed. Under these conditions it is likely that the char content measured is actually lower than at the end of the run.

From the analysis of char content in a char-alumina sample, $C_{char}^{c\text{-}a}$, it is possible to estimate the char content within the fluidized bed, $Total_{fbc}$, by the following equation:

$$Total_{fbc} = \frac{C_{char}^{c\text{-}a}}{100 - C_{char}^{c\text{-}a}} \times Alumina\ Input \qquad (108)$$

The total amount of char produced, $Total_{char}$, could then be calculated:

$$Total_{char} = Total_{fbc} + Elutriated\ Char \tag{109}$$

It is important to note that most of the elutriated char was in the form of pure, fine powder- without associated alumina. For this reason the weights of elutriated char could be added directly to $Total_{fbc}$. Lastly, the total yield of char produced during a run, Y_{char}, can be calculated by:

$$Y_{char} = \frac{Total_{char}}{Total\ Dry\ KBLS\ Fed} \times 100 \tag{110}$$

Results of the above calculations for all the experiments are shown in Table 36.

Sodium, Total Sulphur, and Total Carbon in the Char

Equations 111-113 are used to calculate the weight percent of sodium, sulphur and carbon in KBLS which reports to the char, $D^{Na,\,KBLS}_{Na,\,char}$, $D^{S,\,KBLS}_{S,\,char}$, $D^{C,\,KBLS}_{C,\,char}$, respectively:

$$D^{Na,KBLS}_{Na,char} = C^{char}_{Na} \cdot Y_{char} \cdot \frac{1}{C^{KBLS}_{Na}} \tag{111}$$

$$D^{S,KBLS}_{S,char} = C^{char}_{S} \cdot Y_{char} \cdot \frac{1}{C^{KBLS}_{S}} \tag{112}$$

$$D^{C,KBLS}_{C,char} = C^{char}_{C} \cdot Y_{char} \cdot \frac{1}{C^{KBLS}_{C}} \tag{113}$$

where

C^{char}_{Na}, C^{char}_{S}, C^{char}_{C} = weight percent of sodium, total sulphur, and total carbon in the char (Table 22 - Table 35)

C^{KBLS}_{Na}, C^{KBLS}_{S}, C^{KBLS}_{C} = weight percent of sodium, total sulphur, and total carbon in the kraft black liquor solids feed (Table 10)

Table 37 presents a summary of the experimental results. In some experiments the data are incomplete, therefore a brief explanation will be given. Run SG6 does not contain a value for $D^{S,\,KBLS}_{S,\,char}$, since fluidized bed agglomeration prevented sampling immediately after the run. Instead, the bed was allowed to cool over a 10 hour period in a flow of N_2. The sodium sulphide in the char would react with any trace amount of water vapour and CO_2 in the nitrogen during cooling, therefore the sulphur data are not considered accurate. The sodium data are not expected to vary significantly.

The data for the elements sodium, sulphur and carbon in the char shown in Table 37 are also contained in Table 13 and Table 19, as part of the total mass balance. The data for carbon in runs SG1 and SG6 show two different quantities. Since these runs resulted in fluidized bed agglomeration, it was not possible to take a char-alumina sample immediately after the end of an experiment. Instead, the sample was taken about 10 hours later. For this reason, the actual data for carbon may be too low since some carbon volatilization occurred. The bracketed values represent estimates of the true char content

at the end of the run. These values for char carbon are calculated by performing a mass balance as shown in Table 13. The mass balance closure stream was assigned the same value as steam gasification run SG5 (i.e., 9 ±3 g C/ 100 g C in KBLS). The amount of carbon reporting to the gas was taken as the sum of $D_{C,i}^{C,KBLS}$, for i= CO, CO_2, and CH_4 in Table 40 - Table 43. The estimated amount of carbon in char was then found by difference.

Organic Carbon in the Char

In kraft black liquor solids over 90 wt% of the carbon is bound as organic carbon in lignin and hydroxy acids. The remainder is present mostly as inorganic carbonate. During pyrolysis some of the carbon will be removed as condensables and gases, leaving a solid char mass containing amorphous organic carbon and inorganic carbonate salts.

The chemical analyses performed include: (a) total carbon content of char (C_C^{char}) and KBLS (C_C^{KBLS}); (b) the inorganic carbonate fraction of char ($C_{CO_3^{2-}}^{char}$) and KBLS ($C_{CO_3^{2-}}^{KBLS}$). Table 22 - Table 35 give the values of C_C^{char} and $C_{CO_3^{2-}}^{char}$ for the experiments. Table 10 gives values of 6.66 ±0.33 wt% and 37.65 ±1.95 wt% for $C_{CO_3^{2-}}^{KBLS}$ and C_C^{KBLS}, respectively.

Equations 114-115 are used to calculate the organic carbon content of both the kraft black liquor solids, C_{OC}^{KBLS}, and the char, C_{OC}^{char} , as follows;

$$C_{OC}^{KBLS} = C_C^{KBLS} - \left(\frac{12}{60} \cdot C_{CO_3^{2-}}^{KBLS}\right) \tag{114}$$

$$C_{OC}^{char} = C_C^{char} - \left(\frac{12}{60} \cdot C_{CO_3^{2-}}^{char}\right) \tag{115}$$

The amount of organic carbon in the char as a percent of total input carbon, $D_{OC,char}^{C,KBLS}$, and organic carbon in the feed KBLS, $D_{OC,char}^{OC,KBLS}$, can now be obtained from Eqs. 116-117. Table 38 shows the results of these calculations.

$$D_{OC,char}^{C,KBLS} = C_{OC}^{char} \cdot Y_{char} \cdot \frac{1}{C_C^{KBLS}} \tag{116}$$

$$D_{OC,char}^{OC,KBLS} = C_{OC}^{char} \cdot Y_{char} \frac{1}{C_{OC}^{KBLS}} \tag{117}$$

In Table 18 the estimated amount of organic carbon in char, C_{OC}^{char} , is shown to be 12.8 ±5.5 wt% for SG1 and 19.0 ±2.4 wt% for SG6. A sample calculation for SG6 follows. The total wt% of carbon in char,

C_C^{char} , is calculated using the estimated value for $D_{C,char}^{C,KBLS}$ in Table 37, the carbon content of KBLS, C_C^{KBLS} , and the total yield of char, Y_{char} , as follows:

$$C_C^{char} = D_{C,char}^{C,KBLS} \cdot C_C^{KBLS} \cdot \frac{1}{Y_{char}} \tag{118}$$

$$= (34.1 \pm 5.5)(37.65 \pm 1.95) / (45.1 \pm 4.7)$$

$$= 28.5 \pm 5.6 \text{ g C/ 100 g char}$$

To obtain the organic portion of the total carbon in char, C_{OC}^{char} , it is necessary to subtract the amount of carbon as CO_3^{2-} (Table 35),

$$C_{OC}^{char} = (28.5 \pm 5.6) - (12/60)\{47.5 \pm 1.7\}$$

$$= 19.0 \pm 2.4 \text{ g organic C / 100 g char}$$

This value is inserted into Eqs. 116, 117 in order to estimate $D_{OC,char}^{C,KBLS}$, $D_{OC,char}^{OC,KBLS}$ which are shown in Table 38 as the bracketed terms. Furthermore, in Figure 24, the estimated value for $D_{OC,char}^{OC,KBLS}$ is plotted as the organic carbon yield at 700°C.

Organic-bound Oxygen in the Char

In order to estimate the amount of organic-bound oxygen present in char, an oxygen balance was performed for run P8. A direct measurement could not be made for char since alumina would strongly interfere with this analysis. The calculations were based on data from Table 29, Table 36, Table 40, and Table 41 for the char and gases, as well as pyrolysis water data (20 g H_2O/ 100 g KBLS) from Feuerstein (1966). It was assumed that oxygen in char was mostly in the form CO_3^{2-} and that CO and CO_2 represented the majority of oxygen in the gas phase. The following balance was found: 35 wt% as CO_3^{2-} in the char, 5 wt% in the gases, 50 wt% as pyrolysis water, and 10 wt% unaccounted. In the KBLS, about 20 wt% of the oxygen is bound as the inorganic species CO_3^{2-}, SO_4^{2-}, $S_2O_3^{2-}$, and OH^-; and, 80 wt% is associated with the organic hydrocarbon matrix. It would be reasonable to assume that at least some of the 10 wt% unaccounted O is still associated with the organic fraction of char. Experimental data on the oxygen content of char for similar temperatures by Li (1989) showed that 7 wt% was organic-bound oxygen, which is in the range calculated for our work. At the high end of the estimate, this would represent about 25 mmol O per g carbon and a molar ratio of sodium to organic oxygen, $Na:O_{org}$, of ~1.3.

Sulphur Species in the Char

The total sulphur content in kraft black liquor solids, C_S^{KBLS}, was 1.67 ±0.05 wt%. About 80 wt% of this amount is inorganic sulphur (S^{2-}, SO_4^{2-}, SO_3^{2-} and $S_2O_3^{2-}$) and the remainder is organic. During

pyrolysis and gasification the sulphur is distributed mostly in the char and gas phases with the remainder reporting as condensables. Equations 119-122 are used to calculate the weight percent of total sulphur present in KBLS which reports as sulphur in species i in the char, $D_{S,i}^{S,KBLS}$. Table 39 gives the calculated results for the experiments. These results are also plotted in Figure 27 - Figure 29.

$$D_{S,SO_4^{2-}}^{S,KBLS} = C_{SO_4^{2-}}^{char} \cdot Y_{char} \cdot \frac{1}{C_S^{KBLS}} \cdot \frac{32}{96} \tag{119}$$

$$D_{S,SO_3^{2-}}^{S,KBLS} = C_{SO_3^{2-}}^{char} \cdot Y_{char} \cdot \frac{1}{C_S^{KBLS}} \cdot \frac{32}{80} \tag{120}$$

$$D_{S,S_2O_3^{2-}}^{S,KBLS} = C_{S_2O_3^{2-}}^{char} \cdot Y_{char} \cdot \frac{1}{C_S^{KBLS}} \cdot \frac{64}{112} \tag{121}$$

$$D_{S,S^{2-}}^{S,KBLS} = C_{S^{2-}}^{char} \cdot Y_{char} \cdot \frac{1}{C_S^{KBLS}} \tag{122}$$

where $C_{SO_4^{2-}}^{char}$, $C_{SO_3^{2-}}^{char}$, $C_{S_2O_3^{2-}}^{char}$, $C_{S^{2-}}^{char}$ = weight percent of sulphate, sulphite, thiosulphate and sulphide in the char, respectively (Table 22 - Table 35).

A useful measure of recovery boiler performance used in the pulp and paper industry is the so-called reduction efficiency. This is defined as the ratio of sodium sulphide weight in the char to the weight of all sodium-sulphur inorganics in the char. The following equation can be used to estimate this quantity:

$$\textit{Reduction Efficiency} = \frac{C_{Na_2S}^{char}}{C_{Na_2S}^{char} + C_{Na_2SO_4}^{char} + C_{Na_2SO_3}^{char}} \cdot 100 \tag{123}$$

The individual terms in the ratio can be evaluated by Eqs. 124-127 wherein the second term is simply the amount of sodium bound with the various sulphur anions:

$$C_{Na_2S}^{char} = C_{S^{2-}}^{char} + (C_{S^{2-}}^{char} \cdot \frac{1}{32} \cdot 2 \cdot 22.98) \tag{124}$$

$$C_{Na_2SO_4}^{char} = C_{SO_4^{2-}}^{char} + (C_{SO_4^{2-}}^{char} \cdot \frac{1}{96} \cdot 2 \cdot 22.98) \tag{125}$$

$$C_{Na_2SO_3}^{char} = C_{SO_3^{2-}}^{char} + (C_{SO_3^{2-}}^{char} \cdot \frac{1}{80} \cdot 2 \cdot 22.98) \tag{126}$$

In some experiments, sodium thiosulphate was also measured. As mentioned in Chapter 5, this is the result of sodium sulphide oxidation during analysis. Therefore, the amount of sodium sulphide in Eq. 123 is adjusted to include the amount owing to oxidation. Given the sodium thiosulphate content as,

$$C_{Na_2S_2O_3}^{char} = C_{S_2O_3^{2-}}^{char} + (C_{S_2O_3^{2-}}^{char} \cdot \frac{1}{112} \cdot 2 \cdot 22.98) \tag{127}$$

then the additional amount of sodium sulphide owing to oxidation would be $C_{Na_2S_2O_3}^{char} \cdot 2 \cdot (78/158)$.

One of the important variables which affects the reduction efficiency is the residence time of char in the fluidized bed. Due to continuous feeding of solids into the reactor, those particles which were injected at the beginning of the run will have a longer residence time than those at the end of the run. However, since the mass feed rate of KBLS is constant, it is possible to assign a mean residence time, t_{med}, to the entire char mass. Also, an additional amount of time was spent by the entire char mass between the cessation of feeding and sampling of the bed, hence the mean residence time is calculated as,

$$\begin{matrix}\text{Mean} \\ \text{Residence Time}\end{matrix} = \left\{\frac{\text{KBLS feed time}}{2}\right\} + \left\{\begin{matrix}\text{additional time} \\ \text{needed for sampling}\end{matrix}\right\} \qquad (128)$$

The information required for this calculation can be found in Table 22 - Table 35. The second term in the equation is found by subtracting the "Bed Sampling Time" by "KBLS Feed Time".

FIXED GASES

Gas samples were taken periodically throughout an experiment and the results are plotted in Figure 40 - Figure 51. The scatter in the data can be explained by difficulties encountered using the sampling method. The most recurring problem was that of gas leakage from the syringes. A second source of error was due to the condensables or particles present in the gas stream which entered the syringe. In either case, the corresponding gas analysis was always found to be too low compared to other gas samples.

In the discussion which follows the average molar flow rate, F_i^{ave}, and average carbon yield, $D_{C,i}^{C,KBLS}$, refer to a period of time during a run where the time-sampled gas analysis was relatively constant over time. In practice, this means that the average gas composition consists of a minimum of 3 data points covering a period of 30 minutes prior to shut down. Due to the small feed rate of solids and steam to the system compared to the flow of fluidizing nitrogen gas, any continuous increase in concentration of gases was probably masked by the experimental errors of the sampling technique.

In order to close the carbon balance it is essential to know how much carbon reported to the gas phase. Since the amounts of fixed gases are typically about 10-50 times higher than the sulphur compounds, the latter were ignored in the carbon balance calculations.

Table 40 - Table 43 summarize the following data for the fixed gas, *i*: the average molar gas yield, Y_i^{ave} ; the average carbon yield, $D_{C,i}^{C,KBLS}$. Equations 129 and 130 show the calculations used to determine the average molar gas yield and carbon yield.

$$Y_i^{ave} = \frac{F_i^{ave}}{F_{KBLS}} \cdot 60 \tag{129}$$

$$D_{C,i}^{C,KBLS} = \left\{ \frac{Y_i^{ave} \cdot M_C}{C_C^{KBLS} \cdot 1000} \right\} \cdot 100 \tag{130}$$

where

F_i^{ave} = average molar flow rate of i (mol i·min^{-1})
F_{KBLS} = feed rate of dry KBLS (kg·h^{-1})
M_C = atomic weight of carbon (12 g·mol^{-1})
C_C^{KBLS} = carbon content of KBLS (0.3765 ±0.0195 kg C·kg KBLS^{-1})

The values of $D_{C,i}^{C,KBLS}$ for CO, CO_2 and CH_4 are added together and shown in Table 19 as the total carbon content in the gas stream.

Equations 131 and 132 show the corresponding calculation for H_2 gas in the case of pyrolysis and steam gasification, respectively. The reason for the separate equations is that the hydrogen yield in steam gasification should be compared to the total hydrogen input to the reactor; namely, from the KBLS and steam. The hydrogen yield data for each experiment are given in Table 42.

$$D_{H,H_2}^{H,INPUT} = \left\{ \frac{Y_{H_2}^{ave} \cdot M_{H_2}}{C_H^{KBLS} \cdot 1000} \right\} \cdot 100 \tag{131}$$

$$D_{H,H_2}^{H,INPUT} = \frac{Y_{H_2}^{ave} \cdot M_{H_2}}{\left(\frac{F_{KBLS}}{60} \cdot C_H^{KBLS} \cdot 1000\right) + \left(F_{H_2O} \cdot \rho_{H_2O} \cdot \frac{2}{18}\right)} \cdot 100 \tag{132}$$

where

M_{H_2} = molecular weight of hydrogen gas (2 g H·mol^{-1} H_2)
C_H^{KBLS} = wt% of elemental H in KBLS (0.0344±0.0007 kg H· kg KBLS^{-1})
F_{H_2O} = feed rate of H_2O (mL·min^{-1})
ρ_{H_2O} = density of H_2O @ 25°C (1 g·mL^{-1})

SULPHUR GASES

The calculations performed for the sulphur gases follow the same reasoning as shown for the case of the fixed gases and will therefore not be discussed further. Figure 40 - Figure 51 give the time-sampled molar flow rate of sulphurous gases for pyrolysis and steam gasification runs. Table 44 - Table 47 summarize the following data for the sulphur-bearing gas, *i*: the average molar gas yield, Y_i^{ave}; and the average sulphur yield, $D_{S,i}^{S,KBLS}$.

It is noted that runs P3 and P5 do not present data for CH_3SH and $(CH_3)_2S$. The reason for this is that an isothermal gas chromatographic technique was employed. Compared to the temperature programmed method used for all other runs, this method could only resolve the H_2S and COS peaks. The method was used because column contamination led to problems of peak resolution using temperature programming. In Table 19 the total amount of sulphur contained in the gases for each run can be obtained by the summation of $D_{5,i}^{5,KBLS}$ for H_2S, CH_3SH, $(CH_3)_2S$ and COS.

APPENDIX B

SPECIFICATIONS, SUPPLIERS OF MAJOR EQUIPMENT AND MATERIALS

Since much of the material used in this work was based on English units, these are included for completeness where appropriate.

EQUIPMENT	SUPPLIER	SPECIFICATIONS
Pilot Plant Equipment		
Dry Test Meter	Canadian Meter Corp. 3860 Notre Dame Chomedey, Que.	- 200 L/min max. capacity - Model DTM-325-5 Singer Co.
CO Monitors	MSA Canada 1360 Begin St. Laurent, Que.	- Mini CO Model IV, (0-100 ppm) - Toxgard Indicator, Model C #206798
Gate Valves	Crane Supply 4805 Dunn Ave Montreal, Que.	- 1.9 cm (3/4 in) NPT ends, rated for 400°C and 65 psi, Type 304 XU carbon steel
Fluidized-Bed Reactor/ Distributor Gasket	John Crane 3475 Pitfield Montreal, Que.	- 10.80 cm (4.25 in) ID x 12.7 cm (5 in) OD x 1.59 mm (1/16 in) thick Grafoil
PI Controllers	Barber Coleman 580 Meloche Dorval, Que.	- Model 558A-04544-010-0-00 - SCR controllers Model 313-121-47. - 20 A + 204 V, single-phase
Fluidized-Bed Reactor Shell	NGP Steel Erectors 8110 Lafrenaie St. Leonard	- 316 Stainless Steel. Details included in thesis.
Digital Temperature Indicators	Thermoelectric 3005 De Baene Montreal	- (-60-1350°C) ±1°C type K Model 31670-00-012 - (-80-600°C) ±1°C type J Model 31670-00-011
Ball Valves for Underflow and Cyclones	Romatec 635 Henri Bourassa Montreal, Que.	- 1.9 cm (3/4 in) NPT 316 SS ball valve, rated @ 250°C and 100 psi, Model #74-104-01
Caustic Solution Recirculation Pumps	Snowdon Electric Motors 5160 Namur Montreal, Que.	- Little Giant high pressure pump, rated 241.3 kPa (35 psig), Model 35-OM
Process Piping	Firth Brown Steel 4300 Cote de Liesse Montreal, Que.	- 316 SS seamless tubing, wall thickness = 0.89 mm (0.035 in) for all. OD = 4.76 mm (3/16 in), 9.53 mm (3/8 in), 15.88 mm (5/8 in), 19.05 mm (3/4 in), 2.54 cm (1 in)
Screw Feeder Reducer Gear Box	Beel Controls 2650 Pitfield Blvd. St. Laurent, Que.	- 15:1 reduction ratio, Model SUQ-155-TL (45.19 N•m torque)
Screw Feeder DC Motor	" "	- 249 W (1/3 HP) Baldor Motor

EQUIPMENT	SUPPLIER	SPECIFICATIONS
DC Motor Controller	" "	- 10-turn potentiometer, open-loop controller Model SB-600-11
Screw Feeder Auger and Overwrap	Dentech 2075 Cabot Montreal, Que.	- See thesis Chapter 3 for details
Fluidized-Bed Flange Gaskets	MSS Inc 299 Benjamin Hudon Montreal, Que.	- 5" ID x 5 7/8" OD x 1/8" thick Graflock Gaskets (rated to 900°C)
Thermocouples/ Extension Wire	Thermo Electric 3005 de Baene Montreal	- 1/16" x 12" Type K - 1/8" x 12" Type K - 16 gauge wire ext tex/tex Type K - 1/16" x 6" Type J - 20 gauge Type J, extension PVC stranded
Laboratory Air Purification	Furneco 4520 de la Roche Montreal, Que.	- Type 92A filter DX - Type 92A filter BX - 1 Silica Gel absorber Type 62A - 1 Pressure regulator 2 - 150 psi, model 10163 Balston Inc.
N_2 Gas Cylinder Manifold	Matheson P.O. Box 893 530 Watson Street Whilby, Ont.	- Single-row brass manifold, 3-cylinder station with 2-stage pressure regulator, C.G.A. 580 connector
N_2 Fluidizing Gas	Cryo-Gaz 2205 Guenette St. Laurent, Que.	- Size H, Industrial grade N_2 cylinders - 99.99% N_2 minimum purity 20 ppm O_2 max., 80 ppm Ar max., 5 ppm moisture max.
Insulation	Reintjes Construction 1710 St. Regis Dorval, Que.	- 2.54 cm thick Kaowool (max. 1450°C)
Preheaters/ Windbox/ Cyclone Controllers	Thermo Electric	- 0-600°C ON-OFF control with offset, Model 100
Variable Autotransformer	Superior Electric Co Bristol, Conn U.S.A.	- 204 VAC, 15 A
N_2 Rotameter	Emerson Electric 4645 Fairway Lachine, Que.	- Brooks Flowmeter, Model 7-1110 - Monel float, R-7M-25-1
Air Rotameter	" "	- Brooks Flowmeter, Model 7-1110 - Glass float, R-7M-25-1
Differential Pressure Transmitter for Fluidized-Bed Pressure Drop	Foxboro Canada	- Adjustable scale 0-50 kPa, Model 613
Fluidized-Bed Heating Wire	Pyradia 430 Guimond Longueuil, Que.	- Type A-1, 20 gauge wire (max. T = 1400°C), Kanthal Inc.
Pneumatic N_2 Rotameter	Emerson Electric	- Tube #3-65
H_2O Metering Pump	Cole-Parmer	- Masterflex Pump, Model 7520-35
Windbox Heating Tape	Cole Parmer 7425 N Oak Park Ave. Chicago, Illinois	- Model R-3119-10 (Rated 240 VAC) 6.35 cm wide x 305 cm long (max. T = 850°C) Samox Inc.

EQUIPMENT	SUPPLIER	SPECIFICATIONS
Distributor Pressure Drop	Furneco	- Magnehelic, Model 2205C (0-103 kPa), Dwyer Instruments
Scrubber NaOH	DOW Chemical Sarnia, Ont.	- ~0.5 cm diameter beads
Heating Tape (cyclones/windbox)	" "	- 1" x 96", Model R-3117-80, Samox Co.
Analytical Equipment		
Gas Chromatograph/ Sulphur Gases	Hewlett Packard	- Model 5790A, equipped with single flame FPD detector
Gas Chromatograph/ Fixed Gases	Fisher Scientific	- Model 1200 Gas Partitioner, equipped with TCD detector
Ion Chromatograph	Dionex Corp 1228 Titan Way Sunnyvale, CA	- Model 2000i, equipped with ECD and amperometric detectors
Deionization Column	Fisher Scientific	- HN High Capacity DI Barnstead Cartridge - Ultrapure (Mixed Bed DI) Barnstead Cartridge
Ion Analyzer	Cole Parmer	- Microprocessor Ionalyzer Model 901 Orion Research
Oxygen-Bomb Combustion Apparatus	Fisher Scientific	- Parr Oxygen Bomb, Model No. 1108
Gas-Tight Syringes	Chromatographic Specialties 300 Laurier Blvd. Brockville, Ont.	- 10 µL, 100 µL, 500 µL, 1 mL, 2.5 mL, Hamilton Series 1000
Sulphur Gases Permeation-Tube Assembly	VICI Metronics 2991 Corvin Drive Santa Clara, CA	- COS wafer #7600 - CH_3SH #6000 - $(CH_3)_2S$ #6200 - $(CH_3)_2S_2$ #6301 - H_2S #0110 - heat exchanger # 19x415-000 glass U-Tube
Integrators for Gas Chromatographs/ Ion Chromatographs	Hewlett Packard 17500 Trans Canada Hwy Kirkland, Que.	- 3390A Reporting Integrators
Weighing Balances	Canlab 8655 Delmeade Montreal, Que.	- 0-60,000 g (±1 g) Model 3807 - 0-160 g (±.0001 g) Model AE166, Sartorius Co.
Sieves	Fisher Scientific P.O. Box 1020 Montreal, Que.	- Tyler series; 38, 53, 63, 75, 106, 125, 180, 212, 250 µm aperture
Sieve Shaker	Fisher Scientific	- Model RX-24, (110 V, 6.4 A)

APPENDIX C

DERIVATION OF RATE LAWS FOR THE PROPOSED MECHANISMS OF THE CATALYSED C-H_2O REACTION

RATE LAW FOR CO PRODUCTION

For the reactions on the active catalyst sites, Eqs. 84, 32 (Chapter 2), one can assume the steady-state assumption for $[O(*)]$, as follows,

$$\frac{d[O(*)]}{dt} = 0 = j_1 [(*)] p_{H_2O} - j_{-1} [O(*)] p_{H_2} - j_2 [O(*)] [C_{site}] p_{H_2O}$$

Solving for $[(*)]$, gives the following expression,

$$[(*)] = [O(*)] \left\{ \frac{j_{-1} p_{H_2} + j_2 [C_{site}] p_{H_2O}}{j_1 p_{H_2O}} \right\} \tag{133}$$

Recall that the total surface concentration of catalyst sites is given by,

$$[C_{cT}] = [(*)] + [O(*)] \tag{134}$$

Inserting $[(*)]$ from Eq. 133 into Eq. 134, and solving for $[O(*)]$ gives the following expression,

$$[O(*)] = \frac{[C_{cT}]}{\left\{ \frac{j_{-1} p_{H_2}}{j_1 p_{H_2O}} + \frac{j_2 [C_{site}]}{j_1} + 1 \right\}} \tag{135}$$

Invoking the assumptions made by Cerfontain et al. (1987b) for the analogous C-CO_2 reaction, it is noted that the oxygen exchange reaction, Eq. 84 (Chapter 2), is very fast compared to the reduction of the oxidized catalyst, Eq. 32 (Chapter 2), therefore, $j_1 >> j_2$. Also, the equilibrium constant of the oxygen-exchange, Eq. 84 (Chapter 2), is large, and the surface consists mostly of oxidized catalyst sites; this implies that $j_{-1}/j_1 << 1$. From these assumptions it is seen that the denominator of Eq. 135 approaches 1, and $[O(*)] \approx [C_{cT}]$.

Assuming that the concentration of gasification sites, $[C(O)]$, is at steady-state, and also realizing that the forward rates of Eqs. 65, 69 are negligible during catalysed gasification, then at steady state,

$$\frac{d[C(O)]}{dt} = 0 = j_2 p_{H_2O} [O(*)] [C_{site}] - i_2 [C(O)] - i_{-1} p_{CO} [C(O)] - m_{-1} p_{H_2} [C(O)]$$

Solving for $[C_{site}]$, and noting that $[O(*)] \approx [C_{cT}]$ from Eq. 135, then

$$[C_{ate}] = [C(O)]\left(\frac{i_2 + i_{-1}\,p_{CO} + m_{-1}\,p_{H_2}}{j_2\,p_{H_2O}\,[C_{cT}]}\right) \tag{136}$$

The concentration of carbon active sites, $[C_T]$ is given by,

$$[C_T] = [C(O)] + [C_{ate}] \tag{137}$$

Inserting $[C_{ate}]$ of Eq. 136 into Eq. 137, and solving for $[C(O)]$ gives,

$$[C(O)] = \frac{[C_T]}{\left\{1 + \left(\frac{i_2 + i_{-1}\,p_{CO} + m_{-1}\,p_{H_2}}{j_2\,p_{H_2O}\,[C_{cT}]}\right)\right\}} \tag{138}$$

The rate determining step for the overall gasification is given by Eq. 67, therefore,

$$-r_n = i_2\,[C(O)]\,S_{a0} \tag{139}$$

Replacing $[C(O)]$ from Eq. 138 into Eq. 139, and recalling that $N_T = [C_T] \cdot S_{a0}$ from Chapter 2, gives the following expression,

$$-r_n = \frac{i_2\,N_T}{\left\{1 + \left(\frac{i_2 + i_{-1}\,p_{CO} + m_{-1}\,p_{H_2}}{j_2\,p_{H_2O}\,[C_{cT}]}\right)\right\}} \tag{140}$$

From the quasi-equilibrium assumption, $i_2 << m_{-1}\,p_{H_2}$, and therefore i_2 can be dropped from the denominator. Also, in gasification systems employing pure steam or H_2/H_2O mixtures, then p_{CO} would be small, and $i_{-1}p_{CO}$ can be ignored. Finally, in the derivation of Eq. 135, if all the concentration terms are converted to units of mol sites/g C by multiplying by S_{a0}, then $[C_{cT}]$ may be replaced by N_{cT}. The simplified rate law is,

$$-r_n = \frac{i_2\,N_T}{1 + \left(\frac{m_{-1}\,p_{H_2}}{j_2 \cdot N_{cT} \cdot p_{H_2O}}\right)} \tag{141}$$

RATE LAW FOR CO_2 PRODUCTION

The mechanism for CO_2 production includes the extra step, Eq. 33, given in Chapter 2. From the steady-state assumption for $[O(*)]$, then

$$\frac{d[O(*)]}{dt} = 0 = j_1\,[(*)]\,p_{H_2O} - j_{-1}\,[O(*)]\,p_{H_2} - j_2\,[O(*)]\,[C_{ate}]\,p_{H_2O} - j_3\,[O(*)]\,[C(O)]\,p_{H_2O}$$

Solving for [(*)],

$$[(*)] = [O(*)]\left\{\frac{j_{-1}\,p_{H_2} + j_2\,[C_{site}]\,p_{H_2O} + j_3\,[C(O)]\,p_{H_2O}}{j_1\,p_{H_2O}}\right\} \tag{142}$$

Inserting [(*)] in Eq. 142 into Eq. 134 shown previously gives,

$$[O(*)] = \frac{[C_{cT}]}{\left\{\frac{j_{-1}\,p_{H_2}}{j_1\,p_{H_2O}} + \frac{j_2\,[C_{site}]}{j_1} + \frac{j_3\,[C(O)]}{j_1} + 1\right\}} \tag{143}$$

From previous arguments, the first two terms in the denominator are small. Also, the oxygen-exchange reaction, Eq. 84 (Chapter 2), is very fast compared to the reduction of an oxidized site by C(O), Eq. 33 (Chapter 2), so $j_1 >> j_3$ and the denominator approaches 1.

For the steady-state concentration of gasification sites, [C(O)],

$$\frac{d[C(O)]}{dt} = 0 = j_2\,p_{H_2O}[O(*)][C_{site}] - i_2[C(O)] - i_{-1}\,p_{CO}[C(O)] - m_{-1}\,p_{H_2}[C(O)] - j_3\,p_{H_2O}[O(*)][C(O)]$$

Solving for $[C_{site}]$,

$$[C_{site}] = [C(O)]\left\{\frac{i_2 + i_{-1}\,p_{CO} + m_{-1}\,p_{H_2} + j_3\,p_{H_2O}\,[O(*)]}{j_2\,p_{H_2O}\,[O(*)]}\right\} \tag{144}$$

Replacing $[C_{site}]$ from Eq. 144 into Eq. 137, and rearranging gives,

$$[C(O)] = \frac{[C_T]}{\left\{1 + \left(\frac{i_2 + i_{-1}\,p_{CO} + m_{-1}\,p_{H_2} + j_3\,p_{H_2O}\,[O(*)]}{j_2\,p_{H_2O}\,[O(*)]}\right)\right\}} \tag{145}$$

As shown previously, one can approximate [O(*)] by $[C_{cT}]$, or N_{cT}. The rate determining step is Eq. 67 (Chapter 2). The terms i_2 and $i_{-1}p_{CO}$ may be dropped since the desorption step is rate determining, and the CO concentration is small for experimental systems that operate differentially in H_2O and H_2. Replacing [C(O)] from Eq. 145 into Eq. 139, and rearranging gives the rate law,

$$-r_n = \frac{i_2\,N_T}{1 + \left(\frac{m_{-1}\,p_{H_2}}{j_2\,N_{cT}\,p_{H_2O}} + \frac{j_3}{j_2}\right)} \tag{146}$$

APPENDIX D

ESTIMATION OF THE MASS TRANSFER RATES OF STEAM TO THE PARTICLES IN THE FLUIDIZED BED

Mass Transfer Relationships

The external mass transfer of steam to the char-alumina particles in the fluidized bed is estimated for the steam gasification runs SG4 (600°C) and SG5 (650°C). These values are then compared to the measured carbon gasification rates after adjusting for the total external surface area in the particulate phase.

Neglecting the particle curvature and assuming dilute concentrations of diffusing species, the average molar flux of steam to the char-alumina surface, W_{H_2O}, is given by (Fogler, 1986):

$$W_{H_2O} = k_c \left(C^{bulk}_{H_2O} - C^{*}_{H_2O} \right) \tag{147}$$

where k_c is the average mass-transfer coefficient, and the molar concentration of steam in the bulk fluid and the particle surface are $C^{bulk}_{H_2O}$ and $C^{*}_{H_2O}$, respectively. The average mass-transfer coefficient is estimated from empirical correlations involving the Sherwood number, *Sh*, as follows:

$$Sh = \frac{k_c \, d_p^{*}}{D_{H_2O\text{-}m}} \tag{148}$$

where $D_{H_2O\text{-}m}$ is the overall diffusion coefficient of steam in the bulk fluid of the particulate phase and d_p^{*} is the diameter of the particle.

La Nauze and Jung (1986) give a summary of the correlations for the mass transfer to particles in fluidized-bed combustors in terms of the Sherwood number. The simplest expression that also gives the lowest estimate of the mass transfer coefficient is that of Avedesian and Davidson (1973). They assume no forced or natural convection in the particulate phase and reason that the Sherwood number is equal to $2\cdot\varepsilon_{mf}$, where ε_{mf} is the bed voidage at minimum fluidization. The bed voidage does not vary significantly with temperature and is estimated as 0.54 from the data of Kunii and Levenspiel (1977) for 200 μm sharp sand particles.

Estimating the Particle Diameter

For non-spherical particles, the equivalent diameter is used in the Sherwood number and is given by the following expressions (Fogler, 1986):

$$d_p^{*} = 0.564 \sqrt{A_p} \tag{149}$$

$$A_p = \phi \cdot \pi \, d_p^{\,2} \tag{150}$$

where A_p is the external surface area of the particle (i.e., $6.8 \cdot 10^{-8}$ m^2), ϕ is the sphericity as defined by Kunii and Levenspiel (1977), and d_p is the surface-area-mean particle size measured and reported in Chapter 3 (i.e., 180 μm). The sphericity is estimated as 0.67 from micrographs of char-alumina. This is similar to the value quoted by Kunii and Levenspiel for sharp sand. The equivalent diameter of the particle, d_p^*, is therefore calculated as $147 \cdot 10^{-6}$ m.

Estimating the Overall Diffusion Coefficient

For steady-state diffusion in multicomponent systems where all the species except steam are assumed to be stagnant, the effective diffusion coefficient of steam in the bulk fluid of the particulate phase, $D_{H_2O\,m}$ (cm^2/s), can be found from the expression (Treybal, 1980):

$$D_{H_2O\text{-}m} = \frac{1 - y^p_{H_2O}}{\sum_{i=1}^{n} \frac{y_i^p}{D_{H_2O\text{-}i}}} \tag{151}$$

where $y^p_{H_2O}$ and y^p_i are the mole fractions of steam and gaseous species i in the particulate phase, respectively. The mole fractions of the species considered are obtained from a knowledge of the molar flow rates of the major gases at the exit of the reactor and assume that the particulate phase is well-mixed. The molar flow rates of the sulphur gases were ignored because they are one order of magnitude smaller than for the fixed gases. The species considered were CO_2, CO, H_2O, N_2, and H_2. The molar flow rates for CO_2, CO, and H_2 are obtained from Table 40 - Table 42. For example, in run SG5 these are 0.061, 0.016, and 0.157 mol·min^{-1}, respectively.

The flow rate of N_2 in the particulate phase is essentially identical for both runs SG4 and SG5 at ~0.60 mol/min. This is based on the two-phase theory of fluidization and neglects interphase transport from the bubbles. It is calculated as 27% of the total inlet molar flow rate to the fluidized bed (i.e., 2.23 mol/min).

The molar flow rate of steam at the exit of the particulate phase, $F^p_{H_2O}$, is calculated from a steady-state mole balance in the particulate phase and assumes negligible interphase transfer of steam from the bubbles. It is given as the difference of the inlet flow rate to the particulate phase (i.e., 27% of 0.56 mol/min) and the sum of consumption rates of steam, ξ_{40} and ξ_{41}, obtained from Table 15 and repeated in Table D.1 for both runs SG4 and SG5. Finally, the mole fractions for the various species are tabulated in Table D.1.

Table D.1 - Values of Key Parameters Used in the Mass Transfer Calculations

Parameter		Run SG4	Run SG5
Alumina Input (kg)		5.504	6.311
A_{total}	(m^2)	31.2	35.4
$F^P_{H_2O}$	($mol\,min^{-1}$)	0.12	0.019
$(\xi_{40} + \xi_{41})$	($mol\,min^{-1}$)	0.04	0.132
$C^{bulk}_{H_2O}$	($mol\,min^{-1}$)	2.92	0.46
$y^P_{N_2}$		0.72	0.71
$y^P_{H_2}$		0.088	0.18
$y^P_{CO_2}$		0.034	0.072
y^P_{CO}		0.010	0.019
$y^P_{H_2O}$		0.15	0.022
$D_{H_2O\text{-}N_2}$	($10^{-4}\ m^2 s^{-1}$)	1.73	1.91
$D_{H_2O\text{-}H_2}$	($10^{-4}\ m^2 s^{-1}$)	5.78	6.37
$D_{H_2O\text{-}CO_2}$	($10^{-4}\ m^2 s^{-1}$)	1.38	1.52
$D_{H_2O\text{-}CO}$	($10^{-4}\ m^2 s^{-1}$)	1.69	1.87
$D_{H_2O\text{-}m}$	($10^{-4}\ m^2 s^{-1}$)	1.84	2.13
k_c	($m s^{-1}$)	1.35	1.56
W_{H_2O}	($mol\,m^{-2} s^{-1}$)	3.94	$7.2 \cdot 10^{-1}$
$-r''_w$	($mol\,m^{-2} s^{-1}$)	$9.7 \cdot 10^{-6}$	$3.2 \cdot 10^{-5}$

The binary diffusivity of steam in i, $D_{H2O,i}$ (cm^3/s), can be obtained by the Fuller, Schettler, and Giddings correlation given in Reid et al. (1977):

$$D_{H_2O\text{-}i} = \frac{10^{-3}\, T^{1.75}\, [(M_{H_2O} + M_i)/M_{H_2O} \cdot M_i]^{1/2}}{P\, [(\Sigma v)^{1/3}_{H_2O} + (\Sigma v)^{1/3}_i]^{\,2}} \qquad (152)$$

In this expression M_{H2O} and M_i are the molecular weights of steam and species i, respectively. The atomic diffusion volumes, Σv ($cm^3 \cdot g^{-1} \cdot mol^{-1}$), for the species $H_2O_{(v)}$, CO, CO_2, H_2, and N_2 are 12.7, 18.9, 26.9, 7.07, and 17.9, respectively. The corresponding mass-transfer coefficients calculated for runs SG4 and SG5 using Eq. 148 are given in Table D.1.

Calculating the Mass Transfer Rate

If the mass transfer of steam to the char-alumina particle controls the gasification of carbon then $C^s_{H_2O}$, in Eq. 147 is negligible. The bulk concentration of steam in the particulate phase, $C^{bulk}_{H_2O}$, is estimated as the product, F^P_{H2O}, given in Table D.1 and $1/U_{mf} \cdot A$. It is noted that the flow rate of gas at minimum

fluidization, $U_{mf} \cdot A$, does not vary greatly with temperature and can be taken as ~0.012 $m^3 \cdot min^{-1}$ (i.e., 0.025 m/s x $7.85 \cdot 10^{-3}$ m^2) for both SG4 and SG5. Table D.1 lists the calculated bulk steam concentrations. Eq. 147 can now be used to estimate the molar flux of steam to the char-alumina surface. For runs SG4 and SG5, W_{H_2O} is found to be 3.94 and $7.2 \cdot 10^{-1}$ $mol \cdot s^{-1} \cdot m^{-2}$, respectively.

The carbon consumption rate per unit external surface area, $-r_w''$, can be found by dividing ξ_{40} from Table 15 by the total external surface area of char-alumina, A_{total}, where the latter quantity can be estimated from the equation:

$$A_{total} = \frac{Alumina\ Input \cdot A_p}{\rho_{Al_2O_3} \cdot \frac{4}{3} \Pi (d_p/2)^3} \tag{153}$$

The Alumina Input to the fluidized bed for runs SG4 and SG5 is given in Table 33 - Table 34, and the density of alumina, $\rho_{Al_2O_3}$, is 3965 $kg \cdot m^{-3}$. The values of $-r_w''$ for runs SG4 and SG5 are $9.7 \cdot 10^{-6}$ and $3.2 \cdot 10^{-5}$ $mol \cdot m^{-2} \cdot s^{-1}$, respectively.

Comparison of W_{H_2O} and $-r_w''$ shows that the mass transfer of steam to the char surface is greater than the flux of carbon by a factor of 10^5 times at 600°C and 10^4 times at 650°C. It is therefore reasonable to assume that kinetics control the gasification rate of carbon at these temperatures.